



**HAL**  
open science

# Development and characterization of luminescent molecular materials and their application in technical textiles

Tarik Aaboub

► **To cite this version:**

Tarik Aaboub. Development and characterization of luminescent molecular materials and their application in technical textiles. Optics / Photonic. Université de Rennes; Université Hassan II (Casablanca, Maroc), 2023. English. NNT: 2023URENE003 . tel-04405046

**HAL Id: tel-04405046**

**<https://theses.hal.science/tel-04405046v1>**

Submitted on 19 Jan 2024

**HAL** is a multi-disciplinary open access archive for the deposit and dissemination of scientific research documents, whether they are published or not. The documents may come from teaching and research institutions in France or abroad, or from public or private research centers.

L'archive ouverte pluridisciplinaire **HAL**, est destinée au dépôt et à la diffusion de documents scientifiques de niveau recherche, publiés ou non, émanant des établissements d'enseignement et de recherche français ou étrangers, des laboratoires publics ou privés.

# THESE DE DOCTORAT EN COTUTELLE DE

L'ÉCOLE NORMALE  
SUPERIEURE DE RENNES

ÉCOLE DOCTORALE N° 601  
MATISSE  
Spécialité : Photonique

L'UNIVERSITE HASSAN II  
DE CASABLANCA

CENTRE D'ÉTUDE DOCTORALE  
*Sciences et Application*  
*Spécialité : Sciences des matériaux*

**Tarik AABOUB**

**Développement et caractérisation de matériaux moléculaires  
luminescents et leur application dans des textiles techniques**

Thèse présentée et soutenue à la Faculté des Sciences Ben M'sik Casablanca le 15 mai 2023

## Unités de recherche

Systèmes et Application des Technologies de l'Information et de l'Energie (SATIE UMR CNRS 8029)  
Laboratoire Ingénierie des MATériaux (LIMAT)

## Rapporteurs avant soutenance :

**Lionel PATRONE**

Chargé de recherche, HDR, Aix Marseille université, France

**Bouchaib MANOUN**

Professeur d'université, université Hassan I, Maroc

## Composition du Jury :

Président : **Bouchaib MANOUN**

Professeur d'université, université Hassan I, Maroc

Examineurs : **Lionel PATRONE**

Chargé de recherche, HDR, Aix Marseille université, France

**Najma LAAROUSSI**

Professeur d'université, université Mohammed V, Maroc

**Abdeslam EL BOUARI**

Professeur d'université, université Hassan II, Maroc

**Boujemaa JABER**

Professeur d'université, UATRS, CNRTS, Maroc

Dir. de thèse : **Martinus H.V. WERTS**

Chargé de recherche, HDR, ENS Rennes, France

Co-dir. de thèse : **Said GMOUH**

Professeur d'université, université Hassan II, Maroc

## Invité(s)

**Aicha BOUKHRISS**

Docteur en chimie des matériaux, ESITH, Maroc



For the electronic version of my thesis report as well as the slides presented during my thesis defense, please scan the following QR code and follow the link



PS : Maybe in 3 4 years, these QR codes will disappear,  
Especially with the recent artificial intelligence (AI) development.



## Résumé en français

Cette thèse s'inscrit dans deux domaines complémentaires. Le premier concerne le développement des matériaux avec des fonctions dotées de propriétés nouvelles à travers la chimie moléculaire, et leur intégration dans une matrice, mettant en relief le textile comme substrat, en utilisant la chimie de surface. Le deuxième est plutôt technique, et concerne les développements et les innovations dans les instruments de caractérisation, en spécifiant les méthodes optiques et spectroscopiques. L'objectif ultime serait d'élaborer des textiles techniques avec la propriété auto-lumineuse en utilisant différents procédés de fonctionnalisation et leur caractérisation optique et spectrale.

Les humains sont incroyablement ingénieux dans leur capacité à trouver des moyens d'améliorer leur vie sur terre. L'une des manifestations les plus évidentes de cette ingéniosité est notre capacité à transformer les ressources naturelles en matériaux qui répondent à nos besoins. La révolution industrielle a marqué un tournant vers l'utilisation de matériaux synthétiques, souvent dérivés de précurseurs naturels mais nécessitant une grande quantité d'énergie pour être produits. Malgré cela, la commodité et la polyvalence de ces matériaux synthétiques ont fait d'eux une partie intégrante de notre vie quotidienne.

Parmi les matériaux existants, certains ont la propriété de produire de la lumière lorsqu'ils sont excités par une source d'énergie, comme un courant électrique, de la chaleur ou une réaction chimique. Ces matériaux sont appelés luminescents et incluent la fluorescence, qui libère immédiatement de la lumière après avoir absorbé de l'énergie, la phosphorescence qui stockent de l'énergie avant de la libérer plus tard, et les matériaux

électroluminescents qui produisent de la lumière lorsqu'un courant électrique les traverse, comme dans le cas des tubes néon et des diodes électroluminescentes (LEDs). Ces matériaux luminescents ont trouvé des applications variées, notamment en biologie pour le marquage cellulaire et la recherche moléculaire, ainsi que dans le développement de techniques spectroscopiques telles que la spectroscopie de fluorescence, la spectroscopie Raman, la spectroscopie à excitation par laser ou plasma. Encore, la luminescence est également utilisée dans la décoration, l'art et les loisirs.

Grâce à l'innovation technologique et technique, ces matériaux ont pu être employés dans de nouvelles applications et sont maintenant utilisés dans des exploitations concrètes par l'intermédiaire de la fonctionnalisation de surface. Cette dernière est connue depuis longtemps, et utilisée depuis des siècles, notamment dans les procédés de teinture de textiles, mais ses applications se sont considérablement développées avec les avancées technologiques récentes. Ce traitement de surface est utilisé pour donner des propriétés nouvelles ou améliorer des propriétés existantes, par le biais de modification de leur surface. La fonctionnalisation de surface est utilisée dans de nombreux domaines tels que la chimie des matériaux, la physique des matériaux, la biochimie, les nanotechnologies entre autres. Les techniques de fonctionnalisation de surface sont utilisées pour conférer des propriétés comme la conductivité électrique, la réactivité chimique, l'hydrophobie, l'adsorption, etc.

La fonctionnalisation de surface par la méthode sol-gel est l'une des méthodes de fonctionnalisation, et qui consiste à créer des revêtements polymériques transparents, flexibles et résistants à la corrosion et à l'oxydation. Le sol-gel est une réaction chimique qui consiste à préparer des sols colloïdaux à partir de précurseurs chimiques, puis à faire

coaguler ces sols pour former des gels. Ces gels peuvent ensuite être traités thermiquement ou chimiquement pour obtenir des matériaux solides tels que des céramiques, des verres, des métaux, des polymères, des nanoparticules et des composites. La technique sol-gel s'est avérée efficace sur de nombreux aspects, particulièrement en termes de résultats obtenus et de facilité d'utilisation. Elle présente également l'avantage d'être économe en énergie et en solvants, ainsi que respectueuse de l'environnement avec un minimum de rejets.

Cette thèse se concentre sur l'intégration de matériaux dotés de propriétés spécifiques dans des matrices textiles par fonctionnalisation. L'accent est mis sur les matériaux luminescents, qui seront intégrés dans un réseau sol-gel et fixés à la surface des textiles. Les outils et techniques liés aux fibres optiques sont utilisés tout au long du processus, depuis la molécule jusqu'au produit final.

Ce projet peut être décomposé en trois étapes : (i) la préparation des matériaux ayant les propriétés désirées, (ii) les méthodes pour transférer ces propriétés au substrat cible, et (iii) les techniques permettant une caractérisation complète des matériaux et des substrats, notamment en termes de caractéristiques optiques. Chapitre 1 décrit l'état de l'art des principaux sujets abordés dans ce travail, en discutant l'aspect théorique des colorants, les fluorophores et les luminophores. Nous avons également examiné les méthodes spectroscopiques de caractérisation de ce type de matériaux à caractère luminescent, spécifiquement les méthodes de détermination des rendements quantiques des molécules fluorescentes ainsi que les récents développements en matière d'instruments et de techniques.

Le chapitre 2 examine les instrumentations et les méthodes utilisées dans cette thèse, en se concentrant sur les types d'équipements spectroscopiques développés pour la



fonctionnalisation des textiles. La première partie de ce chapitre décrit les matériels et méthodes utilisés pour atteindre cet objectif, y compris les matériaux, les produits chimiques, les méthodes et les appareils utilisés, spécifiant les méthodes de traitement et fonctionnalisation des textiles. La deuxième partie souligne les aspects techniques des méthodes de mesure spectroscopique basées sur des dispositifs couplés à des fibres optiques, en fournissant des détails sur l'étalonnage des spectres, les corrections et les paramètres expérimentaux à prendre en compte lors de l'utilisation de ces instruments.

Le chapitre 3 discute de l'utilisation de la chimie sol-gel pour la fonctionnalisation des textiles et de sa convenance pour l'incorporation avec des matériaux, en commençant par utiliser des colorants modèles pour teindre les tissus en coton. Ce dernier a été étudié optiquement en termes de paramètres expérimentaux dont le but d'établir un processus générique de teinture par la méthode sol-gel, qui est optimisé et respectueux à la nature.

Le chapitre 4 contient deux parties complémentaires. Dans la première partie, nous rapportons une nouvelle méthode instrumentale développée pour déterminer les rendements quantiques de photoluminescence des molécules fluorescentes en solution en utilisant une mesure simultanée des spectres d'absorption et d'émission du fluorophore à travers des dispositifs couplés à des fibres optiques. La validité de la méthode et son efficacité ont été démontrées en utilisant des fluorophores bien documentés comme références standards. Dans la deuxième partie, quatre molécules fluorescentes ont été synthétisées et caractérisées en utilisant la méthode décrite dans la première partie. De plus, ces molécules de fluorophores ont été utilisées pour préparer des tissus textiles fluorescentes par le processus développé dans le chapitre 3, ce qui est une étape essentielle dans le processus de préparation de textiles lumineux.

Dans le chapitre 5, nous nous dirigeons vers le développement de textiles affichant une luminescence longue persistante, qui est l'objectif ultime de ce travail. Pour obtenir des tissus qui émettent de la lumière pendant une période prolongée, il est nécessaire d'utiliser des matériaux avec une émission de luminescence forte et durable. Selon les recherches bibliographiques, les phosphores inorganiques à base de strontium aluminate sont actuellement les matériaux lumineux persistants les plus efficaces à cet effet. Cependant, il y a également un intérêt croissant pour l'utilisation de matériaux lumineux organiques, qui ont montré des comportements lumineux persistants prometteurs. Dans la première partie de ce chapitre, une sélection de composés organiques, qui ont été rapportés dans la littérature pour afficher une luminescence longue persistante à l'état cristallin, est présentée. Leurs propriétés lumineuses sont investiguées avec un ensemble spécifique de spectroscopie luminescente à temps résolu qui a été développé lors de ce travail. Dans la deuxième partie, des phosphores aluminate de strontium ont été étudiés et comparés aux matériaux lumineux organiques. La luminescence persistante des matériaux inorganiques s'est révélée être beaucoup plus intense avec une durée d'émission assez longue. La troisième partie du chapitre décrit l'incorporation des phosphores inorganiques à luminescence persistante dans les textiles et la caractérisation de leur luminescence.

A l'issue de ce travail de thèse, Nous avons examiné l'utilisation de la méthode de fonctionnalisation par sol-gel pour créer un processus écologique de teinture de textiles en alternative aux méthodes existantes. Nous avons également amélioré et testé l'efficacité de ce processus pour intégrer des molécules luminescentes afin de produire des textiles fluorescents. Nous avons mis en place un montage expérimental pour mesurer les rendements quantiques de fluorescence en solution et un montage spectro-temporel pour mesurer les paramètres photophysiques de l'analyte luminescent. Nous avons réussi

à préparer des molécules organiques luminescentes à température ambiante, mais ces matériaux présentaient un temps d'émission court insuffisant pour notre objectif principal. En conséquence, nous avons opté pour des matériaux phosphorescents inorganiques et avons réussi à créer des textiles luminescents avec une émission persistante longue en utilisant une méthode directe simple.

---

## Acknowledgement

Alhamdulillah, Allah gave me everything.

This Ph.D. was completed as a co-shared thesis (Cotutelle) between Hassan II university of Casablanca in Morocco and the Ecole Normale Supérieure de Rennes in France. The program was fully funded through the French-Moroccan partnership Hubert Curien Toubkal. For these reasons and a few more, I would like to express my gratitude toward the CEDoc Ben M'Sick, CNRST, ED MathSTIC (N°601, currently MATISSE) of the University of Rennes, the administration of ENS Rennes, SATIE of Paris-Saclay (UMR 8029), and PHC Toubkal. I thank them for their assistance in facilitating the paperwork and giving me the opportunity to participate in this program, which allowed me to benefit from this unique collaboration.

Expressing gratitude can be difficult, especially when it comes to thanking those who have made a significant impact on my life. Finding the right words to convey my appreciation can be challenging, and a brief mention is not enough to fully express my appreciation to all of the people who have supported me with their smiles, love, presence, laughter, and guidance. There have been so many people in my life who have contributed to my growth and success, and I am deeply grateful for each and every one of them.

I am heartily thankful to my parents; I am in debt for your kindness, support, love, and devotion in raising me. My wonderful little siblings, Fadwa and Anasse, thank you for your existence; I could not be prouder of you and your achievement thus far, wishing you all the best and success. My big brother Anouar, sister-in-law Asma, and superb nephews Yazane and Ons, thank you for being in my life and having me in Paris; you have made my arrival in France easy. Nada, your presence has dramatically improved my life, and I am deeply grateful for your love, support, thoughtfulness, and faith in me as we journey together. Thank you.

I want to thank my thesis directors sincerely. It has been my good fortune to do my thesis under the supervision of Pr. Said Gmouh (Hassan II university, Morocco) and Dr. Martinus H.V. Werts (ENS Rennes, France), who are both great researchers and supervisors. I thank them for their guidance, constant concern for my improvement, and helpful support through

---

---

critical comments. I have learned several notions from them that I could use and apply in my thesis. I truthfully thank them for all the guidance and sustainably assistance. Martin, I am so grateful for everything you have taught me and the new skills I have gained under your guidance. Your help with my writing and your suggestions were invaluable, and your insights while revising my thesis report were constructive. Your help during the preparation of my presentation and your advice were of great help. The coffee breaks and walking talks we shared were also greatly appreciated and made me feel at home. Thank you for everything.

I am also thankful to my co-supervisor, Aicha Boukhriss (ESITH, Morocco), who first believed in me and saw my potential. Her help with my thesis research was a surplus. I wish her the best of luck on her new journey.

I was lucky to conduct numerous experiments at the REMTEX laboratory, providing me unlimited access to their resources and materials. I want to express my gratitude to Pr. Omar Cherkaoui, the head of the R&D department at the laboratory, as well as Dr. Mehdi El Bouchti, the lab's responsible and every colleague in this wonderful lab. Thank you.

I have always believed in the butterfly effect and how small actions or events can have unforeseen consequences. Abdelkrim Batan, my bachelor's thesis supervisor and the catalyst for where I am now. He is the person who introduced me to "the sol-gel chemistry" and surface functionalization and encouraged me to pursue research and explore international opportunities. I am deeply thankful.

I want to show my appreciation to all my thesis committee members, starting with Pr. Bouchaib Manoun, Pr. El Bouari, Pr. Patrone for their thorough revision and wise comments. Thank them all for taking the time to be present and carefully revise my manuscript and contribute to a long discussion during my thesis defense. I am also thankful for Pr. Najma Laaroussi, Pr. Boujema Jaber for the fruitful discussions before and during my thesis defense and I thank them for taking the long road to be present in Casablanca knowing that they were not present in Morocco at the time .

A second appreciation word to Lionel and Martin (Pr. Patrone and Pr. Werts), with whom I shared great moments in Morocco, discovering Rabat and Casablanca. I want to thank you for

---

coming and for the friendly discussions during our long walks in the streets. Thank you for the gifts (From Brittany and Axe-en-Provence) and see you next time in France.

Finally, my colleagues from REMTEX, LIMAT, and the Mechatronic department at ENS Rennes. A special thanks goes to Lancelot and Moura, my deskmates in E-047, for their friendship. Lancelot, thank you for sharing your expertise with the microscope and gold nanoparticles with me. I wish you the best in your new endeavors. Moura, it was a pleasure to speak our native language together while being in a foreign country. It reminded me of home. Lastly, I am grateful for all the moments I shared with my numerous friends, whom I cannot even begin to count.

Tarik AABOUB, May 17<sup>th</sup>, 2023, Casablanca, Morocco

---

# Table of content

<i>Résumé en français</i> .....	<i>i</i>
<i>Acknowledgement</i> .....	<i>vii</i>
<i>Table of content</i> .....	<i>x</i>
<i>List of figures</i> .....	<i>xiv</i>
<i>List of tables and schemes</i> .....	<i>xvii</i>
<b>General introduction</b> .....	<b>1</b>
<i>Research framework and thesis outline</i> .....	<i>2</i>
<b>Chapter 1 Scientific background and state of the art</b> .....	<b>4</b>
<i>1.1. Introduction</i> .....	<i>4</i>
<i>1.2. Concept of color</i> .....	<i>5</i>
<i>1.3. Dyes and pigments</i> .....	<i>6</i>
1.3.1. Chromophores.....	<i>6</i>
1.3.2. Auxochromes.....	<i>7</i>
1.3.3. Interlude.....	<i>10</i>
<i>1.4. Luminescence</i> .....	<i>10</i>
1.4.1. Background and history of luminescence.....	<i>10</i>
1.4.2. Photoluminescence of organic chromophores.....	<i>11</i>
<i>1.5. Fluorescence</i> .....	<i>13</i>
1.5.1. Overview.....	<i>13</i>
1.5.2. Quantum yield and efficiency of fluorescence.....	<i>14</i>
1.5.3. Measurement of Quantum Yield (QY).....	<i>15</i>
1.5.4. Recent developments in QY measurement.....	<i>18</i>
1.5.5. Interlude.....	<i>21</i>
<i>1.6. Phosphorescence</i> .....	<i>21</i>
1.6.1. Phosphorescence from inorganic materials.....	<i>21</i>

---

1.6.2. Long-lived phosphorescence from the triplet excited state .....	24
1.6.3. Long-persistent luminescence (LPL) of organic materials .....	28
1.6.4. Interlude .....	38
1.7. Conclusion.....	39
1.8. Property to material transfer .....	40
<b>Chapter 2 Materials, methods, and instrumentation .....</b>	<b>42</b>
2.1. Introduction.....	42
2.2. Materials and chemicals .....	43
2.2.1. Substrate .....	43
2.2.2. Chemicals .....	43
2.3. Textile functionalization techniques.....	44
2.3.1. Functionalization by the pad-dry-cure method.....	44
2.3.2. Functionalization by the doctor-blade coating method .....	45
2.3.3. Functionalization by the spray coating method.....	46
2.4. Characterization equipment and apparatus.....	47
2.4.1. Nuclear magnetic resonance spectroscopy (NMR) .....	47
2.4.2. Attenuated total reflectance infrared spectroscopy (ATR-IR) .....	47
2.4.3. UV-visible extinction spectroscopy .....	47
2.4.4. Scanning Electron Microscopy with Energy Dispersive Spectroscopy .....	50
2.4.5. Colorimetric measurements.....	51
2.5. Devices .....	52
2.5.1. Light source.....	52
2.5.2. Samples   sample holder .....	55
2.5.3. Detectors   spectrophotometers .....	56
2.5.4. Detector calibration .....	58
2.5.5. Optical fibers and accessories .....	59
2.5.6. Integrating sphere.....	61
<b>Chapter 3 A sol-gel process for dyeing cotton in the perspective of functionalized textiles ....</b>	<b>63</b>
3.1. Introduction.....	63
3.2. Sol-gel chemistry .....	63
3.2.1. Overview .....	63

---



---

3.2.2. Sol-gel reactions .....	64
3.2.3. Sol-gel in surface coatings .....	65
3.2.4. Experimental conditions.....	66
3.3. <i>Practical realization</i> .....	69
3.3.1. Preparation of dye molecules .....	69
3.3.2. Optical characterization of the dyes in solution .....	69
3.3.3. Preparation of sol-gel dyeing solutions .....	71
3.3.4. Dyeing the cotton fabrics .....	71
3.3.5. Surface morphology and composition characterizations.....	74
3.3.6. Optical investigation of the fabrics .....	76
3.3.7. Exhaustion and monitoring of the dyeing baths .....	76
3.3.8. Colorimetric measurements.....	77
3.3.9. Diffuse reflectance and Kubelka-Munk relation .....	78
3.4. <i>Optimization of the sol-gel dyeing process</i> .....	80
3.4.1. Duration of impregnation .....	80
3.4.2. Number of dyeing cycles.....	82
3.4.3. Dyeing temperature .....	83
3.4.4. Dye concentration .....	85
3.4.5. Optimized sol-gel dyeing process .....	86
3.5. <i>Colorfastness and durability</i> .....	87
3.5.1. Experimental and measurements.....	87
3.5.2. Results .....	88
3.5.3. Amelioration of the dye fixation .....	89
3.6. <i>Conclusion</i> .....	92

<b>Chapter 4 Molecular fluorophores: Synthesis, measurement of their fluorescence quantum yields, and application to textiles .....</b>	<b>96</b>
4.1. <i>Introduction</i> .....	96
4.2. <i>Theoretical background for the SAFER method</i> .....	96
4.3. <i>Practical realization of the SAFER method</i> .....	105
4.3.1. Chemicals .....	105
4.3.2. Measurement set-up .....	106
4.3.3. Experimental conditions.....	107

---

---

4.3.4. Some examples of how PLQY measurement is done with the SAFER method .....	108
4.3.5. Validation of the SAFER method .....	112
4.4. <i>Synthesis of fluorophores and measurement of their PLQYs in solution using the SAFER method</i> .....	116
4.5. <i>Development of fluorescent textiles</i> .....	120
4.6. <i>Conclusion</i> .....	124
<b>Chapter 5 Organic and inorganic materials with long persistent luminescence and development of persistently luminescent textile fabrics</b> .....	<b>140</b>
5.1. <i>Introduction</i> .....	140
5.2. <i>Set-up for spectrotemporal characterization of luminescence</i> .....	141
5.3. <i>Synthesis of organic room temperature molecules</i> .....	143
5.3.1. <i>Chemicals</i> .....	143
5.3.2. <i>Synthesis routes</i> .....	144
5.3.3. <i>Spectroscopic measurements</i> .....	146
5.4. <i>LPL of the host molecule alone</i> .....	147
5.5. <i>Host-guest binary molecule / doping</i> .....	149
5.6. <i>Ion exchange / metathesis</i> .....	151
5.7. <i>Summary</i> .....	153
5.8. <i>Characterization of phosphors in their powder form</i> .....	154
5.9. <i>Sample preparation</i> .....	157
5.10. <i>Morphological aspect of the textile fabrics</i> .....	158
5.11. <i>Visual aspect of the samples as a function of the time</i> .....	159
5.12. <i>Conclusion and future perspectives</i> .....	160
5.12. <i>General conclusion</i> .....	160

---

---

## List of figures

<b>Figure 1.1.</b> Electromagnetic spectrum.....	5
<b>Figure 1.2.</b> Examples of chromophoric groups present in some organic dyes .....	6
<b>Figure 1.3.</b> Color enhancement by an auxochrome .....	7
<b>Figure 1.4.</b> Chemical structure of 2,4,6-trinitroaniline (TNA) .....	8
<b>Figure 1.5.</b> Representation of donor-acceptor system linked with $\pi$ -conjugated bonds.....	8
<b>Figure 1.6.</b> Effect of substituent groups within an azo-dye system.....	9
<b>Figure 1.7.</b> Jablonski diagram of energy levels and the transitions between them.....	12
<b>Figure 1.8.</b> Chemical structures of fluorescent fused-ring compounds .....	13
<b>Figure 1.9.</b> Representation of setup used in the absolute QY determination.....	16
<b>Figure 1.10.</b> Excitation and emission spectra of incident light and emitted light.....	16
<b>Figure 1.11.</b> Schematical representation of absorption spectra and standard reference .....	18
<b>Figure 1.12.</b> A representation of a double-beam measurement using a CCD detector.....	20
<b>Figure 1.13.</b> Zinc sulfide phosphor, atomic arrangement of ZnS in FCC lattice.....	22
<b>Figure 1.14.</b> Different proposed persistent luminescence mechanisms.....	24
<b>Figure 1.15.</b> Simplified Jablonski energy diagram with an explanation of LPL.....	25
<b>Figure 1.16.</b> Molecular structures of some triplet-state phosphorescent compounds.....	27
<b>Figure 1.17.</b> Photoinduced charge transfer of a single molecule with D-A moieties .....	29
<b>Figure 1.18.</b> The process of creating long-lasting charge-separated states. ....	30
<b>Figure 1.19.</b> The charge recombination (CR) process after the excitation source is ceased. ....	31
<b>Figure 1.20.</b> Simple preparation of amorphous room phosphorescent films.....	32
<b>Figure 1.21.</b> Long persistent luminescence from intermediate (exciplex) emission. ....	32
<b>Figure 1.22.</b> Electro-donor TMB and polymeric electro-acceptor PBPO .....	34
<b>Figure 1.23.</b> different polymeric films doped with fluorescent or organic dye.....	35
<b>Figure 1.24.</b> Energy diagram of the charge-separation matrix and the emitter dopant. ....	36

---

## List of figures

---

<b>Figure 1.25.</b> Mechanism for organic LPL based on trapping electron .....	37
<b>Figure 1.26.</b> Chemical structure of the donor-acceptor single molecule .....	38
<b>Figure 2.1.</b> Molecular structure of cellulose, a natural polymer.....	43
<b>Figure 2.2.</b> Dip coating and pad-dry-cure process.....	45
<b>Figure 2.3.</b> Doctor-blade coating and cure-pad processes .....	46
<b>Figure 2.4.</b> spray coating process .....	46
<b>Figure 2.5.</b> Representation of the dual-beam UV-vis spectrometer .....	49
<b>Figure 2.6.</b> Representation of a single-beam fluorimeter for emission measurements.....	49
<b>Figure 2.7.</b> Representation of fiber-coupled single beam UV-vis measurement setup .....	50
<b>Figure 2.8.</b> CIELab and CIELCH color spaces. ....	51
<b>Figure 2.9.</b> LS-1 tungsten halogen lamp, Avalight-HAL-S--Mini lamp .....	53
<b>Figure 2.10.</b> Corrected emission spectra of the fiber-coupled LEDs used for excitation.....	54
<b>Figure 2.11.</b> Stability of the LEDs emission after three hours of excitation .....	54
<b>Figure 2.12.</b> Spectral output of AVALIGHT-Xe-Hp with ZWB1 bandpass filter.....	55
<b>Figure 2.13.</b> Single-cell holders.....	56
<b>Figure 2.14.</b> The four spectrometers used during the preparation of this thesis.....	58
<b>Figure 2.15.</b> Spectral lines of calibration mercury-argon Hg-1 lamp.....	59
<b>Figure 2.16.</b> Representation of the anatomy of an optical fiber .....	60
<b>Figure 2.17.</b> Representation of fiber collimator principle .....	61
<b>Figure 2.18.</b> Representation of the working principle of the integrating sphere setup.....	62
<b>Figure 3.1.</b> Sol-gel hydrolysis step .....	64
<b>Figure 3.2.</b> Sol-gel condensation steps. Water condensation, alcohol condensation.....	65
<b>Figure 3.3.</b> NaOH effect on TEOS-based sol-gel solution .....	67
<b>Figure 3.4.</b> Extinction spectra of TEOS sol-gel solution when NaOH is added.....	67
<b>Figure 3.5.</b> Optical microscope images of TEOS and nPTES coatings of a thin glass slide .....	68
<b>Figure 3.6.</b> Absorption spectra of the dyes in H <sub>2</sub> O, EtOH, NaOH, and PBS .....	70

---

---

<b>Figure 3.7.</b> Conditions for dyeing of textile fabrics. ....	72
<b>Figure 3.8.</b> Representation of the formed thin film on the surface of the cotton fabric. ....	73
<b>Figure 3.9.</b> SEM images of untreated and dyed fabric with the sol-gel .....	74
<b>Figure 3.10.</b> EDS spectra of untreated and dyed fabric with the sol-gel .....	75
<b>Figure 3.11.</b> How optical monitoring is performed for the fabrics and the dyeing baths.....	76
<b>Figure 3.12.</b> Reflectance spectrum of tissue fabric and its conversion to K/S spectrum.....	79
<b>Figure 3.13.</b> Dye bath exhaustion and KS as a function of the duration of dyeing .....	81
<b>Figure 3.14.</b> Dye bath exhaustion and KS as a function of the number of dyeing cycles. ....	82
<b>Figure 3.15.</b> Dye bath exhaustion and KS as a function of the dyeing temperature.....	84
<b>Figure 3.16.</b> Dye bath exhaustion and KS as a function of the concentration.....	85
<b>Figure 3.17.</b> Initial sol-gel dyeing process and optimal generic sol-gel dyeing process .....	87
<b>Figure 3.18.</b> Representation of hybrid class I weak bonds and class II strong bonds .....	89
<b>Figure 4.1.</b> Set-up used for simultaneous light absorption and fluorescence emission .....	106
<b>Figure 5.1.</b> Set-up for the spectrotemporal measurement of solid LPL.....	142
<b>Figure 5.2</b> Synthesis route of the prepared organic persistent luminescent materials .....	145
<b>Figure 5.3.</b> Excitation and emission intensities as a function of time and wavelength .....	146
<b>Figure 5.4.</b> Excitation and emission intensities over cycles as a function of time .....	146
<b>Figure 5.5.</b> TPPC3Br2 molecule and crystal at daylight and under 254 nm excitation lamp.....	148
<b>Figure 5.6.</b> Emission spectra of crystalline TPPC3Br2 upon excitation using 260 nm LED .....	148
<b>Figure 5.7.</b> Averaged decay luminescence of TPPC3Br2, PL decay profile.....	149
<b>Figure 5.8.</b> Shows a crystal of TPPC3Br2_TMB, under excitation .....	150
<b>Figure 5.9.</b> Emission spectra of TPPC3Br2_TMB when excited using 260 nm LED .....	150
<b>Figure 5.10.</b> Averaged decay luminescence of TPPC3B2_TMB. PL decay profile .....	151
<b>Figure 5.11.</b> Crystal of TPPC3Br1_Pf6 under excitation source (260 nm).....	152
<b>Figure 5.12.</b> Shows the emission spectra of TPPC3Br1_Pf6 when excited by a 260 nm. ....	152
<b>Figure 5.13.</b> Averaged decay luminescence of TPPC3B1_Pf6. PL decay profile.....	153

---

## List of figures

---

<b>Figure 5.14.</b> Persistent luminescence spectra of sample TA1 and TA2 .....	156
<b>Figure 5.15.</b> Decay luminescence profiles on a semi-logarithmic scale of TA1 and TA2.....	156
<b>Figure 5.16.</b> The strategy to prepare PL fabrics using the spray coating technique.....	158
<b>Figure 5.17.</b> SEM photographs of a spray coating samples.....	159
<b>Figure 5.18.</b> Photographs of farics at after turning off the excitation.....	159

## List of tables and schemes

<b>Table 1-1.</b> Rates of absorption and emission comparison .....	26
<b>Table 3-1.</b> Maximum absorption and molar extinction coefficient of the dyes.....	71
<b>Table 3-2.</b> Molar concentration of the prepared sol-gel solutions .....	71
<b>Table 3-3.</b> Visual aspects of the dyes in ethanol and the final aspect of the fabrics.....	73
<b>Table 3-4.</b> Elemental analysis of the fabrics dyed via the sol-gel process.....	75
<b>Table 3-5.</b> Amount of bath exhaustion using the sol-gel process .....	77
<b>Table 3-6.</b> CIELab coordinates of the samples obtained from the Datacolor.....	78
<b>Table 3-7.</b> Reflectance and color strength (K/S) of the fabrics (tissues) .....	79
<b>Table 3-8.</b> Colorimetric CIE coordinates as a function of the dyeing time .....	81
<b>Table 3-9.</b> Colorimetric CIE coordinates as a function of the number of dyeing cycles.....	83
<b>Table 3-10.</b> Colorimetric CIE coordinates as a function of dyeing temperature .....	84
<b>Table 3-11.</b> Colorimetric CIE coordinates as a function of dyeing temperature. ....	86
<b>Table 3-12.</b> Results of color fastness test by diffuse reflectance and UV-vis spectroscopies .....	88
<b>Table 3-13.</b> Crosslinking results of color fastness test .....	91
<b>Table 4-1.</b> Quantum yields of different fluorophores in solution using the SAFER method .....	112
<b>Table 4-2.</b> Images of the fluorophores dissolved in dichloromethane.....	118
<b>Table 4-3.</b> Photophysical parameters of different fluorophores in solution .....	119

---

<b>Table 4-4.</b> Images of cotton fabrics obtained via the sol-gel method.....	122
<b>Table 4-5.</b> Images of cotton fabrics obtained via doctor-blade coating.....	123
<b>Table 5-1.</b> Summary of the three materials.....	153
<b>Table 5-2.</b> Photographs of the compounds TA1 and TA2 .....	155
<b>Scheme 3-1.</b> Hydrolysis and polycondensation processes between dye and nPTES.....	90
<b>Scheme 4-1.</b> Synthesis of the stilbene and fluorene-based fluorophores.....	117

---

# General introduction

Human beings are incredibly resourceful when it comes to finding ways to improve their lives on Earth. One of the most interesting examples of this is how we transform natural resources into materials that serve our needs. The industrial revolution marked a shift towards using synthetic materials, often derived from natural precursors and requiring a significant amount of energy to produce. Despite this, the convenience and versatility of synthetic materials have made them an integral part of our daily lives.

Chemistry played the key role in this natural-to-synthetic evolution, enabling tremendous new applications of materials, either by modifying the existing materials (modification, functionalization) or by creating new ones (chemical reactions, simulation, imagination). Molecular and surface chemistry participated noticeably in this evolution alongside technological developments. Molecular chemistry was deeply involved in elaborating and creating new molecules and materials. Some of them were inspired by nature, and others were accidentally discovered. Surface chemistry was also an asset, permitting the application of molecular chemistry to materials. The developed materials can then be used in a beneficial application that can serve humankind.

This thesis focuses on molecules and molecular materials that can absorb light and emit a visible response through colorful emissions (such as dyes, fluorophores, and luminophores). These materials have the property of light emission that can be transferred from the molecule to a substrate through surface chemistry. In this work, textile fabrics are selected as the substrate and will be given this new property through surface functionalization.

---



## General introduction

---

The written account of the research of this thesis covers two main areas of research. The first area involves synthesizing and integrating molecular materials with tailored properties, specifically those that exhibit luminescence, into textile materials. The second area focuses on the technical aspect of the research, including the development and use of specialized measurement instruments and techniques, such as spectroscopic methods, to study the materials. Both of these aspects are important for understanding the properties and potential applications of the materials being developed.

### *Research framework and thesis outline*

This thesis project aims to create luminescent textiles using persistently luminescent materials through surface functionalization. Throughout the three years of this thesis, the research focused on developing a sustainable process for functionalizing textiles to incorporate various functionalities while also working towards sustainability goals related to the environment, society, and the textile industry.

The thesis work was carried out as part of the LUMITEX project, which was funded by the France-Moroccan "Partenariat Hubert-Curien Toubkal" program. Three laboratories participated in this project. The first laboratory is LIMAT/UH2C<sup>1</sup>, where different materials were synthesized and structurally characterized. The textile material and its expertise were achieved in REMTEX/ESITH<sup>2</sup>, and finally, these materials were fully characterized by spectroscopic techniques developed at SATIE/ENS-Rennes<sup>3</sup>. The main objectives of the project were to identify suitable luminescent materials, with a focus on new materials (such as recent organic room-temperature luminophores, the first of which was developed in 2017) and to apply these materials to textiles to create luminescent fabrics using a sustainable process.

The thesis is organized into five chapters:

---

<sup>1</sup> Université Hassan II de Casablanca (FSBM), Morocco

<sup>2</sup> Ecole supérieure des industries de textile et de l'habillement (ESITH), Morocco

<sup>3</sup> Ecole normale supérieure de Rennes (ENS), France

## General introduction

---

- Chapter 1 deals with the scientific background and state of the art, focusing on the explanation of phenomena and theory underlying the molecules and materials: (i) dyes, (ii) fluorescent dyes, and (iii) after-glow materials. It also highlights the recent advances in the technical side of measurement instruments and methodologies in the disposition for the characterization of these materials.
- Chapter 2 is devoted to the materials and methods used in this thesis, including a brief discussion on the textile substrate and textile processing. In addition, the instrumental methods and experimental set-ups developed during this thesis are described.
- Chapter 3 discusses the use of sol-gel chemistry for the functionalization of textiles and its suitability for incorporation with materials, starting by using model dyes for dyeing cotton fabrics via the sol-gel process. The latter was studied in terms of experimental parameters that were optimized.
- The first part of Chapter 4 includes a new measurement technique developed during the thesis work that uses non-monochromatic LEDs in the measurement of photoluminescent quantum yields of luminescent materials. This new technique is called the SAFER method. The apparatus, the calibration of the spectrometers, sample preparation, and the experimental protocol will be detailed. In the second part, the synthesis and characterization of fluorescent molecules are outlined. The fluorophores were subsequently used to prepare fluorescent textiles using the optimized sol-gel process established in Chapter 3.
- Chapter 5 is concerned with organic and inorganic “persistently luminescent” (or “phosphorescent”) materials. Following the present literature, we will refer to these materials as LPL (“long persistent luminescence”) materials. The chapter highlights the experimental and optical investigation of materials, both prepared in our lab and obtained from commercial sources, and their use for the preparation of phosphorescent textile fabrics. It will explain some of the difficulties that have been encountered during the preparation of these room-temperature phosphorescent materials. Also, insights into future perspectives for this area of research are given, along with challenges and limitations.

---

# **Chapter 1 Scientific background and state of the art**

## **1.1. Introduction**

In this chapter, we will focus on the scientific foundation relevant to the research presented in this thesis. We will emphasize the theoretical and practical considerations relevant to the work described in the thesis and draw attention to recent developments and research in the field related to the theme of the thesis. This chapter aims to provide a comprehensive overview of the scientific context in which the work presented in this thesis is situated.

Also, we will review the basic knowledge about the materials and compounds used in this work, such as dyes and their role in producing visible coloration and appearance. We will also provide an overview of the background and history of the luminescence phenomenon, its different types, and the theoretical mechanisms behind it. In addition, we will spotlight the technical advances in the field of luminescence characterization and measurement. This information will provide a solid foundation for understanding this thesis work.

Finally, this chapter will include a brief overview of the process of creating the final materials through surface functionalization, with more detailed information provided in subsequent chapters pointing out the use of textile fabric as substrate. This will give readers an understanding of how the materials were developed and prepared for the research described in this thesis

### 1.2. Concept of color

The human eye can distinguish different wavelengths of light, which we perceive as different colors. The visible spectrum of light, which ranges from 400-700 nanometers, is the range of wavelengths that the human eye can detect. This ability to perceive color is an important aspect of our visual system and allows us to see and interpret the world around us.

Various phenomena might occur when the light wave enters in contact with matter. The light is either absorbed, transmitted, reflected, refracted, diffracted, scattered, or polarized as a function of the nature and the composition of matter, as well as the energy that holds the wave. In the case of reflection, the incident light hits the surface of matter and rebounds either totally or partially. If this latter happens, a part of the light power is absorbed by matter, causing electronic excitations in the materials. These two phenomena (*i.e.*, absorption and reflection) define the perceived color of an object. In the case of partial reflection, some wavelengths are absorbed more strongly than others, and the reflected wavelengths give the perceived color by the human eye. For example, when white light hits a blue object, all of the components of the white light are absorbed except the blue wavelengths, which are reflected or scattered in different directions.

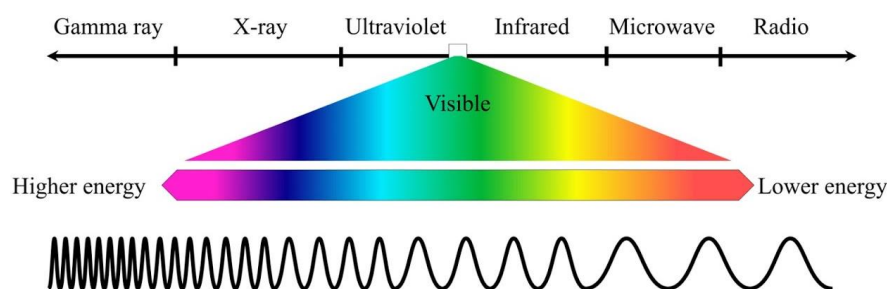


**Figure 1.1.** Electromagnetic spectrum

Light wavelengths outside the visible range are not detectable by the human eye and do not contribute to our visual perception. However, certain materials may absorb ultra-violet light and then emit light in the visible range (photoluminescent emission), as in the case of fluorescence.

### 1.3. Dyes and pigments

The term “color” is closely related to dyes and pigments, which are compounds that are used to produce color in various materials. These compounds are primarily organic molecules but differ in some characteristics.

To be considered as a dye, a molecule must meet certain criteria. These include the ability to absorb light in the visible range of the electromagnetic spectrum, the presence of a chromophore, which is the part of the molecule responsible for the color, the existence of a  $\pi$ -conjugated system, and the presence of electron resonance in the molecular structure. If any of these conditions are not met, the molecule will not be able to produce color [1–3].

#### 1.3.1. Chromophores

The region that is responsible for the coloration of a molecular compound is the chromophore. It is the part of the molecular system where the difference in energy between two separate molecular orbitals is within the visible range of the electromagnetic spectrum. The chromophore functions by altering the energy in the delocalized electron cloud of the molecule (dye), which allows the compound to absorb light [2].

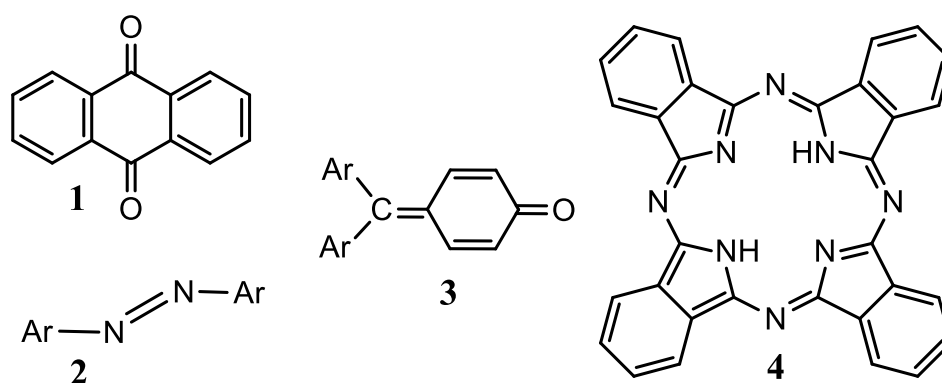


**Figure 1.2.** Examples of chromophoric groups present in some organic dyes

Chromophores, which are shown in *Figure 1.2*, can be classified into several types. Some, like the azo group (2), are colorless and are known as chromogens. Others, such as quinoid rings (1 and 3), consist of a close conjugated system of simple and double bonds with attachment

points that extend the atoms involved in the delocalization of electrons. This results in significant shifts in wavelength and the production of intensely colored compounds. The phthalocyanine group (4) comprises four isoindole groups linked by a nitrogen atom ring, forming an 18  $\pi$ -conjugated electron system. This makes phthalocyanines frequently used in dye preparation, particularly when they contain a transition metal [3].

### 1.3.2. Auxochromes

To enhance the usefulness of chromophores as dyes, it is often necessary to introduce an auxochrome. Otto Witt introduced auxochromes in 1876 as groups that can be added to dyes to improve their color and solubility in solutions [4]. For example, carboxylic (-COOH), sulfonic (-HSO<sub>3</sub>), and hydroxyl (-OH) groups. These auxochromes help to improve the color and solubility of dyes, making them more practical for use in various applications

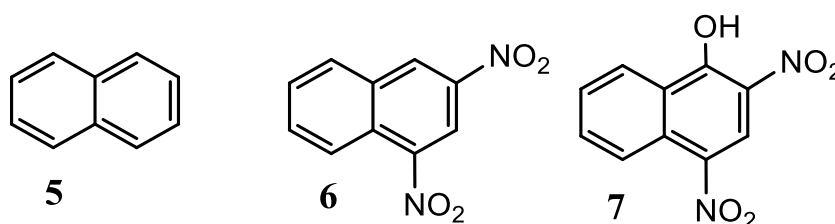


**Figure 1.3.** Color enhancement by an auxochrome

Naphthalene (*Figure 1.3, (5)*) is a colorless compound with an absorption maximum at 275 nm in cyclohexane, indicating that it has a close conjugated system. However, when nitro groups<sup>1</sup> are added to naphthalene, as in 2,4-dinitronaphthalene (*Figure 1.3, (6)*), the resulting compound exhibits a pale-yellow color. This is because the nitro groups function as chromophores, absorbing light and contributing to the overall color of the compound. When an auxochrome, such as a hydroxyl group, is present in the compound (*Figure 1.3, (7)*), the resulting molecule, 2,4-dinitronaphthalen-1-ol, exhibits a deep yellow color with an absorption

---

<sup>1</sup> Nitro groups can function as a chromophore and an auxochrome, depending on the context in which they are used.

maximum at 432 nm in methanol. The presence of the auxochrome enhances the color and solubility of the compound.

A remark that should be noted is that the presence of both chromophore and auxochrome does not implicitly indicate that the substance can be used as a dye. For instance, 2,4,6-trinitroaniline (**8**) is not useful as a dye despite the presence of NH<sub>2</sub> as an auxochrome group. This is because of the basic character of the auxochrome group that is neutralized by the strongly acidic character of the chromophore, *i.e.*, nitro group (NO<sub>2</sub>) [1,3].

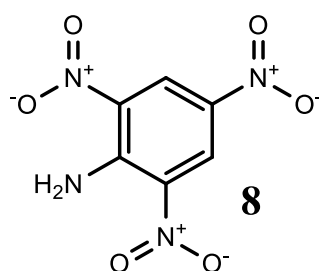


**Figure 1.4.** Chemical structure of 2,4,6-trinitroaniline (TNA) with three chromophores and one auxochrome

Later, it was discovered that auxochromes are either electron-donating or electron-accepting groups with respect to the  $\pi$ -conjugated system. The presence of one or more auxochromes introduces a modification in the electronic structure of the conjugated system and the delocalization of the electron cloud.



**Figure 1.5.** Representation of donor-acceptor system linked with  $\pi$ -conjugated bonds

A special situation occurs when both a donor and acceptor auxochromes are connected in the right manner to the conjugated system. Such systems are known as push-pull dyes. Depending on the strength of the electron donor and the electron acceptor, the position of the intramolecular charge transfer (ICT) band can be modified along the visible range of the electromagnetic spectrum [5,6].

In short, the color of a molecular dye is determined by two main factors. First, the presence of an auxochrome group can influence the color of the dye by acting as an electron donor or electron acceptor, leading to changes in the electron cloud of the compound. Second, the length of the conjugated system can affect the color of the dye. Generally, the longer the conjugated system, the longer the wavelength of absorbed photons and the more intense the color of the dye. Systems with fewer than eight  $\pi$ -conjugated bonds absorb light only in the ultraviolet range and are seen as colorless by the human eye. However, for each additional double bond in the system, the absorption of photons of longer wavelengths is possible, allowing the dye to absorb light over a wider range of the visible spectrum [7,8].

As shown in *Figure 1.6*, adding groups of increasing electron-donating ability causes the conjugated system (the molecule) to have a longer wavelength absorption, case of (**9**,  $\lambda_{\text{abs}}= 347$  nm) *vs.* (**10**,  $\lambda_{\text{abs}}= 386$  nm) since the amino group is a stronger electro-donor than hydroxyl group. Introducing an electron acceptor to the structure with the presence of an electron donor causes to extend of the conjugated system, providing a bathochromic effect (**11**,  $\lambda_{\text{abs}}= 443$  nm).

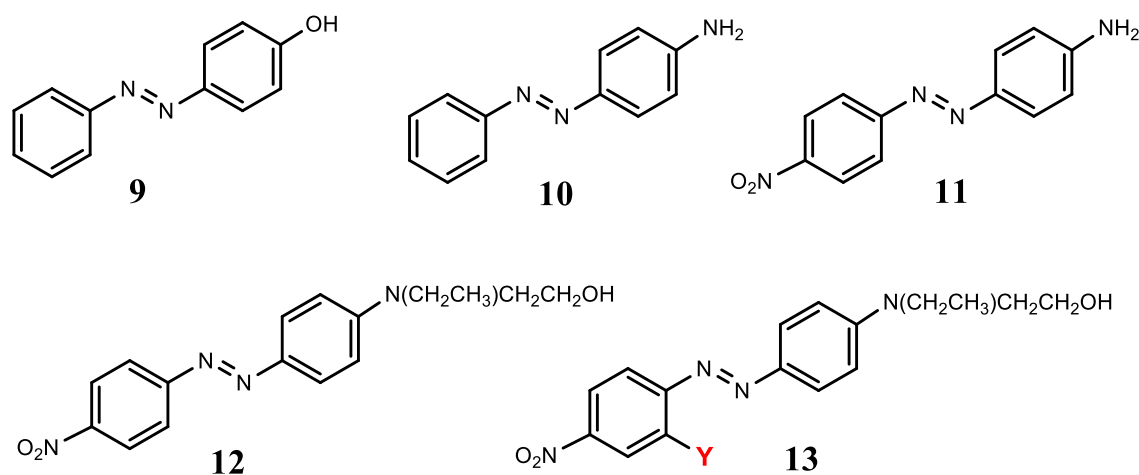


**Figure 1.6.** Effect of substituent groups within an azo-dye system

When alkyl groups are added to an electron donor, this enhances its strength and causes a bathochromic effect (**12**,  $\lambda_{\text{abs}}= 502$  nm). The presence of additional auxochromic groups also modifies the resonance of electron clouds and causes either a bathochromic effect (if deactivating) or a hypsochromic effect (if activating) in the electron cloud in the aromatic ring (**13**).



### 1.3.3. Interlude

It has been mentioned that when light enters into contact with the matter, the absorbed energy causes the electrons to become more energized, which means that the electron passes from the ground state to the excited state. This absorbed energy is not destroyed. Thus, some phenomena may occur depending on the case. For most dyes, the return of electrons to the ground state is not accompanied by any visual observation. However, it might cause the fading of the coloration as time passes. For some dyes, relaxation from the excited state to the ground state occurs with the emission of the energy as light in a process called fluorescence. The emitted light contains less energy than the absorbed light. Therefore, the emitted light is always at longer wavelengths than the absorbed radiation. In certain cases, the excited molecule can undergo a transition from the excited singlet state to a triplet state. This triplet state usually decays without light emission at room temperature.

### 1.4. Luminescence

This section will present a short background on luminescent materials, with examples of this phenomenon. Afterward, we will discuss materials that exhibit emission resulting from a photoexcitation, *i.e.*, photoluminescence<sup>1</sup>.

#### 1.4.1. Background and history of luminescence

Light emission after exposure to ultraviolet, infrared radiations, electron-bombardment, or X-rays and any excitation source has attracted earlier interest since the 1900s [9,10]. A luminescent material emits light because of the energy absorbed after an excitation occurs.

Although the phenomenon of luminescence has been observed for centuries, its systematic scientific understanding has only developed in recent centuries. In 1852, Stokes reported materials that exhibited strong luminescence under ultraviolet excitation light [11]. A few

---

<sup>1</sup> It is a form of luminescence, that is resulting of absorption of photon (energy) and the emission of light. It takes three forms, fluorescence, phosphorescence, and chemiluminescence.

---

years later, Wiedemann (1888) proposed the term "luminescence" broadly to refer to any materials that emit light, distinguishing this "cold light" from "hot light" produced by incandescent sources [12,13].

Wiedemann defined various types of luminescence based on the type of energy that is transformed into light. For instance, chemiluminescence, in which the light emission is due to chemical reactions, *e.g.*, white phosphorous undergoing slow oxidation at room temperature [14]. When the emitted light results from the prior absorption of light radiation, the occurring phenomenon is known as photoluminescence. Further, if the emission time is short, the photoluminescence is better known as fluorescence, for example, observed with chlorophyll [15,16]. Otherwise, when the emitted light delays ( $> 1\text{ms}$ ) and lasts for a while (up to hours), the photoluminescence is called phosphorescence, as observed with the Bologna stone [17,18].

Radioluminescence is observed when high-energy photons irradiate samples, such as X-rays,  $\gamma$ -rays, or particles (neutrons) [19]. Triboluminescence is when light emission occurs due to breaking bonds, *e.g.*, flash quartz rocks and lifesavers [20–23]. In neon light tubes, an electric field passes through a gas (for LEDs, electric current through semiconductors) is known as electroluminescence [24–26]. Some living organisms, such as fireflies, bacteria, and sea creatures, can produce light through chemical reactions in specific biological centers, a phenomenon known as bioluminescence, which is the biological equivalent of chemiluminescence [27–30].

Regarding this thesis work, we showed interest in luminescence from the point of view of photoluminescence, *i.e.*, fluorescence and phosphorescence, with further emphasis on "persistent" long-lived luminescence.

### 1.4.2. Photoluminescence of organic chromophores

As previously stated, photoluminescence is a process in which a material absorbs energy from light and then re-emits that energy in the form of light. This process can occur in various materials, including semiconductors, minerals, and organic molecules. Photoluminescence

can be further classified into fluorescence and phosphorescence depending on the light emission time.

When considering organic chromophores, the classification is related to the electronic states (*i.e.*, singlet and triplet) of the luminescent species that maneuver the back-to-ground of the electron. The electronic states of photoluminescent molecules are represented via the Jablonski state diagram that shows the transitions between different states (*Figure 1.7*).

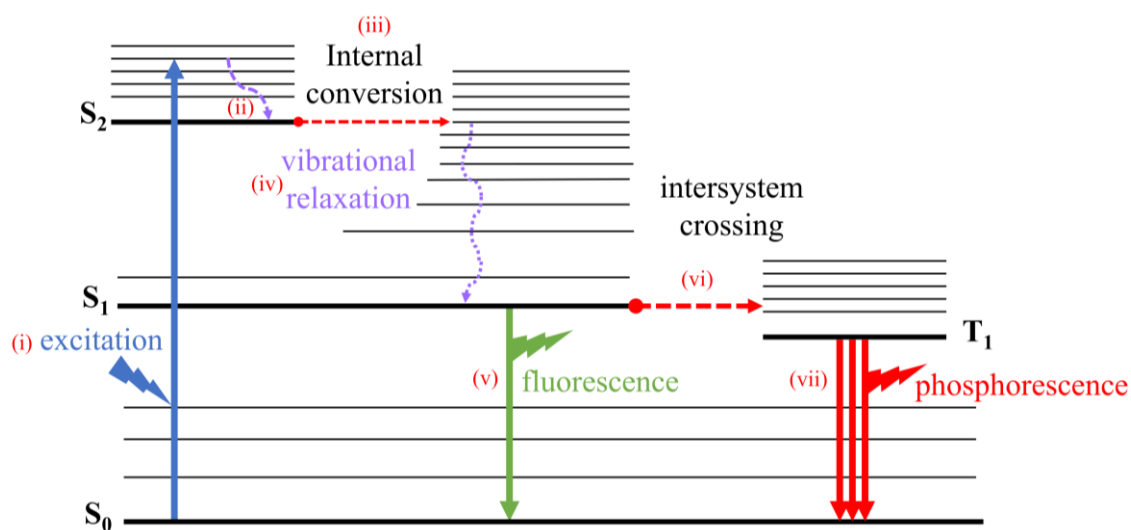


**Figure 1.7.** Jablonski diagram of energy levels and the transitions between them

When an electron is excited by absorbing a photon of a particular wavelength (*i*), the electron relaxes to levels of the lowest excited state (S<sub>1</sub>) via non-radiative transitions (vibrational relaxation<sup>1</sup> and internal conversion<sup>2</sup>) (*ii*, *iii*, and *iv*). From this excited (S<sub>1</sub>) state, the molecule may decay non-radiatively back to the ground state. Alternatively, it may relax with the emission of a fluorescence photon (*v*).

If the relaxation process is entirely non-radiative, the molecule will not fluoresce, and all absorbed energy will be dissipated as heat. The probability of radiative events occurring

---

<sup>1</sup>Vibrational relaxation is an extremely rapid and non-radiative transition accompanied by energy dissipation as heat to neighboring molecules or solvent.

<sup>2</sup>Also a non-radiative transition that describes the transition of higher singlet excited state into a vibrational state of a lower excited state of the same energetic level.

compared to fully non-radiative relaxation determines a fluorophore's quantum yield and how brightly it will shine, as will be detailed in the upcoming paragraphs (*section 1.5.2*).

A third possibility is that the excited chromophore undergoes intersystem crossing (*vi*) to a triplet state resulting in the emission of light observed as phosphorescence (*vii*). In this case, the relaxation of the chromophore is slow and is accompanied by the emission of light for an extended period of time.

## 1.5. Fluorescence

### 1.5.1. Overview

Similarly to other organic molecular dyes, fluorescent dyes (from this point, they will be referred to as fluorophores) are conjugated systems with alternating simple-double bonds. Fluorophores can absorb in the ultra-violet and the visible ranges, accompanied by emission in the visible range, and can be extended to emit in the near-infrared region.

The most intense fluorophores are compounds containing aromatic groups with low-energy  $\pi$ - $\pi^*$  transitions. Simple heterocycles such as pyridine (**14**) and pyrrole (**15**) do not exhibit fluorescence, but fused-ring structure such as quinoline (**16**) and 1-indole (**17**) compounds indeed exhibit fluorescence emission.

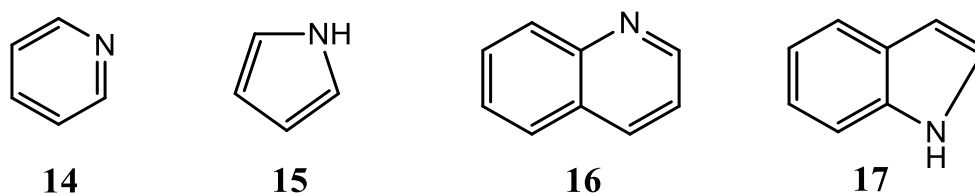


**Figure 1.8.** Chemical structures of pyridine (**16**) and pyrrole (**17**) as non-fluorescent heterocyclics. Quinoline (**18**) and indole (**19**) as fluorescent fused-ring compounds

Other molecular systems that are commonly considered strong fluorescent molecules are dipolar push-pull systems. These are based on an electron-donating auxochromic group (EDG) connected to an electron-withdrawing group (EWG) that are connected via a  $\pi$ -conjugated system, similar to what has previously been seen for some dyes (*Figure 1.5* and *1.6*). The classical push-pull molecules have a large conjugated system with extended

intramolecular charge transfer (ICT) between the EDG and EWG. Further research reported small push-pull fluorophores based on the same principle with small ICT between the donor and the acceptor [31–35], with pronounced emission ability in both solution and solid-state [36,37].

### 1.5.2. Quantum yield and efficiency of fluorescence

Fluorescence compounds convert excitation energy into photons, and this conversion is not 100% efficient (in most cases) due to losses that occur through other (non-radiative) deactivation paths. Quantum yield is the probability that a photon is emitted after the system has been excited [38]. Historically, the first definition and use of quantum yield for any molecular quantum process were given by Rubin and Braslavsky in 1925 [39], which was ultimately defined according to the IUPAC as the following [40]:

$$\Phi(\lambda) = \frac{\text{Nb of events}}{\text{Nb of absorbed photons}} \quad (1.1)$$

Where  $\Phi(\lambda)$  is usually used for light emission and can also be used for photophysical processes such as intersystem crossing, luminescence, and photophysical reaction in the case of fluorescence. Equation (1.1) is often written as follows:

$$\Phi_F(\lambda) = \frac{\text{Nb of emitted fluorescence photons}}{\text{Nb of absorbed photons}} \quad (1.2)$$

As written, Equation (1.2) is not time-dependent, and the quantum yield reflects the relative importance of both radiative and non-radiative processes. Equation (1.2) will extend to become:

$$\Phi_F(\lambda) = \frac{\text{Nb of emitted fluorescence photons}}{\text{Nb of absorbed photons}} = \frac{K_r}{K_r + \sum K_{nr}} \quad (1.3)$$

$K_r$  is the radiative transition rate (*i.e.*, emission), and  $K_{nr}$  as the non-radiative transition rates (*i.e.*, internal conversion, intersystem crossing, vibrational relaxation). In general, the quantum yield is often smaller than 100% (1 photon emitted per 1 photon absorbed). This value can only be obtained in the case of resonance systems.

### 1.5.3. Measurement of Quantum Yield (QY)

The methods of measurement of fluorescence quantum yield of solutions were reviewed by Demas and Crosby [41]. Let us recall the property that absorbed light after passing through the fluorescent solution is either emitted as light (fluorescence) or dissipated as heat (generally to the solvent or adjacent molecules).

Based on this remark, we define three ways to measure fluorescence QY. First, using photothermal methods that measure the dissipated temperature (heat) or sound waves, for instance, photoacoustic spectroscopy (PAS) [42,43], thermal blooming (TB) [41,44,45], or thermal lenses (TL) [41,46–48]. The emitted light is then obtained by subtracting the dissipated intensity from the absorbed intensity. However, these photothermal methods require special care and present significant potential errors [49,50]. Second, using optical measurements, either employing the absolute method [51–56], *i.e.*, using an integrating sphere setup to measure the absolute emitted light directly. Alternatively, using the relative method [41,57–59], *i.e.*, by comparing with a standard fluorescent compound with known quantum yield.

Both comparative and absolute methods are used in practice and can precisely determine quantum yield with a few percent. Nevertheless, the absolute method using an integrating sphere has proven its effectiveness for being more robust and delivering fluorescence quantum yields, but it is still subject to calibration errors [49,60]. The following sections will present the relative and the “absolute” fluorescence measurement methods.

#### 1.5.3.A. “Absolute” measurement of fluorescence QY using an integrating sphere

In addition to determining the fluorescence QY of solutions, the absolute method is more effective when investigating scattering materials, solid-state fluorescent materials (*e.g.*, solid-state organic emitters and particles), films, and fabrics. Contrarily to the relative method, the absolute method does not require a reference sample, and among its advantages is that it allows the collection of all the emitted and scattered light by the sample. Also, several problems and experimental errors are eliminated in the absolute determination of QY, for example, raises in concentration, re-absorption of emitted light (inner filter effect), aggregation, and fluorescence quenching. In addition, the absolute approach involves

---

calculating the ratio of the photon absorbed versus the photon emitted directly from the fluorescence spectrum.

However, the “absolute” method is not really absolute since it still needs a carefully calibrated detection system.

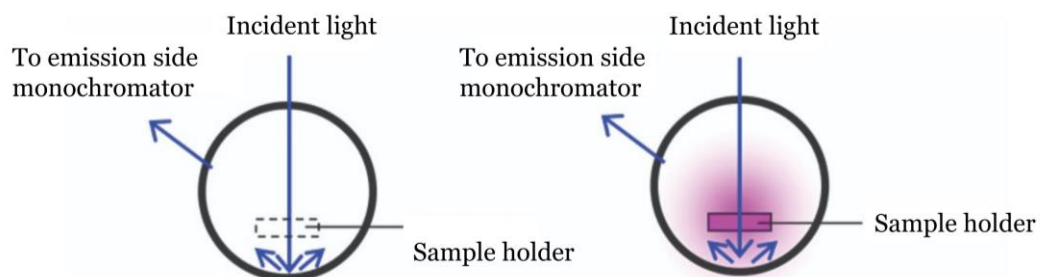


**Figure 1.9.** Representation of measurement setup used in the absolute approach for QY determination. The incident light measurement with nothing inside (left) and the sample (right).

To measure the photoluminescence quantum yield, an integrating sphere with an optical fiber coupled to a spectrometer is often used (*Figure 1.9*). The spectrometer is typically equipped with monochromatic light sources such as lasers for excitation. The first step is to record the spectrum of an empty holder. Then, the sample is placed in the center of the sphere at a slight angle to prevent the light from being reflected back out through the entrance port. The spectrum is then recorded again. The quantum yield is calculated as the ratio of the number of emitted photons to the number of absorbed photons, which is determined by integrating the two shaded regions in the spectra as demonstrated in *Figure 1.10*.

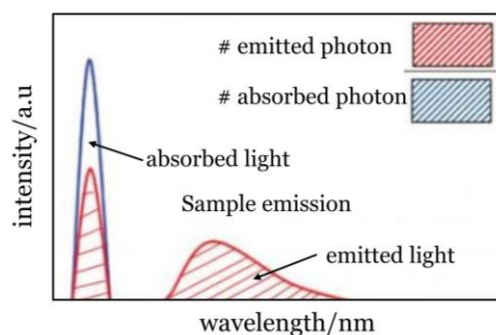


**Figure 1.10.** Excitation and emission spectra of incident light (from empty sphere/blue) and emitted light (in the presence of the sample/red). The ratio of integrals determines the quantum yield of fluorescence.

Overall, the integrating sphere-based absolute measurement is simple, rapid, and requires no complicated sample preparation. The absolute method delivers results with an accuracy of 10-15% with good statistics (3 to 5 measurements at least) [38,56,60–62].

### 1.5.3.B. Relative measurement of fluorescence QY

Regardless of various disadvantages of the relative method, including utilizing a standard reference with known QY with similar excitation and emission properties as the sample under examination, introduction of refractive indexes of the solvent, problems related to the solid angle, and other experimental limitations, this approach is the most used for the determination of fluorescence quantum yield, pointing out fluorescent solutions.

To perform QY measurement through the relative method, two separate apparatuses are needed. The first system (*section 2.4.3*) is usually a double beam absorption setup used to record absorption spectra of the sample with unknown QY. The second system (*see also section 2.4.3*) is a single beam absorption used to excite the fluorescent solution and record the emitted light at 0°/90° geometry montage.

Equation (1.2) is further developed to give Equation (1.4), which will be used to determine fluorescence quantum yields.

$$\Phi = \Phi_R \frac{n^2 F^i f_R}{n_R^2 f_i F^R} \quad (1.4)$$

Where  $\Phi_R$  is the known QY value of the reference.  $n$  and  $n_r$  are solvent refractive indexes of the sample and the reference, respectively.  $f_i$  and  $f_R$  are absorption coefficients of the sample and the reference, respectively.  $F^i, F^R$  are the integrated photon fluxes of the emitted light for the sample and the reference, respectively.



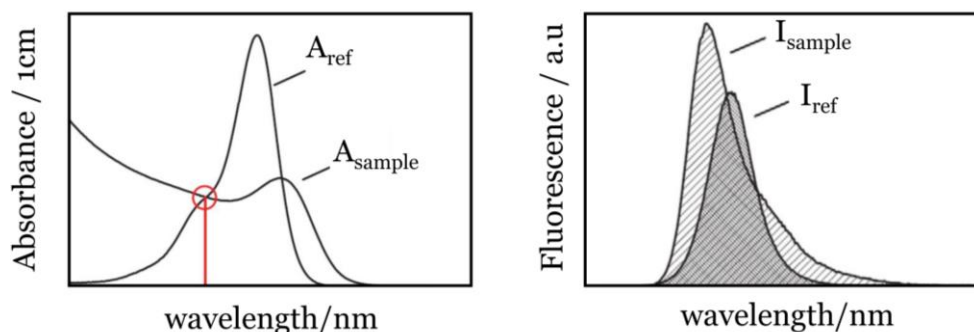


**Figure 1.11.** Schematic representation of absorption spectra of the sample ( $A_{sample}$ ) and standard reference ( $A_{ref}$ ); the red circle/line indicates the optimal wavelength for excitation (left). Uncorrected emission spectra of the sample ( $I_{sample}$ ) and reference ( $I_{ref}$ ) (right). Spectra were obtained from [60] with modifications

Since the fundamental concept of this approach is that two solutions that have the same absorbance can be assumed to be absorbing the same number of photons, the absorption coefficients  $f_i$  and  $f_R$  must be the same to allow comparison between the reference and the sample. Determining the absorption coefficient requires meticulous care since it is considered a potential source of errors related to concentrations and the position of the cuvette and spectrometer angles. The relative integral photon fluxes  $F^i, F^R$  are obtained by measuring the fluorescence spectra of the sample and the reference using the single beam spectrometer [41,49,60,63–68] (*Figure 1.11*). More details concerning the measurement of QY using the relative method are reported in Chapter 4, *section 4.2*.

#### 1.5.4. Recent developments in QY measurement

As previously mentioned, the measurement methods for quantum yields (QYs) have been well-established and thoroughly reviewed in terms of experimental protocols, output corrections, and mathematical formulas [41,64,69,70]. Subsequent improvements were made possible by advancements in optical technologies, which led to the development of more advanced instruments.

In 2017, Nawara and Waluk presented a valuable improvement in the relative method for fluorescence quantum yield determination. The approach relies on the simultaneous absorption and emission of light using one single commercial instrument. The proposed method, namely “SAFE” for simultaneous absorption and fluorescence emission, consists of

using a spectrofluorimeter (FS5 spectrofluorometer Edinburgh Instruments) equipped with three separate detectors, one for the emission, one for the reference, and a third one for the transmittance. This improvement eliminates several problems related to using different instruments for absorption and emission measurements. Using the recommended standards, Nawara and Waluk validated the measurement methods and confirmed that the “SAFE” approach provides reliable results with differences in the mean value that does not exceed 2.5 % compared to the comparative method. The method was further validated using a very challenging compound to measure due to the vibrational absorption peaks, which is anthracene. In contrast, the proposed approach might produce absorption spectra of lower quality since they were recorded on a transmittance channel. However, the method gives highly accurate values of quantum yields [71].

A further practical improvement in the context of the instrumental protocol of fluorescence quantum yield measurement was introduced by Nawara and Waluk (2020). The previous experimental apparatus is extended to allow in-situ “SAFE” measurement based on simultaneous double-beam absorption. The experimental apparatus is based on the previous FS5 spectrofluorimeter to which they introduce Peltier module-controlled cuvette holder (model - Qpod, Quantum Northwest) directly into the spectrometer sample chamber [72]. Contrary to their previous work, the absorbed light was not recorded on the transmittance detector but on a CCD line camera with high sensitivity.

As shown in *Figure 1.12*, a part of the CCD camera was eliminated by the excitation beam light (incident light  $I_0$ ). In contrast, the second part was illuminated by the transmitted light through the sample (transmitted light  $I$ ), allowing real-time transmittance determination, therefore, a precise determination of the absorption factor.

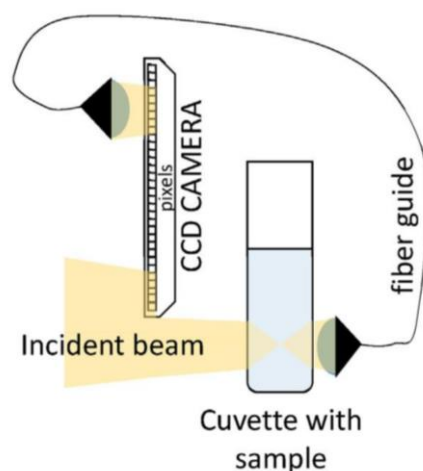


**Figure 1.12.** A representation of a double-beam absorption measurement using a CCD detector used in work [72]

As for the fluorescence spectrum, they were collected at the standard right-angle geometry described in the previous paragraph simultaneously with the CDD camera, *i.e.*, the SAFE method. The method was validated using standard fluorophore (quinine in perchloric acid) and anthracene in ethanol. The results agree with the literature value with an uncertainty of measurement equal to 0.007 (for quinine). As for anthracene, the reported value is 0.01 higher than the previous work reported in the previous section. The dual-beam measurement provides high stability and reproducibility by reducing the signal drift related to the fluctuation of the light source or the detector instability [73].

During this research work, the instrumental setup of QY determination is further developed. In Chapter 4 we present a measurement approach based on the simultaneous measurement of absorption and fluorescence emission spectra as in the SAFE method, but when a relatively broad-band light source is used as the excitation source, for example, light-emitting diodes (LEDs). As will be seen, the spectral photon flux is not constant over the narrow emission range, and considering only the specified maximum emission wavelength is generally not satisfactory for typical LEDs used for fluorescence applications. In the proposed SAFER method, modifications were entered to consider the full spectral distribution of the excitation light. The method was validated using various fluorophores, including recommended standards, and the obtained QY values were consistent with literature values [74].

### 1.5.5. Interlude

Fluorescence is a phenomenon in which a substance absorbs light at a specific wavelength and reemits it at a different wavelength. Many systems exhibit this type of emission, and the measurement of fluorescence quantum yield is an important aspect of studying this phenomenon. There are several methods for quantifying fluorescence quantum yield, and these methods are continuously being improved and refined due to advancements in the field of instrumentation. This part of the literature review will provide readers with an overview of the advancements and improvements in photoluminescence quantum yield measurement techniques discussed in this thesis, including the method presented in Chapter 4. This will give readers a comprehensive understanding of the current state of the field and the contributions made by this thesis.

### 1.6. Phosphorescence

Before further explaining the phenomenon of phosphorescence, one must be aware that three different phenomena can produce light after the excitation is removed, and all of them are considered phosphorescence: (i) Persistent “glow in the dark” photoluminescence, commonly known from the inorganic phosphors. (ii) Long-lived phosphorescence from the triplet excited state of organic molecules. (iii) Long persistent luminescence (LPL) observed in purely organic molecules resulting from exciplex charge recombination [17,75]. In this section, these types of phosphorescence will be reviewed, as well as the recent work in the field.

#### 1.6.1. Phosphorescence from inorganic materials

##### 1.6.1.A. Overview

A wide variety of inorganic phosphors are known to the art. These compounds generally belong to one of the two classes of industrially produced phosphors: Zinc sulfide and strontium aluminate. Current phosphorescent materials are made with these inorganic pigments to produce various non-radioactive self-illuminating products. These two systems

will be described in the following, with further explanations about the theory and origin of this persistent phosphorescence.

Zinc sulfide phosphors doped with copper or cobalt have been widely used in markets for centuries [76,77]. These compounds exhibit broad-band green emission centered at 540 nm, and the resulting emission remains visible for several hours after the excitation is turned off. However, the resulting after-glow remains relatively weak, not to mention the rise of safety concerns about using cobalt and copper [78,79].

Zinc sulfide phosphors are obtained by mixing sodium sulfide with zinc salt, *e.g.*, zinc chloride, following the reaction  $\text{Zn}^{2+} + \text{S}^{2-} \rightarrow \text{ZnS (s)}$ . The precipitation of ZnS in the presence of copper ions ( $\text{Cu}^{2+}$ ) and its annealing in high temperatures yields phosphorescent particles [80,81]. Also, several works were conducted to elaborate nanoparticles through the sol-gel method instead of co-precipitation [76,82].

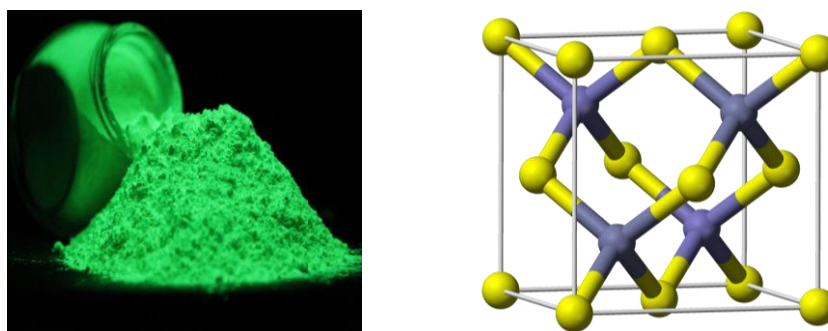


**Figure 1.13.** Zinc sulfide phosphor (left), atomic arrangement of ZnS that crystallize in FCC lattice, yellow: Zn atoms, gray: S atoms; (right)

With the discovery of  $\text{Eu}^{2+}$  and  $\text{Dy}^{3+}$ -doped strontium and calcium aluminates in 1996, new long-lasting phosphors with strong emission and long after-glow invaded the phosphors market [83]. Afterward, this phenomenon has also been observed in metal ion-doped aluminates, silicates, phosphates, and oxysulfides [84,85].

Based on the emission color, the persistent phosphors are divided into five groups: red, green, blue, white, and NIR. In addition to the emission color, the commonly used classification is based on the dopant type. Lanthanide and transition metal ions are the most used [86]. Despite the existence of several efficient compounds that exhibit long-lasting afterglow, the number of

known materials in this category is relatively low. Among the available options,  $\text{SrAl}_2\text{O}_4:\text{Eu}$  co-doped with dysprosium is currently considered one of the best persistent phosphorescent materials due to its high afterglow intensity and duration [87].

### 1.6.1.B. Suggested long-lasting phosphorescence mechanism

After more than 25 years after the discovery of  $\text{SrAl}_2\text{O}_4:\text{Eu}^{2+}$  co-doped with  $\text{Dy}^{3+}$ , the mechanism behind its long-lived photoluminescence emission is still unclear [87,88]. Most scientists agree on the existence of a long-lived trap level, where, after the excitation, charge carriers (in this case,  $\text{Eu}^+$ ) get trapped inside the forbidden band gap with a very long lifetime. Once the excitation ceases, the charge carriers are gradually released from this trap resulting in the emitted light [87–89]. In what follows, we briefly describe the most known theoretical models of this after-glow emission (*Figure 1.14*).

- **Matsuzawa model**

In this model, Matsuzawa assumed that  $\text{Eu}^+$  ions are created upon excitation of  $\text{Eu}^{2+}$ , leaving a hole that can be transferred to the valence band (VB). Holes are then captured by trivalent rare earth ions, such as  $\text{Dy}^{3+}$ , thus creating  $\text{Dy}^{4+}$  ions. At a high temperature, to release the trapped charges, the holes are released and migrate through the valence band back to the  $\text{Eu}^+$  and create the excited state of  $\text{Eu}^{2+}$  accompanied by a photon release [83,90].

- **Dorenbos model**

Dorenbos proposed another explanation of the mechanism for this lasting after-glow, pointing out that the  $\text{Eu}^+$  and  $\text{Dy}^{4+}$  ions cannot exist based on the difference in energy gaps between the energy levels [85,91]. After the excitation, the 4f level of the europium should not be interpreted as an actual hole that can accept an electron. Furthermore, the 5d level of the europium is located right below the conduction band (CB), and the  $\text{Dy}^{2+}$  level is around 0.9 eV below the conduction band (CB) [85]. For these reasons, Dorenbos claims that electrons are thermally promoted from  $\text{Eu}^{2+}$  to the conduction band (leaving  $\text{Eu}^{3+}$ ) and migrate through it to be trapped by a trivalent co-dopant ( $\text{Dy}^{3+}$  ions), and therefore recharging it to the divalent ion ( $\text{Dy}^{2+}$ ). After the thermal relaxation of the trapped electron

(from  $Dy^{2+}$ ), it will recombine upon reaching the luminescent center ( $Eu^{2+}$ ) and transit to the ground state with photon emission [87].

- **Clabau model**

It is similar to the Dorenbos model but differs in some points; importantly, there is no migration of electrons through the conduction band, but with the aid of a direct transition between the traps, that can occur based on the assumption that levels are located close to each other [92,93] (*e.g.*, europium ion and the lattice defects).

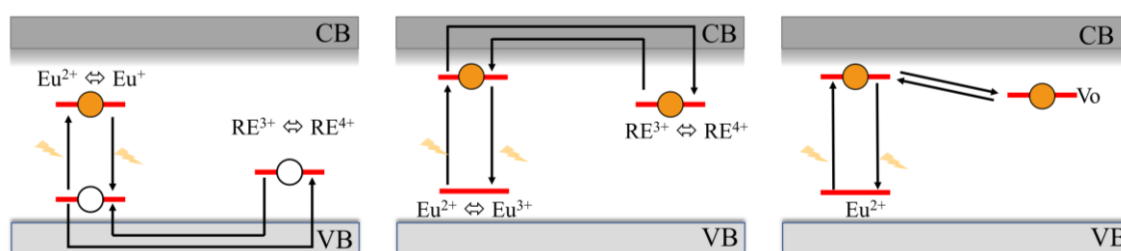


**Figure 1.14.** Different proposed persistent luminescence mechanisms for  $SrAl_2O_4:Eu$  co-doped with  $Dy$ . Left: Matsuzawa's model, middle: Dorenbos's model, right: Clabau's model. RE: rare earth

Despite extensive research, the mechanism behind persistent luminescence in materials is still not fully understood. Several models have been proposed to explain this phenomenon, but none of them have been supported by sufficient experimental evidence to identify the afterglow cause definitively. The Matsuzawa model, which used to be a widely accepted explanation, is now less popular. The role of lattice defects, such as oxygen vacancies, in persistent luminescence has been suggested as a possible factor, but it is unclear if this is sufficient to explain the phenomenon [89].

### 1.6.2. Long-lived phosphorescence from the triplet excited state

#### 1.6.2.A. Overview

In this section, the triplet state phosphorescence of organic compounds is reviewed. Phosphorescence and fluorescence have some common points, or according to the gold book (IUPAC), long-lived phosphorescence from organic compounds describes the emission of light that involves the change in spin multiplicity, typically from triplet state to singlet state [40].

The triplet state occurs and can only be accessed via non-radiative intersystem crossing transition. Furthermore, the direct transition singlet to triplet is forbidden contrary to fluorescence in which transitions are allowed [94].

### 1.6.2.B. Mechanism of long-lived phosphorescence from the triplet state

For a better understanding of long-lived phosphorescence and its difference from fluorescence, some quantum mechanical selection rules must be reviewed [95,96]. Except for molecular oxygen, which exists in the triplet state, all other molecules exist in the singlet state. In most compounds (*Figure 1.15*), the ground state ( $S_0$ ) is a singlet state with two unpaired electrons with opposite spins (+1/2 and -1/2). When a molecule absorbs energy from an external source and becomes excited, an electron is "promoted" to the excitation singlet state ( $S_1$ ) while maintaining its spin orientation (-1/2 or +1/2). At this stage, as the molecule relaxes back to its ground state, the electron may either return to the ground state with the emission of light (spin neutral), resulting in fluorescence, or it may migrate through intersystem crossing to a less energetic triplet state ( $T^1$ ). The relaxation from the triplet state back to the singlet ground state is accompanied by the slow release of energy as phosphorescence, which may last for a few microseconds to as long as one second after the excitation is removed [84].

In the case of long-lived phosphorescence, the non-radiative process dissipates more energy than fluorescence. Therefore, the energy difference between the absorbed and the emitted photon is larger, resulting in more considerable wavelength shifts.

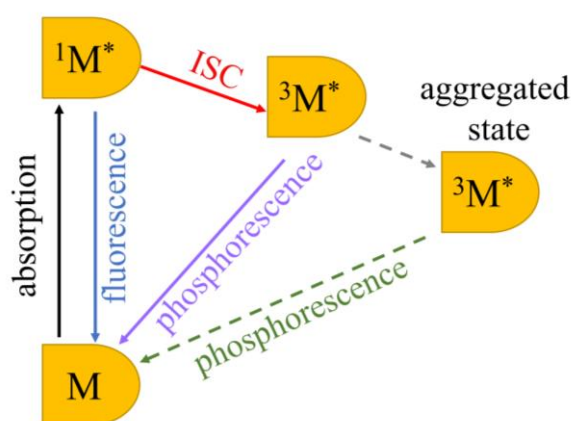


**Figure 1.15.** Simplified Jablonski energy diagram with an explanation of long-lived phosphorescence of organic compounds from triplet-state emission



*Table 1.1* compares fluorescence and long-lived phosphorescence absorption and emission rates. The photoexcitation and photon absorption are very rapid. Fluorescence allows transitions from the excited singlet state to the ground singlet state; therefore, the emitted light is immediate. Phosphorescence, on the other hand, is a forbidden transition, but it can be observed because of spin-orbit coupling. Hence, its radiative constant is typically low. The rest of the non-radiative transitions are very rapid compared to fluorescence and long-lived phosphorescence.

**Table 1-1.** Rates of absorption and emission comparison [16,97,98]

Process	Transition	Timescale (s)
Photoexcitation	$S_0$ to $S_n$	$\sim 10^{-15}$ (instantaneous)
Internal conversion	$S_n$ to $S_1$	$10^{-14}$ to $10^{-11}$
Vibrational relaxation	$S_n^*$ to $S_n$	$10^{-12}$ to $10^{-10}$
Intersystem crossing	$S_1$ to $T_1$	$10^{-11}$ to $10^{-6}$
Fluorescence	$S_1$ to $S_0$	$10^{-9}$ to $10^{-6}$
long-lived phosphorescence	$T_1$ to $S_0$	$10^{-3}$ to 1

### 1.6.2.C. Examples of compounds with long-lived phosphorescence from the triplet state

The triplet state phosphorescence is widely observed in some aromatic carbonyl molecules, carbon dots, some organometallic chelates, and complexes with heavy atoms [99,100].

For instance, (5,5-dioxido-10H-phenothiazin-10-yl)(phenyl)methanone (**18**) in its crystalline form shows a phosphorescence emission of 455 ms at room temperature. This molecule, which is based on the phenothiazine structure, contains a “d-p $\pi$ ” bond between the partially filled d-orbital on the transition metal atom and the partially filled p-orbital on a ligand atom [101]. Also, some benzoic acid derivatives show a visible persisting afterglow. Isophthalic acid (**22**), for example, in its aggregate form, is a molecule-based carbonyl group, presenting

---

phosphorescence emission at room temperature of 970 ms after being excited with a 405 nm blue LED flashlight (*Figure 1.16*) [102].

Tris(8-hydroxy-quinolato)aluminum (**20**) is a coordination complex that is widely used in OLEDs electronics and presents a phosphorescence of a few microseconds [103]. The presence of a heavy atom in the molecular structure as in 9-(4-((4-iodophenyl)sulfonyl) phenyl)-9H-carbazole (**19**) bonded covalently to the structure, or through ionic bonding as in 2,3,4,5-tetraphenylloxazol3-ium bromide (**21**) has an effect due to the charge transfer to the skeleton of the molecule, which results in room-temperature phosphorescence emission of 19 ms and 10 ms, respectively (*Figure 1.16*) [104–106].

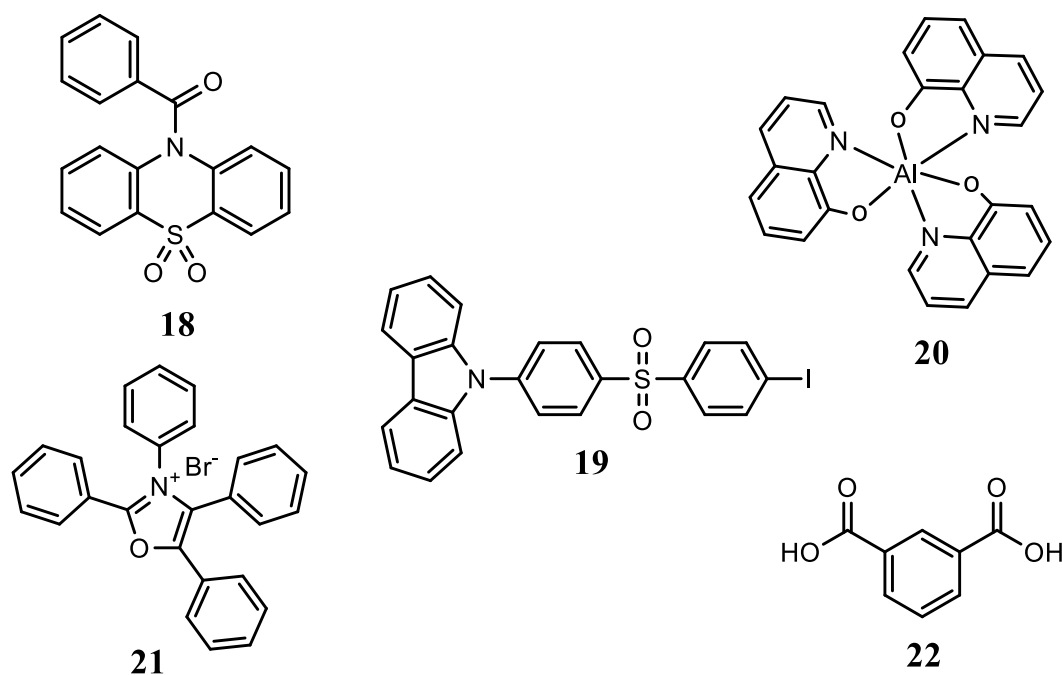


**Figure 1.16.** Molecular structures of some triplet-state phosphorescent compounds

These long-lived phosphorescence compounds have a long luminescence lifetime compared to fluorescence, which opens wide fields of application in biology and spectroscopy. In contrast, they are short-lived compared to the persistent inorganic phosphors (*section 1.6.1*) that emit for hours, limiting their application fields, *e.g.*, incorporation in matrixes and functionalization on surfaces [107].

### 1.6.3. Long-persistent luminescence (LPL) of organic materials

#### 1.6.3.A. Overview

In recent years, long-persistent luminescence (LPL) has garnered significant interest. However, for decades, this slow emission was only observed in organic materials at cryogenic temperatures and inert conditions [108], severely limiting its practical applications. The mechanism behind and the relationship between the structure and properties of long-persistent luminescent organic materials are still not fully understood [109,110]. In the following sections, recent research on long-persistent luminescent materials will be reviewed, as well as the proposed mechanisms for this emission.

#### 1.6.3.B. Historical and theoretical background

The first introduction of organic long persistent luminescence (OLPL) closely was through the photo-ionization of organic molecules [111]. The photo-ionization of organic molecules, when incorporated into polymer media for stabilization of the radical cation of the guest molecule, was found to generate hours of lasting luminescence at very low temperatures (20 K) [112]. Overall, the energy of the excitation light is used to create the ionized charge-separated (CS) states [113]. Subsequently, the electrons from the photo-ionized molecules, which are stabilized in a rigid system (*e.g.*, polymer, crystalline state), are slowly released to recombine with the radical cation and generate the excitation states of the guest with a theoretical ratio of 75 % triplet states and 25 % singlet states. As a result, the guest molecule's fluorescence and phosphorescence are observed after the charge recombination [112].

This charge-separated (CS) system was also noticed in some single molecules containing twisted donor-acceptor moieties at low temperatures (77 K) [114]. For instance (*Figure 1.17*), 9-mesityl-10-methyl-acridinium ion compound (**23**), which has an electron donor mesitylene ((**24**), Mes) and an acceptor cation 10-methylacridinium ((**25**), Acr<sup>+</sup>) connected directly to each other.

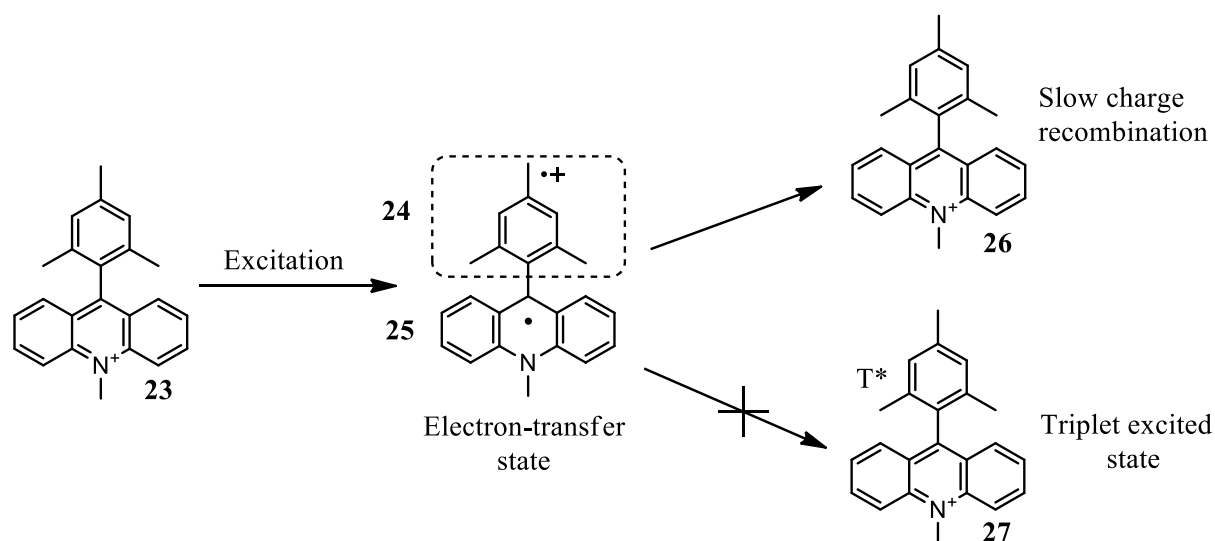


**Figure 1.17.** Photoinduced charge transfer (ET) of a single molecule with donor-acceptor moieties

Even though the presence of a direct bonding and proximity, there is no  $\pi$ -conjugation between the two moieties [115]. This molecule exhibits an extended charge transfer (CT) lifetime and higher energy (2.37eV) compared to other donor-acceptor-linked molecules [115]. However, there are claims that the formation of triplets excited state (27) occurs rather than the charge transfer (CT) due to energy differences [116,117]. After that the excitation ceases, the back-charge transfer (CR- charge recombination) to the ground state (26) becomes extremely slow, accompanied by phosphorescence emission that lasts for more than 2 hours, except that this long lifetime is noticed only at very low temperatures (77 K) [118].

### 1.6.3.C. Recent works on organic long persistent luminescence (OLPL)

In 2017, the first room-temperature organic long persistent luminescent (OLPL) film utilizing two sample organic molecules was reported by Kabe and Adachi [119]. The discovery opened a new window to understand OLPL and ameliorate their physical and photophysical properties. The successful system is based on binary donor-acceptor exciplex<sup>1</sup> that emits upon the recombination of long-lived charge-separated states, a system in which an electron donor

<sup>1</sup> An exciplex (blend word of excited complex) is an aggregate of two molecules, one of which is excited

molecule and an electron acceptor molecule form charge-separated states (CS) under photoexcitation [118,120].

The process underlying this phenomenon (long-lived charge-separated states) starts when an electron is photoexcited from the highest occupied molecular orbital (HOMO) to the lowest unoccupied molecular orbital (LUMO) of the acceptor molecule (*Figure 1.18*). Then, charge transfer (CT) occurs from the HOMO of the donor to the HOMO of the acceptor molecules. The electron on the LUMO travels between the acceptor's LUMO states, forming the separation of charges to create the charge-separated state (CS).

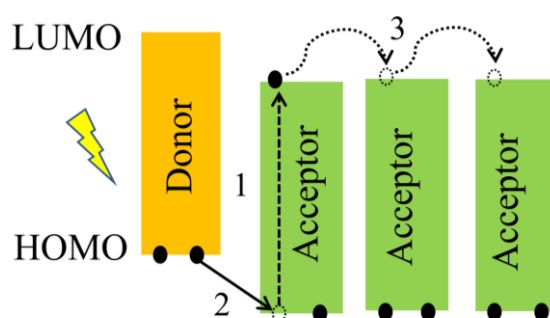


**Figure 1.18.** The process of creating long-lasting charge-separated states. 1: absorption of excitation light. 2: charge transfer (CT). 3: charge separation (CS) between acceptor molecules

At this point, we consider that the charges are separated, and the photoexcitation has not ceased yet. Once the excitation is turned off (*Figure 1.19*), the charge recombination (CR) of lasting-separated charge states (CS) occurs gradually in the radical anions and radical cations. The charge recombination (CR) of the separated charges (CS) results in the desired emission [119], precisely the LPL exciplex emission<sup>1</sup>.

---

<sup>1</sup> It is mandatory to mention that the exciplex is a state formed during the photo-excitation, and does not involve any formation of new compound or molecule

---

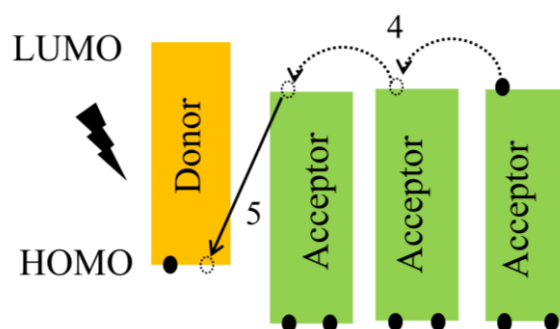


**Figure 1.19.** The charge recombination (CR) process after the excitation source is ceased. 4. Charge recombination (CR), and 5. exciplex emission

To achieve long-lived charge-separated states (CS), Adachi and Kabe used a strong electron donor with highly stable radical cation *N,N,N',N'*-tetramethylbenzidine ((29), TMB), and a strong electron acceptor with high triplet state energy *2,8-bis(diphenylphosphoryl)dibenzo[b,d]thiophene* ((28), PPT) that provides a rigid amorphous environment. The blend of the two molecules was melted over the melting point under the nitrogen atmosphere and rapidly cooled to room temperature resulting in amorphous films, as shown in *Figure 1.20*.

The films that were produced showed a strong and broad emission centered at 526 nm when 1 mol% of TMB was used as a dopant in the PPT host material. Upon excitation with a 340 nm LED for 180 seconds, the phosphorescence emission of the films lasted for more than 5000 seconds after the excitation source was removed.

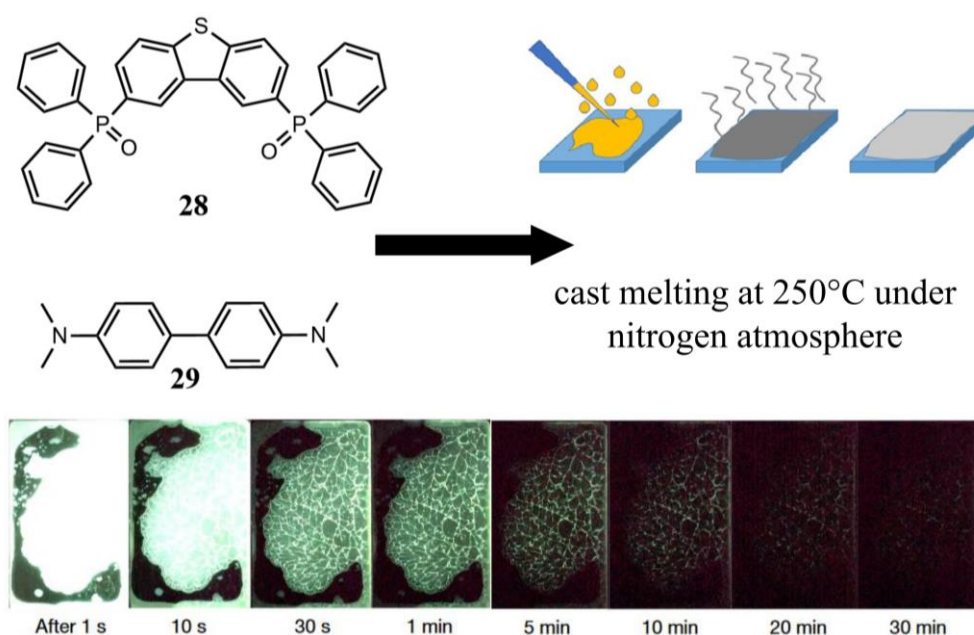


**Figure 1.20.** Simple preparation of amorphous room phosphorescent films. The blend of TMB (29) and PPT (28) is melted at 250 °C under a nitrogen atmosphere. Photographs of LPL from a 1 mol% TMB: PPT films

For a long persistent luminescence (LPL) [121], the binary system must be highly efficient in terms of photo-induced charge separation (CS) and the emission from the recombination of charges (CS and CR). A blend of donor-acceptor (D-A) molecules offers, indeed, an effective way to create this charge separation [119,122].

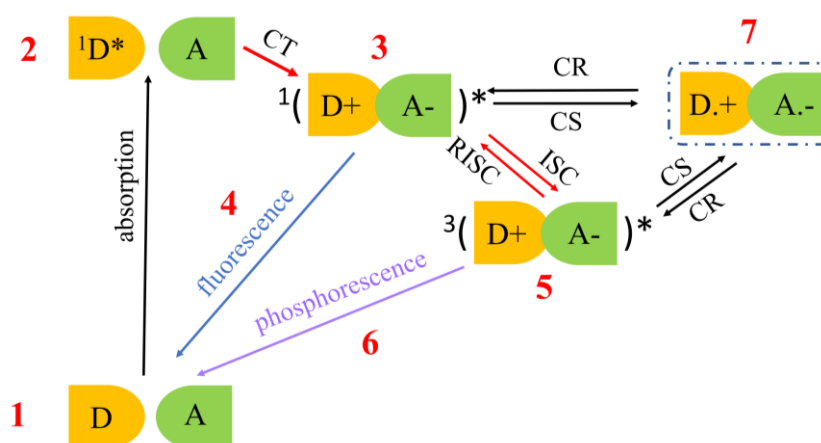


**Figure 1.21.** Long persistent luminescence from intermediate (exciplex) emission by charge-separated and recombined states. D: donor molecule. A: acceptor molecule. CT: charge transfer. CS: charge separation. CR: charge recombination. ISC: intersystem crossing. RISC: reverse intersystem crossing.

The mechanism of this emission is explained in *Figure 1.21*. When the molecule (1) is excited (2), the singlet states of the donor (D) are excited, accompanied by charge transfer (CT), creating by that an exciplex state (3). As the photo-excitation ends, some of the singlet states of the exciplex are liberated as fluorescence (4), or can cross to the triplet states of the exciplex (5) via ISC accompanied by extended persistent luminescence emission (6).

Some exciplex excitons (3) separate into radical ions (7) through charge separation (CS). Once the excitation is off, the charge recombination (CR) of the radical ions occurs via both exciplexes singlet (3) and triplet states<sup>1</sup> (5), resulting in LPL with slow emission decay. In addition, the small gap energy between the S<sub>1</sub> and T<sub>1</sub> of the exciplexes allows reverse intersystem crossing by thermal activation [121,122,124].

The process is similar to what has been observed in a single D-A molecule (*Figure 1.17*), with a difference in the presence of two separated molecules instead of one [106,122].

Further works published by Jinnai *et al.* (2018) from the same research laboratory as Adachi and Kabe in which they extended the emission range of the prepared films by using a variety of emitter dopants molecules (charge separation matrix of TMB: PPT + emitter dopant). The composition of the material can change the color and the emission time of the prepared films. The light emission comes from the emitter dopant to which the exciplex energy was transferred via Förster resonance energy transfer (FRET) [125].

Lin and co-workers (2018) prepared the first polymeric exciplex-based LPL material that exhibits a green emission peaked at 526 nm with a lifetime of 7 minutes under ambient conditions. The host matrix is a strong electron-accepting polymer that provides a rigid environment, enhancing charge separation and decreasing non-radiative transitions. Doping this matrix with a strong electro-donor allows the creation of an exciplex state via charge transfer, separation, and recombination steps. The prepared films were a blend of electro-

---

<sup>1</sup> Theoretically, the triplet states of exciplexes should be higher in energy than the triplet states of the donor or the acceptor alone. This is because the energy levels of the triplet states are directly related to the highest occupied molecular orbital (HOMO) of the donor and the lowest unoccupied molecular orbital (LUMO) of the acceptor [123].



acceptor, poly(arylene ether phosphine oxide) (**30**, PBPO), and electro-donor *N,N,N',N'*-tetramethylbenzidine (**29**, TMB) that were mixed (1:99 wt% TMB/PBPO) in dimethylacetamide and drop-casted on a substrate at 110 °C for 1 hour (*Figure 1.22*).

The films produced in this work are highly flexible and possess excellent mechanical properties without exhibiting cracks, as seen in *Figure 1.20*. This is likely due to the inherent characteristics of the host material used [121].

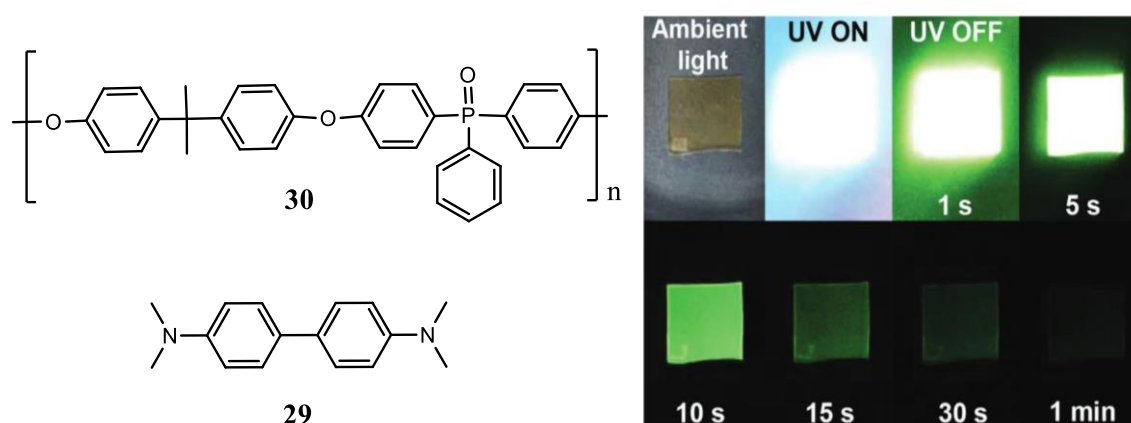


**Figure 1.22.** Electro-donor TMB (**31**) and polymeric electro-acceptor PBPO (**34**) were dissolved in dimethylacetamide and drop-casted under a nitrogen atmosphere (left). The elaborated films at 298 K under the ambient light, during 365 nm excitation, and at various times in the dark (right)

For a better understanding of the influence of the binary donor-acceptor molecules on the luminescence properties of exciplex, Nishimura and Adachi (2020) published a paper in which they explained the dependence of the emission to the energy gap ( $\Delta E$ ) between the charge-transfer excited state (CT) and the lowest localized triplet ( $^3LE$ ) excited state of the donor. When the energy level of  $^1CT < ^3LE$ , the mixture of donor and acceptor exhibits LPL from  $^1CT$  (fluorescence-based LPL). When  $^3LE < ^1CT$ , LPL emission is mainly obtained from emissive  $^3LE$  of the donor (phosphorescence-based LPL). Otherwise, when  $^3LE$  of the acceptor is the lowest, then the emission is quenched. Therefore, the observed color depends directly on the energy difference ( $\Delta E$ ) between the HOMO and LUMO of the exciplex, and from any pathway, the relaxation takes place [122].

Several works were also conducted in which different polymeric molecules were used as a rigid matrix to incorporate the host-guest binary system [126–132]. The polymeric matrix reduces the non-radiative decay rate of the triplet exciton state and decreases the speed of the charge recombination between the D-A system. In addition, the nature of the polymer, *i.e.*, low oxygen permeability, reduces emission quenching. A wide range of polymers is compatible with containing the donor-acceptor systems, polymethyl methacrylate (PMMA), polylactic acid (PA), or polyvinyl alcohol (PVA) (*Figure 1.23*).

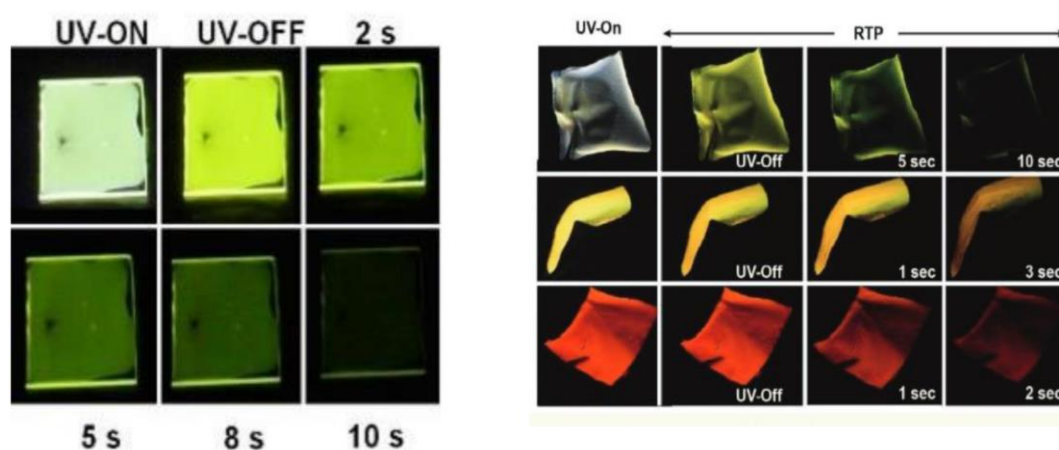


**Figure 1.23.** different polymeric films doped with fluorescent or organic dye to enable emissions with tunable colors. PMMA films (left) and PVA films (right) with different thicknesses. Photographs are obtained from [126,127]

One of the benefits of using a polymer matrix is that it promotes the Förster resonance energy transfer (FRET). This process enables the use of emitter dopant molecules, usually to extend the emission color range. The FRET from the long-lived singlet or triplet state of donor molecules to the singlet state of fluorescent acceptors would provide an emission through this latter, as shown in *Figure 1.24* [125,133,134].

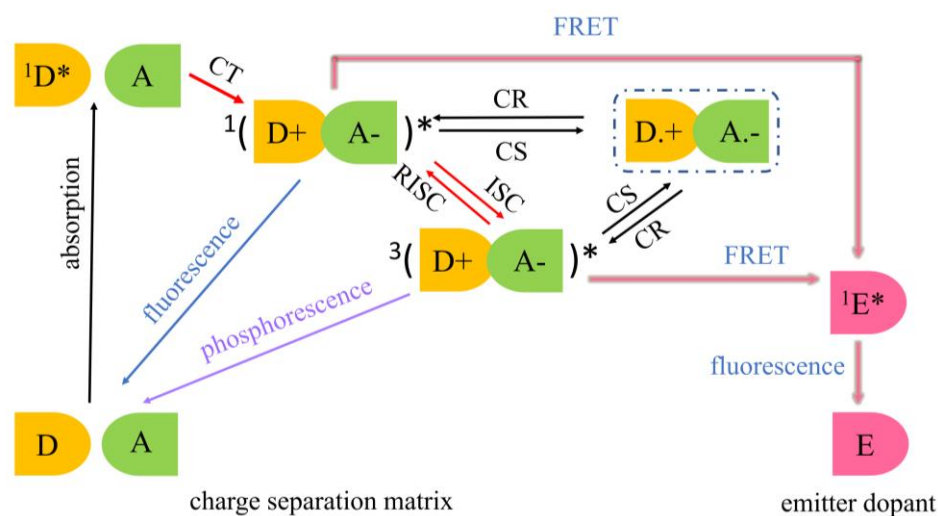


**Figure 1.24.** Energy diagram of the charge-separation matrix and the emitter dopant. The FRET permits the energy transfer from the singlet or triplet state of the donor molecule and emits through the singlet state of the emitter dopant

In 2020, Alam *et al.* published a paper in which they presented a different kind of OLPL materials: crystalline materials. These crystals exhibit room temperature emission due to the formation of exciplexes between the crystal host and a guest dopant molecule. By using dimethylamine (**31**, DMA) as an electron-donor dopant and triphenylphosphonium cation (**32**,  $TPP^+$ ) as an electron-acceptor, Alam and colleagues were able to prepare crystals that exhibit long-persistent luminescence through a simple process of co-crystallization assisted doping.

As shown in *Figure 1.25*, under photoexcitation (254 nm UV source), the charge transfer (CT) of the electrons from the guest to the host occurs. At this point, the charge is separated (CS) between host molecules (acceptors) and acts as a molecular trap that could capture the electrons and release them gradually when the excitation is ceased. The LPL emission is observed due to the recombination (CR) of radical cation of donor recombines with the radical anion of the acceptor. The prepared crystals exhibit green emission at 520 nm, lasting over 7 hours under ambient conditions [135].

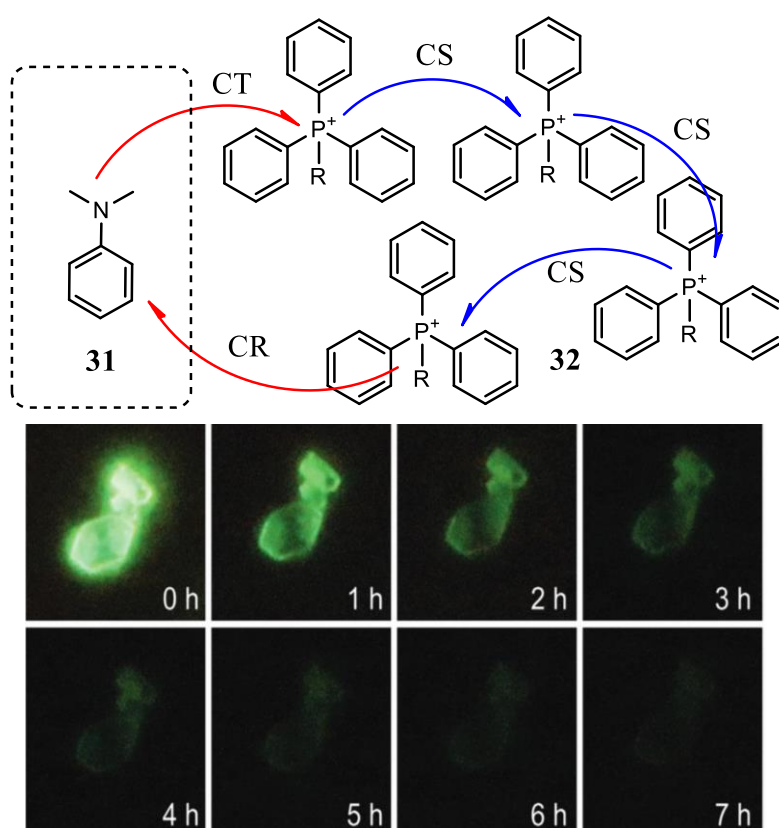


**Figure 1.25.** Mechanism for organic long-persistent luminescence based on trapping electron in cationic quaternary phosphonium core. The charge recombination (CR) resulting in OLPL (left). Photographs of TPP-R: DMA crystals after 365 nm excitation and its subsequent after-glow

So far, the most effective approach for creating OLPL emission has been to use binary donor-acceptor exciplex systems to access charge-separated states. In 2022, Alam and co-workers published a new work in which they designed a single molecule with two moieties (**Figure 1.26**). *N,N'*-dimethylamine moiety (*dashed lines*) that acts as an electron donor (guest) and a phosphonium moiety as an electron acceptor (host). Using a single compound binary system has several advantages in creating OLPL systems. One such advantage is that it facilitates the transfer of charge (CT) from the donor to the acceptor, as well as stabilizing and protecting the system. This can improve the efficiency and longevity of the OLPL system. The lifetime of the compound can also be affected by the type of counterion present in its structure, with certain counterions resulting in longer lifetimes (*i.e.*, Br<sup>-</sup>, I<sup>-</sup>, PF<sub>6</sub><sup>-</sup>).

These counterions may also act as donors of electrons, which ameliorate the emission lifetime and efficiency by favoring the intersystem crossing (ISC) and singlet-triplet charge separation [124].

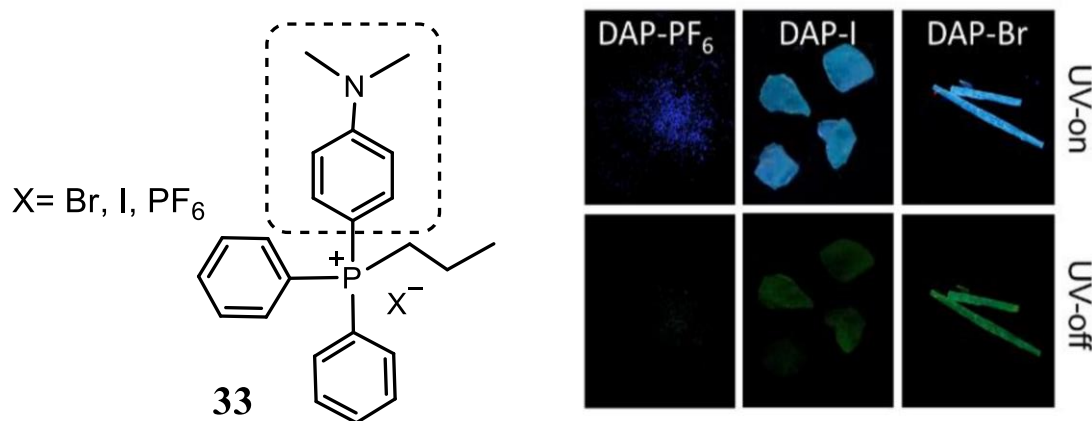


**Figure 1.26.** Chemical structure of the donor-acceptor single molecule, images of crystals under 365 nm excitation, and when it ceased

The compounds described in the previous statement can produce light, or luminesce, in their crystalline form. However, when these compounds are dissolved in a solution at room temperature, they lose their ability to produce light. This has been previously reported in the scientific literature and is thought to be caused by the oxygen-quenching process that occurs in solution. The crystalline structure of these compounds creates a dense, rigid network of aggregates that helps prevent non-radiative deactivation and protects the triplet-exciton from being quenched by oxygen [136–138].

### 1.6.4. Interlude

Phosphorescence, or the emission of light after being excited, can be caused by various mechanisms and phenomena. One common type is the "glow in the dark" phosphorescence from inorganic compounds, such as zinc sulfide and strontium aluminates with various dopant phosphors. The mechanism for this emission type is not fully understood, but many

scientists believe it involves an electron-hole trap mechanism in which the electron becomes trapped when excited, and its relaxation emits a slow glow (*section 1.6.1*).

Another type of phosphorescence is the emission from the triplet excited state, which is observed in some organic compounds at very low temperatures. This type of emission is caused by the excitation of a molecule to its singlet excited state, followed by a non-radiative intersystem crossing to the triplet state. The relaxation back to the ground state from the triplet to the singlet state emits decayed light. This type of phosphorescence emission from the triplet state has also been observed at room temperature in some aromatic carbonyl molecules, carbon dots, some aggregates, and organometallic chelates (*section 1.6.2*).

Long-persistent-luminescence (LPL) is another type of phosphorescence observed in some pure organic molecules that can form exciplex states. LPL emission is observed in donor-acceptor binary systems and results from charge transfer from a guest molecule to a host molecule. The charge is separated over the guest molecule states before being recombined back to the initial state after the excitation is turned off. The slow charge recombination releases light as luminescence emission (*section 1.6.3*).

### **1.7. Conclusion**

In the literature review of this thesis report, the current state of knowledge on luminescent textile development was examined. The main goals and objectives of the research were identified, and the review focused on three main areas:

The nature and classification of molecular materials that produce luminescence, the methods for transferring materials to a substrate through surface functionalization, and the technical aspects of measurement setup development. Inorganic compounds were found to be particularly effective at producing intense, long-lasting emissions, but their insolubility limits their practical applications.

Moreover, organic long persistent luminescent compounds (OLPL) have attracted much interest, showing promising results.

## 1.8. Property to material transfer

The goal of creating molecules and materials is typically to utilize their properties and functions to achieve a desired result or benefit. It is helpful to consider how the materials being developed can add value to their intended application. One way to do this is to transfer (give) the properties of a molecular material to another material by incorporating it into the host material through surface functionalization. This results in the desired properties being present on the surface of the host material rather than throughout its bulk. The performance of the material is mainly dependent on the surface because it is the surface that determines the material's interactions with its environment and how it functions. By understanding and carefully designing the surface properties of a material, it is possible to significantly enhance its performance and usefulness in a given application.

The focus of this thesis is on the creation of textiles with specific luminescent properties and functions. To achieve this, the surface of the textiles will be modified. It is possible to modify the surface of textiles in various ways due to their natural or synthetic character [139]. In Chapter 2, cotton textiles will be discussed as the chosen substrate for modification, and the reason for selecting them will be explained.

One way to modify the textile surfaces is through surface functionalization, which processes through various methods and techniques, such as chemical or physical treatments, coatings, or the incorporation of functional molecules [139,140]. Functionalization of textiles, or the modification of the surface of textiles to give them specific properties, is a particularly important area of research due to the widespread use of textiles. This could involve making the textile more durable, improving its appearance or feel, or imbuing it with unique properties such as antimicrobial or water-resistant capabilities applications [141–143].

Textile functionalization is a well-studied area with a wealth of information available in the literature [144–147]. In this thesis, the methods and techniques used for functionalization will be described in detail in Chapter 2 as where utilized. This will provide a thorough

## Chapter 1

---

understanding of the process and allow for replication or further experimentation in the future.

This thesis aims to explore sustainable and eco-friendly methods for transferring materials to a substrate, focusing on surface functionalization techniques. This literature review highlights various approaches, including physical and chemical treatments. Our goal is to establish a material-substrate relationship in an environmentally responsible manner. On the technical side of this literature review, the ongoing developments in measurement instrumentation and characterization techniques were reviewed, pointing out optical investigations as will be discussed in details on the upcoming chapter.



---

## **Chapter 2 Materials, methods, and instrumentation**

### **2.1. Introduction**

This chapter reviews the instrumentations and methods used in this thesis, specifying the developed spectroscopic types of equipment. The first part of this chapter is the classical material and methods of thesis reports, describing the used materials, chemicals, methods, and employed apparatuses. The second part highlights more the technical side of developed spectroscopic measurement methods based on fiber-coupled devices with further details on the calibration of spectra and their corrections, as well as some experimental parameters to consider while using the fiber-coupled instruments.

Herein, most optical spectroscopic equipment dedicated to determining the absorption and emission of light are commonly known and well documented and, therefore, will be briefly addressed. However, new setups were constructed during our work on luminescence materials and long persistent luminescent compounds. These setups will be discussed in more detail in Chapters 4 and 5, especially a trouble-free instrument for measuring the photoluminescent quantum yields of fluorescent molecules using a non-monochromatic LED as an excitation source.

## Part One : Material and methodologies

### 2.2. Materials and chemicals

#### 2.2.1. Substrate

Cotton is collected from the cotton plants. The fiber is almost pure cellulose (*Figure 2.1*), a condensed polymer formed by bio-synthesis from carbon dioxide and water, along with glucose as an intermediate monomer [148]. Since cellulose molecule constitutes most of the cotton matter, it provides an important count of hydroxyl groups (-OH) that offers a potential site for bonding with other chemicals. At the time of its collection and its assembly to become a fabric, it may undergo certain modifications, *e.g.*, contact with impurities and electrostatic charging. Therefore, two pre-treatment steps must be conducted before using the cotton fabric as a substrate. The first is eliminating impurities and adjusting surface proprieties through the boiling-off process, followed by hot and cold washings [149]. The second is surface activation by alkaline treatment of cellulosic fibers that promotes more active sites and ameliorates shrink-age resistance, luster, and dye affinity [141]. In this work, nonwoven treated cotton fabrics of density 168 g.m<sup>-2</sup> were supplied by ESITH industry (Morocco) and used as substrates in the form of small cuts (depending on the application and the employed technique).

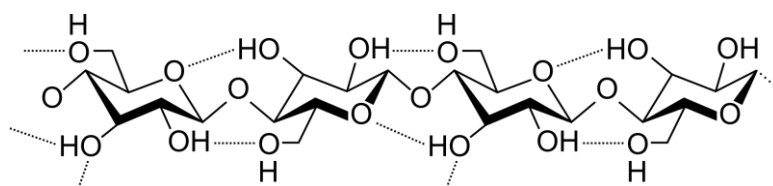


Figure 2.1. Molecular structure of cellulose, a natural polymer

#### 2.2.2. Chemicals

All chemicals used during the preparation of this thesis were purchased from Sigma Aldrich/Merck and used as received without further purification unless where indicated. Solvents and reagents were at least of spectroscopic or analytical grade (> 95%). Commercial raw polyurethane (R-PU) (Fixamin PU K New) and polyacrylate (PA) are supplied by

Impocolor (Morocco), with a density that varies between 1.08 and 1.12. commercial cross-linking agent (KNITTEX CHN) from DICRYLAN. Thickener (HV 30) supplied by BASF.

### 2.3. Textile functionalization techniques

Surface functionalization is enabled by a wide range of technologies and methods designed to modify the initial property of the surface and creates another structure that is suitable for the upcoming acquired functionality. These functionalization doings vary from traditional primitive solution treatments to some new advanced methods, thanks to recent technological developments [142].

In the following, we review some surface modification techniques<sup>1</sup> that are mostly used in the textile industries and laboratories, singling out the physicochemical techniques for modifying the surface of the textile.

#### 2.3.1. Functionalization by the pad-dry-cure method

The pad-dry-cure method (*Figure 2.2*) is one of the most common methods for easy-care and durable press finishes applied to cellulosic fibers and fabric blends with high cellulose content [150]. It permits the creation of coatings on the substrate after passing through simple steps, basically starting with dipping the substrate into the bath solution and passing by roller pressers that enable uniform and homogenized distribution and assure the penetration of coating in the textile structure. After, the substrate undergoes thermal treatment to dry and evaporate solvents and enhance the crosslinking reaction of the coated layer, which is obtained during the curing step. Even though that the dip-pad-dry-cure method is mostly used in textile processing, it has some limitations related to the use of apparatus, consuming energy, and also problems related to the dispersion of the additives and the formation of aggregates on the surface of the treated substrate.

---

<sup>1</sup> a duly special note about the confusion between the method and the technique. The method is the process by which the functionalization of textile is done, while the technique is the practical aspect of the functionalization

In this work, the steps of dip-pad-dry-cure were separately performed<sup>1</sup>, whereas the dipping of the fabric was carried out in a glass crystallizer containing the solution-to-apply. As for the padding step, an automatic MU504A Lab Padder was used, followed by the application of infrared irradiation for the drying and curing steps.

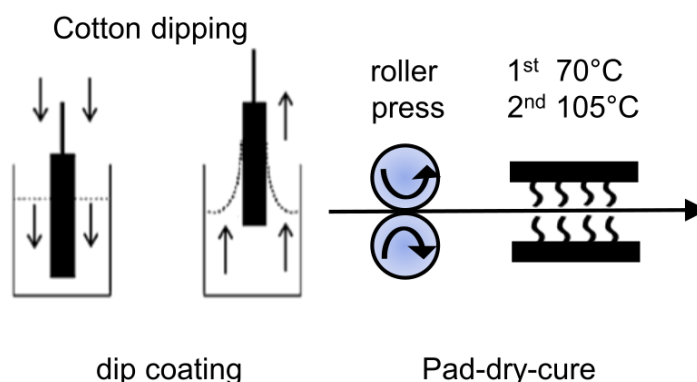


**Figure 2.2.** Dip coating and pad-dry-cure process

### 2.3.2. Functionalization by the doctor-blade coating method

Another commonly used method in the textile industry is the doctor-blade coating (*Figure 2.3*). It works by placing a sharp blade at a fixed distance from the surface that needs to be covered. The coating formulation is then placed in front of the blade, and the blade is moved across in-line with the surface, creating a wet film with precise thickness [151]. Afterward, the sample is thermally treated to enhance the chain-growth polymerization and form atom-transfer radical-polymerization [152] coatings. Regardless of the limitations of this coating method, notably the change in mechanical properties of the fabric, it showed promising results and large-scale applicability, pointing out the ability to integrate insoluble inorganic particles and pigments (contrarily to the dip-pad-dry-cure method).

---

<sup>1</sup>In general, the process may be continuous using specific-designed apparatus for this purpose

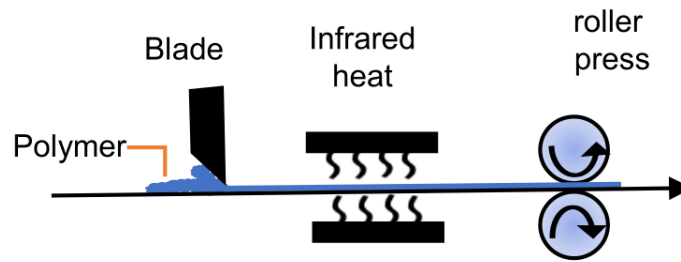


Figure 2.3. Doctor-blade coating and cure-pad processes

### 2.3.3. Functionalization by the spray coating method

Spray coating on textile fabrics (*Figure 2.4*) is emerging as a promising technique to overcome the limitations of textile functionalization with the previously mentioned conventional methods (*e.g.* suitability, solubility, aggregates, mechanical modification, etc.) . It has been introduced as a direct-facile, eco-friendly, and low-cost technique to coat different substrates and reduce water and chemical consumption [153]. Furthermore, the spray coating prevents agglomeration and assures homogenous distribution of the uploaded substance to the substrate while preserving its mechanical properties. The spray coating method appears to be the appropriate direct way to apply formulations to textile fabric, thus assuring a regular coating layer over the surface [154]. In this thesis, the spray coating formulation was prepared, uploaded into the spray gun cavity, and applied directly to one side of the fabric with multiple passes (coatings) from a distance of 20 cm to the substrate (using filtered air, 4 bar, controlled medium flow rate). The fabrics were left to dry in air at atmospheric conditions for 30 minutes, followed by thermo-fixation under infrared heat for 5 minutes.

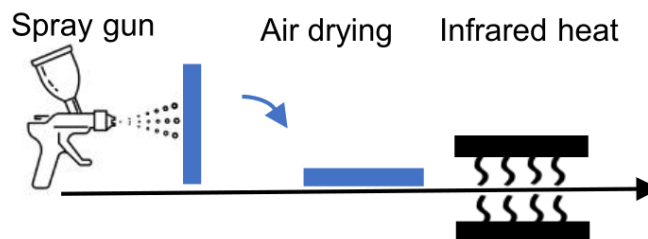


Figure 2.4. spray coating process

In this thesis, I had the opportunity to work and utilize these three functionalization methods of textile fabrics. The choice of a method over another is further explained in each Chapter.

The experimental details, including coating formulation preparation and thermal treatment conditions, are also reported where used.

### **2.4. Characterization equipment and apparatus**

In this thesis work, various instruments and techniques were employed to identify and study molecules in solution as well as the characterization of materials, including the investigation of textile surfaces.

#### **2.4.1. Nuclear magnetic resonance spectroscopy (NMR)**

Most commonly known as NMR spectroscopy, a technique that is used to observe local magnetic fields around atomic nuclei. The NMR analysis is performed in chemistry to determine organic compounds' molecular identity and structure. Herein,  $^1\text{H}$ -NMR was recorded on a Bruker Avance Topspin (300 MHz) using TMS as an internal reference and heavy water ( $\text{D}_2\text{O}$ ) or deuterated methanol as solvent. The used splitting patterns are s (singlet), d (doublet), dd (double-of-doublet), t (triplet), and m (multiplet).

#### **2.4.2. Attenuated total reflectance infrared spectroscopy (ATR-IR)**

Infrared spectroscopy (IR) analyzes the interaction of infrared radiation with the matter by absorption, emission, or reflection. It studies and identifies functional groups in molecular substances through their vibrations. Nowadays, IR instruments come up accompanied by an attenuated total reflectance (ATR) accessory, which enables samples to be examined directly in the solid or liquid state without further preparation. Infrared spectra were recorded on a Nicolet iS20 FTIR instrument in ATR mode, with a mid-infrared beam splitter, with Ever-Glo and tungsten/halogen as sources. It has a spectral range of  $4000\text{-}750\text{cm}^{-1}$  and has a resolution better than  $0.4\text{ cm}^{-1}$ .

#### **2.4.3. UV-visible extinction spectroscopy**

UV-vis extinction spectroscopy is used in diverse applied and fundamental fields, particularly in analytical chemistry for quantitative measurements. When light interacts with a sample, its

intensity is attenuated due to two factors: absorption by the sample and scattering by particles within the sample. The former is described by its absorbance density and the latter by its turbidity. This light attenuation (or extinction) is commonly referred to as the optical density<sup>1</sup> (OD), which is a function of wavelength  $\lambda$ . The principle of this technique is based on the illumination of a sample (incident light intensity  $I_0$ ) and the recording of the amount of light that reaches the detector (transmitted light intensity  $I$ ). The optical density is then defined as the base-10 logarithm of the ratio of intensities (*Equation. (2.1)*).

$$OD(\lambda) = -\log_{10} \frac{I(\lambda)}{I_0(\lambda)} = \log_{10} \frac{I_0(\lambda)}{I(\lambda)} \quad (2.1)$$

When the solution does not scatter light, the optical density is equal to the absorbance (scattering is zero), and the well-known Beer-Lambert Bouguer law (*Equation (2.2)*) that describes the linear relationship between the concentration ( $C$ ) and the measured absorbance can be applied, where  $\varepsilon(\lambda)$  represents the wavelength-dependent extinction coefficient of the analyte in 1 cm pathlength.

$$Abs(\lambda) = OD(\lambda) = \varepsilon_{(\lambda)} l C \quad (2.2)$$

For this thesis, a double-beam Thermo-Fisher Evo 300 PC spectrophotometer was used to record absorbance spectra and calibration curves. *Figure 2.5* represents the working principle of a dual-beam spectrometer. When the lamp source (usually a deuterium/tungsten lamp) produces light, it passes via a monochromator to select the desired wavelength of light. Aided by mirror systems that separate and split the incident beam ( $I_0$ ), the light passes through the sample (S) and the reference (R) simultaneously, and a detector collects the emitted light (I) to give output data.

---

<sup>1</sup> The optical density is often referred to as the absorbance of a sample, though this nomenclature can be confusing since the attenuation of light in a sample is due to both absorbance and scattering.

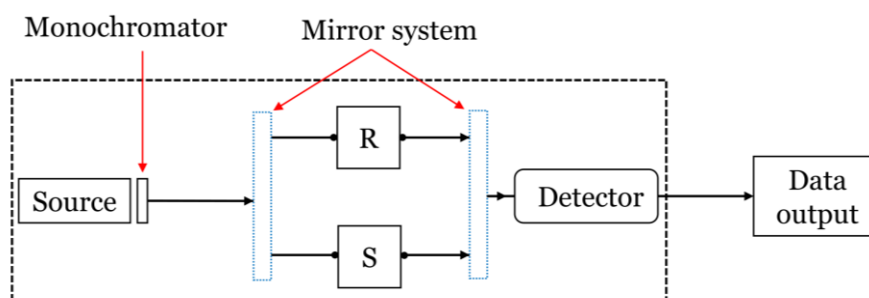


**Figure 2.5.** Representation of the dual-beam UV-vis spectrometer

For emission measurements, a single-beam fluorimeter is used (*Figure 2.6*). The working principle is similar to an absorption spectrometer except for the position of the detector. The measurement is performed in  $90^\circ$  geometry, permitting the record of the emission spectra. In general, this setup configuration is used in the measurement of fluorescence.

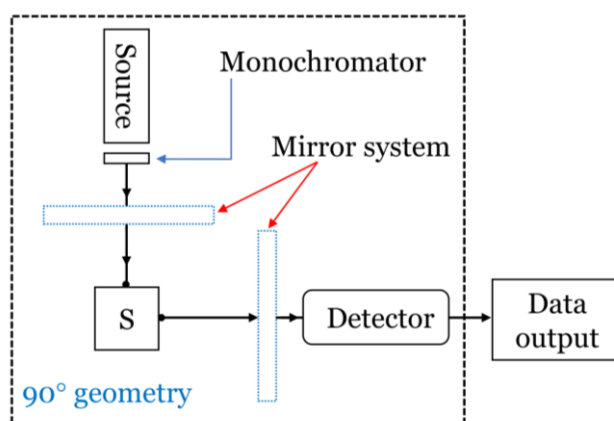


**Figure 2.6.** Representation of a single-beam fluorimeter designed for emission measurements ( $0/90^\circ$ )

Another instrument based on fiber-coupled spectrophotometers was also used during this thesis work (*Figure 2.7*). The setup is based on single-beam absorption using a tungsten-halogen lamp to illuminate, through optical fibers, the analyte and record the transmitted light on a spectrometer (*setup used in section 3.3.2*). The setup requires first to correct for the dark signal (baseline) and record the reference spectrum as the blank sample (usually pure solvent).



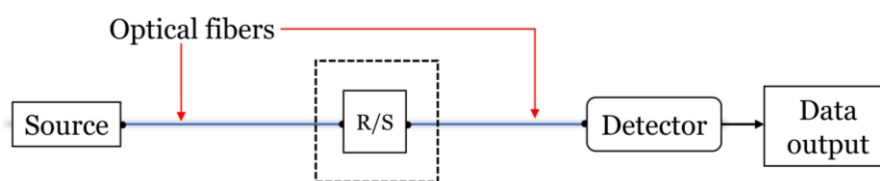


**Figure 2.7.** Representation of fiber-coupled single beam UV-vis measurement setup

For the investigation of the photophysical properties of the dyes, poly(methyl methacrylate) PMMA single-use 1cm cuvettes<sup>1</sup> (cells) were employed. However, working on the ultra-violet region of the optical spectrum requires the use of quartz cells, as the case in Chapter 4.

#### 2.4.4. Scanning Electron Microscopy with Energy Dispersive Spectroscopy

Scanning electron microscopy (SEM) is a type of electron microscopy that produce images of a sample by scanning the surface with a focused beam of electrons. When the beam (with high energy) enters into contact with the matter, several signals are produced (backscattered), including secondary electrons (SE) and X-rays. The former signal is translated into spectral peaks of varying intensity, resulting in a topology profile of the sample, allowing for targeted analysis of sample surfaces, and used in this work to observe textile fabrics. The latter signal (X-rays) produces characteristic peaks of a unique atomic structure, obtained through the energy dispersive spectroscopy (EDS) detector, and permits determining which chemical elements are present in a sample and estimating their relative abundance.

SEM-EDS were recorded on two instruments: (i) a Quattro ESEM™ electron microscope operating at 30kV at a pressure of 2 mbar, not requiring any specific sample preparation. (ii) an SH-4000M with a SED detector and dark background, operating at 5kV at a high vacuum, gold coatings were applied on the textile samples to enhance their conductivity. Energy dispersive spectroscopy (EDS) analysis was recorded with electron backscatter diffraction (EBSD) coplanar with wavelength dispersive X-ray spectroscopy (WSD).

---

<sup>1</sup> Polystyrene cells were also tested; however, these cuvettes are limited in terms of compatibility with some solvents (*e.g.*, ethanol) which causes them to crack and break.

## 2.4.5. Colorimetric measurements

When color-bearing compounds (dyes, pigments, fluorophores, luminophores) are applied to textiles, it is essential to characterize and manage the obtained coloration to have consistent results, including evaluating the success and robustness of the dyeing. Each color is represented by a “color point” with variables named “color coordinates”, indicating the position of the color in the corresponding marks (space).

To this end, the Datacolor instrument is used, which is designed to analyze flat samples such as plastic and textile to objectively evaluate the difference of colors between samples using Equation (2.3)

$$\Delta E = \sqrt{\Delta L^{*2} + \Delta a^{*2} + \Delta b^{*2}} \quad (2.3)$$

Before explaining these variables and what they refer to, it is essential to understand the concept of color space, a three-dimensional model that mathematically describes a set of colors in relationship to each other. Colors are mapped along axes representing different aspects that vary depending on the type of color space.

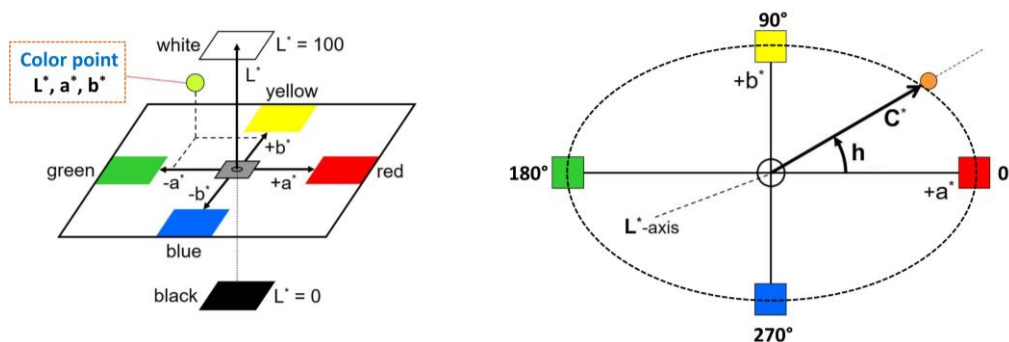


**Figure 2.8.** CIELab (left) and CIELCH (right) color spaces representing cartesian and polar coordinate systems, respectively.  $L^*$  (0-100) represents lightness.  $a^*$  ( $+a^*$ ,  $-a^*$ ) act for red and green colors, respectively.  $b^*$  ( $+b^*$ ,  $-b^*$ ) are yellow and blue, respectively. On the other side, chroma ( $C^*$ , also called saturation) is a parameter that expresses the distance from the lightness axis. The hue angle ( $h^\circ$ , the color tone) is expressed in degrees, with  $0^\circ$  being a location on the  $+a^*$  axis, continuing to  $90^\circ$  for the  $+b^*$  axis,  $180^\circ$  for  $-a^*$ ,  $270^\circ$  for  $-b^*$ , and back to  $360^\circ = 0^\circ$ . Note that, for CIELCH, the  $L$  axis is perpendicular to  $a^*$  and  $b^*$  axes.

Historically, it stated with CIE RGB color space (1931) whereby human observers find, for any spectrum of light, a matching mixture of three chosen primary lights, which are typically

monochromatic at wavelengths that are: (R) for red, green (G), and blue (B). After, CIE Lab color space (1976, *Figure 2.8\_left*) was introduced to be perceptually uniform by representing the parameters ( $a^*$ ), ( $b^*$ ), and ( $L^*$ ) in rectangular Cartesian coordinates. When represented in cylindrical polar coordinates (CIELCH, *Figure 2.8\_right*), lightness ( $L^*$ ), hue ( $h^\circ$ ), and chroma ( $C^*$ ), the chromatic relationships are relatively easy to see, so people often prefer these coordinates to the rectangular ones—even though the color difference equation looks just a bit more complicated [155–157].

The color difference specification between two samples is presented according to ISO/CIE 11664-6:2014 standard. The colorimetric analysis was performed using a Datacolor 600™ Dual-beam  $d/8^\circ$  spectrophotometer, with a pulsed xenon light source filtered to approximate D65-wavelength from 360 to 700 nm  $\pm$  10 nm. The outcome data are averaged three times based on at least three independent measurements.

### ***Part Two : Development of fiber-coupled spectroscopic setup***

Throughout this thesis project, I had the opportunity to discover and work with fiber-coupled spectroscopic equipment. Such equipment has proven its effectiveness for various spectroscopic measurements, for instance, absorption, emission, transmission, fluorescence, extinction, scattering, and even colorimetric measurements. Herein, we will introduce fiber-coupled components for optical spectroscopy, with further details on the montage in Chapters 4 and 5.

## **2.5. Devices**

To conduct optical spectroscopic measurements, the presence of three items is needed: a light source, a sample, and a detector.

### **2.5.1. Light source**

#### **2.5.1.A. LS-1 tungsten halogen lamp**

Tungsten-halogen lamps, a type of incandescent halogen lamp, are often used in illumination systems. They produce light over a wavelength range of 360-2000 nm, which makes them

suitable for UV-visible spectroscopy. The LS-1 series white-light tungsten halogen light source (from OceanOptics, *Figure 2.9\_left*) was utilized for measurements in the VIS-shortwave NIR range, offering high color temperature and a long bulb lifetime.

In this thesis, the LS-1 lamp was employed in various investigations, including optical densities, diffuse-reflectance measurements, colorimetric measurements, and extinction and scattering measurements. The LS-1 lamp was used with a color-corrector FG3 conversion filter (Schott) that enhances the blue and red regions of the visible spectral range by reducing the intensity of the green part of the light spectrum.

### 2.5.1.B. AVALIGHT-HAL-S-MINI LAMP

The AVALIGHT lamp (*Figure 2.9\_right*) was also used for investigations requiring a robust light source. The AVALIGHT lamp is also a Halogen lamp and resembles the LS-1 excitation light, except for some ameliorations in terms of stability, long bulb lifetime, and broad wavelength range (360-2500 nm).



**Figure 2.9.** LS-1 tungsten halogen lamp from OceanOptics (left), AVALIGHT-HAL-S-MINI lamp from AVANTES (right)

### 2.5.1.C. LIGHT-EMITTING DIODES (LED)

In the last two chapters, the ultraviolet and visible regions of the electromagnetic spectrum were investigated when studying luminescent molecules. Usually, the excitation source (*e.g.*, deuterium high-intense lamp) of spectrometers built for measuring in the ultraviolet region is fitted with grating monochromators to isolate the specific peak (wavelength) for measurements. Four LED light sources (LS-series) purchased from OceanOptics, providing various wavelengths (340 nm, 380 nm, 450 nm, and 518 nm), were employed during the preparation of this thesis. The LEDs are contained in a housing similar to the LS-1 housing (*Figure 2.9\_left*) and can be set on continuous or pulsed excitation mode, making them suitable

for luminescent measurements. Herein, light-emitting diodes (LEDs) were used in our experiments on the ultraviolet and visible edges. These sources are referred to by means of the wavelength of their emission maximum, but contrary to 'monochromatic' light sources (lasers and lamp-monochromator combinations), the LEDs have relatively broad spectra, as shown in *Figure 2.10*.

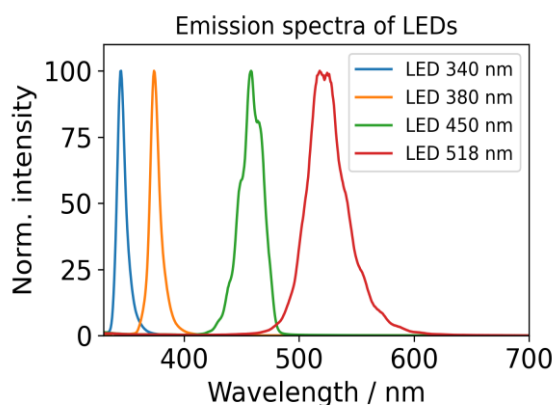


**Figure 2.10.** Corrected emission spectra of the fiber-coupled LEDs used for excitation

Also, we investigated the stability of LED light sources by measuring their intensity as a function of time. Two LEDs source lights (380 nm and 450 nm) were studied for 3 hours and recorded emission spectra every 2 minutes to observe any signal fluctuations; thus, slight fluctuations were noticed for the first few spectra after switching the LEDs on, and afterward, the emission of the LED stabilized (*Figure 2.11*).

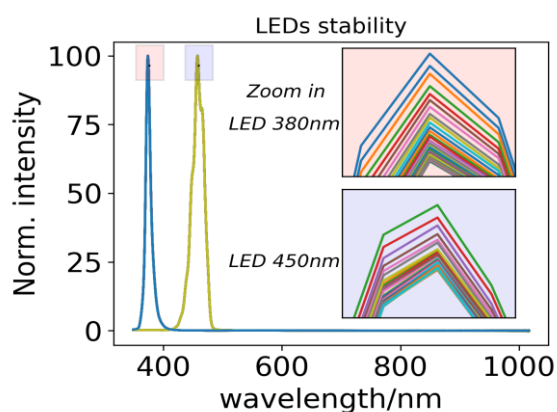


**Figure 2.11.** Stability of the LEDs emission (380 nm and 450 nm) after three hours of excitation (right). The zoom is done on the top of spectra following the colors, red for 380nm LED, and blue for the 450nm LED

LEDs presented a good level of stability with fluctuations that varied between 1 % and 1.5 % over the three hours of the experiment, making them very stable for spectroscopic measurements (which can be achieved in several minutes).

### 2.5.1.D. AVALIGHT XE-HP

For some applications, *e.g.*, in the ultraviolet range, incandescent light may be unsuitable. In such cases, a pulsed Xenon light source can be helpful despite its extreme intensity (*Figure 2.12*). The XE-HP source light (from Avantes) covers a range from 200 nm to 1000 nm and performs pulses up to 150 Hz. Since this lamp is very intense, a thinner optical fiber (50  $\mu\text{m}$ ) was used to reduce its intensity. Also, the ZWB1 (UG11 Schott) bandpass filter was employed to reduce the intensity between ( $\sim 450\text{-}650\text{ nm}$ ).

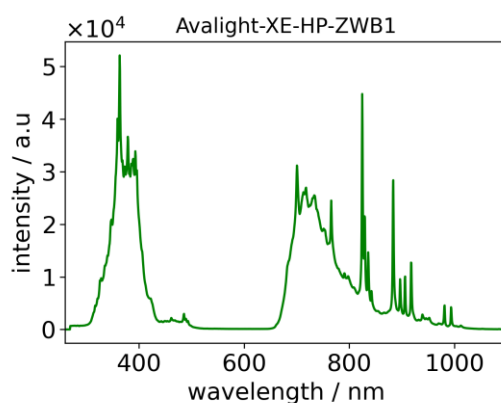


**Figure 2.12.** Spectral output of Avalight-Xe-Hp with ZWB1 bandpass filter

These previously seen light sources present a universal SMA 905 output connector that enables connecting with other components, basically terminal-SMA optical fibers. SMA 905 connector is compatible with standard multimode fibers.

## 2.5.2. Samples | sample holder

### 2.5.2.A. Single-cell holder

The single-cell holder (CUV-UV Fiber Optic Cuvette Holder / Ocean Optics, *Figure 2.13\_left*) is designed for small-footprint systems to measure the absolute absorbance of aqueous solutions with 1-cm pathlength cuvettes, couples efficiently via optical fibers to spectrometers

and light sources passing by two collimating lenses (74-UV f/2 fused silica lenses). The holder is optimized for 200-2000 nm applications, has a built-in filter slot, and features spring-loaded ball plungers for precise cuvette positioning. It also presents a cover slot that permits blocking ambient light from the sample chamber.

### 2.5.2.B. Qpod cell holder

Qpod holder (Peltier-controlled Qpod / OceanOptics *Figure 2.13\_right*) is also a single-cell, but it has four ports for mounting optics, which means two other outputs of optical fibers that can be used for absorbance and fluorescence measurements. It offers a precise temperature-controlled ( $\pm 0.15$  °C from 0 °C to + 80 °C) and is built with an internal magnetic stirrer. Similarly to the previously seen holder, the compartment has mounting rings on every four sides, allowing for connecting optical components (*i.e.*, collimating lenses).



**Figure 2.13.** Single-cell holders: CUV-UV Fiber Optic Cuvette Holder (left). Peltier-controlled Qpod (right)

### 2.5.3. Detectors | spectrophotometers

Regardless of the broad spectral range covered by the excitation light or how much the sample holders are optimized to offer a sizeable spectral domain, it is meaningless if the responsive range of the detector (*i.e.*, spectrometer) is limited. In this thesis work, four spectrometers from Ocean Optics (currently Ocean Insights) and Avantes were used (*Figure 2.14*). The properties, characteristics, and specifications of each spectrophotometer will be outlined here.

### 2.5.3.A. Ocean Optics USB4000 fiber-optic spectrometer

USB4000 is a miniature fiber-optic spectrometer with high performance and speed, covering the range from 350 nm to 1038 nm. It features a high-sensitivity linear CCD<sup>1</sup> array that provides high responsivity and excellent optical resolution and operates within integrating time from 3.8 ms to 10 seconds. The USB4000 is perfect for rapid absorption and transmission measurements, as well as it can be used for colorimetric investigations when coupled with an integrating sphere, as will be seen in subsequent paragraphs.

### 2.5.3.B. Flame VIS-NIR spectrometer

The Flame spectrometer covers approximately the same range from 350 nm to 1100 nm with an integrating time from 1 ms to 65 seconds. It is also a CDD silicon-based multi-channel array detector, suitable for applications requiring repeatability and reproducibility.

### 2.5.3.C. AvaSpec ULS2048 CL-Evo spectrometer

The AvaSpec spectrometer is based on a CMOS<sup>2</sup> detector array instead of a CDD detector array. The spectrometer from Avantes has become a genuine competitor to CDD detectors to be used in cameras and spectrometers and has proven its effectiveness due to the fast reading of pixels, making it suitable for some applications that require higher framerates (which will be seen in the last chapter of this thesis). The AvaSpec offers more or less the same spectral range of the already seen spectrometers (330 nm-1060 nm) and an integrating time from 9  $\mu$ s to 59 seconds. The problem with CMOS technology is being more susceptible to noise, so the ratio signal-to-noise (S/N) is more critical (undesired signal). Also, the light sensitivity of the CMOS chip tends to be lower due to the location of transistors next to it. Overall, the CMOS is

---

<sup>1</sup> CCD or charge coupled device is a highly sensitive photon detector with large number of light-sensitive small areas known as pixels. Each pixel has three multi-channels (max) that are sensitive to light, UV, visible and near-infrared light (200-1100 nm)

<sup>2</sup> CMOS, or complementary metal oxide semiconductor, is a fast and rapid sensor that converts light into electrons/electrical signals. The working principle is the several transistors amplify and move the charge (electron) on each pixel through integrated circuit (IC).



rapidly improving in performance, suitable for particular applications, but CCD sensors may still be required for some demanding applications.

### 2.5.3.D. QE65000 High-Sensitivity Fiber Optic spectrometer

The QE65000 spectrometer is the most sensitive spectrometer used, achieving up to 90% quantum efficiency. The QE65000 from Ocean Optics is suitable for low-light-level applications and operates in a spectral range from 360 nm to 1000 nm. Furthermore, it has an integration (exposure) time ranging from 8 ms to approximately 15 minutes. The QE65000 features a back-thinned FFT-CDD detector (Hamamatsu S7031-1006S) with a 2D arrangement of pixels (1044 horizontal x 64 vertical). The particularity of this spectrophotometer is the integrated thermos-electric (Peltier) cooler that cools the detector down to 10 °C. This reduces dark noise, provides signal stability, and enables low integration times.



**Figure 2.14.** The four spectrometers used during the preparation of this thesis. From left to right, we have USB4000, Flame VIS-NIR, ULS 2048CL EVO, and QE65000. These spectrometers also have SMA 905 input connectors.

### 2.5.4. Detector calibration

Eventually, due to the environmental and experimental conditions, the wavelength of all spectrometers will drift slightly as time passes. It is why regular calibration of spectrometers is needed. Herein, we are reviewing the calibration of the spectrometers QE65000 and ULS2048CL to correct (calibrate) the wavelength.

In general, the calibration of spectrometers is conducted using a spectral calibration lamp, in our case, the Hg-1 low-pressure mercury-argon lamp (Ocean Optics). The Hg-1 lamp is coupled through an optical fiber (preferably with a small internal diameter, *e.g.*, 50  $\mu\text{m}$ ) with the spectrometer and records the obtained spectra. *Figure 2.15* shows the spectral lines of the

Hg-1 lamp recorded on both QE65000 from Ocean Optics (red plot) and ULS2048CL from Avantes (blue plot). The data of these spectral lines will be used to solve Equation (2.4), which connects pixel numbers and wavelengths (third-order polynomial equation).

$$\lambda_p = C_0 + C_1p + C_2p^2 + C_3p^3 \quad (2.4)$$

Where:  $\lambda$  is the wavelength of pixel  $p$ ;  $C_0$  is the wavelength of pixel 0; and  $C_1$ ,  $C_2$ , and  $C_3$  are the first, second, and third coefficients, respectively. The equation can be resolved using any calculator program that performs third-order polynomial regression (Excel, Python). After executing the regression, the obtained values will be used to correct the wavelengths of the spectrometers by saving the new calibration coefficients directly on the spectrometer via USB mode (the detailed procedure is well documented and available online).

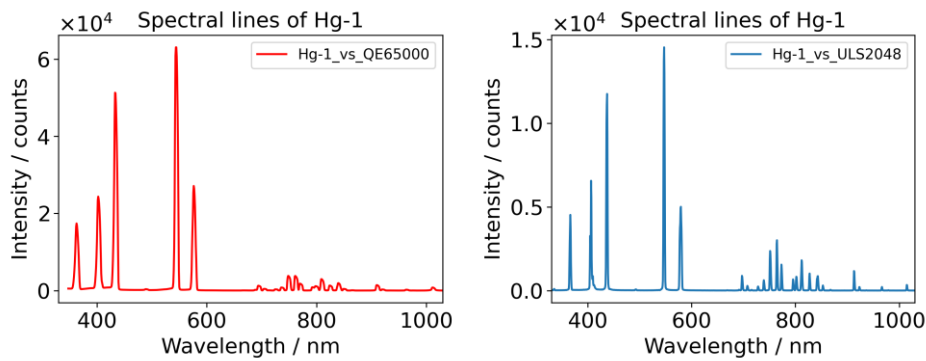


**Figure 2.15.** Spectral lines of calibration mercury-argon Hg-1 lamp recorded on QE65000 and ULS2048CL using 50 $\mu$ m internal diameter optical fiber

## 2.5.5. Optical fibers and accessories

### 2.5.5.A. Optical fibers

Optical fibers link the previously described devices through standard subminiature assembly connectors (SMA 905) that are present in the light source, spectrometers, sample holders, and other fiber-coupled accessories. Optical fibers are generally built similarly by drawing a thin strand of silica glass from a glass rod called the preform. The cladding wraps the thin strand (the core) to hold the light inside and, finally, the coating (buffer) to protect the entire system, as shown in *Figure 2.16*.

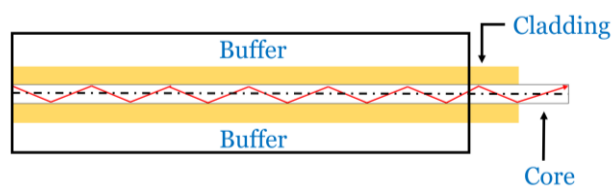


**Figure 2.16.** Representation of the anatomy of an optical fiber

The working principle of optical fibers is based on the refraction and reflection of light. It consists of guidance of rays of light propagating through the fiber, precisely through the core. The core must have a refractive index higher than that of the cladding, which means that each time the ray of light hits the interface between the cladding and the core, it will be reflected back to the core (total internal reflection). This difference in refractive indexes is resulting the guidance of light along the length of the fiber with very low attenuation [158,159].

These silica-core fibers are labeled through boot collar color depending on the nature of the wrapping buffer, indicating the type and most efficient wavelength range and to which applications are compatible. For example, the gray boot collar indicates that the fiber is solarization-resistant and most efficient for applications like fluorescence, the red boot collar for applications in the VIS-NIR range, and the blue boot collar for UV-VIS applications.

In this thesis work, and depending on the conducted experiment, mainly how much the light source is intense<sup>1</sup>, we used in our investigations a 50  $\mu\text{m}$ -optical fiber for calibrations, 100  $\mu\text{m}$  for transmittance measurements, 400  $\mu\text{m}$  for absorption and fluorescence measurements, 600  $\mu\text{m}$  for colorimetric measurements (supplied from Ocean optics and Avantes).

### **2.5.5.B. Collimators and optics**

In fiber-coupled equipment, collimators convert divergent light into parallel rays, which allows a well-controlled field of view (FOV), a focalized beam of light, and the efficiency of the transmitted light. The collimators can easily be inserted or removed and attached directly to the optical fibers through the standard SMA 905 connector.

---

<sup>1</sup> It is essential when using an intense potent light source to not saturate the spectrometer, a reason to use thinner optical fiber

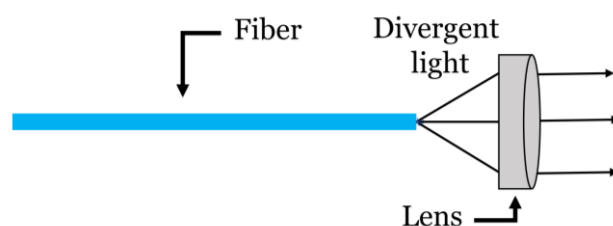


**Figure 2.17.** Representation of fiber collimator principle

### 2.5.5.C. Filters and color correctors

Filters can absorb light in a particular region of the electromagnetic spectra. They can be inserted on the top of the assembly, *i.e.*, next to the source light, or on the bottom, *i.e.*, next to the spectrometer. In general, there are three types of glass filters: high-pass filters used in fluorescence and Raman spectroscopy to block excitation energy, correction filters (balancing) that aims to absorb energy in a particular region and let pass the rest, and finally, bandpass filter employed to transmit the light in the selected range. For some experiments, we employed high-pass filters recommended in luminescence measurements and color correction filters, ideally for absorption and transmission; for instance, the FG3 filter was employed to enhance the blue and red region, and the OF2-GG395 filter transmits wavelengths  $> 395$  nm to reduce the emission of the excitation LED.

### 2.5.6. Integrating sphere

An integrating sphere (IS) is an optical component consisting of an empty spherical cavity covered with white reflective layers permitting light diffusion, widely used in photometry to test light bulbs and LEDs intensities. The IS principle is based on Lambertian reflectance theory, which assumes that introduced rays of light are scattered uniformly in a diffusing way and therefore assure equal distribution in the whole system. Inside the sphere, there is a baffled detector that collects uniform light signals, whereas the role of the baffle is to prevent the first reflection to enters the detector, and only homogenized reflections are collected.

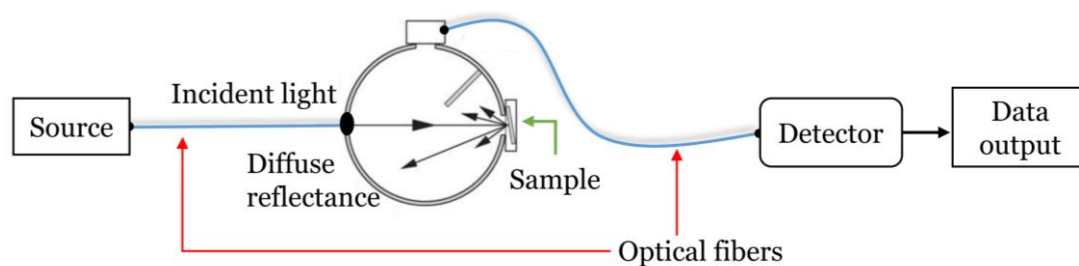


**Figure 2.18.** Representation of the working principle of the integrating sphere setup

In this work, an integrating sphere setup (*Figure 2.18*) was employed to measure the total integrated reflectance of solid surfaces, *i.e.*, textiles, based on the diffuse reflectance spectroscopy (DRS)<sup>1</sup> principle, allowing for the conduction of colorimetric and fluorescence experiments on textile fabrics. Avasphere 30 is connected via optical fibers to a white light source (LS-1 or Avalight HAL) and one of the spectrophotometers (USB4000 or QE65000).

In this chapter, the instruments and techniques that were used in this thesis work were addressed with more given details in the following chapters and especially where used.

---

<sup>1</sup> DRS is a technique that measures the reflectance based on absorption and scattering, both of which vary with wavelength to produce the reflectance spectrum.

---

---

## **Chapter 3 A sol-gel process for dyeing cotton in the perspective of functionalized textiles**

### **3.1. Introduction**

The coloring of textiles is an essential step in textile production. In this chapter, we aimed to dye cotton fabrics using functional surface coatings as an alternative to traditional dyeing methods. We used sol-gel processing to create thin coatings on the surface of the textile substrate that contain dye molecules, giving the fabric its color. We studied and improved the process to make it more environmentally friendly and sustainable.

### **3.2. Sol-gel chemistry**

#### **3.2.1. Overview**

There has been a vivid interest in using sol-gel<sup>1</sup> chemistry to modify the surface properties of substrates and impart new functionalities for specific applications. It has been recognized that the sol-gel process is a powerful tool for modifying substrates. Originally developed by Stöber in 1968 for the synthesis of silica nanoparticles, the method has gained widespread recognition for its ability to produce size- and shape-controlled particles [160]. Afterward, the sol-gel

---

<sup>1</sup> Is a type of soft-chemistry that uses reactions at room-temperature to produce solid materials from the assembly of small molecules typically monomers into integrated polymeric networks. The solid phase is obtained after thermal treatment.

process has been used not only for nanoparticle synthesis but also for applying thin layers (or multiple layers) onto chosen substrates by promoting the growth of polymers on the treated substrate, resulting in the deposition of thin layers with specific properties. These thin layers give the substrate new functionality and performance.

Silica-based sol-gel formulations remain to be the most explored, studied, and discussed, and yet more to come. The most known is tetraethyl orthosilicate (TEOS), which is mainly used as a crosslinker in silicone polymers and as a precursor to silicon dioxide for the preparation of semiconductor materials [161,162]. Later, various metal-alkoxide-based precursors were employed to prepare sol-gel formulations, *e.g.*, titanium, hafnium, thorium, and zirconium alkoxides [163–165].

### 3.2.2. Sol-gel reactions

The sol-gel reaction passes through the hydrolysis and condensation steps:

**First step:** The hydrolysis, as shown in (*Figure 3.1*) is the reaction permitting to obtain of silanols monomers by transforming OR to OH groups (1). The hydrolysis process depends on how much water is present in the media and the type of catalyst used.

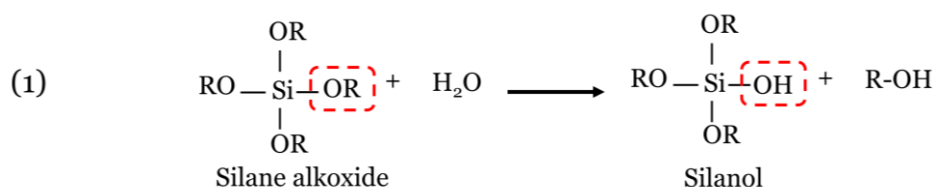


**Figure 3.1.** Sol-gel hydrolysis step

**Second step:** The condensation step is the polymerization of silanols to form siloxanes. These silanols can be obtained from the condensation of hydroxyl groups of the silanols to form siloxane with the liberation of water (2) or the reaction of silanol with unreacted silane alkoxide with the liberation of alcohol (3), as shown in *Figure 3.2*.

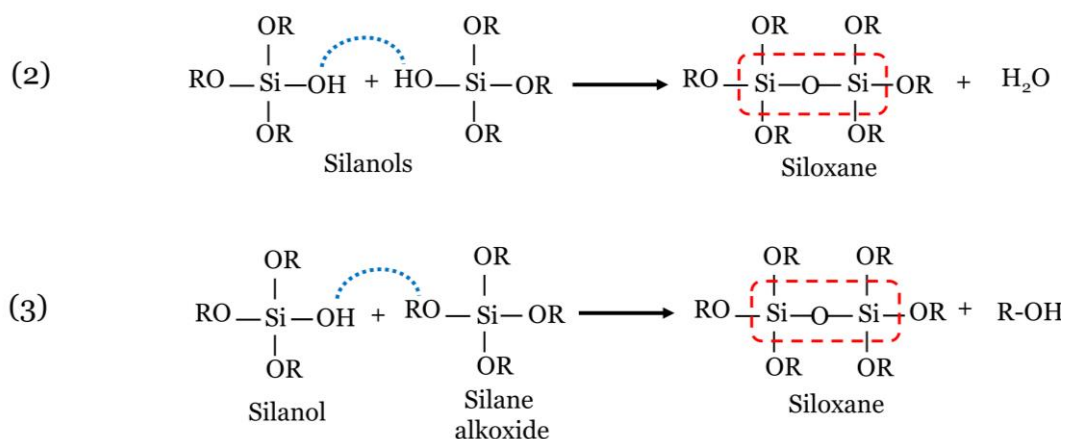


**Figure 3.2.** Sol-gel condensation steps. Water condensation (2), alcohol condensation (3)

Once the reaction ends, a network will be formed (called wet-gel). The prepared formulation can be deposited as a thin film or treated to elaborate nanoparticles and aerogels.

These sol-gel formulations are not standardized. Many factors can interact and affect the final aim, *e.g.*, type of precursor, temperature, reaction time, alkoxide concentration, the concentration of other reagents, type of catalyst, presence or absence of catalyst, and other factors [166–169].

### 3.2.3. Sol-gel in surface coatings

The interest of the sol-gel process is that it is suitable for various substrates, *e.g.*, ceramic, glass, and metallurgic materials [170,171]. Since this process allows the integration of organic compounds (among others) in alkoxide skeletons organized to form thin layers, offering, by that, several advantages compared to other functionalization techniques (*e.g.*, doctor blade coating). The sol-gel process permits the addition of valuable functionalities to textile fabrics and gives them new properties for specific applications.

As previously seen, plenty of works were conducted to incorporate functional materials into textile fabrics through the sol-gel method, including organic compounds and nanoparticles that are applied to the textile fabric via different techniques. These techniques can be simple such as spray and dip coatings (*see sections 2.3.1 and 2.3.3*), or require a specific dispositive, for example, the electrospinning and or chemical vapor deposition (CVD)[172,173].



### **3.2.4. Experimental conditions**

Regarding the works conducted in this thesis, the following conditions were respected and investigated for further improvements:

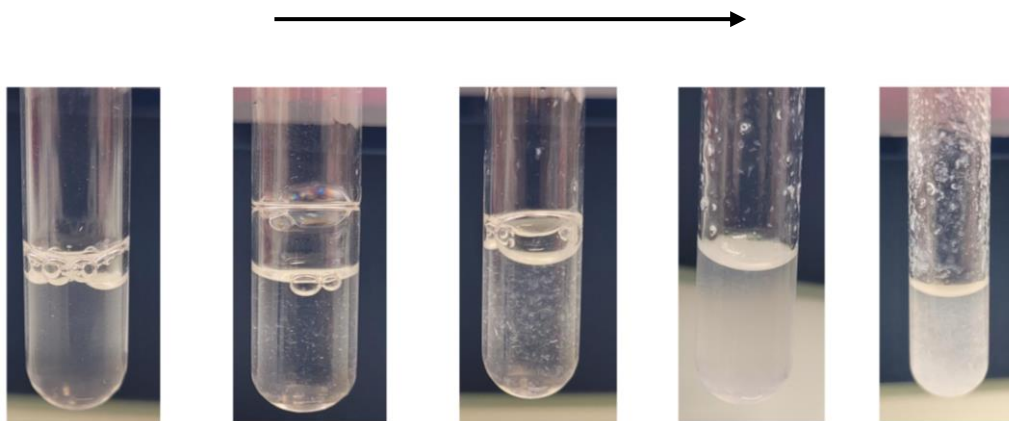
- The molar ratio for the sol-gel formulations was respected based on previous works conducted by our research team in the same field of textile functionalization [143,174,175]. This ratio is (5:0.008:55:60) for (precursor:HCl:EtOH:H<sub>2</sub>O).
- Acid is used as a catalyst in the sol-gel formulation, and its use in small amounts is to avoid the deterioration of cellulosic fiber when high acidic concentrations are employed.
- The choice of the precursor is basically related to cost and availability. In this work, *n*-propyltriethoxysilane (*n*PTES) and TEOS were investigated. Nevertheless, the TEOS precursor was quickly discarded from the list for two reasons, which will be discussed in the next section.

#### **3.2.4.A. Why TEOS is not a suitable precursor for our studies**

Since this chapter is dedicated to dyeing and using dyes, TEOS and *n*PTES-based sol-gel formulations were prepared using commercial dyes as additives. The dyes were supplied by the CHT group (Tübingen, Germany), which produces dyestuffs destined for the textile industry. However, the supplier does not provide the chemical structure, purity, or any information other than the final color in the aqueous medium.

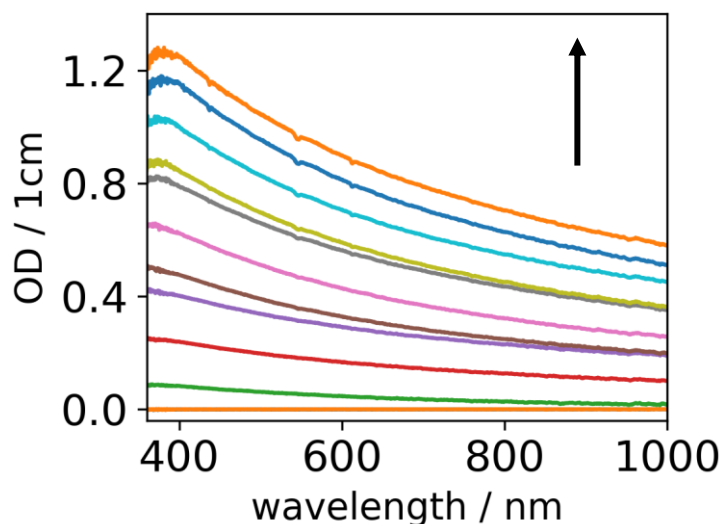
After the sol-gel reaction ends, in a few minutes, the TEOS-based solution starts hardening and becoming gel, which was not noticed for the *n*PTES-based solution. A phenomenon that was explained later by the basicity of the dye that causes the solution to form colloids and, therefore, a hardened gel. In fact, the dye, which acted like an alkaline catalyst, accelerated the polymerization and caused the rapid formation of large-size particles.

Figure 3.3 shows a separate experiment in which TEOS-based sol-gel solution without the presence of dye, to which small amounts of NaOH are added. Note that the solution before any addition of NaOH is limpid and transparent.



**Figure 3.3.** NaOH effect on TEOS-based sol-gel solution. The arrow direction indicates more NaOH added

Furthermore, this phenomenon was studied using extinction spectroscopy to observe the effect of adding NaOH to the TEOS-based sol-gel solution. To this end, a cuvette was filled with a known volume of sol-gel solution to which  $1.5 \times 10^{-6}$  mol of NaOH was added each time with stirring and recorded absorption spectra between each add.



**Figure 3.4.** Extinction spectra of TEOS sol-gel solution when NaOH is added

Adding NaOH causes an increase in the optical density of the solution (*Figure 3.4*). This increase is caused by light scattering<sup>1</sup>. The light scattering by the solution results from the formation of silica particles that was accelerated by adding NaOH.

Another reason not to use TEOS as a precursor for the elaboration of coatings is explained through the study of gold nanoparticles and their immobilization in sol-gel frameworks. Here, different sol-gel solutions with gold nanoparticles were prepared using *n*PTES and TEOS precursors with respect to the conditions mentioned in *section 3.2.4* and used to coat glass slides (used in optical microscopy). The polycondensation of the 3D network forms a thin film on the surface of the glass; after drying and annealing, TEOS coating films break and shatter into pieces, causing their separation from the substrate. In contrast, *n*PTES-based films demonstrate good homogeneity, as shown in *Figure 3.5*.

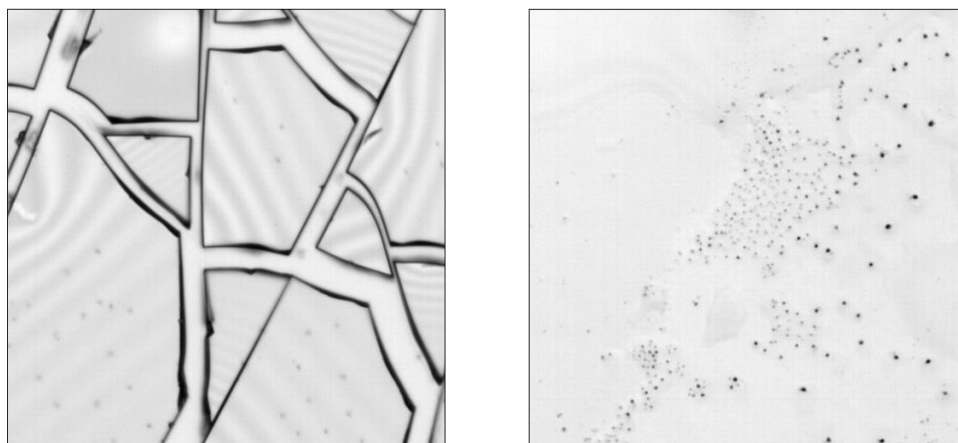


**Figure 3.5.** Optical microscope images (obj x20 times, long-pass filter cut-on at 550 nm) of TEOS (left) and *n*PTES (right) coatings of a thin glass slide, incorporating 80 nm gold nanoparticles (black spots)

According to the literature, TEOS can easily form siloxane bonds (Si-O-Si) after complete hydrolysis of the alkoxides, especially when an excess of water is present. TEOS is employed to elaborate silica glass and silica nanoparticles (SiO<sub>2</sub>) and is not suitable for coating applications (especially applications in which flexibility is required) unless mixed with other

---

<sup>1</sup> Light scattering is the process by which small particles scatter light, causing deviate from straight trajectory.

precursors such as PDMS (polydimethylsiloxane), VTES (vinyltrimethoxysilane) or other silica-free monomers as MMA (methyl methacrylate) [176–178]. As far as we are concerned, we confirmed that using TEOS in the coating formulation for textiles does not give satisfactory results. Even if the coating does not break, the brittle character of this coating will change the rigidity and mechanical properties of the fabric.

For these reasons, we employed *n*PTES as the primary precursor to prepare sol-gel formulations in the conducted sol-gel experiments of this thesis.

### 3.3. Practical realization

#### 3.3.1. Preparation of dye molecules

As previously seen in *section 3.2.4.A*, we decided to preferably synthesize our own dyes with controlled acidity and known chemical structures to avoid the accelerated gelation of the sol-gel solution. We chose to synthesize azoic dyes because of their simple obtain and also because of their various use in the dyeing and finishing of textile fabrics. To this end, four dye molecules were synthesized in the process of dyeing cotton fabric with the sol-gel method. The classic synthesis procedure of azoic dyes was followed, with minor changes involving diazotization and the coupling steps [179,180]. The dyes are labeled TA01...TA04. The details on the synthesized molecules are gathered as *appendixes* at the end of this chapter.

#### 3.3.2. Optical characterization of the dyes in solution

Besides the molecular characterization of the dyes, the photophysical properties of these synthesized molecules were investigated, precisely absorption and molar attenuation coefficients in solution and how they behave in different solvents. Traditionally, absorption measurements are performed in cuvettes using UV-visible spectroscopy based on the Beer-Lambert-Bouguer law.

These color-bearing molecules are highly soluble in water due to the presence of sulfonic groups in the molecular structure; in contrast, they are not well soluble in ethanol.

Concentrated stock solutions of the chromophores were prepared using highly purified water as the solvent. Afterward, the stock solutions were diluted using different solvents, *i.e.*, water, absolute ethanol, phosphate-buffered saline solution (PBS), and 0.1M sodium hydroxide (NaOH) to have an optical density inferior to 1 ( $OD < 1$ ). Measurement set-up was reported in section 2.4.3.

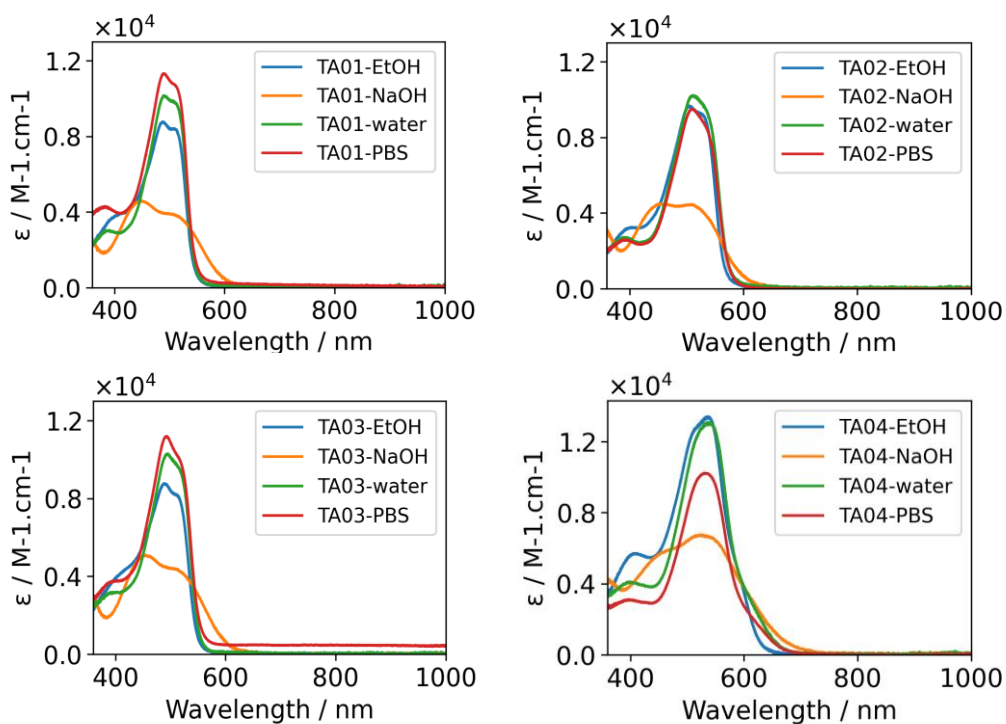


**Figure 3.6.** Absorption spectra of the dyes in H<sub>2</sub>O, EtOH, NaOH, and PBS

Generally, the chromophores display similar absorption spectra in water, ethanol, and PBS, with minor shifts in wavelengths and different molar attenuation coefficients. However, in alkaline media, the addition of NaOH can cause changes in the shape of the absorption spectra, resulting in hypsochromic and hypochromic shifts related to the protonation or deprotonation of the molecule. Azoic dyes contain conjugated systems with a large number of delocalized  $\pi$ -bonds [181], and their behavior can be affected by pH changes, sometimes resulting in a change in coloration, which allows them to be used as indicators such as methyl orange and congo red [182–185]. *Table 3-1* lists the maximum absorbance of the dyes in different solvents and their corresponding molar attenuation coefficients.

**Table 3-1.** Maximum absorption wavelength and corresponding molar extinction coefficient of the dyes in different solvents

<i>Dyes</i>	$\lambda_{\text{max}}$ (nm) (H <sub>2</sub> O)	$\epsilon$ water (M <sup>-1</sup> .cm <sup>-1</sup> )	$\lambda_{\text{max}}$ (nm) (EtOH)	$\epsilon$ EtOH (M <sup>-1</sup> .cm <sup>-1</sup> )	$\lambda_{\text{max}}$ (nm) (PBS)	$\epsilon$ PBS (M <sup>-1</sup> .cm <sup>-1</sup> )	$\lambda_{\text{max}}$ (nm) (NaOH)	$\epsilon$ NaOH (M <sup>-1</sup> .cm <sup>-1</sup> )
TA01	490	10130	489	8769	490	11330	448	4580
TA02	512	10180	505	9600	509	10220	445	4460
TA03	495	10200	490	8634	492	11780	454	5100
TA04	539	13045	537	13250	532	10100	450	5800

### 3.3.3. Preparation of sol-gel dyeing solutions

The chromophores (TA01... TA04) were used to prepare sol-gel dyeing solutions following our previous work [143]. Molar ratios of (5:0.008:55:60) for (precursor: HCl: EtOH: H<sub>2</sub>O) were mixed, followed by adding the dye to have a concentration of 2.0 g.L<sup>-1</sup>. The mixture is stirred for 3 hours at 70°C, cooled down, and transferred to a capped glass storage bottle. The prepared solutions are kept in the fridge at 4°C until their use.

**Table 3-2.** Molar concentration of the prepared sol-gel solutions

Samples	TA01	TA02	TA03	TA04
Dye's concentration in the sol-gel	4.90x10 <sup>-3</sup> mol/L	4.56x10 <sup>-3</sup> mol/L	4.52x10 <sup>-3</sup> mol/L	4.42x10 <sup>-3</sup> mol/L

### 3.3.4. Dyeing the cotton fabrics

To apply the sol-gel solutions to the fabrics, the dip-pad-dry-cure method was used with a 1:8 (*w/v*) fabric-to-solution ratio, meaning that 1 g of fabric was dyed using 8 ml of sol-gel process solution. This method involves immersing the fabric in the dye bath and then pressing it with a roller to evenly distribute the dye throughout the fabric (*section 2.3.1*). The samples were dyed under the following conditions: a dye bath concentration of 2.0 g.L<sup>-1</sup> for 1 minute at room

temperature, with only one dyeing cycle (referred to as the initial sol-gel dyeing process). The dyed fabrics were then subjected to thermal treatment using infrared heat to enhance the polycondensation of the deposited films and improve the mechanical properties of the final fabric. *Figure 3.7* shows the dyeing conditions for the conventional (1) and initial sol-gel (2) dyeing processes.

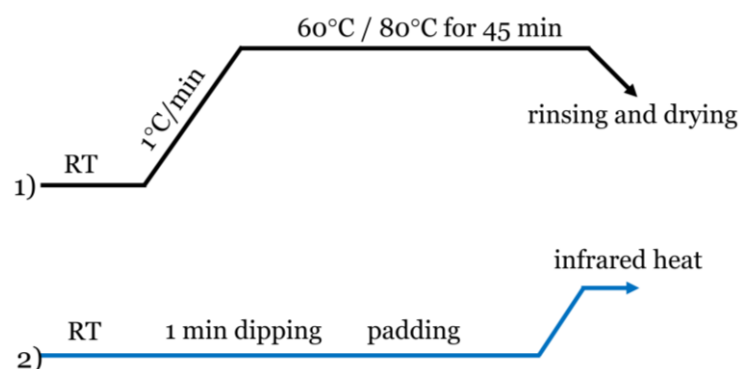


**Figure 3.7.** Conditions for dyeing of textile fabrics. (1) Conventional dyeing process. (2) Sol-gel dyeing process

Conventional dyeing systems require the use of heat while dyeing by raising the temperature by 1°C per minute for approximately 35 minutes up to 60°C, then stabilizing the temperature for 40-45 minutes between 60-80°C with continuous mechanical agitation, followed by washing the samples with hot and cold water respectively [186,187]. In contrast, the sol-gel process performs dyeing at room temperature (RT) in a matter of several minutes. Only afterward a thermal treatment is required [188] to evaporate solvents and enhance the polycondensation of the sol-gel matrix. In this case, *n*PTES silane precursor was employed to prepare the sol-gel dyeing solution that acts as the mordant and links the dye to the cellulosic fiber with hydrogen and electronic bonding, as demonstrated in *Figure 3.8*.

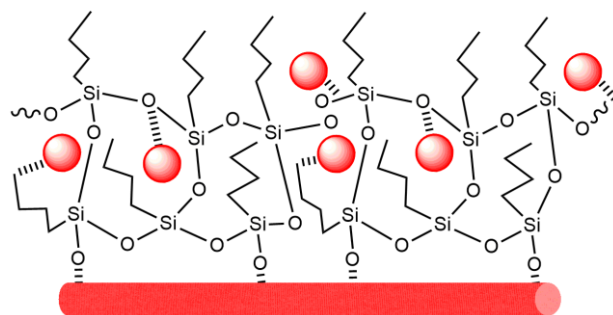


**Figure 3.8.** Representation of the formed thin film on the surface of the cotton fabric. In general, this type of silane precursor permits to create weak bonding, such as hydrogen and Van Der Waals interactions, to form a three-dimensional framework

*Table 3-3* collects the visual aspect of the dyes diluted in (EtOH) and also the final shades of the cotton fabrics dyed via the sol-gel method using the process depicted in *Figure 3.7*. Among the advantages of dyeing by the sol-gel is that the deposited thin film does not affect the mechanical properties of the final fabrics and keeps its flexibility and touch, contrarily to the knife-coating, for example, that adds a whole new thick layer to the surface of the textile that changes the mechanical characteristics of the fabric.

**Table 3-3.** Visual aspects of the dyes dissolved in ethanol (first row) and the final aspect of the textile fabrics (second row)

Samples	TA01	TA02	TA03	TA04
Aspect in ethanol solution diluted to ~0.01 mM				
Fabrics prepared via the sol-gel method				



### 3.3.5. Surface morphology and composition characterizations

SEM analysis was conducted to observe the sol-gel film and its adhesion to the cotton. As expected, untreated cotton represents a slight level of natural irregularity. In contrast, the SEM micrograph of the dyed sample with the sol-gel process shows the presence of welds and fillings between the yarns, with certain homogeneity of deposits consisting of silica layers (*Figure 3.9*). The deposited film aims to protect and encapsulate the dye and create different bonding frameworks of silica-based dye.

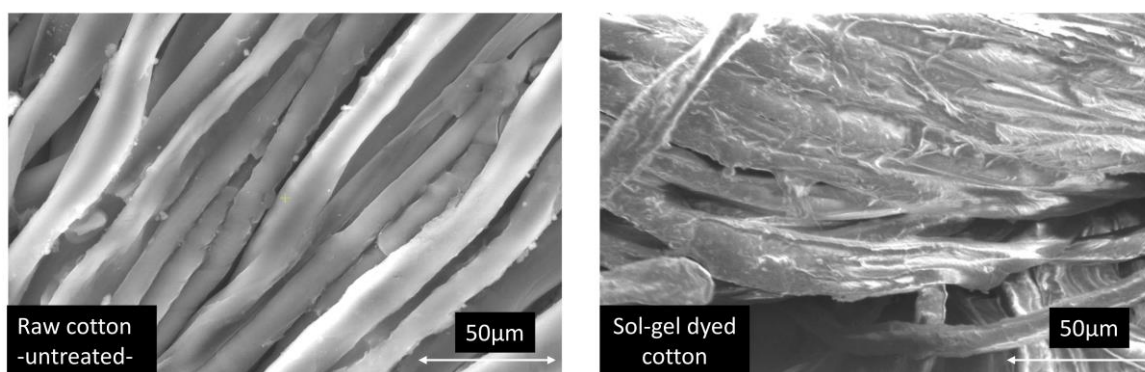


**Figure 3.9.** SEM images of untreated white cotton (left) and dyed fabric with the sol-gel (case of TA02, right)

The chemical composition of untreated and treated fabrics was determined by elemental analysis using EDS, as represented in *Figure 3.10* and *Table 3-4*. The analysis of raw cotton showed the presence of common elements like C, O, Na, Cl, and Ca. As for the samples after dyeing, Si and N elements appear, resulting from the silane precursor and the dye's azo group (-N=N-).

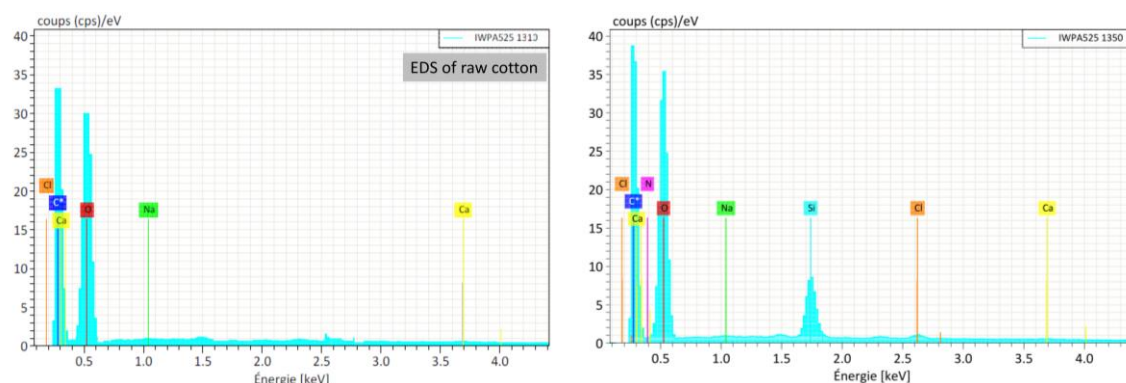


**Figure 3.10.** EDS spectra of untreated white cotton (left) and dyed fabric with the sol-gel (case of dye 02, right)

*Table 3-4* assembles the atomic and weight rates of the chemical elements of the raw cotton fabric as untreated and the dyed fabrics using the sol-gel method (TA01...TA04). These data were collected from the original EDS analysis of the fabrics. The chemical composition of the fabrics remains approximately the same with minor variations, and since the same sol-gel dyeing process was performed for all the fabrics, these slight differences are probably due to the molecular structure of the dyes.

**Table 3-4.** Elemental analysis of the fabrics dyed via the sol-gel process

Sample	C		N		O		Na		Si		Cl	
	weight %	atomic %	weight %	atomic %	weight %	atomic %	weight %	atomic %	weight %	atomic %	weight %	atomic %
<b>Raw</b>	37.80	45.57	o	o	57.81	52.33	1.40	0.88	o	o	0.01	0.01
<b>TA01</b>	37.38	44.91	4.35	4.74	59.13	53.34	0.71	0.45	1.77	0.91	0.70	0.28
<b>TA02</b>	38.29	40.94	6.46	5.74	56.83	51.39	0.66	0.41	1.65	0.81	0.65	0.22
<b>TA03</b>	35.58	42.24	4.38	4.38	61.39	54.37	0.87	0.60	0.32	0.63	2.50	3.24
<b>TA04</b>	37.56	43.37	5.45	5.59	56.83	51.87	0.92	0.57	1.43	1.03	0.19	0.08

### 3.3.6. Optical investigation of the fabrics

In this part, we describe the optical properties of the dyed fabrics and also monitor the dye bath of the sol-gel dyeing process, as schematized in *Figure 3.11*.

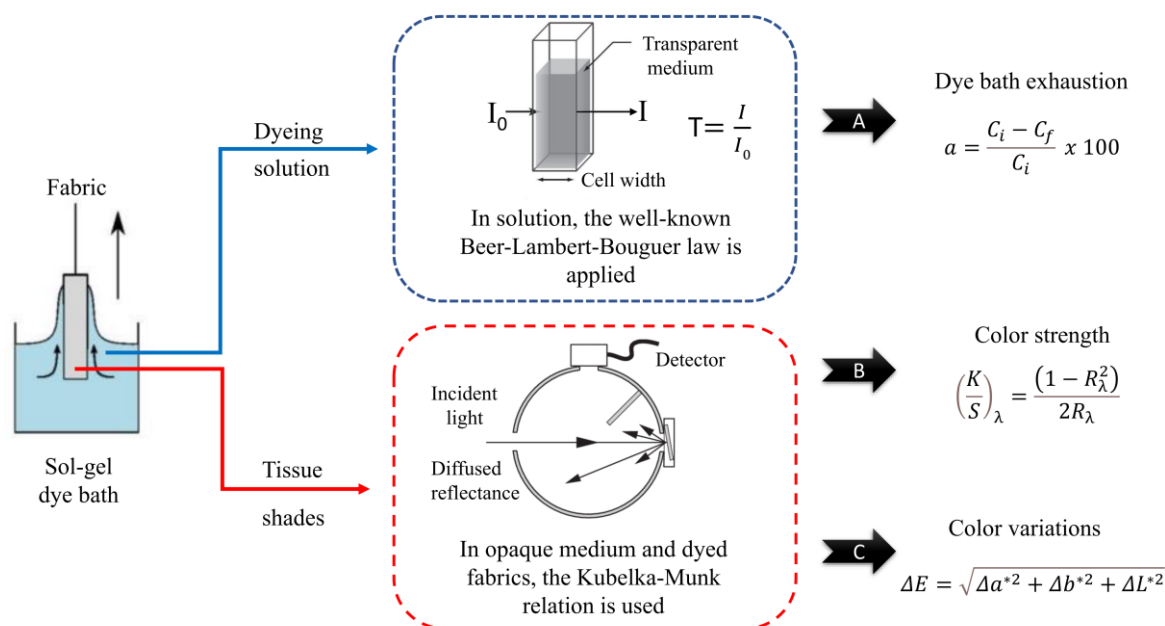


**Figure 3.11.** How optical monitoring is performed for the fabrics and the dyeing baths

The analysis focused on monitoring the dyeing solution before and after the dyeing process to determine the amount of dye transferred from the bath to the fabric. This analysis is done using UV-vis spectroscopy, and the calculated parameter is commonly known as the pick-up rate, adds-in rate, or also exhaustion rate, expressed in percentage. Further, on the fabric's side, the colorful aspect of the fabrics was evaluated using two different instruments, even though both are based on the same principle: diffuse-reflectance spectroscopy. This analysis was done using an integrating sphere and Datacolor instrument (As shown in sections 2.4.5 and 2.5.6).

### 3.3.7. Exhaustion and monitoring of the dyeing baths

To determine the exhaustion rate of the sol-gel dyeing bath, calibration curves for each dye were recorded first on the UV-vis instrument and used to measure the concentration of the

bath before and after the dyeing process ( $C_i$  and  $C_f$ ). The amount of absorbed dye ( $a$  %) on the fabric is calculated using Equation (3.1) and expressed as the exhaustion rate.

$$a = \frac{C_i - C_f}{C_i} \times 100 \quad (3.1)$$

where  $C_i$  is the initial concentration and  $C_f$  is the final concentration of the dye in the bath. The calculated amounts of dye that were transferred from the bath to the textile fabric are listed in *Table 3-5* with given average values based on three independent measurements.

**Table 3-5.** Amount of bath exhaustion/dye pick up using the sol-gel primary process, measured using UV-visible, applying equation (3.1)

Sample	TA01	TA02	TA03	TA04
Dyeing conditions	1 min/ 1cycle/ RT °C	1 min/ 1cycle/ RT °C	1 min/ 1cycle/ RT °C	1 min/ 1cycle/ RT °C
$a$ % Exhaustion	3.13± 0.83%	10.26± 0.94%	3.77± 1.01%	11.91± 0.79%

As can be noticed, the fabrics differ in the amount of bath exhaustion, although the same dyeing conditions were respected for all the samples—this difference is related to the affinity of the dyes.

### 3.3.8. Colorimetric measurements

Tissues were evaluated utilizing the Datacolor instrument (2.4.5) and Equation (3.2), which connect the CIELab parameters to give a response of color difference. In general, lower  $\Delta E$  values indicate greater accuracy; contrariwise, high  $\Delta E$  values indicate a significant mismatch.  $a^*$ ,  $b^*$  are the four unique colors of human vision, and  $L^*$  represents lightness [157,189,190] (details in section 2.4.5). The reported values are based on at least three dependent measurements.

$$\Delta E = \sqrt{\Delta a^{*2} + \Delta b^{*2} + \Delta L^{*2}} \quad (3.2)$$

*Table 3-6* gathers the colorimetric parameters of the untreated white fabric used as the reference and the treated dyed fabrics using the sol-gel method. Visually, with the naked eye,

the fabrics are dyed with pale orange, red, orange, and purple, respectively. Indeed, the colorimetric measurement demonstrates coherence between the visualized color and the given coordinates; whereas and taking TA04 as an example,  $a^*$  is a positive value that tends to the red area, and  $b^*$  is a negative value that corresponds to the blue region, in addition, the hue angle value  $h^\circ$  matches undeniably the violet zone.  $\Delta E$  is usually used to compare two samples that are similar in coloration; however, here, it has no significant indication since a white sample (untreated) is compared to colored samples, which delivers colossal difference values.

**Table 3-6.** CIELab coordinates of the samples obtained from the Datacolor instrument under D65 daylight and d/10° observer

Samples	L*	a*	b*	C*	h°	ΔE
Untreated	89.94± 0.19	00.72± 0.23	03.43± 0.09	03.50± 0.03	78.13± 1.62	0.01 <sup>#</sup>
TA01	67.56± 0.29	32.66± 0.18	17.09± 0.21	36.86± 0.59	27.62± 0.20	41.32± 0.31
TA02	58.96± 0.44	44.52± 0.22	01.13± 0.06	44.53± 0.29	01.45± 0.08	53.69± 0.13
TA03	66.79± 0.71	34.16± 0.13	17.38± 0.25	38.32± 0.73	26.96± 0.41	43.00± 0.32
TA04	41.85± 0.49	21.48± 0.24	-20.63± 0.19	29.78± 0.28	316.14± 0.35	57.64± 0.11

<sup>#</sup> The shown value expresses the difference between the three dependent measurements of the untreated white fabric. No value can be given since  $\Delta E$  is a comparative parameter, and this sample is the reference itself

### 3.3.9. Diffuse reflectance and Kubelka-Munk relation

Fabric samples were optically investigated using diffuse reflectance spectroscopy, which characterizes light reflectance from opaque materials. For ideally opaque diffusing materials, reflectance obeys the Lambert cosine law [191]. However, textiles and painted paper are not considered ideal diffusers nor ideal absorbers. The diffuse reflectance of these materials can be described in the Kubelka-Munk (KM) theory. KM theory calculates a parameter ( $K/S$ ) that connects the intrinsic absorption and the scattering of the colored, diffusing material to the measured reflectance, as given in Equation (3.3).

$$\left(\frac{K}{S}\right)_\lambda = \frac{(1 - R_\lambda^2)}{2R_\lambda} \quad (3.3)$$

Here,  $K$  and  $S$  are the absorbance and the scattering, respectively, and  $R_\lambda$  is the measured reflectance at the wavelength ( $\lambda$ ). KM theory models the appearance of painted films and how

the coloration changes by additional coatings and their thicknesses. According to KM theory, the (K/S) parameter at a given wavelength is proportional to the dye content in the tissue, as expressed in Equation (3.4).

$$\left(\frac{K}{S}\right)_{dye_i, C_i, \lambda} = P_{i, \lambda} \cdot C_i \quad (3.4)$$

Here,  $P_{i, \lambda}$  is the coefficient that depends on the used dye in the same wavelength [149,189]. This linearity is no longer accurate when high concentrations of the dye content occur, and significant deviations may be observed [192].

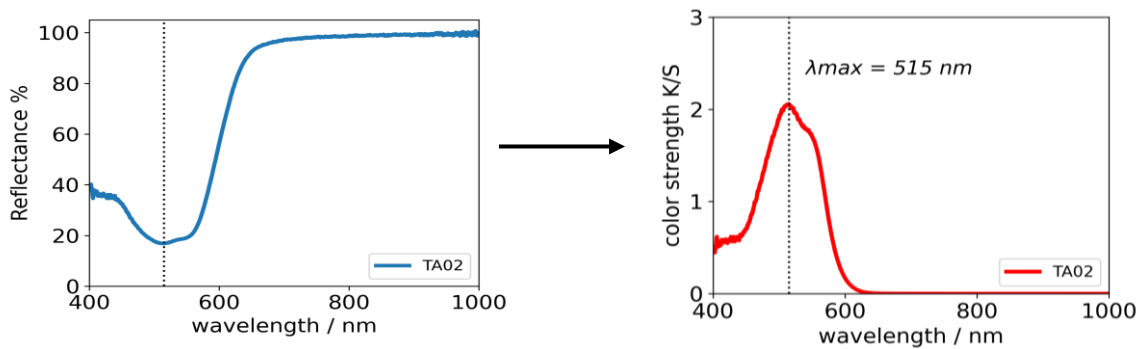


**Figure 3.12.** Reflectance spectrum of tissue fabric (averaged based on three measurements) and its conversion to K/S spectrum utilizing Kubelka-Munk relation expressed in equation 3.3. TA02 was used as an example

From this point, only the value of K/S (color strength) in the corresponding maximum wavelength will be presented. All values were given averaged based on three dependent measurements.

**Table 3-7.** Reflectance (%) and color strength (K/S) of the fabrics (tissues) on the corresponding maximum wavelength, obtained via the integrating sphere measurement

Sample	$\lambda_{max}$	Reflectance %	Color strength K/S
TA01	481 nm	20.60	1.53
TA02	515 nm	16.83	2.05
TA03	486 nm	17.85	1.89
TA04	543 nm	15.70	2.35

These optical investigations (*Figure 3.11*) constitute a complementary system to evaluate and monitor the dyeing process on both the fabric and the sol-gel dyeing bath and, therefore, will be the utilized analysis for the upcoming sections.

Hence and forward, and for clarity, only the studies of the dye TA02 and TA04 will be parallelly reported. The choice of TA02 and TA04 is related to the affinity and color strength that present these two dyes (*Table 3-5*).

### 3.4. Optimization of the sol-gel dyeing process

The initial sol-gel dyeing process is further studied to determine the most favorable conditions for dyeing. The experimental conditions affect the interaction between the sol-gel, the dye, and the cotton. Thus, there is a need to optimize the parameters that influence the final aspect of the dyed fabrics and the efficiency of the dyeing process. To this end, the exhaustion of the dye bath was monitored as well as the properties of the final dyed sample when a parameter was varied. The dye bath exhaustion, which was calculated using Equation (3.1), was studied side-to-side with the color strength (K/S) at the corresponding wavelength for each parameter. In addition, the colorimetric CIELab coordinates were also measured. The bath exhaustion and the K/S value measured on the dyed cotton are complementary parameters, quantifying the transfer of the dye (the coloration) from the bath to the textile fabric. These parameters are (i) dyeing temperature, (ii) dye concentration, (iii) impregnation time, and (iv) the number of dyeing cycles. These parameters will be detailed in the upcoming sections.

#### 3.4.1. Duration of impregnation

The duration of impregnation determines the time given to the dye and the sol-gel material to diffuse and become adsorbed at the surface, inside, and between the fibers. Depending on the nature of the dye, the optimal duration of impregnation differs. We have prepared a series of samples in which the duration of impregnation varies from 1 min, 30 min, 1 hour, 2 hours, 3 hours, and 4 hours. The dyeing was systematically performed at 23°C with a dye concentration of 2.0 g.L<sup>-1</sup> for only 1 dyeing cycle.

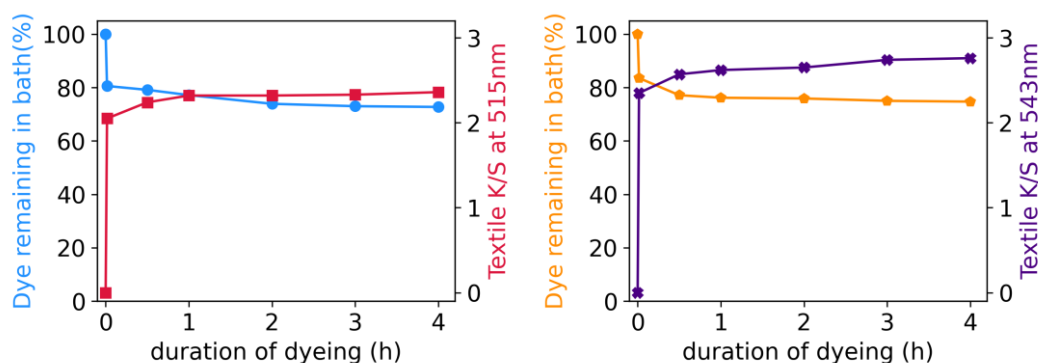


**Figure 3.13.** Dye bath exhaustion and the color strength of the dyed textile at the maximum corresponding wavelength are represented as a function of the duration of dyeing with the sol-gel process. Sample TA02 (left), sample TA04 (right)

As shown in *Figure 3.13*, the dye transfer in our sol-gel process is generally rapid. After only one minute, the dye remaining in the bath strongly decreases, and the color strength on the textile (K/S) increases to be close to the plateau value. This plateau is fully reached after 1 hour of exposure to the cotton in the bath. Beyond that duration, a slow increase takes place.

**Table 3-8.** Colorimetric CIE coordinates, reflectance (%R), and (K/S) color strength of the dyed cotton textile as a function of the dyeing time. The CIE cylindrical parameters were used because they give a more meaningful indication

Duration	CIE coordinates (D65/8°)						Kubelka-Munk (at $\lambda_{max}$ )					
	L*		C*		h°		$\Delta E$		R%		K/S	
Fabrics	TA02	TA04	TA02	TA04	TA02	TA04	TA02	TA04	TA02	TA04	TA02	TA04
Reference	89.9	89.9	3.5	3.51	78.1	78.1	o	o	100.0	100	o	o
1 min	52.0	39.7	51.0	30.9	5.6	323.1	o	o	16.86	15.29	2.05	2.35
30 min	51.3	36.3	51.6	31.3	5.5	319.5	1.43	2.15	15.82	14.27	2.24	2.57
1 hour	51.0	35.4	51.9	32.1	5.3	318.4	0.49	0.68	15.42	14.06	2.32	2.69
2 hours	51.0	35.8	52.1	32.2	5.0	316.9	0.26	0.88	15.42	13.95	2.32	2.65
3 hours	50.7	33.3	52.3	32.3	5.0	316.6	0.43	0.93	15.37	13.62	2.33	2.75
4 hours	50.4	33.1	52.4	32.4	4.8	316.3	0.56	0.99	15.22	13.55	2.36	2.76



Concerning the colorimetric characterization (*Table 3-8*),  $L^*$  (lightness) and  $C^*$  (chromaticity) change in opposite directions as the dyeing progress: if one increases, the other decreases. As for the  $h^\circ$  hue angle, it tends to  $0^\circ$  (or  $360^\circ$  for TA04) with prolonged exposure, meaning that the coloration becomes more red-tinted (violet-tinted for TA04) as positioned in the cylindrical CIELab colorimetric system (*see section 2.4.5*) [156,190]. Overall, the color difference ( $\Delta E$ ) indicates that after 30 minutes, the samples are similar in coloration since this value is inferior to 1. In conclusion, the colorimetric measurements confirm that the coloration gets deeper and darker when time increases, but most of the dyeing takes place in the first minutes of the dyeing process.

### 3.4.2. Number of dyeing cycles

The number of dyeing cycles was studied with the aim of seeing the effect of additional coatings on the obtained shade of color. It is imagined that each dyeing cycle adds a new "layer" of dye. Thus, fabrics were prepared in a way to have 4 samples for each dye: the first fabric is dyed only once, the second fabric is dyed twice, the third fabric is layered thrice, and the fourth fabric is dyed four times. For each dyeing cycle, the same sol-gel dye solution was re-used, *i.e.*, the dye solution was not refreshed between dyeing cycles on the same fabric, monitoring the exhaustion of the dye bath. The duration of impregnation was for 1 minute, at  $23^\circ\text{C}$ , in a solution of  $2.0\text{ g.L}^{-1}$  dye content.

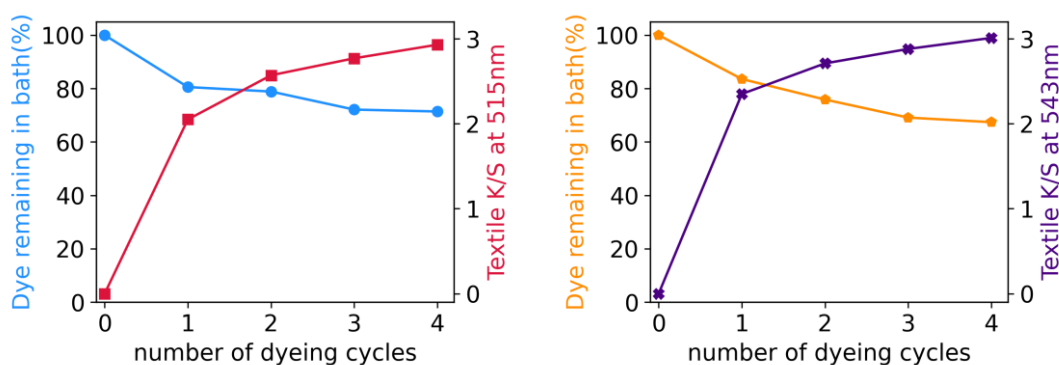


**Figure 3.14.** Dye bath exhaustion and the color strength of the dyed textile at the maximum corresponding wavelength are represented as a function of the number of dyeing cycles. Sample TA02 (left), sample TA04 (right)

Figure 3.14 shows the effect of the number of dyeing cycles on the sol-gel process. The dye bath exhaustion decreases significantly for the first process cycle, and the dye uptake continues for each additional deposited layer. Color strength K/S on the other hand, increases for each additional coating, which is in good agreement with the colorimetric measurements that show a diminution in the lightness of the samples and a hue angle that tends to 0° for the sample TA02 (red hue) as shown in Table 3-9. As for ΔE, the reported value indicates a difference between the samples, except for the last one.

**Table 3-9.** Colorimetric CIE coordinates, reflectance (%R), and (K/S) color strength of the dyed cotton textile as a function of the number of dyeing cycles. The CIE cylindrical parameters were used because they give a more meaningful indication

Duration	CIE coordinates (D65/8°)						Kubelka-Munk (at λ <sub>max</sub> )					
	L*		C*		h°		ΔE		R%		K/S	
Fabrics	TA02	TA04	TA02	TA04	TA02	TA04	TA02	TA04	TA02	TA04	TA02	TA04
Reference	89.9	89.9	3.5	3.51	78.1	78.1	o	o	100.0	100	o	o
1 cycle	52.0	39.7	51.0	31.9	5.6	323.1	o	o	16.86	15.29	2.05	2.35
2 cycles	48.3	35.0	52.6	32.4	5.5	325.9	3.50	4.11	14.29	13.69	2.57	2.71
3 cycles	46.8	33.7	52.9	32.7	4.8	327.4	0.96	0.31	13.50	13.11	2.77	2.88
4 cycles	46.4	32.6	52.9	30.0	4.7	322.1	0.82	0.85	12.93	12.62	2.93	3.01

In short, further intensification in shades requires multiple dyeing cycles instead of prolonged exposure time in a single cycle. We recall that the same dye solution was used for these multiple sol-gel cycles, further reducing the amount of dyes and chemicals used. These results suggest that several slabs of cotton may be dyed each for several cycles using the same dye bath.

### 3.4.3. Dyeing temperature

Existing dyeing processes use high temperatures (section 3.3.4). It is our goal to understand the effect of temperature on this sol-gel process and to use the lowest possible temperature. We performed dyeing at 23°C, 40°C, 60°C, and 80°C respectively, with only one dyeing cycle for 1 minute in a solution of 2.0 g.L<sup>-1</sup>.

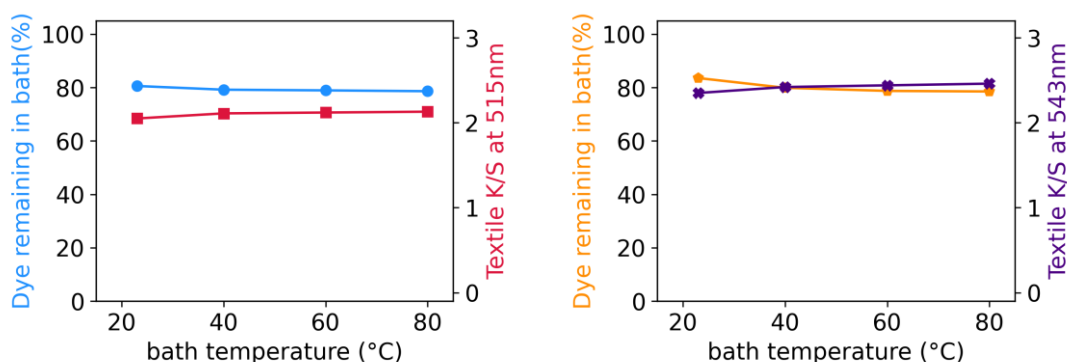


**Figure 3.15.** Dye bath exhaustion and the color strength of the dyed textile at the maximum corresponding wavelength are represented as a function of the dyeing temperature. Sample TA02 (left), sample TA04 (right)

The dye transfer from the bath to the textile depends weakly on temperature, as evident from *Figure 3.15*. At temperatures beyond 40°C, the transfer reaches an optimum. K/S value measured on the dyed cotton also obeys the same pattern of constancy with no significant increase in dyeing efficiency.

**Table 3-10.** Colorimetric CIE coordinates, reflectance (%R), and (K/S) color strength of the dyed cotton textile as a function of dyeing temperature. The CIE cylindrical parameters were used because they give a more meaningful indication

Duration	CIE coordinates (D65/8°)							Kubelka-Munk (at $\lambda_{max}$ )				
	L*		C*		h°		$\Delta E$	R%		K/S		
Fabrics	TA02	TA04	TA02	TA04	TA02	TA04	TA02	TA04	TA02	TA04	TA02	TA04
Reference	89.9	89.9	3.5	3.51	78.1	78.1	o	o	100.0	100	o	o
23 °C	52.0	39.7	51.0	31.9	5.6	323.1	o	o	16.85	15.29	2.05	2.35
40 °C	52.4	40.3	50.6	32.1	4.5	325.5	0.49	0.40	16.51	14.92	2.11	2.42
60 °C	53.8	41.9	51.0	31.9	4.4	325.4	0.58	0.47	16.46	14.83	2.12	2.44
80 °C	52.7	40.8	52.2	31.0	5.2	321.4	0.77	0.48	16.40	14.77	2.13	2.46

Colorimetric analysis shows that values are very close to each other, which means that the samples are similar in coloration and, more obviously, from the  $\Delta E$ , indicating that the samples are similar in coloration (*Table 3-10*). We understand that temperature has no binding effect on the dye affinity for the textile or the appearance of the dyed fabric. In fact, and as previously mentioned, dyeing at room temperature is considered as an advantage of the sol-gel dyeing method compared to traditional dyeing processes, wherein high temperatures are required to perform dyeing.

#### 3.4.4. Dye concentration

The point of raising the concentration of the dye in the sol-gel solution is to observe its effect on the obtained shade on the fabrics. For that, samples are dyed with solutions with concentrations of 1.0 g.L<sup>-1</sup>, 2.0 g.L<sup>-1</sup>, and 5.0 g.L<sup>-1</sup>. The dyeing was performed at room temperature for only 1 minute and 1 dyeing cycle.

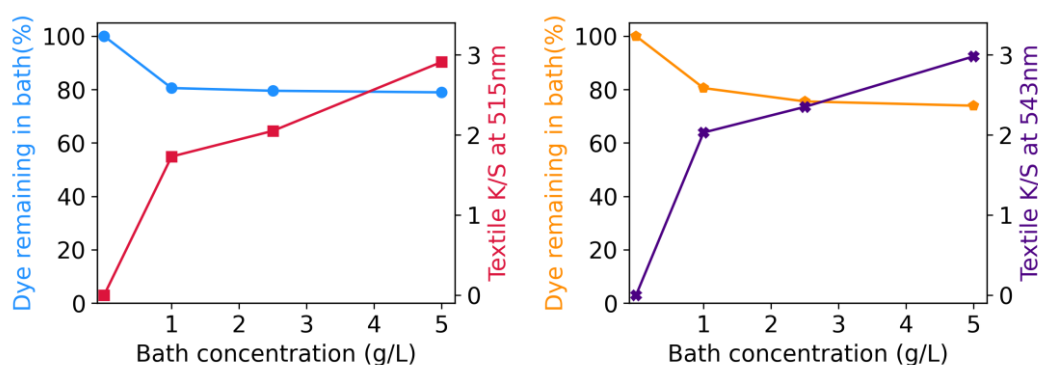


**Figure 3.16.** Dye bath exhaustion and the color strength of the dyed textile at the maximum corresponding wavelength are represented as a function of the concentration. Sample TA02 (left), sample TA04 (right)

The concentration of dye in the sol-gel dyeing solution has a remarkable influence. However, the remaining dye in the bath remains nearly constant. In contrast, color strength (K/S) increases as a function of raising the concentration of the dye (*Figure 3.16*).

**Table 3-11.** Colorimetric CIE coordinates, reflectance (%R), and (K/S) color strength of the dyed cotton textile as a function of dyeing temperature. The CIE cylindrical parameters were used because they give a more meaningful indication

Duration	CIE coordinates (D65/8°)								Kubelka-Munk (at $\lambda_{max}$ )			
	L*		C*		h°		$\Delta E$		R%		K/S	
Fabrics	TA02	TA04	TA02	TA04	TA02	TA04	TA02	TA04	TA02	TA04	TA02	TA04
Reference	89.9	89.9	3.5	3.51	78.1	78.1	o	o	100.0	100	o	o
1.0 g/L	60.3	42.3	49.1	32.1	7.1	325.5	4.82	1.46	18.97	16.97	1.73	2.03
2.0 g/L	52.0	39.7	51.0	31.9	5.6	323.1	o	o	16.86	15.29	2.05	2.35
5.0 g/L	47.0	37.0	53.7	30.3	4.4	321.2	5.41	1.44	13.00	12.77	2.91	2.98

Colorimetric analysis concurs with the previous observations whereby fabric gets less lightness, more deep saturation, and more redness (more purple for TA04), as *Table 3-11* shows. Coming to an end, the concentration in the sol-gel solutions has its effect on the obtained shades.

### 3.4.5. Optimized sol-gel dyeing process

Having investigated these operational parameters of the sol-gel process, an optimized sol-gel dyeing process is proposed in *Figure 3.17*. The following conclusions were applied:

The exposure time is fixed to be 30 minutes to allow ample time for the dye and the sol-gel material to diffuse into the fabric. Since the temperature has no remarkable influence, room temperature dyeing was chosen to perform dyeing. In contrast, the number of layers and the dye content notably influence dyeing; Hence, we choose 2 coatings to be performed at a dye bath concentration of 2.0 g.L<sup>-1</sup>. Considering that the final fabric was not washed at the end of the process, contrarily to the conventional fabric. This remark is essential and will be discussed in the following section.

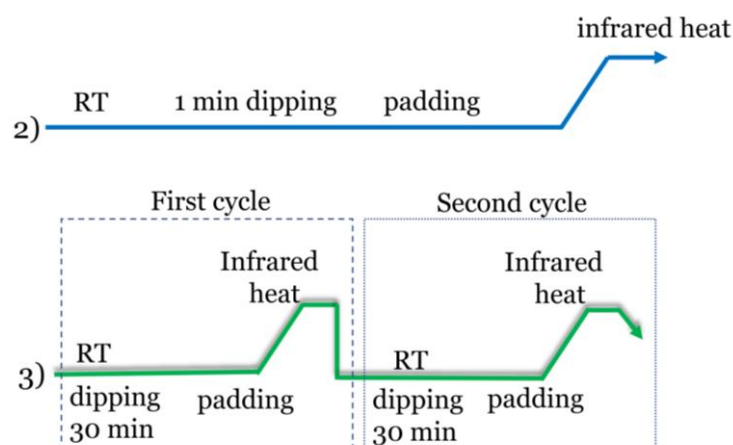


**Figure 3.17.** Initial sol-gel dyeing process previously discussed (2). Optimal generic sol-gel dyeing process by the sol-gel method, derived from the results of the present study (3). The fabric is dipped in the dye bath for 30 minutes with no mechanical agitation; afterward, aided by roller presses, the fabric is padded and then thermally heated to evaporate solvent (first cycle). The process is repeated again, guarding the same steps (second cycle)

The optimized sol-gel dyeing process, obtained based on the previous study, presents a list of advantages: performing dyeing at room temperature (RT), the total consumption of the dyeing solution, and reasonable dyeing time.

### 3.5. Colorfastness and durability

Now that the dyeing process was studied and the dyeing conditions were established to their optimum, it is essential to test the durability of the coloration. To this end, the color fastness test was conducted according to standards ISO105-C01, GB/T5713, and ISO 105X12, GB/T3920 for the color fastness to water and to rub, respectively.

#### 3.5.1. Experimental and measurements

Dyed fabric cuts of approximately 2x3 cm were placed separately in an oven-dried round bottom flask containing 30 ml of distilled water and 15 small iron balls, heated to 40°C, and stirred for 15 minutes. Diffuse reflectance spectroscopy and colorimetric parameters were investigated before and after the fastness test, as previously shown in *Figure 3.11*. Colorfastness was also evaluated via UV-vis spectroscopy using Equation (3.5).

Where  $C_{abs}=C_i-C_f$  is the amount of the absorbed dye on the fabric (*previously calculated using Equation 3.1*), and  $C_s$  is the concentration of the solution after the test (*i.e., the disgorging/leached amount*).





$$\beta = \frac{C_s}{C_{abs}} \times 100\% \tag{3.5}$$

### 3.5.2. Results

After the colorfastness test, the naked-eye analysis shows a difference in coloration compared to its state before the test (*Table 3-12*). Diffuse reflectance analysis showed approximately a 30% decrease in color strength for both samples. The colorimetric coordinates were explored here in delta ( $\Delta$ ) to show the difference between the two samples before and after the colorfastness test, whereas the lightness ( $\Delta L$ ) and the hue angle ( $\Delta h^\circ$ ) are larger indicating a significant difference before and after the washing test.

Two colors are considered similar when the color difference ( $\Delta E$ ) does not exceed the 1.0 value. Here, both samples have  $\Delta E > 1$ . Furthermore, based on Equation (3.5), the rate ' $\beta$ ' of leached dye in solution shows that the quantity leached in the solution is 31.7 % and 24.8 % for TA02 and TA04, respectively. From our standpoint, a significant amount of the leached dye can be explained by the fact that the fabrics were not washed after the dyeing process (*as mentioned in section 3.4.5*). Therefore, the unfixed dye leaches quickly in the solution. Another factor for consideration is the type of the formed bonding; since they are considered weak bonds and can break with the agitation and heat that were applied in the colorfastness test.

**Table 3-12.** Results of color fastness test provided by diffuse reflectance and UV-vis spectroscopies, and Datacolor

Fabrics	Before	After	K/S		$\Delta L$	$^1\Delta h^\circ$	$^1\Delta E$	% $\beta$
			Before	After				
Dye 02			2.18± 0.32	1.53± 0.22	15.76	19.69	8.52	31.74%
Dye 04			2.54± 0.13	1.81± 0.40	12.33	15.54	7.66	24.81%

### 3.5.3. Amelioration of the dye fixation

At this point, and henceforward, only the dyed fabric TA02 will be studied. Here, experiments were conducted to add more value to the dyeing process and force it with solid fixation of the dye through the cross-linking<sup>1</sup> process. Here, we aimed to fix the dye molecule covalently to the silica hybrid network through a two-step sol-gel process. Before discussing experimental details and preparation methods, it is essential to understand the different types of hybrid materials. Hybrid organic-inorganic systems can be classified into class I and class II, depending on if the interaction of the phases is weak or strong, respectively [193,194]. In general, the former type consists of interactions that do not need much energy to break, for instance, Van der Waals, hydrogen, and electrostatic interactions. On the other hand, class II hybrid consists of creating covalent bonds that involve sharing electrons to form electron pairs between atoms. These bonds require important energy to break [195]. In hybrid materials, it is also possible to meet the two types of interactions coexisting in the same system [193], as shown in *Figure 3.18*.

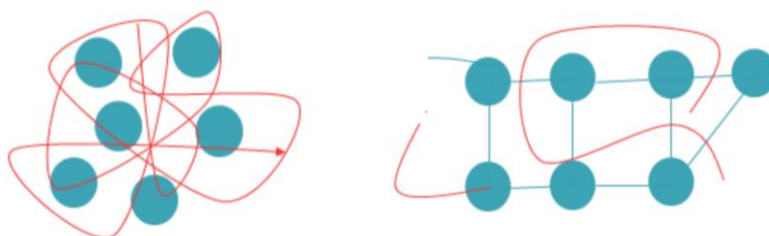


**Figure 3.18.** Representation of hybrid class I with weak bonds (left) and class II with strong bonds (blue links, right)

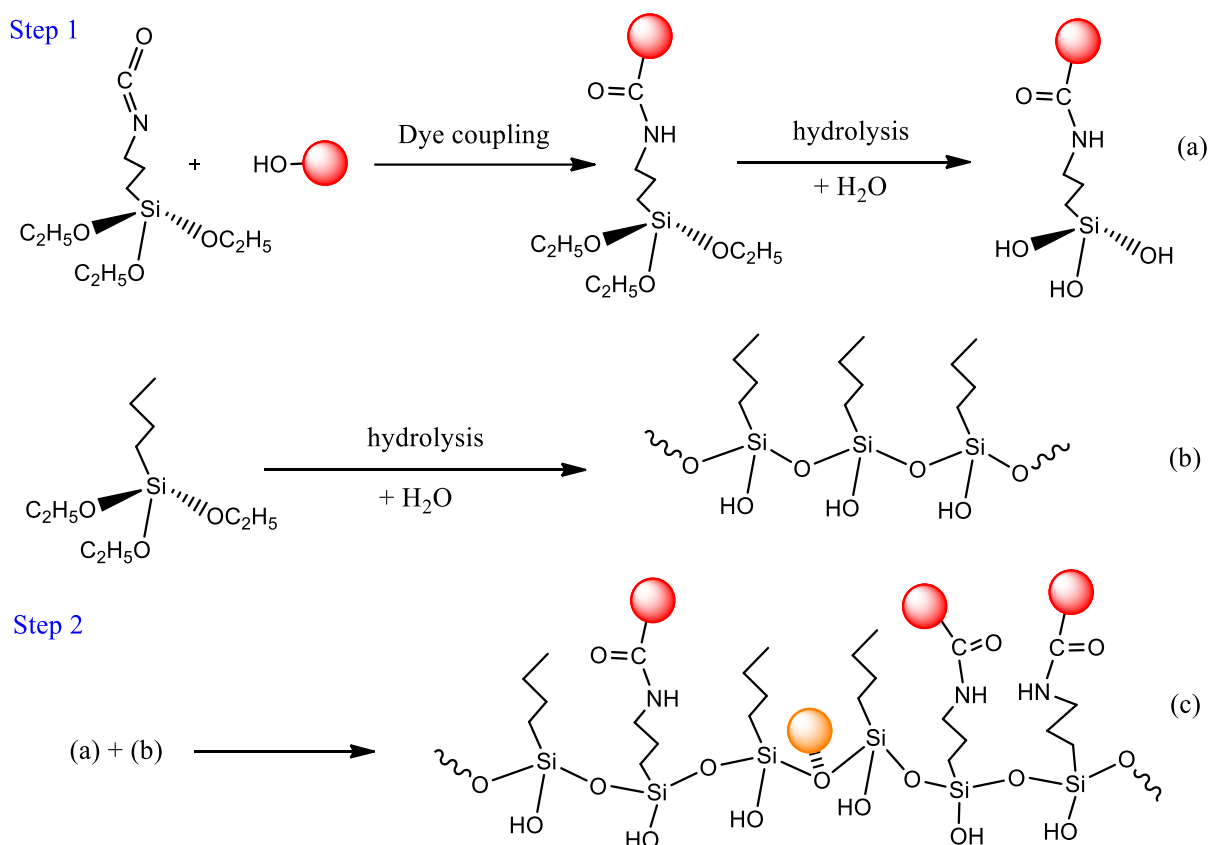
The two steps sol-gel process consists of first grafting the molecule to the silica framework by covalent bonds (step 1), utilizing a very reactive isocyanate function. After, the silane-based molecule is used to prepare the sol-gel solution aided by *n*PTES as a silane co-precursor

---

<sup>1</sup> Cross-linking is the art of chemically joining two or more molecules covalently using reagents with reactive functional end groups (primary amine, epoxy ring, sulfhydryls, etc.) that creates genuine bonds.



(step 2) following references [196–198] with minor changes (*Scheme 3-1*). Details on the synthesis and the characterization will be given as an appendix at the end of this chapter.



**Scheme 3-1.** Hydrolysis and polycondensation processes between the cross-linked dye and nPTES co-precursor. (a) : cross-linking of dye using 3-(triethoxysilyl)-propyl isocyanate as a precursor. (b) : formation of 3D sol-gel silica network using n-propyltriethoxysilane as co-precursor. (c) : polycondensation of (a) and (b) to form a 3D network of class II type, whereby genuine covalent bonds are formed (red), also weak bonds can be found (orange)

We consider the ungrafted and grafted samples, namely TA02 and TA020, to be tested for colorfastness to investigate the effect of grafting the dye to the silica network.

Results show that (*Table 3-13*): The naked-eye analysis shows a difference in coloration compared to its state before the test. Diffuse reflectance analysis showed a 20.64 % decrease in the color strength of sample TA02 versus only 9.86 % when the dye is grafted with the isocyanate function (TA020). The colorimetric coordinates were explored here in delta- $\Delta$  to show the difference between the two samples before and after the colorfastness test, whereas the lightness ( $\Delta L$ ) and the hue angle ( $\Delta h^\circ$ ) are more significant for the sample TA02, compared to TA020.

Objectively, two colors are similar when the color difference ( $\Delta E$ ) does not exceed the 1.0 value. Here, both samples have  $\Delta E > 1$ ; nevertheless, for the sample TA020, this value tends to be 1 and shows that the sample margin is smaller than the sample TA02.

**Table 3-13.** Crosslinking results of color fastness test provided by diffuse reflectance and UV-vis spectroscopies, and Datacolor

Fabrics	Before	After	K/S		$\Delta L$	$\Delta h^\circ$	$\Delta E$	% $\beta$
			Before	After				
TA02 (no crosslinking)			2.18± 0.32	1.53± 0.22	15.76	19.69	8.52	31.74
TA020 (crosslinking)			2.23±0.18	2.01±0.11	8.57	2.93	1.93	10.17

Diffuse reflectance spectroscopy and colorimetric CIELab coordinates confirm that using the two steps sol-gel process and grafting the dye covalently before its application improves the colorfastness of the samples. Furthermore, based on Equation (3-5), the rate ' $\beta$ ' of leached dye in solution shows that more than 30 % leached in the solution *vs.* 10 % for the sample TA020. This demonstrates that grafting the dye significantly enhances the colorfastness of the samples.

### **3.6. Conclusion**

This chapter reported a functionalization approach to dye textile fabrics employing the sol-gel process. Cotton fabrics were successfully dyed using an optimized low-temperature sol-gel method. In combination with the sol-gel, the dyes show a good affinity for the textiles and give a color nuance of adequate quality. The sol-gel dyeing was achieved via the pad-dry-cure process using sol-gel solutions. The study of four critical parameters (temperature of dyeing, time of impregnation, number of dyeing cycles, concentration of the dye in the bath) that might affect the dyeing efficiency and the shade of the color was carried out. It was found that dyeing with the sol-gel process could be carried out efficiently at 23°C, using an impregnation time of 30 minutes with two dyeing cycles. In conclusion, dyeing textiles by the sol-gel process gives satisfactory results and is an exciting alternative to existing dyeing processes.

As the present sol-gel process may be used with functional materials other than the model dyes used in this study, these results open perspectives toward the inclusion of other functionalities (other dyes, nanoparticles) into cotton textiles using the sol-gel process. This will be investigated in the following chapters.

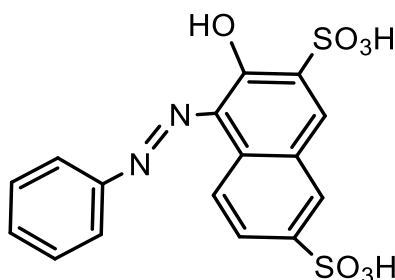
### Appendix 3.1. Materials and chemicals

Cotton fabric cuts were treated as described previously [149,199] and used as substrates for the dyeing process. Reagents are used without further purification, unless where indicated: Aniline (99.5%), o-anisidine (99%), 4-chloroaniline (98%), 2-methoxy-5-methylaniline (99%), sodium nitrite, 3-hydroxynaphthalene-2,7-disulfonic acid, ethyl alcohol (99% EtOH), hydrochloric acid (37% HCl), *n*-propyltriethoxysilane (97% *n*PTES), 3(triethoxysilyl) propylisocyanate (99% ICPTES) were commercially purchased from Sigma-Aldrich, SolvaChem, and Fluka Analytical.

### Appendix 3.2. Synthesis and preparation of the dyes

The classic synthesis procedure of azoic dyes was followed, with minor changes involving diazotization and the coupling steps [179,180].

#### 3.2.1. Synthesis of the dye TA01

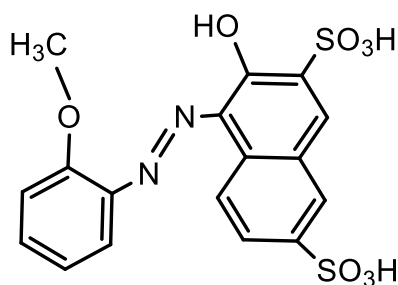


*(E)*-3-hydroxy-4-(phenyldiazenyl)naphthalene-2,7-disulfonic acid

One gram (0.011mol) of aniline is solubilized in 5 ml of ethanol and stirred in an ice bath, maintaining the temperature between 2-3°C. Then, 1.34 ml (0.044 mol) of concentrated hydrochloric acid (37%) is added. Afterward, 0.965g (0.014 mol) of sodium nitrite is added. Subsequently, 6.08g (0.020mol) of 3-hydroxynaphthalene-2,7-disulfonic acid was solubilized in water (pH 9-10). Solvents were removed by evaporation and the obtained product that is washed with (2x3ml) of diethyl ether and (6 x 5ml) of ethanol, which was centrifuged for 5 min at 9000 rpm. Finally, at a pH of 2, using hydrochloric acid solution (1M), absolute alcohol is added and heated to the boiling point; the solution is left to cool down slowly and filtered. The residue is left to dry for two nights at room temperature. *Yield: 82.3%. Molecular weight:*

408.01 g.mol<sup>-1</sup>. IR-ATR:  $\nu$  cm<sup>-1</sup>:  $\nu$ (N=N) (~1393-1465cm<sup>-1</sup>),  $\nu$ (-OH) (~3310-3520 cm<sup>-1</sup>),  $\nu$ (Ar C=C) (~1600-1620cm<sup>-1</sup>);  $\nu$ (C-S, S=O, S-O-H) (~1020-1038-1081-1197cm<sup>-1</sup>);  $\nu$ (C-O) (~1118 cm<sup>-1</sup>);  $\nu$ (C-N) (~1270-1285cm<sup>-1</sup>). <sup>1</sup>H NMR: (300MHz, D<sub>2</sub>O, 298K):  $\delta$  (ppm) 2.05 (s, 2H, OH), 5.40 (s, 1H, ArOH), 7.31-7.33 (m, 2H), 7.70 (t, 3H), 7.91 (d, H), 8.05 (s, 2H), 8.27 (d, 1H).

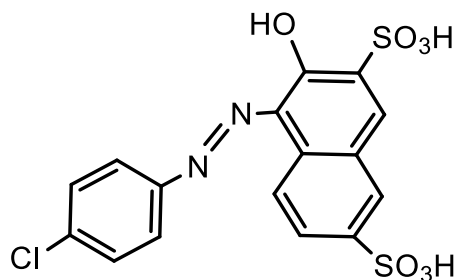
### 3.2.2. Synthesis of the dye TA02



(E)-3-hydroxy-4-((2-methoxyphenyl)diazenyl)naphthalene-2,7 disulfonic acid

The same synthesis procedure was followed using o-anisidine as primary amine and 3-hydroxynaphthalene-2,7-disulfonic acid in an equimolar ratio. Yield: 85.5%. Molecular weight: 438.02 g.mol<sup>-1</sup>. IR-ATR:  $\nu$  cm<sup>-1</sup>:  $\nu$ (N=N) (~1390-1460cm<sup>-1</sup>);  $\nu$ (-OH) (~3300-3500cm<sup>-1</sup>);  $\nu$ (C=C) (~1601-1618cm<sup>-1</sup>);  $\nu$ (C-S, S=O, S-O-H) (~1012-1035-1084-1197cm<sup>-1</sup>);  $\nu$ (C-O) (~1117cm<sup>-1</sup>);  $\nu$ (C-N) (~1271-1282cm<sup>-1</sup>). <sup>1</sup>H NMR: (300MHz, D<sub>2</sub>O, 298K):  $\delta$  (ppm) 2.05 (s, 2H, OH), 3.92 (s, 3H, OH), 5.40 (s, 1H, ArOH), 6.93 (m, 1H), 7.26-7.33 (m, 2H), 7.59 (t, 1H), 7.70 (d, H), 7.89-7.94 (m, 2H), 8.27 (d, 1H).

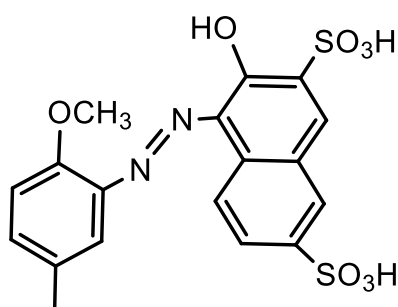
### 3.2.3. Synthesis of the dye TA03



(E)-4-((4-chlorophenyl)diazenyl)-3-hydroxynaphthalene-2,7-disulfonic acid

The same synthesis procedure was followed using 4-chloroaniline as primary amine and 3-hydroxynaphthalene-2,7-disulfonic acid in an equimolar ratio. *Yield: 79.0% Molecular weight: 441.97 g.mol<sup>-1</sup>. IR-ATR:  $\nu$  cm<sup>-1</sup>:  $\nu$ (N=N) (~1395-1465 cm<sup>-1</sup>);  $\nu$ (-OH) (~3305-3501 cm<sup>-1</sup>);  $\nu$ (C=C) (~1600-1620 cm<sup>-1</sup>);  $\nu$ (C-S, S=O, S-O-H) (~1014-1035-1081-1191 cm<sup>-1</sup>);  $\nu$ (C-O) (~1120 cm<sup>-1</sup>);  $\nu$ (C-Cl) (~830 cm<sup>-1</sup>);  $\nu$ (C-N) (~1275-1285 cm<sup>-1</sup>). <sup>1</sup>H NMR: (300MHz, D<sub>2</sub>O, 298K):  $\delta$  (ppm) 2.05 (s, 2H, OH), 5.40 (s, 1H, ArOH), 7.33 (m, 1H), 7.70 (m, 1H), 7.74 (m, 2H), 7.89 (s, 1H), 7.99 (dd, 2H), 8.27 (d, 1H).*

### 3.2.4. Synthesis of the dye TA04



*(E)-3-hydroxy-4-((2-methoxy-5-methylphenyl)diazenyl)naphthalene-2,7-disulfonic acid*

The same synthesis procedure was followed using 2-methoxy-5-methyl aniline as primary amine and 3-hydroxynaphthalene-2,7-disulfonic acid in an equimolar ratio. *Yield: 83.8%. Molecular weight: 452.03 g.mol<sup>-1</sup>. IR-ATR:  $\nu$  cm<sup>-1</sup>:  $\nu$ (N=N) (~1390-1460 cm<sup>-1</sup>);  $\nu$ (-OH) (~3390-3510 cm<sup>-1</sup>);  $\nu$  Ar(C=C) (~1602-1619 cm<sup>-1</sup>);  $\nu$ (C-S, S=O, S-O-H) (~1020-1037-1083-1193 cm<sup>-1</sup>);  $\nu$ (C-O) (~1115cm<sup>-1</sup>);  $\nu$ (C-N) (~1270-1289 cm<sup>-1</sup>). <sup>1</sup>H NMR: (300MHz, D<sub>2</sub>O, 298K):  $\delta$  (ppm) 2.05 (s, 2H, OH), 2.39 (s, 3H), 3.92 (s, 3H, OH), 5.40 (s, 1H, ArOH), 7.12 (d, 1H), 7.33-7.37 (m, 2H), 7.70 (t, 1H), 7.80 (d, 1H), 7.89 (d, 1H), 8.27 (d, 1H).*

---

## **Chapter 4 Molecular fluorophores: Synthesis, measurement of their fluorescence quantum yields, and application to textiles**

### **4.1. Introduction**

This chapter contains two complementary parts. In the first part, we will report a new instrumental method developed to determine the photoluminescence quantum yields (PLQY) of fluorescent molecules in solution using simultaneous measurement of absorption and emission spectra of the fluorophore through fiber-coupled devices. The validity of the method and its effectiveness were demonstrated using well-documented fluorophores as standard references. In the second part, four fluorescent molecules were synthesized and characterized using the method described in the first part. Furthermore, these fluorophore molecules were employed to prepare fluorescent textile fabrics, which is an essential step in the process of preparing luminescent textiles.

***Part One : A method for determining photoluminescence quantum yields in solutions using light-emitting diodes as the excitation source***

### **4.2. Theoretical background for the SAFER method**

PLQY is an essential photophysical property in the characterization and evaluation of fluorophores and other molecular or nanoscale photoluminescent species in solution. The determination of the PLQY using standard "right-angle" spectrofluorimeters has been amply

---

discussed and reviewed in the literature [200–205] as reported in the art of this thesis report. The standard comparative fluorimetric method, in which the photoluminescence intensity of a solution of a fluorophore with unknown quantum yield is compared to a standard solution of known PLQY, is now well established. This method (we will refer to it as the "standard method") is relatively easy to apply, provided that all requirements pertaining to the samples and the apparatus have been strictly satisfied [201–203,205].

These requirements result from the assumptions and approximations made in the underlying theoretical analysis. The solution to be characterized should contain one single light-absorbing species, typically a pure fluorescent molecular compound. The photoluminescence (PL) of this species is required to have Kasha-Vavilov behavior [206], *i.e.*, the excited state from which PL is emitted should always be the same and be reached quasi-instantaneously upon excitation, independently of the excitation wavelength. The solute should be perfectly dissolved without the formation of aggregates. The sample solutions should be limpid and display no scattering, *i.e.*, the overall light extinction should be equal to the overall light absorption. The PL emission should be isotropic, and light polarization effects should be negligible. Measurements should be carried out on optically dilute solutions, *i.e.*, the optical density should be inferior to 0.1.

On the instrumental side, the excitation wavelength should best be the same for the sample and the PLQY standard. If this is not the case, a quantum counter should be used to correct the differences in excitation light intensity [207]. Furthermore, all PLE spectra used in the measurement should be fully corrected, which means that any electronic dark signal has first been subtracted, followed by applying suitable wavelength-dependent correction factors [207] such that the spectrum represents the relative spectral photon flux [208] as a function of wavelength<sup>1</sup>.

---

<sup>1</sup>In practice, this is often colloquially referred to as "intensity in photon units".



The standard method furthermore relies on the assumption that the excitation light is monochromatic. It also relies on precise optical density measurement at the excitation wavelength, typically done on a different instrument. This introduces additional experimental uncertainties, a question recently addressed by Nawara and Waluk, who improved on the standard method by measuring sample absorbances simultaneously with the measurement of the PLE spectrum inside the spectrofluorimeter using a separate transmittance detector [209]. This method is called the SAFE method referring to "simultaneous absorption and fluorescence emission". It was demonstrated to be more robust than the standard comparative method. The experimental apparatus was later extended to allow *in situ* double-beam absorption measurement, further increasing reproducibility [73].

Both the standard and the SAFE methods do not address the case where a relatively broadband light source is used as the excitation source, such as a light-emitting diode (LED). In such a case, the temptation may exist to use the approximation that the (relatively) broadband source is monochromatic, taking the specified (maximum) emission wavelength, or that its spectral photon flux is constant over a specified wavelength range. These approximations are generally unsatisfactory for typical LEDs used for fluorescence excitation [210–213], which have relatively broad emission spectra.

Here, we consider a fluorimetric method for comparative measurement of PLQYs in solution in which light absorption and light emission are measured simultaneously, as in the SAFE method, with the modification that the full spectral distribution of the excitation light and its absorption are measured. The method is tentatively called the "SAFER" method and is particularly useful when using LEDs as the fluorescence excitation source. It may also be applied to monochromator-based sources to directly monitor the spectrum of the light exiting the excitation monochromator.

The photoluminescence emission quantum yield,  $\Phi$ , is given as the ratio of the number of luminescence photons emitted ( $N_{em}$ ) and the number ( $N_{abs}$ ) of photons absorbed by the sample. Starting from this definition and assuming an isotropic emission intensity

distribution, we arrive at Eqn. (4.1) for the experimental measurement of the PLQY in a standard right-angle fluorimetric configuration.

$$\Phi = \frac{N_{em}}{N_{abs}} = \frac{K_m \int_0^{\infty} I_m(\lambda) d\lambda}{K_x \int_0^{\infty} I_{abs}(\lambda) d\lambda} \quad (4.1)$$

$I_m(\lambda)$  is the corrected emission spectrum of the fluorophore in the solvent. It is corrected such that  $I_m(\lambda)$  is proportional to the number of photons emitted per unit of time by the fluorophore at that wavelength, *i.e.*, all wavelength dependencies of the spectrometer have been accounted. As a result,  $K_m$  does not depend on wavelength and accounts for geometrical factors in light detection efficiency (including refractive index effects on the detected emission intensity, *vide infra*). It also considers any arbitrary scaling that has been applied to the correction factors used for the correction of the emission spectrum. Furthermore, all background signals not coming from the fluorophore (*e.g.*, Rayleigh and Raman scattering by the solvent) have been subtracted from the emission spectrum, as expressed in Eqn. (4.2)

$$I_m(\lambda) = I_{m1}(\lambda) - I_{m0}(\lambda) \quad (4.2)$$

Here,  $I_{m1}(\lambda)$  is the corrected emission spectrum<sup>1</sup> of the solution of the fluorescent compound and  $I_{m0}(\lambda)$  is the corrected emission spectrum of the illuminated solvent alone. With sufficiently bright fluorophores, we have  $I_m(\lambda) \approx I_{m1}(\lambda)$ , and contributions from the solvent background due to Rayleigh and Raman scattering will be negligible. For consistent SAFER measurement, the emission spectrum of the solvent alone  $I_{m0}(\lambda)$ , is systematically recorded, enabling the subtraction of weak Rayleigh and Raman signatures, particularly for weakly emitting fluorophores.

---

<sup>1</sup>A corrected (photon) emission spectrum has the detector dark current subtracted, the correction for wavelength-dependent overall photon detection efficiency applied and represents the relative spectral photon flux as a function of wavelength.

---

The solvent background spectrum  $I_{m0}(\lambda)$  is recorded simultaneously with the corrected spectrum of the excitation light that has traversed the pure solvent,  $I_{x0}(\lambda)$ . Subsequently, the spectrum  $I_{m1}(\lambda)$  (solvent with fluorophore added) is recorded simultaneously with the corrected spectrum of the excitation light transmitted through the same solution,  $I_{x1}(\lambda)$ .

From  $I_{x0}$  and  $I_{x1}$ , we obtain the spectrum of the absorbed light intensity,  $I_{\text{abs}}$ , a relative measure of how many photons are absorbed per wavelength (under the condition that the light extinction is due to absorption alone, *i.e.*, the sample is a limpid solution).

$$I_{\text{abs}}(\lambda) = I_{x0}(\lambda) - I_{x1}(\lambda) \quad (4.3)$$

Since  $I_{x0}(\lambda)$  is measured with the cuvette only containing the solvent, it already includes all light losses due to the cuvette (reflection losses at the optical interfaces) and losses due to the solvent (residual light absorption, scattering). The contributions of Rayleigh and Raman scattering to these losses are exceedingly small compared to the other losses. The only difference between  $I_{x0}(\lambda)$  and  $I_{x1}(\lambda)$  being the presence of the fluorophore,  $I_{\text{abs}}(\lambda)$  purely represents the light absorption by the fluorophore, just as  $I_m(\lambda)$  is purely the light emission from that fluorophore, free from all artifacts already subtracted.

The quantity  $I_{\text{abs}}$  appears in Eqn. (4.1) together with the constant  $K_x$  which is the (unknown) factor that would convert these relative transmitted excitation photon fluxes into absolute numbers of photons.

At this point, we consider the impact of the refractive index of the solvent on the detection efficiency of the emission channel. In the case of a conventional right-angle fluorimetric set-up, the light collection factor  $K_m$  includes a contribution of the solution's refractive index, which changes the solid angle over which emission light is collected [203]. This refractive index contribution can be factored out of  $K_m$  to have it appear explicitly in the expression of the detected emitted light intensity (Eqn. (4.4))

$$K_m = n^2 K'_m \quad (4.4)$$

With this change, Eqn. (4.1) then becomes Eqn. (4.5).

$$\Phi = \frac{n^2 K'_m \int_0^\infty I_m(\lambda) d\lambda}{K_x \int_0^\infty I_{\text{abs}}(\lambda) d\lambda} \quad (4.5)$$

The ratio  $K'_m/K_x$  can be determined using a solution of a reference fluorophore with known photoluminescence quantum yield  $\Phi_R$  [200] :

$$\frac{K'_m}{K_x} = \frac{\Phi_R \left[ \int_0^\infty I_{Rm}(\lambda) d\lambda \right]^{-1}}{n_R^2 \left[ \int_0^\infty I_{Rabs}(\lambda) d\lambda \right]} \quad (4.6)$$

$K'_m/K_x$  depends only on the instrument and is constant for any experimental set. We observed that it might even be constant over several days on our fluorimetric set-up (provided that it is left strictly unperturbed). However, the requirement of measuring a fresh reference for each series of measurements is maintained to validate the determination of the quantum yield of photoluminescence rigorously.

When plugging the expression for  $K'_m/K_x$  of Eqn. (4.6) back into Eqn. (4.5), a general expression is obtained, in the form of (4.7), for measuring the photoluminescence quantum yield of a fluorophore with respect to a reference solution using an excitation source having an arbitrary spectrum. This relies on the applicability of the Kasha-Vavilov law and on having a pure fluorophore in the solution. The aim is to use a light source with a spectrum that is as narrow as possible but that may be relatively large, such as a light-emitting diode or a broadband light source of wavelength-dependent intensity in combination with a band-pass filter.

$$\Phi = \Phi_R \frac{n^2 F^i f_R}{n_R^2 f_i F^R} \quad (4.7)$$

with

$$F^i = \int_0^{\infty} I_m(\lambda) d\lambda = \int_0^{\infty} [I_{m1}(\lambda) - I_{m0}(\lambda)] d\lambda \quad (4.8)$$

$$f_i = \int_0^{\infty} I_{abs}(\lambda) d\lambda = \int_0^{\infty} [I_{x0}(\lambda) - I_{x1}(\lambda)] d\lambda \quad (4.9)$$

$$F^R = \int_0^{\infty} I_{Rm}(\lambda) d\lambda = \int_0^{\infty} [I_{Rm1}(\lambda) - I_{Rm0}(\lambda)] d\lambda \quad (4.10)$$

$$f_R = \int_0^{\infty} I_{Rabs}(\lambda) d\lambda = \int_0^{\infty} [I_{Rx0}(\lambda) - I_{Rx1}(\lambda)] d\lambda \quad (4.11)$$

Expression (4.7) is the formula for determining fluorescence quantum yield known in the literature. In the context of the present work, there is a difference in how the emission ( $F$ ) and absorption ( $f$ ) factors are obtained. The methods described in previous work use various approximations for the integrated absorbed light intensity (Eqns. (4.9) and (4.11)). For the completeness of the discussion, we will briefly review these approximations first.

To understand the 'standard' and SAFE methods, the expression for the absorbed light intensity,  $I_{abs}$  in Eqns. (4.9) and (4.11) can be rearranged by factoring out  $I_{x0}$ . The absorbed light is thus written as the product of the (corrected) spectrum of the relative spectral photon flux of the excitation light that has fully traversed the pure solvent ( $I_{x0}$ ) and the fraction of light absorbed specifically by the fluorophore (4.12).

$$I_{abs}(\lambda) = I_{x0}(\lambda) - I_{x1}(\lambda) = I_{x0}(\lambda) \left[ 1 - \frac{I_{x1}(\lambda)}{I_{x0}(\lambda)} \right] \quad (4.12)$$

The term  $I_{x1}/I_{x0}$  is recognized to be the transmittance of the sample ( $T = I_{x1}/I_{x0}$ ). From the transmittance, the optical density is obtained by definition as  $OD = -\log_{10} T$ . Thus,  $I_{abs}$  may be expressed in optical density (Eqn. 4.13).

$$I_{abs}(\lambda) = I_{x0}(\lambda) - I_{x1}(\lambda) = I_{x0}(\lambda) [1 - 10^{-OD(\lambda)}] \quad (4.13)$$

At this point, the expressions are still general and do not assume a monochromatic excitation source nor an excitation light source with a 'flat' output spectrum. The factoring out of  $I_{x0}$ , as

done in Equations (4.12) and (4.13), is only relevant at wavelengths where the light intensity of the excitation source is not close to zero. To deal with this, the semi-infinite integral over  $I_{\text{abs}}$  of Eqns. (4.9) and (4.11) is replaced by a definite integral between the wavelengths where the light source has significant intensity.

In the hypothetical case of perfectly monochromatic light of wavelength  $\lambda_{\text{exc}}$ , the excitation light intensity  $I_{x0}(\lambda)$  only has intensity at  $\lambda_{\text{exc}}$  and is zero everywhere else. The factor  $K_x$  can be scaled such that that  $I_{x0}$  becomes a Dirac delta function (*i.e.*, it is only non-zero at  $\lambda_{\text{exc}}$  and its integral evaluates to one). Thus, the assumption of perfectly monochromatic light yields (4.14).

$$\int_0^{\infty} I_{\text{abs}}(\lambda) d\lambda = 1 - 10^{-\text{OD}(\lambda_{\text{exc}})} \quad (4.14)$$

It is seen that with perfectly monochromatic light, the conventionally used expression for the determination of the photoluminescence quantum yield is obtained (*i.e.*, the expression used in the 'standard' method).

The SAFE method by Nawara and Waluk makes a more realistic assumption concerning the properties of excitation light. That method is based on the (implicit) assumption that the light intensity of the excitation light exiting the monochromator is constant over a well-defined band from  $\lambda_1$  to  $\lambda_2$ . An additional implicit assumption is that the transmitted light detector (*e.g.*, a photodiode) has a flat spectral response. In that case (and with proper scaling of  $K_x$ ),  $I_{x0}(\lambda)$  has the value of one over the interval  $\lambda_1$  to  $\lambda_2$  and is zero elsewhere. The absorption integral then becomes Eqn. (4.15), leading to the expressions used by Nawara and Waluk in the 'SAFE' method.

$$\int_0^{\infty} I_{\text{abs}}(\lambda) d\lambda \approx \int_{\lambda_1}^{\lambda_2} [1 - 10^{-\text{OD}(\lambda)}] d\lambda \quad (4.15)$$

The "SAFER" method presented here uses Eqn. (4.7) with full measurement of the corrected transmitted and emitted light spectra required for direct evaluation of the integrals in Eqns. (4.8)...(4.11). It does not use any of the developments in Eqns. ((4.12)...(4.15)).

---

The determination of a single PLQY of a solution thus requires recording eight spectra: four spectra each for the sample and the PLQY reference solution, respectively. The four spectra are recorded in pairs, simultaneously measuring the transmitted and emitted light spectra on the same sample in the same sample holder. In spite of the direct evaluation of the integrals in *Eqns. ((4.8)...(4.11))*, without explicit use of the optical density in the calculations, the SAFER method is still subject to working at optical densities below 0.1 (at excitation and emission wavelengths) to avoid inner filter effects.

A further relevant point to consider is the spectral overlap between the broad-band excitation source and the absorption spectrum of the fluorophore, as implied by *Eqn. (4.13)*. Since we have a single emitting species with Kasha-Vavilov behavior, every photon absorbed by the species will have the same probability to trigger the emission of a PL photon, independently of the wavelength of that excitation photon. For the PLQY measurement, it is thus necessary and sufficient to measure the number of absorbed photons integrated over all relevant wavelengths, as expressed by *Eqns. (4.9) and (4.11)*.

Interestingly, in the case of only partial overlap between the spectrum of the excitation source and the absorption spectrum of the fluorophore, the excitation photons that are outside of the absorption band of the fluorophore will simply never contribute to  $f_i$  (or  $f_{Ri}$ ). Excitation photons that are within the absorption band may sometimes contribute to  $f_i$  (or  $f_{Ri}$ ). Even within the absorption band of the fluorophores, only a fraction of the incoming excitation photons is absorbed, in line with the requirement to work at  $OD < 0.1$ . Those photons whose wavelengths fall inside of the absorption band but that were not absorbed do not contribute to  $f_i$  (or  $f_{Ri}$ ), on equal standing with the photons that are outside of the absorption band (and had no chance whatsoever of being absorbed). Of course, there should be sufficient spectral overlap between the excitation source and the fluorophore absorption band to warrant sufficient light absorption for a reliable determination of the integral  $f_i$  (or  $f_{Ri}$ ).

### 4.3. Practical realization of the SAFER method

#### 4.3.1. Chemicals

Fluorescent dyes of spectroscopic purity were obtained from Sigma-Aldrich/Merck or Acros/ThermoFisher and used as received: 2-aminopyridine (2AP), 4-(dicyanomethylene)-2-methyl-6-(4-dimethylaminostyryl)-4H-pyran (DCM), quinine bisulfate (QBS), Fluorescein (Flscn), rhodamine 6G (Rh6G), pyranine, anthracene (Anth), Cresyl Violet (CV), Coumarin-153 (C153), Nile Red (NR). Solvents and aqueous solutions were supplied by Sigma-Aldrich/Merck and were of analytical or spectroscopic grade: water, perchloric acid (60 wt.% in water), aqueous sulfuric acid (0.5 M), aqueous sodium hydroxide solution (1 M), ethanol (EtOH, 96% with 4% water), methanol (MeOH, 99.8%). The neat solvents were carefully examined using extinction and fluorescence spectroscopies to ensure the absence of any background absorption and fluorescence at the wavelengths used. The acid and base solutions were further diluted with water.

Three recommended [200] PLQY reference solutions were used: QBS in 0.1M HClO<sub>4(aq)</sub> [214], Flscn in 0.1M NaOH<sub>(aq)</sub>, and Rh6G in ethanol. Stock solutions were freshly prepared for each measurement campaign. The sample fluorophores were dissolved in suitable solvents as follows: anthracene in ethanol, QBS in 0.05M H<sub>2</sub>SO<sub>4(aq)</sub>, pyranine in 0.01M NaOH<sub>(aq)</sub>, C153 in both methanol and ethanol, CV in methanol, and NR in methanol. Measurements were made on air-equilibrated solutions. A cuvette containing a known volume of pure solvent and a miniature stir bar is inserted in the cuvette holder equipped with a magnetic stirrer. Small quantities from a concentrated dye stock solution, typically 10<sup>-4</sup>...10<sup>-3</sup> M in the same solvent are added, recording transmitted and emitted light spectra after each addition. The cuvette remains in place, avoiding experimental uncertainties related to cuvette replacement. The final concentrations of the dyes in the measured solutions were typically between 10<sup>-6</sup> M and 10<sup>-5</sup> M. In all cases the optical density of the solutions did not exceed 0.1 (typically below 0.05).



### 4.3.2. Measurement set-up

The experimental set-up is based on fiber-coupled spectroscopic equipment, with an excitation light source (choice of LEDs for different excitation wavelengths) and two spectrometers, one for transmitted-light spectra and one for emitted-light spectra. The fiber-coupled LEDs deliver around 50  $\mu\text{W}$  of light to the sample through the illumination optics, which is comparable to the intensity of a Xenon lamp/narrow slit monochromator combination, with the difference that the total intensity is smeared out over a broader range of wavelengths.

The spectral responses of both spectrometers were calibrated using a NIST-traceable incandescent light source and reference solutions of fluorescent compounds with known photon spectra. The dark signal was subtracted from the raw spectra, and the spectra were converted into photon units using the correction factors described at the end of this chapter.

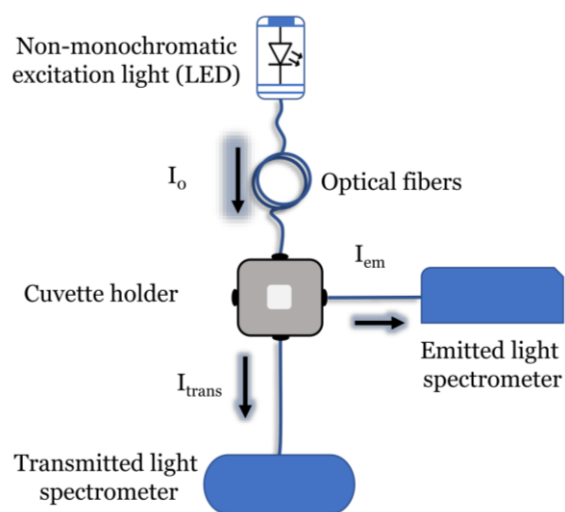


**Figure 4.1.** Set-up used for simultaneous light absorption and fluorescence emission measurements of limpid liquid samples for the determination of photoluminescence quantum yields

The excitation light is fiber-coupled to a thermostated cuvette holder (Quantum Northwest qPod). The light emitted from the solution in the cuvette is collected at a right angle ( $90^\circ$ ) and coupled into a fiber connected to the emitted light spectrometer. The light transmitted

through the cuvette (180°) is also coupled into a fiber connected to the transmitted light spectrometer. The emitted light spectrum is measured using an OceanOptics QE65000 spectrometer. The transmitted light is measured using an Avantes AvaSpec-ULS2048CL-EVO spectrometer.

Corrected (transmitted, emitted) light intensity spectra  $I(\lambda)$  in photon units are obtained from the raw spectrometer data  $I_{\text{raw}}(\lambda)$  by first subtracting the 'dark' spectrum  $I_{\text{dark}}(\lambda)$ , measured in the absence of any excitation light, and subsequently applying correction factors  $K_{\text{corr}}(\lambda)$ .

$$I(\lambda) = K_{\text{corr}}(\lambda)[I_{\text{raw}}(\lambda) - I_{\text{dark}}(\lambda)] \quad (4.16)$$

### 4.3.3. Experimental conditions

For all experiments, standard 10 mm pathlength fluorescence cuvettes are used. These are cleaned by first soaking in 1% Hellmanex solution, followed by washing several times with pure water, spectrograde ethanol, and drying under a gentle flow of filtered air. The cuvette is rinsed with the chosen solvent just before filling it with the solvent. It is then inserted into the cuvette holder (qPod), which offers precise temperature control, fixed to  $23 \pm 0.2^\circ\text{C}$  for all experiments. A little magnetic stirrer is used for mixing in the concentrated analyte solution. Once the cuvette is inserted, it is not removed and re-inserted, further reducing experimental uncertainties.

In the practical implementation of the SAFER procedure, we measure simultaneously  $F$  and  $f$  several times with stepwise increases in the concentration of the fluorophore, starting from zero concentration, *i.e.*, pure solvent ( $I_{m0}$ ,  $I_{x0}$ ,  $I_{Rm0}$ ,  $I_{Rx0}$  in Eqns. (4.8) ... (4.11)). Recording and processing the eight spectra that enter Eqn. (4.7) may seem daunting, but the method is based on the simultaneous recording of pairs of emission and transmitted light spectra in a digital form followed by automated processing using a microcomputer program.

Furthermore, the reference spectra only need to be recorded once for a series of measurements.

The ratios  $F^i/f_i$  and  $F^R/f_r$  in Eqn. (4.7) can be viewed as the slopes of the plots of the (total) emitted light intensity  $F$  as a function of the (total) absorbed light intensity  $f$  at different concentrations of the fluorophores.

#### **4.3.4. Some examples of how PLQY measurement is done with the SAFER method**

The following is an example of a single PLQY measurement for Quinine bisulfate in 0.1M HClO<sub>4</sub>(aq) used as a reference and Fluorescein in 0.1M NaOH(aq) as the analyte sample. The spectra of the excitation light transmitted through the solution and the resulting fluorescence emission are recorded simultaneously at increasing dye concentrations, starting from the pure solvent. All spectra are fully corrected for dark signal and detector response. The spectra are integrated over a band of relevant wavelengths (non-zero intensities) to obtain the integrated intensities for both the transmitted and the emitted light. The integrated absorbed light intensities are calculated from the integrated transmitted light intensities following Eqns. (4.9) and (4.11), using the sum rule of integration. The integrated emitted light intensity is plotted as a function of the integrated absorbed light intensity for both the sample and the reference. Finally, the PLQY is obtained from the ratio of these slopes using Eqn. (4.7). At least three independent PLQY measurements were made for each dye to obtain an estimate of the experimental uncertainty. Additional examples will be found as appendixes at the end of this chapter.

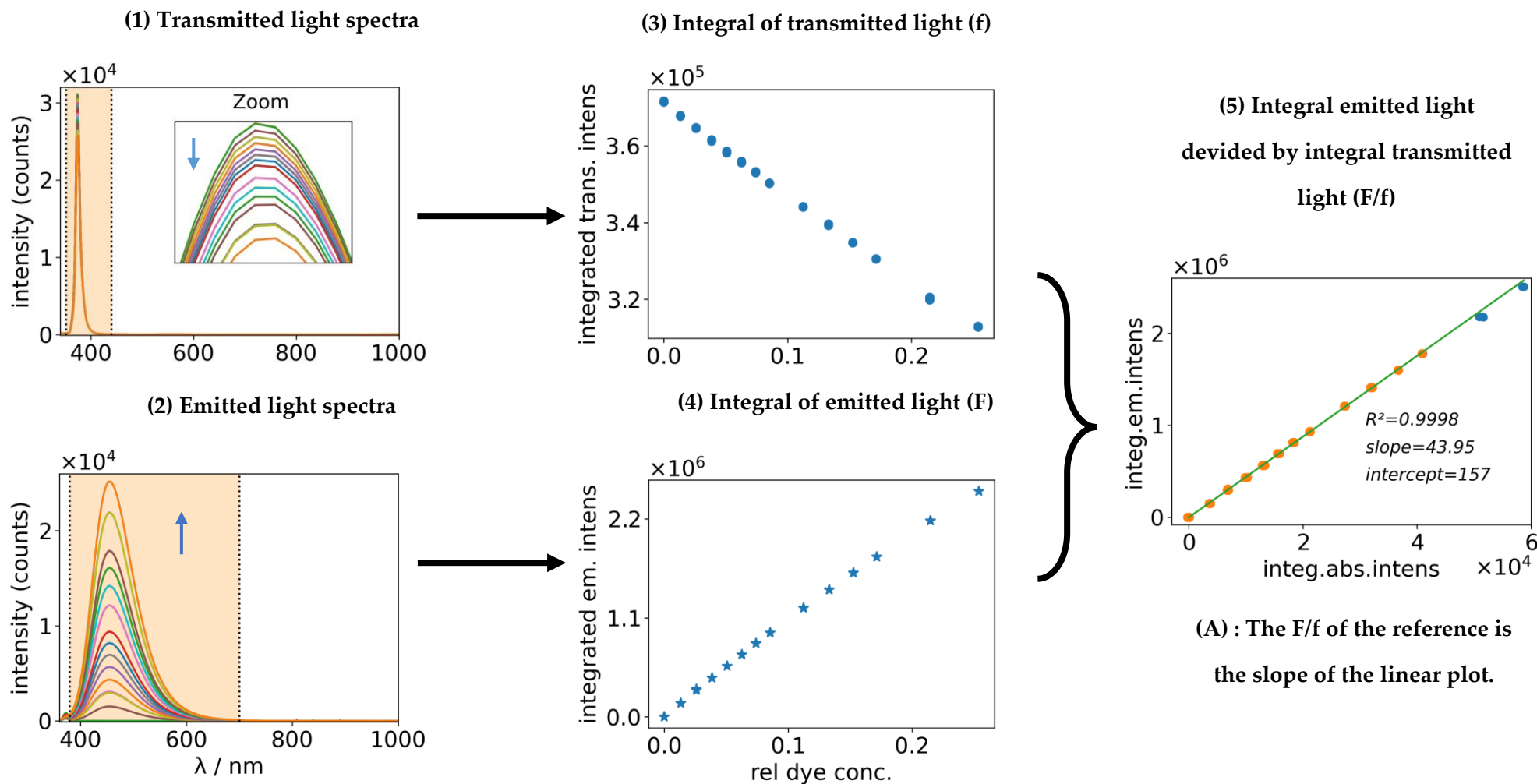
Since the corrected spectra of the excitation light are measured, it is, in principle, possible to use different excitation sources at different wavelengths between the sample and the reference. In the present work, we mainly used the same excitation for both the sample and the reference. This is preferred since it removes one additional source of uncertainty. Also, changing the excitation is relatively tedious in the current set-up and requires carefully replacing the LEDs while the equipment is functioning.

In the case of linear plots for both the sample and the reference, the slopes of the lines give the ratios  $F^i/f_i$  and  $F^R/f_r$  for Eqn. (4.7). Now what is left to do is some calculations using Excel sheets of the parameters of Equation (4.7), including refractive indexes of the used solvents.

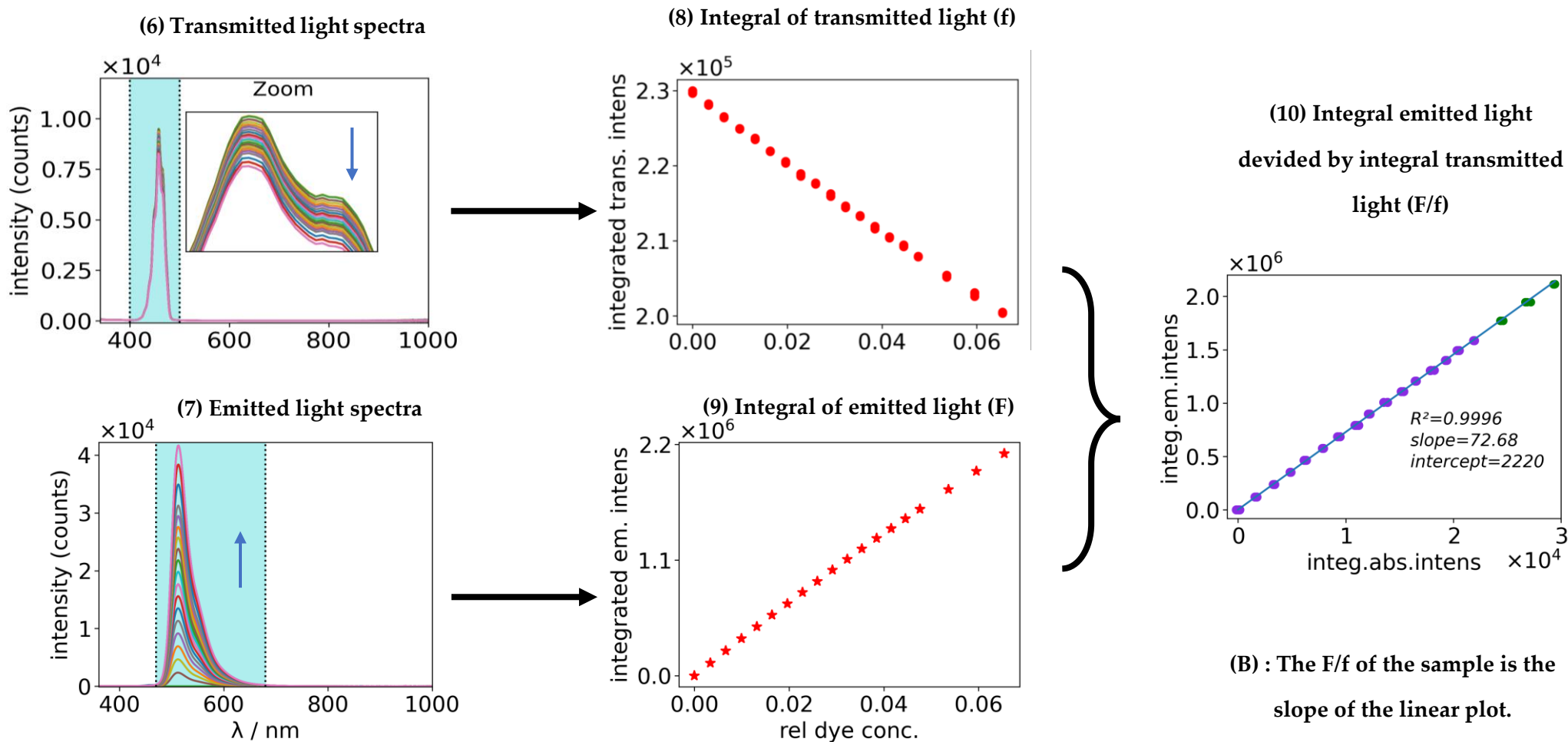
Interestingly, it is not necessary to precisely know the fluorophore concentration for the plot of  $F$  vs.  $f$ , although it may be useful also to study how  $F$  and  $f$  vary with concentration, which will be seen in the upcoming section. For the SAFER measurement, only the plot of  $F$  vs.  $f$  is needed. This must be a straight line going through the origin. If this is not the case, then something is wrong, and a reliable PLQY cannot be determined.

Checking the linearity of  $F$  vs.  $f$  measurements at different concentrations will filter out several problems that can arise with PLQY measurements in solution: solubility problems/dye aggregation, (photo)chemical instability, exceeding the limits on optical density, light source problems, etc. (*see appendix 4.3*).

**Step 1.** Recording emitted and transmitted spectra of a reference molecule (in this case: Quinine bisulfate) and integrating the total absorbed and the total emitted lights. The F/f plot of the reference is presented as the slope of the plot (5)



**Step 2.** Recording emitted and transmitted spectra of a sample molecule (of Fluorescein) and integrating the total absorbed and total emitted lights. The  $F/f$  plot of the sample is presented as the slope of the plot (10)



### 4.3.5. Validation of the SAFER method

The determination of photoluminescence quantum yields of fluorophores in solution using the SAFER method and broadband LED excitation was validated by measuring a series of relatively well-known fluorophore solutions whose PLQYs have been reported in the literature (*Table 4-1*). The reference solutions used were those recommended by Brouwer [200]. QBS in perchloric acid solution, Flscn in aqueous NaOH, and Rh6G in ethanol.

QBS in perchloric acid was preferred over QBS in sulfuric acid, following the work by Nawara and Waluk [214], although we yielded to the temptation to measure the latter as a sample using the former as a reference, confirming the known value. All measurements from this work agree with the literature values.

**Table 4-1.** Quantum yields of different fluorophores in solution, measured at 296K (+/- 1K) compared with recommended PLQY reference standards [200] using the SAFER method. The sample and reference pairs were systematically excited by the same LED light source, except for the Flscn-QBS pair. The last column contains values reported in the literature.

<i>Reference</i>	<i>LED exc. source</i>	<i>Compound</i>	<i>Solvent</i>	$\Phi$ <i>(this work)</i>	$\Phi$ <i>(literature)</i>
QBS/ HClO <sub>4</sub> (aq)	340 nm	Anthracene	EtOH	0.26 ± 0.02	0.28 [215,216]
	380 nm	Pyranine	NaOH	0.96 ± 0.08	~1.0 [217,218]
		QBS	H <sub>2</sub> SO <sub>4</sub>	0.55 ± 0.03	0.55 [200,219-221]
		Flscn <sup>(a)</sup>	NaOH	0.94 ± 0.06	0.93 [200,222,223]
Flscn/ NaOH(aq)	450 nm	Rh6G	EtOH	0.91 ± 0.02	0.95 [200,224,225]
		Pyranine	NaOH	0.99 ± 0.08	~1.0 [217,218]
		C153	EtOH	0.56 ± 0.03	0.54 [226]
		C153	MeOH	0.48 ± 0.02	0.42 [227,228]
Rh6G/ EtOH	518 nm	CV	MeOH	0.53 ± 0.03	0.52 [200,219,221]
		NR	MeOH	0.43 ± 0.03	0.40 [229]

\* Flscn excited with 450 nm LED, QBS reference with 380 nm LED

As a first check of consistency, the PLQY of the Flscn reference was also determined using QBS as the reference, and the PLQY of the Rh6G was also measured against Flscn as a reference. Consistent PLQY values were obtained.

The measurement for the Flscn/QBS pair required to exceptionally change excitation LEDs between the sample (450 nm LED) and reference (380 nm LED), demonstrating that the present SAFER method allows, in principle, to change excitation sources between reference and sample.

Anthracene was measured since it is considered a somewhat challenging case for the traditional comparative method because of its narrow vibronic absorption bands [209] that lead to deviations when light absorption and photoluminescence emission are not measured on the same spectrometer, in particular, because of different bandwidths between the absorption measurement and the excitation light. Our measured value agrees well with the values reported in the literature [215,216]. The overlap between the broadband excitation (340 nm LED) and the narrow anthracene absorption peaks is well considered by the transmitted light spectroscopic measurement in the SAFER method since it measures the integrated absorbed light intensity.

Pyranine, in its fully deprotonated form in basic water, is a well-known strongly fluorescent dye used in certain fluorescent marker pens. The pKa of its phenolic group is 7.2, and the protonated and deprotonated forms have different spectral characteristics, which makes pyranine interesting as a ratiometric pH probe for physiological conditions [230,231]. Pyranine is also a photo-acid, with the pKa\* of the phenolic group dropping to 1.4 in the excited state [232]. It absorbs and emits light in the same spectral range as the fluorescein dianion, with an emission spectrum that has less structure and better photostability [231].



These observations suggest that pyranine may be a superior fluorescence standard compared to Fluorescein. However, there are only a few reports of its PLQY in the literature. A fluorescence quantum yield of 0.82 has been quoted for pyranine in water [233], but neither the pH nor the composition of the aqueous phase nor the experimental conditions were specified. Other two works agree upon a near-unity ( $\sim 1$ ) PLQY for pyranine in basic water [217,218]. Our measurements, using both QBS and Flscn as references, confirm this very high value for the fluorescence quantum yield of pyranine in basic water (0.01 M NaOH). It was observed that, under the experimental conditions used, there are small sample-to-sample variations in the brightness of the pyranine, leading to a somewhat higher uncertainty in the value of the PLQY. We tentatively ascribe this to pH variations of the dilute (10 mM) NaOH solution due to the absorption of CO<sub>2</sub> from the ambient atmosphere. Indeed, upon prolonged exposure of freshly diluted NaOH to air in an open cuvette, the pH may drop to 9.1 at equilibrium, which would lead to the protonation of a small fraction (a few percent) of the pyranine, slightly lowering fluorescence emission. The high dilution for NaOH was chosen following the literature [217,218]. However, a suitable buffer, or more concentrated NaOH solution, should be found in which the fluorescence intensity of pyranine is stable, even in equilibrium with ambient air, before pyranine can act as a standard in fluorescence measurements.

Coumarin-153 (C153) was included since it has been suggested as an emission standard for calibrating the spectral responsivity of spectrometers [234]. It is a highly photostable fluorescent (laser) dye. It may have a double use in the standardization of fluorescence measurements, both as a spectral emission standard and a PLQY standard, for which it has favorable properties.

On the red end of the present study, we have Cresyl Violet (CV) and Nile Red (NR). The former has been considered as a standard for red-emitting fluorophores, and its fluorescence quantum yield was determined with photothermal methods [219]. However, its PLQY has already become concentration-dependent at low concentrations ( $>1 \mu\text{M}$ ) [235], an

observation that is confirmed in the present work. The PLQY measurements for CV were carried out at concentrations below 0.5  $\mu\text{M}$ , where the fluorescence emission intensity is proportional to the absorbed light intensity. NR is an interesting photostable solvatochromic dye [229] that might be considered as a candidate for a future 'red' standard when dissolved in certain polar solvents. Its PLQY in methanol has been reported in the literature [229] but would benefit further confirmation. Our measured value for the PLQY confirms the published value.

Despite the broad spectral range offered by the emission spectrometer of the present set-up, no measurements of near-infrared fluorescence were made for the present study, focusing on more well-established visible-emitting dyes for validation. PLQY standards for the near-infrared are still less developed [200], even though crucial progress has been made recently [236,237]. Measurements in the near-infrared are more challenging due to the presence of significant absorption bands of the solvent [236] (vibrational overtones, *e.g.*, water near 980 nm [238]).

The present validation of the SAFER method has concentrated on known fluorophores with sizeable PLQYs. For the measurement of weakly emitting species with low PLQYs, the SAFER method will encounter the same limitations as the other relative methods. It will depend on the same instrumental capabilities for subtracting any background signals coming from Rayleigh and Raman scattering by the solvent, providing sufficient linear dynamic range in the emission measurement and reducing stray light [239] in the spectrograph. The present setup was not explicitly optimized for weakly emitting samples. We estimate conservatively that without additional precautions, the lowest PLQYs to be determined reliably will be on the order of 0.01.

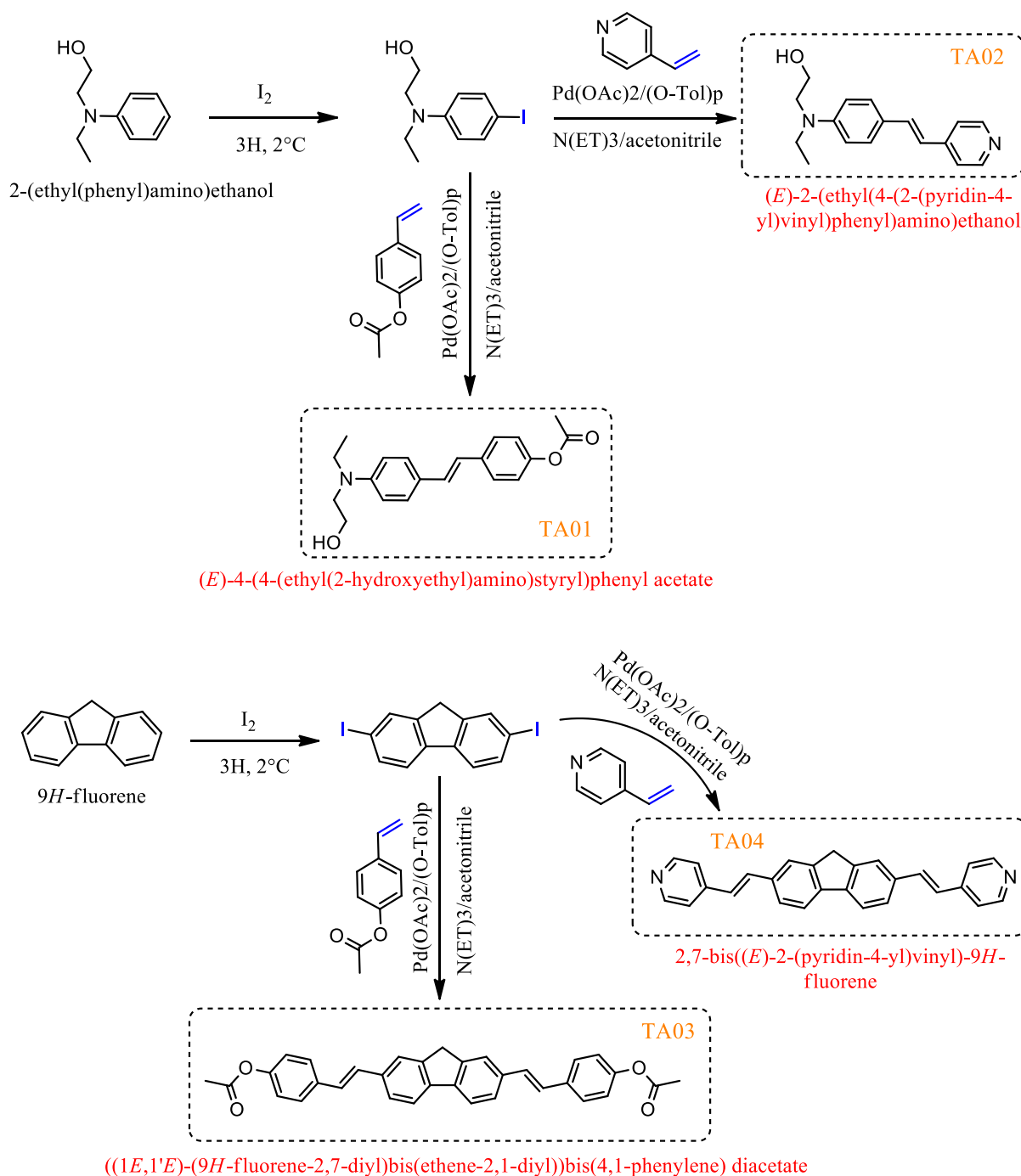
Modifications that could be made to the method to gain reliable access to lower PLQYs are: (i) the use of standards that themselves have low quantum yields [200], (ii) the use of neutral density filters in the emission channel to diminish the intensity of high PLQY standards, and (iii) applying different exposure times between sample and standard [240].

The first modification is preferred. The two latter are instrument-dependent and require further work and validation, *e.g.*, when inserting neutral density filters, an additional correction will be required for the spectral dependence of the optical density of the filter.

## ***Part Two : Synthesis of fluorophores and development of fluorescent textiles***

### **4.4. Synthesis of fluorophores and measurement of their PLQYs in solution using the SAFER method**

Now that the developed SAFER measurement method was validated using standard fluorophore references, it was employed to investigate newly synthesized fluorophores. These stilbene and fluorene-based molecules were prepared via the Mizoroki-Heck coupling with two different arms, as depicted in *Scheme 4.1*. Additional data and characterizations are reported in the appendixes of this chapter.

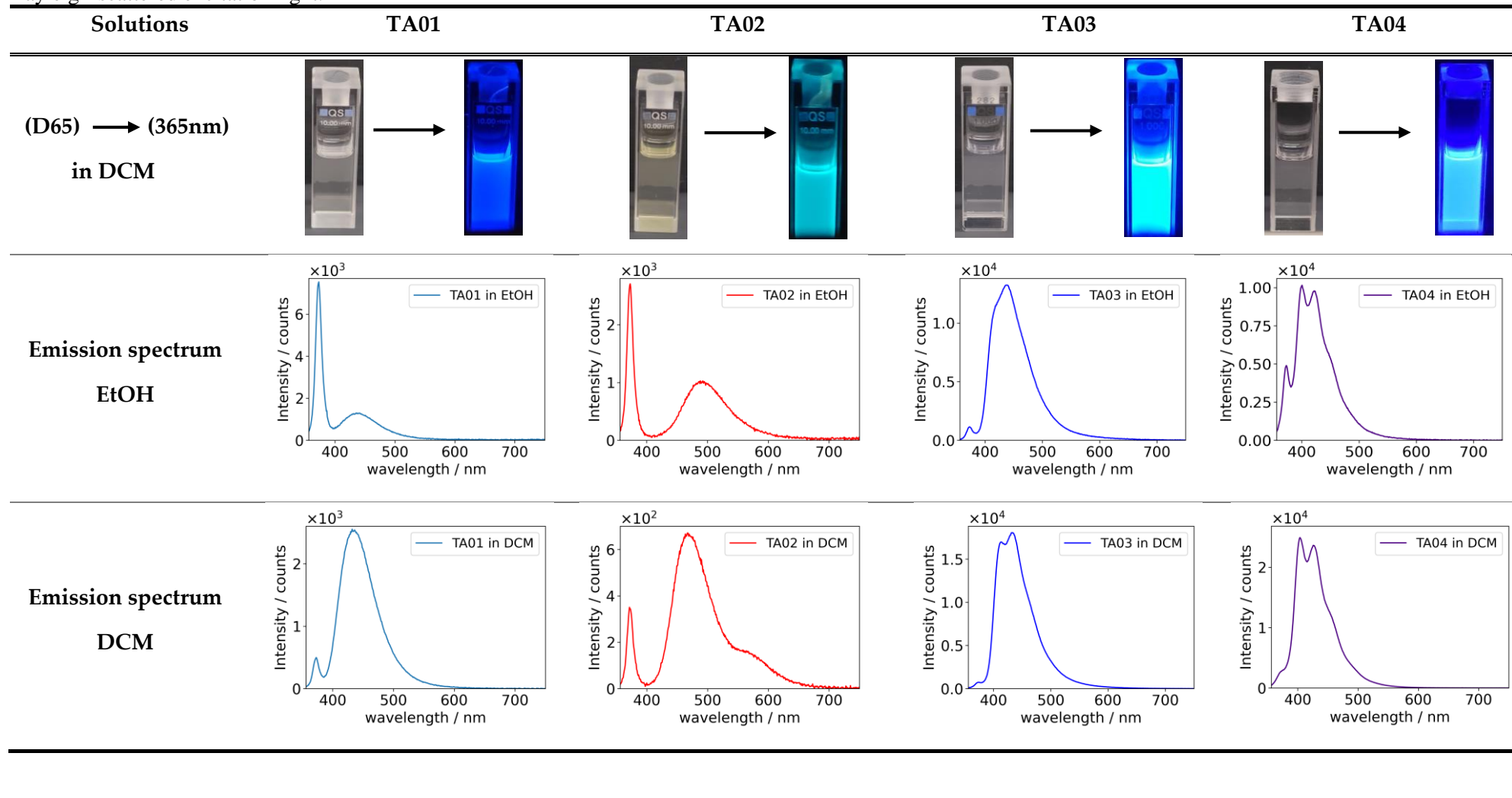


**Scheme 4-1.** Synthesis of the stilbene and fluorene-based fluorophores

The four molecules are referred to as TA01, TA02, TA03, and TA04. **Table 4-2** shows images of cuvettes containing TA01...TA04 dissolved in dichloromethane with a concentration of  $1.2 \times 10^{-5}$  M in daylight and when excited under a 365 nm excitation lamp.

## Molecular fluorophores : Synthesis, measurement of their fluorescence quantum yields, and application to textiles

**Table 4-2.** Images of the fluorophores dissolved in dichloromethane under daylight and 365nm excitation (first row). Emission spectra of the fluorophores in ethanol and dichloromethane, excited under 380 nm LED excitation light (second and third row, respectively). The sharp peaks in most spectra at 371 nm are Rayleigh-scattered excitation light.



The photoluminescence quantum yields of these molecules were determined using the SAFER method. Quinine bisulfate in 0.1M perchloric acid was used as a standard reference in this experiment. The same protocol was followed by first preparing stock solutions from each molecule with a concentration of  $10^{-3}$ ...  $10^{-4}$  mol/L using ethanol and dichloromethane as solvents. The samples were excited using 380 nm LED excitation light at a controlled temperature. *Table 4-3* reports the photophysical parameters of the fluorophore molecules.

**Table 4-3.** Photophysical parameters of different fluorophores in solution, measured at 296K (+/- 1K) compared with QBS in 0.1M perchloric acid reference standards using the SAFER method. The sample and reference pairs were systematically excited by the same LED light source, 380 nm; precisely, its maximum excitation is 371 nm.

<i>Fluorophore</i>	$\lambda_{max\ abs}$ (EtOH)(nm)	$\lambda_{max\ em}$ (EtOH)(nm)	$\Phi$ (EtOH)	$\lambda_{max\ abs}$ (DCM)(nm)	$\lambda_{max\ em}$ (DCM) (nm)	$\Phi$ (DCM)
QBS (0.1M HClO <sub>4</sub> )	347*	451*	0.60*	347*	451*	0.60*
TA01	355	437	0.04± 0.05	370	434	0.06± 0.02
TA02	379	490	0.02± 0.08	385	467	0.02± 0.06
TA03	357	438	0.38± 0.03	366	413/433	0.42± 0.05
TA04	356	403/426	0.41± 0.01	365	400/422	0.75± 0.02

\*measured in 0.1 M of perchloric acid

The reported emission spectra in *Table 4-2* and the photophysical parameters delineated in *Table 4-3* show that the quantum yields of fluorene-based fluorophores is higher than stilbene-based fluorophores. Comparing molecules with the same substituent and different cores (*e.g.*, TA01 and TA03) shows a significant increase in quantum yield values.

The explanation for this relies on the molecular structure of the fluorophores from two points of view. First, the molecules have different lengths and also different donor-acceptor terminal groups. The longer the molecules, the more the  $\pi$ -conjugation system is long and, therefore, significantly increases in emission intensity and photoluminescence quantum yields [241–243]. The second explanation is related to the rigidity and planetary of the molecules.

The more the molecule is rigid and planar, the more intersystem crossing (ISC) from singlet to triplet occurs; therefore, more nonradiative emission (dissipated as heat), which leads to weak quantum yield values, and reversibly [244].

Additionally, these molecules exhibit push-pull skeletons, especially noticed in fluorophore TA02, having a tertiary amine acting like an acceptor and pyridine as a donor (D- $\pi$ -A), a system known for its red-emission shift [245], which explains its longer wavelength absorption compared to other fluorophore dyes (TA01, TA03, and TA04). The other molecular systems have either push-push or pull-pull systems with different  $\pi$ -conjugation lengths [32,33,246].

Regarding the effect of the solvent, the emission spectra of the molecules slightly blue shifts, except for the TA02 molecule, which undergoes a hypsochromic shift from 490 nm to 467 nm, respectively, when going from ethanol to dichloromethane. These emission wavelength changes are due to the polarity of the solvents since ethanol is very polar compared to dichloromethane. Increasing polarity generally results in shifts of the emission spectra to longer wavelengths (redshift/ bathochromic), and decreasing the polarity of the solvent causes shifts to shorter wavelengths (blue shift/ hypsochromic) [247,248]. As for the photoluminescence quantum yields, increasing polarity leads to a decrease in the intensity of fluorescence spectra and therefore decreasing in photoluminescence quantum yields value [249,250], which was noticed in the reported results.

#### **4.5. Development of fluorescent textiles**

In Chapter 3, a sol-gel dyeing process was developed to dye cotton fabrics with organic dyes. This optimized process is suitable for dyes, including fluorescent dyes.

The synthesized fluorophores (TA01 ... TA04) were used to prepare fluorescent textiles using *n*PTES-based sol-gel solutions, which were applied to the fabric by the pad-dry-cure method (*see section 2.3.1*). The experimental protocol remains the same, maintaining all the molar ratios, the fluorophore concentration, and the finishing treatment (*sections 3.3.30 and 3.3.4*).

*Table 4-4* gathers the aspect and the optical characteristics of the prepared fabrics. The emission spectra of the fabrics were evaluated using an integrating sphere and white excitation source (*details on the set-up in section 2.5.6*).

Also, cotton fabrics were prepared using the doctor-blade method (also called the knife coating method) (*section 2.3.2*) using a polyacrylate polymer. The polyacrylate formulation was prepared by adding 2 wt% of each fluorophore to the raw polymer under mechanical stirring. After adjusting pH to equal 10 (using ammonia 25 %), the crosslinking agent and the thickener were added and stirred until having a formulation with a viscosity of 2800 cp (*see sections 2.2.2 and 2.3.2*). As a first check, the polyacrylate has high background fluorescence, which directly affects the emission of the final fabrics, as shown in *Table 4-5*.







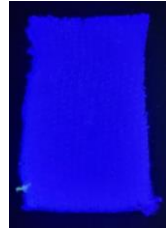
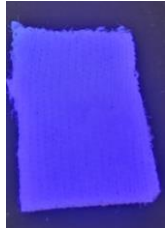
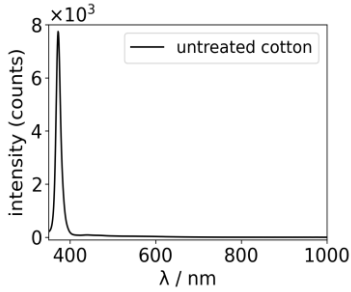
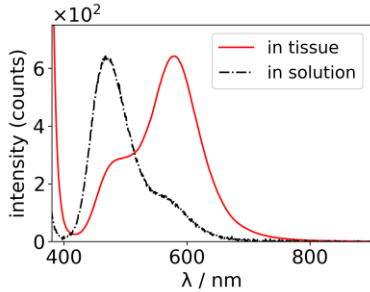
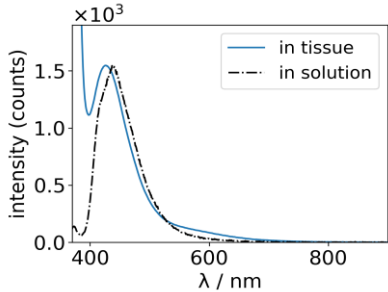
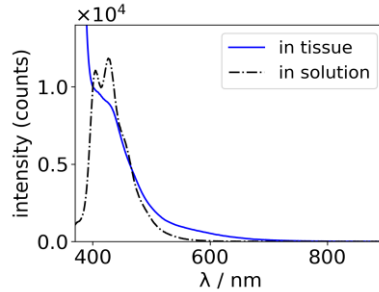
From *Table 4-4*, the emission spectra of the fluorophores dissolved in solution and applied on cotton fabrics generally differ in shape and sometimes have weak emission. This is not surprising since the fabrics were prepared using low fluorophore concentrations in the sol-gel. However, the maximum emission did not change much, except for TA02. The significant redshift noticed for the fluorophore TA02 is attributed to the protonation of the pyridine group, which is caused by the acidic sol-gel medium.

As for the results presented in *Table 4-5*, (fabrics obtained by the doctor-blade coating method), since the raw polymer-based formulation presents a fluorescence emission, which is not negligible and directly affects the absolute emissions of fluorophores, an emission-free polymer must be used. The chosen polymer for the knife-coating method was not a good selection and was not suitable. However, the use of polymer formulation will be beneficial using insoluble compounds, as will be seen in Chapter 5.

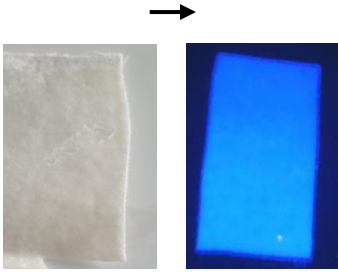
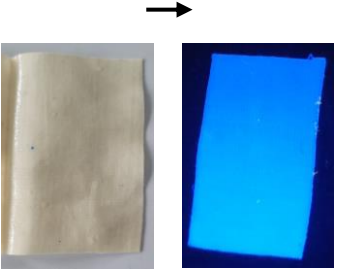
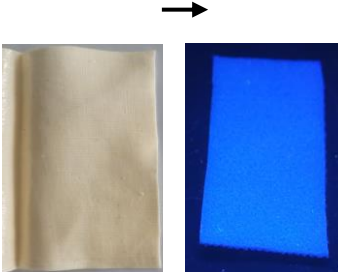
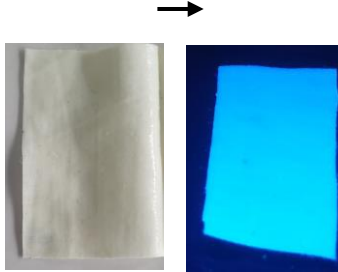
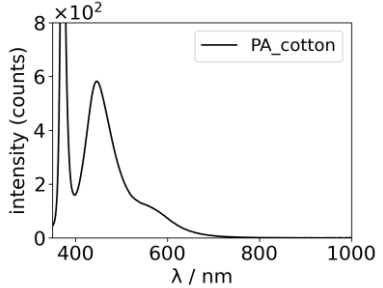
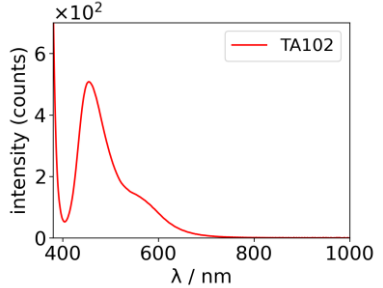
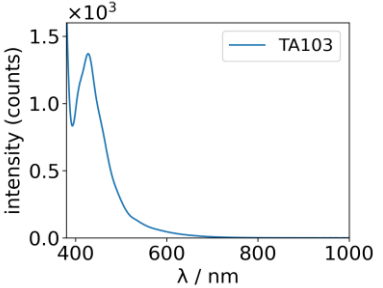
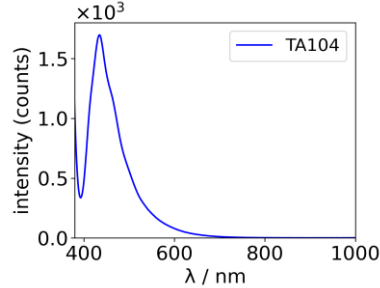


## Molecular fluorophores : Synthesis, measurement of their fluorescence quantum yields, and application to textiles

**Table 4-4.** Images of cotton fabrics obtained via the sol-gel method, pad-dry-cure (first row) of fluorophores-based *n*PTES silane precursor excited under a 365 nm lamp. Emission spectra of fabrics excited under 380 nm LED light (second row) and maximum emission wavelength (third row). The intense peaks in most spectra at 371 nm are Rayleigh-scattered excitation light, which was cut off in the spectra. The dashed spectra correspond to the fluorophores in ethanol solution

Samples	Reference	TA02	TA03	TA04
(D65) → (365nm) sol-gel based- coatings				
				
<b>Emission spectrum</b> <b>(Normalized)</b> <b>(exc = 380 nm)</b>				
<b>Maximum emission</b> <b>wavelength (nm)</b>	--	481 nm _shoulder 579 nm	426 nm	421nm _shoulder

**Table 4-5.** Images of cotton fabrics obtained via doctor-blade coating of fluorophores-based polyacrylate (first row) excited under a 365 nm lamp. Emission spectra of fabrics excited under 380 nm LED excitation light (second row) and maximum emission wavelength (third row). The intense peaks in most spectra at 371 nm are Rayleigh-scattered excitation light, which was cut off in the spectra

Samples	Reference	TA02	TA03	TA04
(D65) → (365nm) Polyacrylate based- knife blade coating				
Emission spectrum (exc = 380nm)				
Maximum emission wavelength (nm)	447 nm 570 nm_shoulder	455 nm 570 nm_shoulder	427 nm	434 nm

## **4.6. Conclusion**

The experimental results obtained in this work indicate that the proposed SAFER method for measuring PLQYs in solution by comparison with a known PLQY standard can successfully be applied for measurements using non-monochromatic excitation light sources, such as LEDs. It relies on simultaneous measurement of the absorbed and emitted light intensity spectra using spectrally calibrated spectrometers. Like other methods, it requires pure samples containing only one light-absorbing species. The methodology was explained and illustrated using several well-established dyes for which the PLQY has been measured by different laboratories using different methods. Furthermore, the values of the PLQY of a few less extensively characterized dyes were confirmed by our measurements.

After establishing the measurement method, organic push-pull fluorophores were prepared and studied spectroscopically using the SAFER method to determine their photoluminescence quantum yields. Further, these fluorophores were used to create fluorescent textiles through their employment in the sol-gel dyeing process, which is an essential step in approaching the primary goal of this thesis project, and toward the development of luminescent textiles.

Appendix 4.1. Detailed drawing of the fluorimetric set-up used in the SAFER method

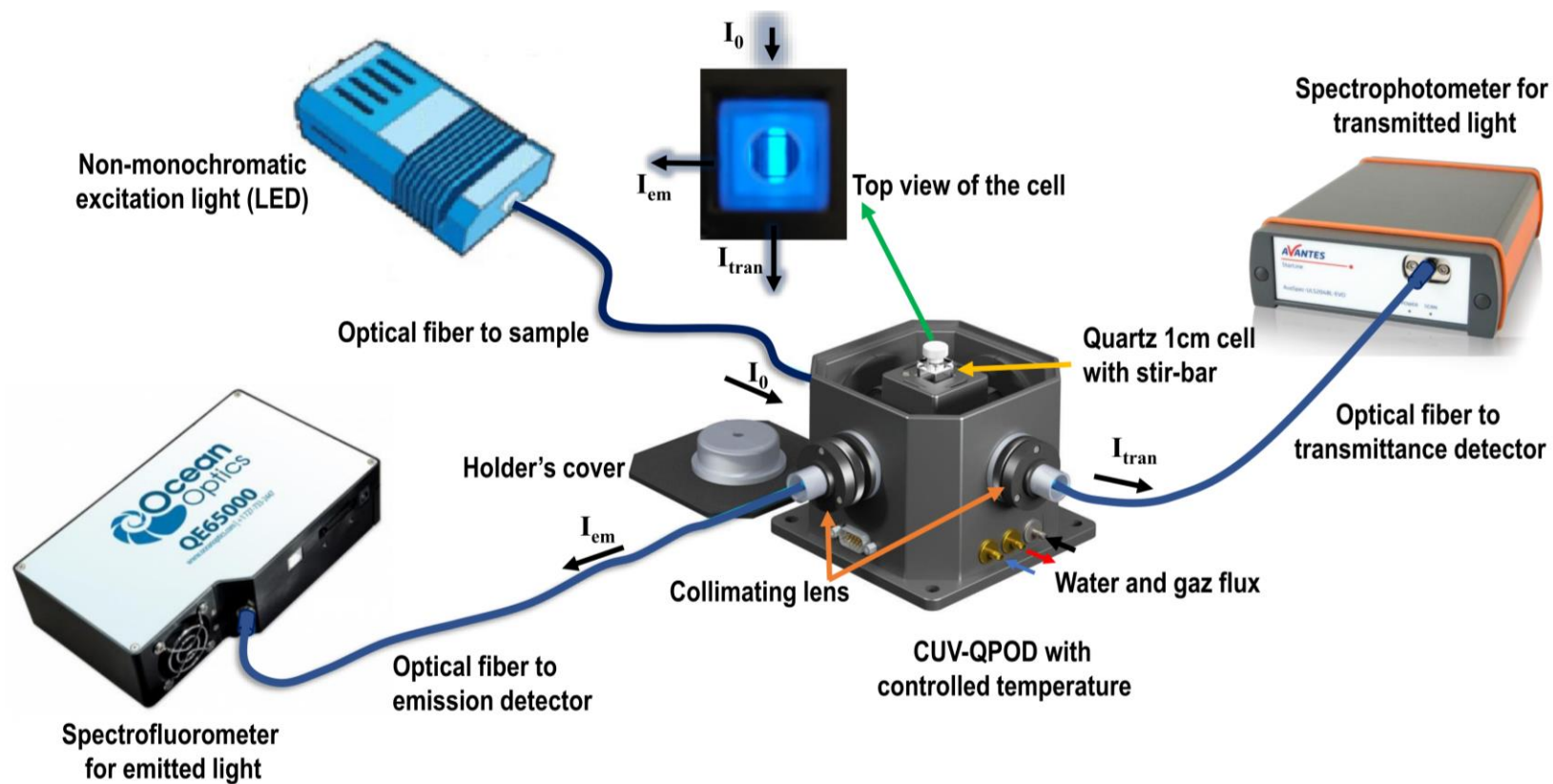


**Figure.App 4-1.** Set-up used for simultaneous light absorption and fluorescence emission measurements of limpid liquid samples for the determination of their photoluminescence quantum yields

## **Appendix 4.2. Spectrophotometers calibration**

### *4.2.1. Spectral correction factors for the spectrometer Ocean Optics QE65000*

The correction factors for the fiber-coupled OceanOptics QE65000 spectrometer (HC1 grating, spectral range 350...1050 nm), which is used for measuring the spectra of the emitted light, were determined using two principal emission reference standards. For the range 350...430 nm, the reference standard was a solution of 2-aminopyridine (2AP) in 0.05M H<sub>2</sub>SO<sub>4</sub>(aq), whose calibrated fluorescence emission spectrum has been reported in the literature[216]. Its fluorescence was excited using a fiber-coupled 280 nm UV LED (Thorlabs M280F5, good optical power 0.8 mW). For the range 410...1050 nm, a fiber-coupled incandescent tungsten-halogen calibration lamp (OceanOptics LS1-CAL) was used. The spectral intensity data for this tungsten-halogen light source is traceable to NIST.

The supplied calibration data were interpolated using spline interpolation and converted to a relative spectral photon flux. The two sets of data (2AP and LS1-CAL) show very good overlap in the zone of spectral overlap, which was used to scale the data sets to make a smooth junction. The resulting merged data set was then scaled such that the minimal value of the set was 1.0. The wavelength of this minimum is where the detection system has the highest overall quantum efficiency. The graph of the final correction factors is shown in *Figure.App 4-2*.

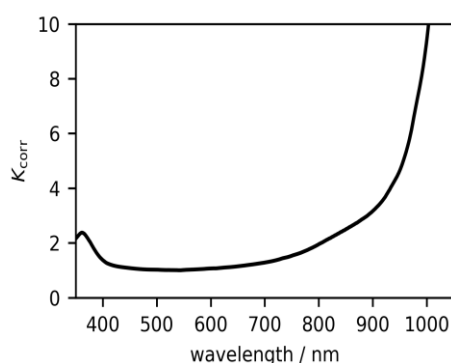


**Figure.App 4-2.** Final correction factor  $K_{corr}(\lambda)$  for the QE65000 spectrometer 350...1050 nm

---

The correction curve for this spectrometer is smooth and reasonably flat up to 920 nm. The spectrometer has good sensitivity in the near-infrared: at 1000 nm, the photon detection efficiency is still 10% of the maximum detection efficiency (reaching near 540 nm). The grating and detector efficiency data were also used to create an alternate set of correction factors. These data were digitized from the documentation supplied by the manufacturer and interpolated using spline interpolation. There was good agreement between these alternate corrections factors and the original correction factors.

Finally, the correction factors were checked by recording the fluorescence emission spectra of samples whose spectra have been accurately described in the open literature. For quinine bisulfate in 0.1M HClO<sub>4</sub>(aq), a reference emission spectrum has been established and published by the United States National Institute of Standards and Technology (NIST) [216,251]. The laser dye DCM in methanol is a red-emitting reference. Its corrected emission spectrum has been measured and published by Gardecki and Maroncelli [234]. The agreement between the published spectra and our corrected spectra is excellent, indicating the accuracy of the correction factors determined for the QE65000 spectrometer and consensus between calibration sources published and measured spectra.

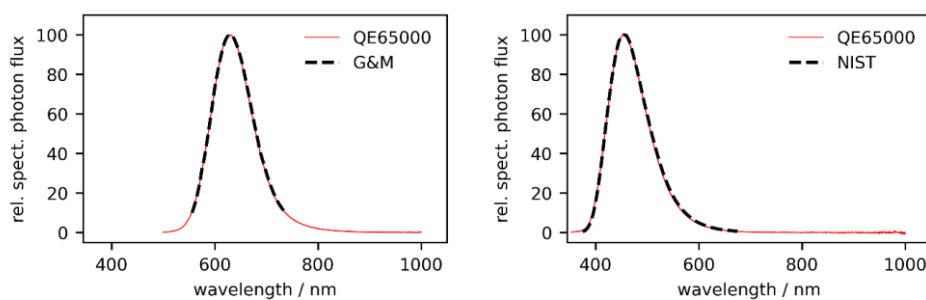


**Figure.App 4-3.** Comparison of corrected fluorescence emission spectra measured using QE65000 spectrometer (solid red line) and spectra from the literature (dashed black line, see Text). Left panel: QBS in 0.1M HClO<sub>4</sub>(aq), excited with 380 nm LED. Right panel: DCM in methanol, excited with a 450 nm LED

### 4.2.2. Spectral correction factors for the spectrometer Avantes ULS2048CL-EVO

The fiber-coupled spectrometer used for measuring the spectrum of the transmitted excitation light (Avantes ULS2048CL-EVO) covers a slightly wider wavelength range

## Molecular fluorophores : Synthesis, measurement of their fluorescence quantum yields, and application to textiles

---

(325...1080nm) than the QE65000 spectrometer. It is equipped with a 25 $\mu$ m slit, which leads to higher spectral resolution and lower sensitivity. The lower sensitivity is a desirable property in this case because of the intensity of the excitation light. The calibration procedure used is very similar to the one described above, using 2AP for the UV and the LS1-CAL tungsten-halogen source for the Vis-NIR window.

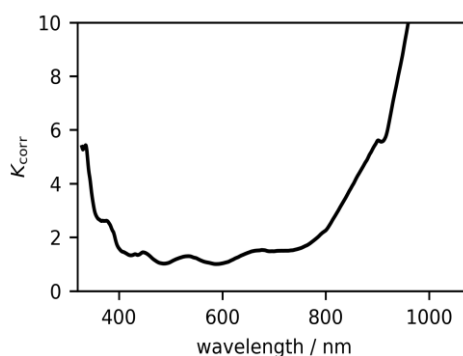


**Figure.App 4-4.** Correction factor  $K_{corr}(\lambda)$  for the ULS2048CL spectrometer 325...1080 nm (right)

The correction factor curve for the ULS2048CL spectrometer shows more structure than the curve for the QE65000 spectrometer. This is due to the ULS2048CL having a CMOS sensor array, whereas the QE65000 has a back-thinned CCD array. Over the years, CMOS light sensors, in particular image sensors, have been the subject of significant improvement in sensitivity, signal-to-noise ratio, read-out speed, and electronic flexibility and can now advantageously replace CCD sensors in several spectroscopy applications. However, (back-thinned) CCDs are still superior in terms of homogeneity, dark current, and smoothness of spectral response.

The correction factors determined were checked by measuring corrected emission spectra using the ULS2048CL like previously done for the QE65000 spectrometer. For this, the spectrometer was temporarily connected to the fiber carrying the emitted light signal. Again, there is an excellent agreement between our corrected spectra and those reported in the literature. The recorded emission spectra are somewhat noisier due to the limited sensitivity of this spectrometer, which is configured for transmitted light (absorbance) measurements.

---

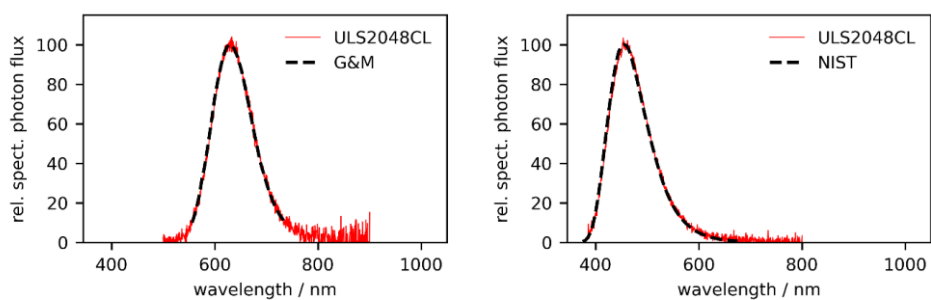


**Figure.App 4-5.** Comparison of corrected fluorescence emission spectra measured using ULS2048CL spectrometer (solid red line) and spectra from the literature (dashed black line, see text above). Left panel: QBS in 0.1M HClO<sub>4</sub>(aq), excited with 380 nm LED. Right panel: DCM in methanol, excited with a 450 nm LED.



### **Appendix 4.3. Proportionality of the emitted light intensity and the integrated absorbed light intensity**

An issue that may occur in the measurement of photoluminescence quantum yield is the re-absorption of the emitted light by the fluorophore, known as the "inner-filter effect," which leads to distorted emission spectra to loss of the proportionality between the emitted light and absorbed light intensities. Furthermore, aggregation or excimer formation might occur for certain compounds as their concentration increases.

To study the loss of linearity in the emitted *vs.* absorbed intensity plot, we performed a series of separate measurements in which the concentration of the dye was deliberately increased above the limit of OD = 0.1 to illustrate the usefulness of successive measurements in increasing concentrations for validation of the PLQY result. As expected, the dependence generally remains linear until OD ~ 0.1. However, there are subtle differences between different fluorophores, depending on the Stokes' shift of the fluorophore, which changes the strength of the inner-filter effect at higher concentrations (and potentially aggregation behavior or excimer formation). For PLQY determinations, only the linear regions of the data are used, working at low concentrations.

#### **Example 1.** Cresyl violet dissolved in methanol under 450 nm LED excitation

Aggregation is known to affect the PLQY of cresyl violet in methanol [235] at concentrations above 1  $\mu\text{M}$  (corresponding to an optical density of 0.07 at the absorption maximum [252]). Indeed, proportionality between absorbed and emitted light intensities are lost when going beyond this limit. For PLQY measurement, we worked at concentrations below 0.5  $\mu\text{M}$ .

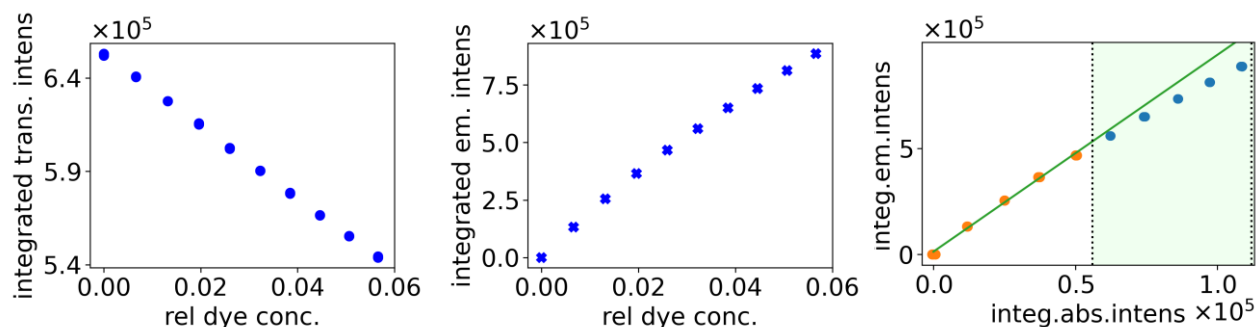


**Figure.App 4-6.** Cresyl violet in MeOH under 450 nm excitation. Integral transmitted light (left). Integralemitted light (center). The linearity (and loss of linearity-green panel) of the plot of the integral emitted light intensity vs the integral absorbed light intensity (right)

**Example 2.** Fluorescein dissolved in 0.1M of NaOH under 450 nm LED excitation

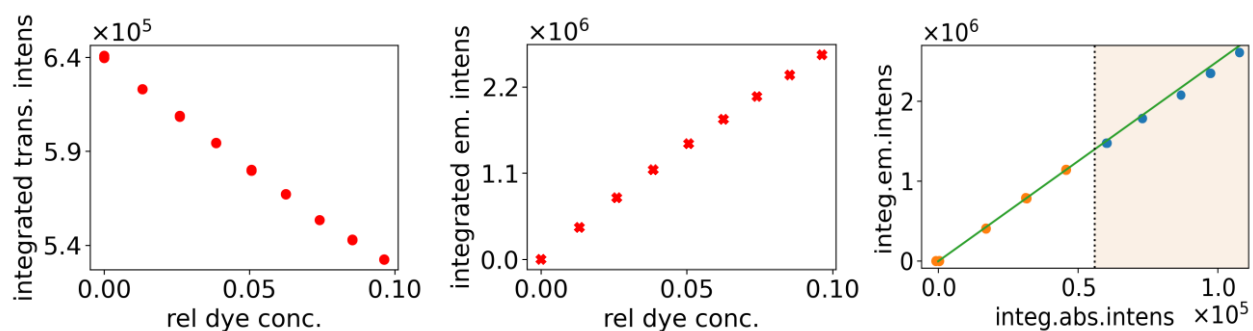
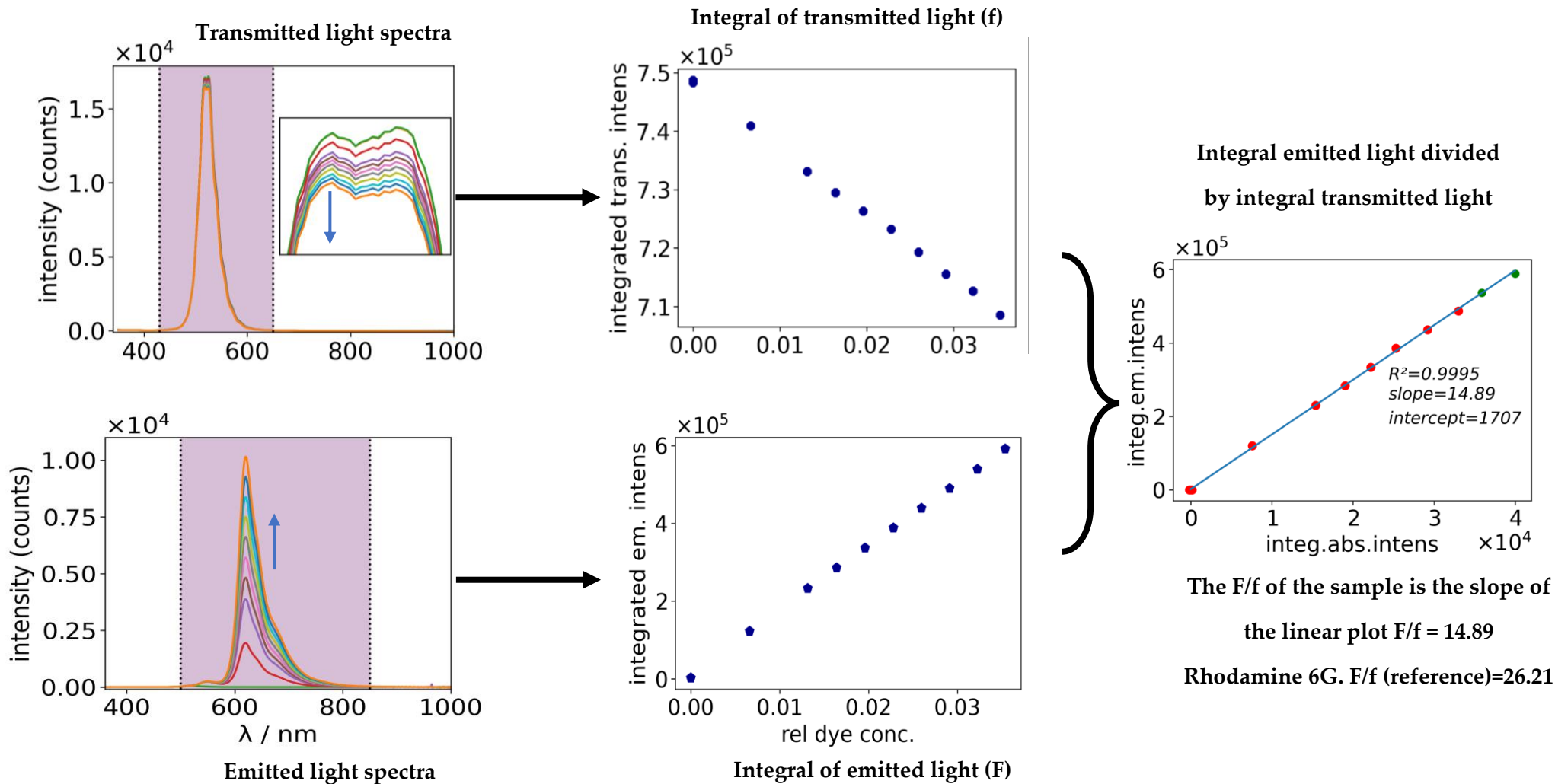


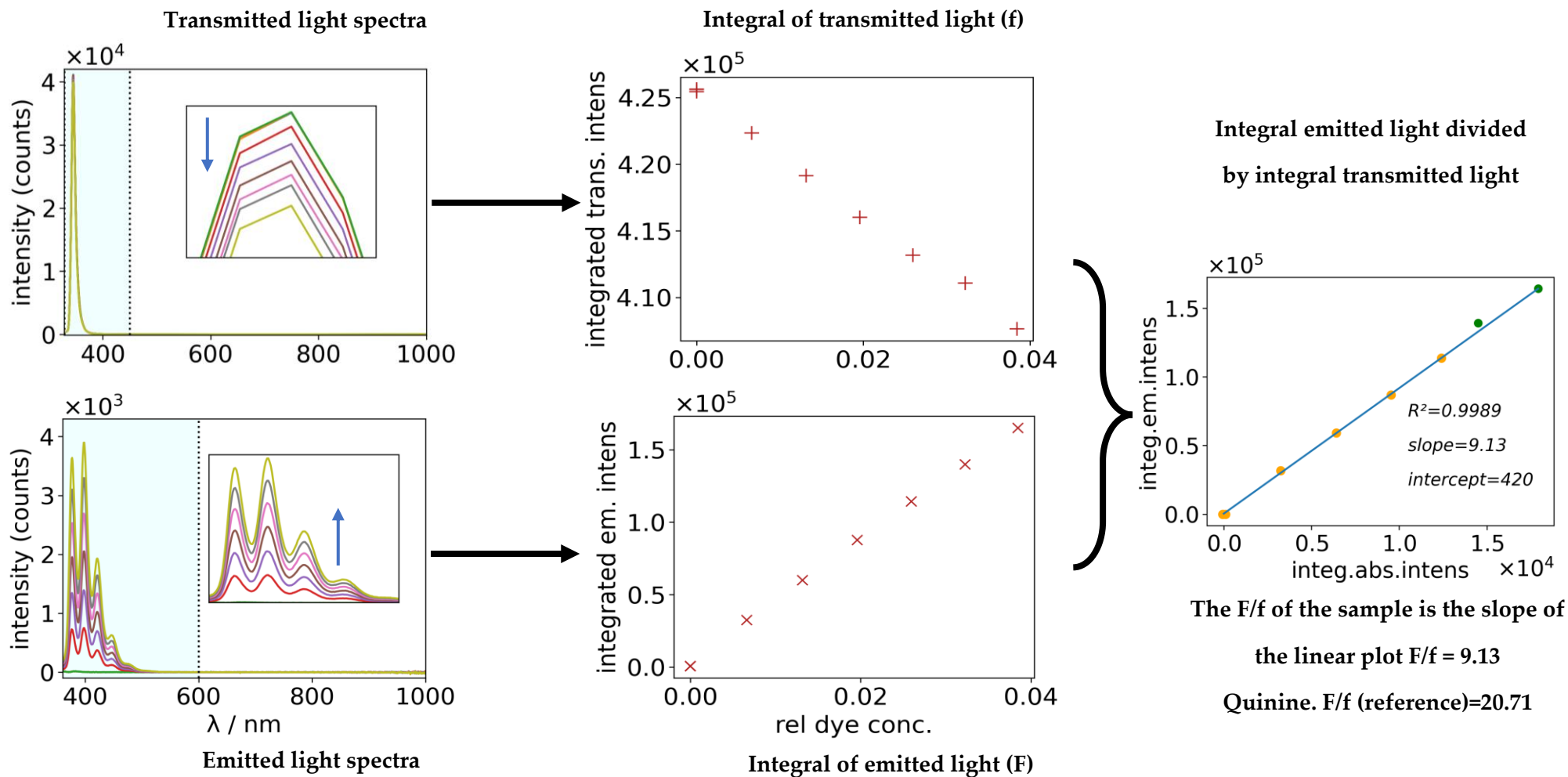
**Figure.App 4-7.** Fluorescein in 0.1M NaOH under 450 nm excitation. Integral transmitted light (left). Integralemitted light (center). The linearity (and loss of linearity-lightorange panel) of the plot of the integral emitted light intensity vs the integral absorbed light intensity (right)

For the PLQY determination to be reliable, this emitted *vs.* absorbed light intensity plot should be linear for the sample and the reference. Our method performs this check explicitly. Note that the amount of absorbed light is directly relevant for PLQY determination. The actual dye concentration is only of secondary relevance. The plot of emitted light intensity *vs.* concentration loses its linearity at lower dye concentrations than the plot of emitted *vs.* absorbed light.

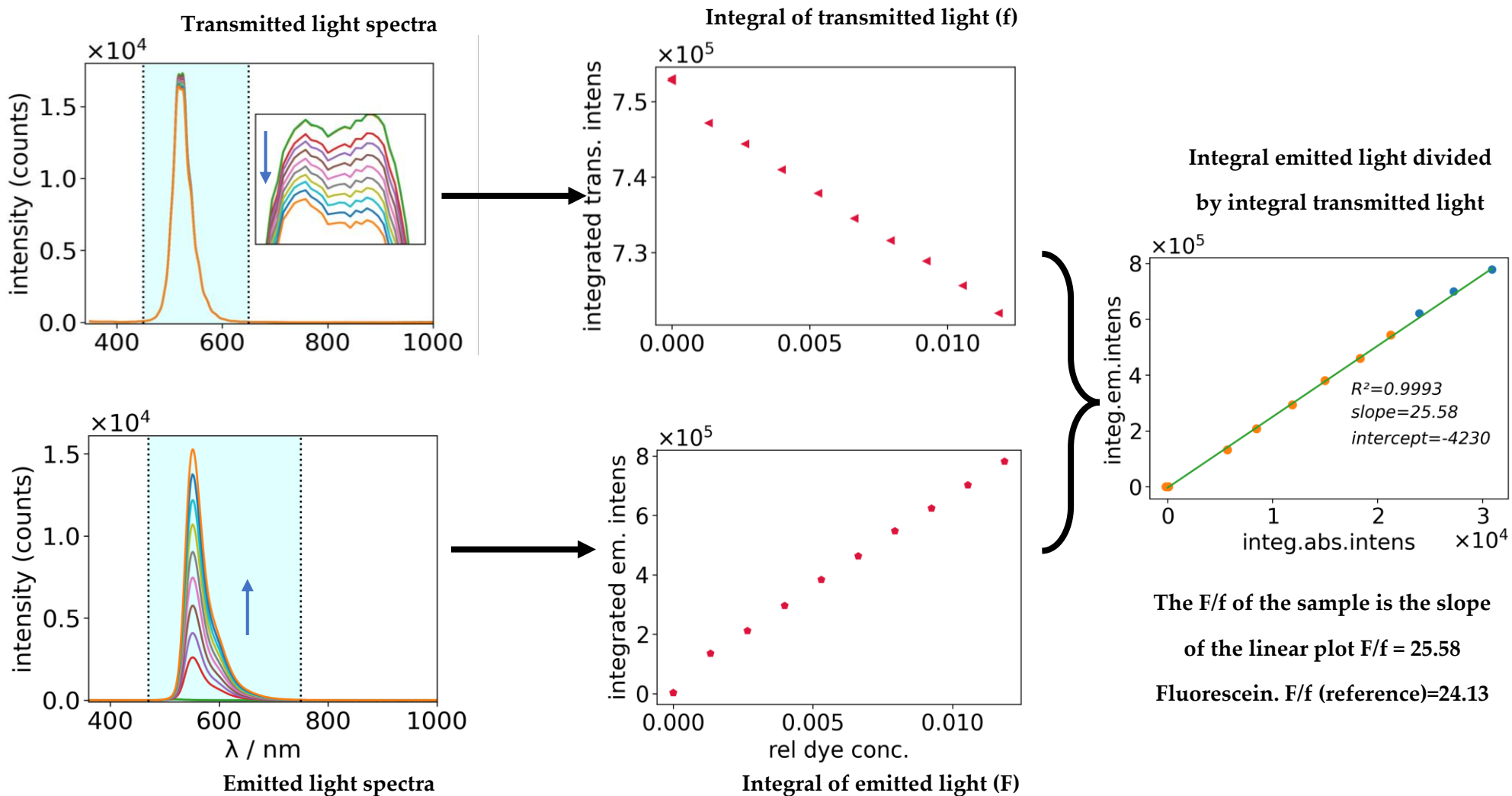
Appendix 4.4. Cresyl violet in methanol excited at 518 nm



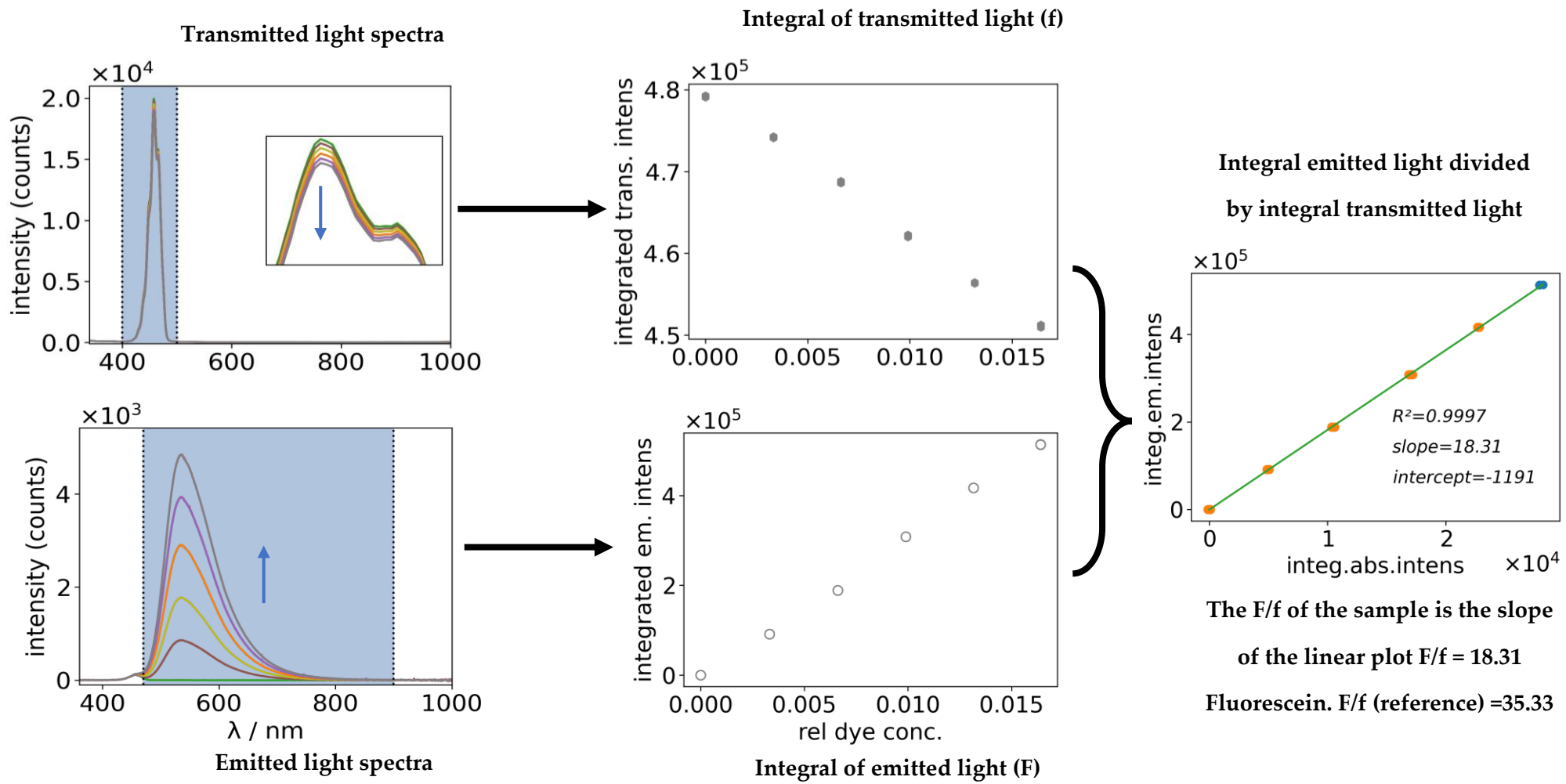
Appendix 4.5. Anthracene in ethanol excited at 340 nm



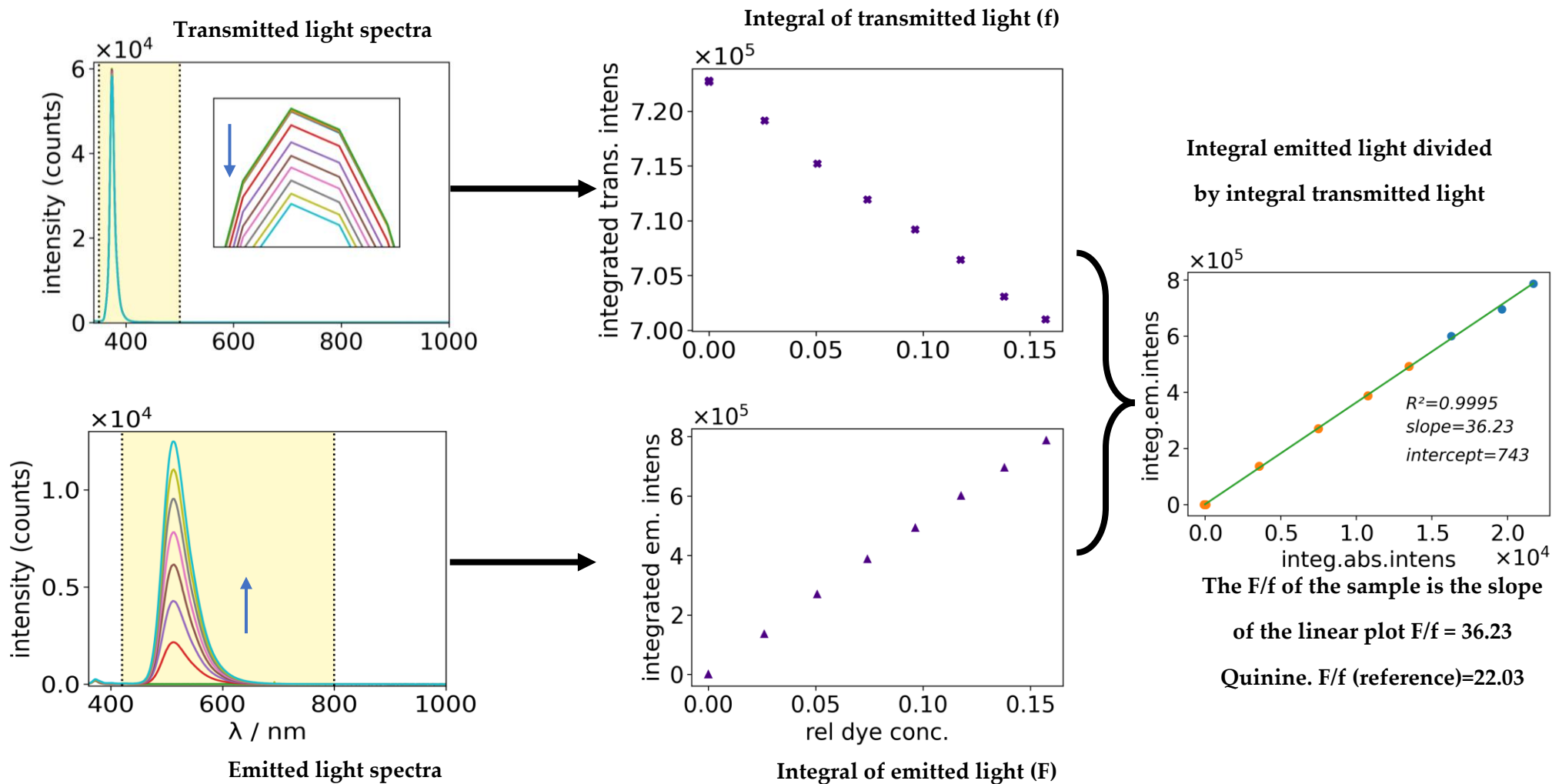
Appendix 4.6. Rhodamine 6G in EtOH excited at 518 nm



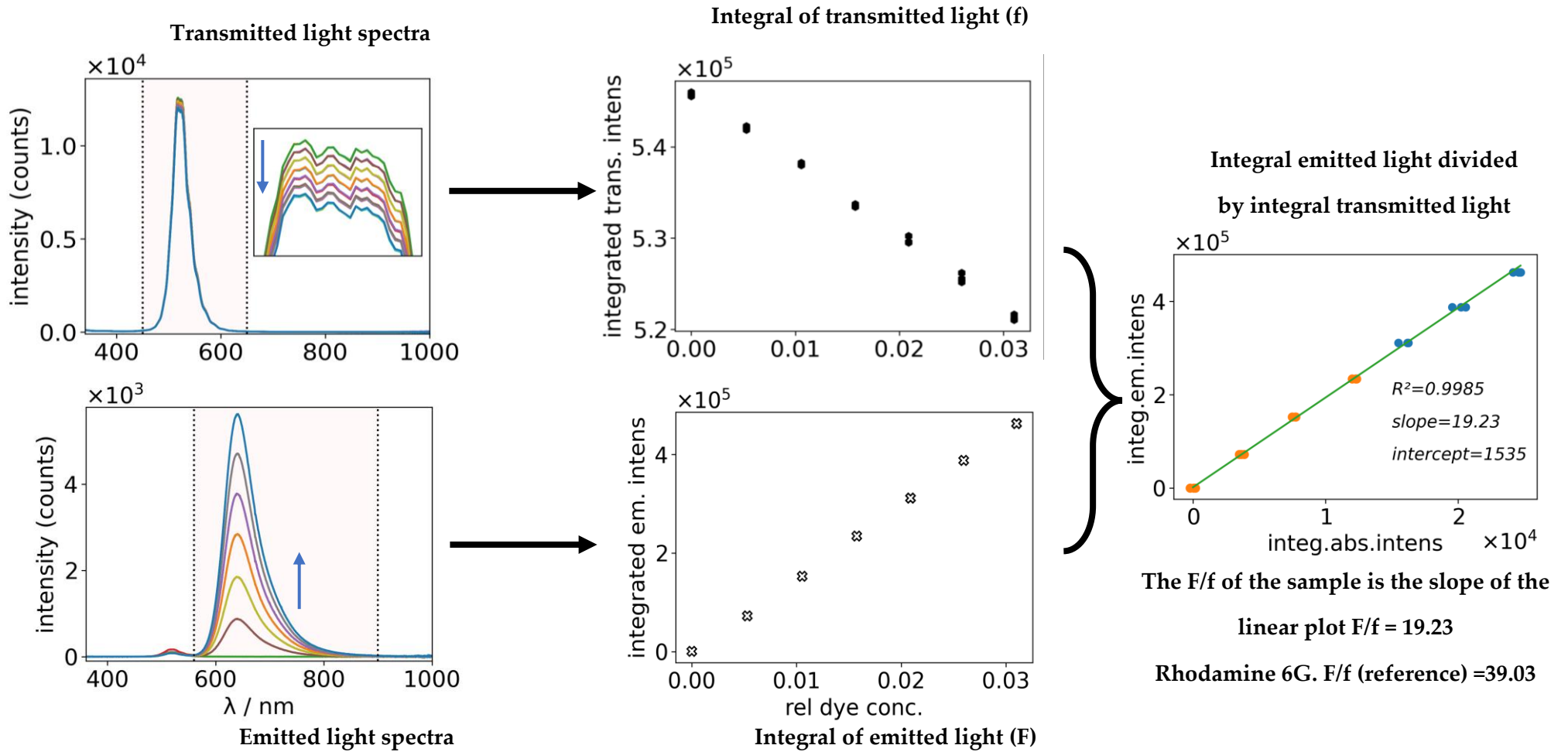
Appendix 4.7. Coumarin 153 in methanol excited at 450 nm



Appendix 4.8. Pyranine in 0.01M NaOH excited at 380 nm



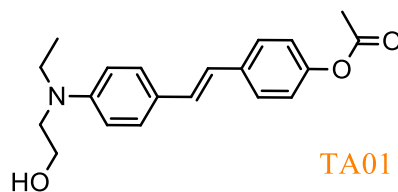
Appendix 4.9. Nile Red in methanol excited at 518 nm





## **Appendix 4.10. Synthesis of stilbene and fluorene-based fluorophores**

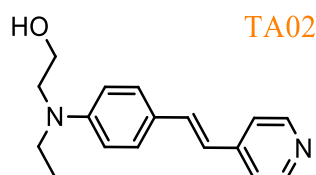
### **4.10.1. Synthesis of TA01**



**(E)-4-(4-(ethyl(2-hydroxyethyl)amino)styryl)phenyl acetate**

One gram (0.034mM) of 2-(ethyl(4-iodophenyl)amino)ethanol is dissolved in 50 ml of acetonitrile under Argon and stirred for 30 minutes at room temperature. After, 1.47 g (0.091mM) of acetoxystyrene, 13.3 mg (0.59mM) of palladium diacetate, 12.13 mg (0.40mM) of tri-*o*-polyphosphine, and 0.92 g (0.091mM) of triethylamine are then added to the mixture and stirred for one night at 95 °C. The residue is purified by chromatographic column using 1:1 ethyl acetate and cyclohexane as eluent. 48% yield brown paste is obtained. ATR-IR ( $\nu$   $\text{cm}^{-1}$ ): 3351 $\text{cm}^{-1}$  ( $\nu$ , -OH), 2965-2877 $\text{cm}^{-1}$  ( $\nu$ , -CH), 1747 $\text{cm}^{-1}$  ( $\nu$ , C=O), 1600-1500 $\text{cm}^{-1}$  ( $\nu$ , C=C Ar), 1353 $\text{cm}^{-1}$  ( $\nu$ , CN), 960 $\text{cm}^{-1}$  ( $\nu$ , =C-H).  $^1\text{H}$  NMR (400 MHz,  $\text{CDCl}_3$ , 298 K):  $\delta$  (ppm) 1.15(t, 3H), 3.41(q, 2H), 3.65(s, OH), 3.73(t, 2H), 4.20(t, 2H), 6.71(q, 2H Ar), 7.26(d, 1H C=C), 7.47(d, 2H Ar), 7.72(d, 1H Ar), 7.91(d, 1H, C=C), 8.54(d, 2H Ar).

### **4.10.2. Synthesis of TA02**

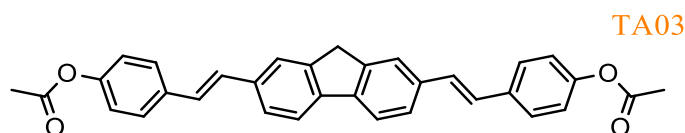


**(E)-2-(ethyl(4-(2-(pyridin-4-yl)vinyl)phenyl)amino)ethanol**

One gram (0.034mM) of 2-(ethyl(4-iodophenyl)amino)ethanol is dissolved in 50 ml of acetonitrile under Argon and stirred for 30 minutes at room temperature. After, 0.82 g (0.078mM) of 4-vinylpyridine, 11.4 mg (0.506mM) of palladium diacetate, 10.47 mg (0.340mM) of tri-*o*-polyphosphine, and 0.79 g (0.078mM) of triethylamine are then added to the mixture and stirred for one night at 95 °C. The residue is purified by recrystallization in acetonitrile. 89 % yield orange powder is obtained. ATR-IR ( $\nu$   $\text{cm}^{-1}$ ): 3351 $\text{cm}^{-1}$  ( $\nu$ , -OH), 2965-2877 $\text{cm}^{-1}$  ( $\nu$ , CH), 3259 $\text{cm}^{-1}$  ( $\nu$ , -OH), 2957-2862 $\text{cm}^{-1}$  ( $\nu$ , -C-H), 1517-1464 $\text{cm}^{-1}$  ( $\nu$ , -C=C Ar), 964

$\text{cm}^{-1}$  ( $\nu$ , -C=C-H).  $^1\text{H NMR}$  (400 MHz,  $\text{CDCl}_3$ , 298 K):  $\delta$  (ppm) 1.15(t, 3H), 2.28(s, 3H), 3.41(t, 2H), 3.65(s, OH), 3.73(t, 2H), 4.20(t, 2H), 6.76(d, 2H Ar), 6.95(s, 2H C=C), 7.29(d, 2H Ar), 7.84(m, 4H Ar).

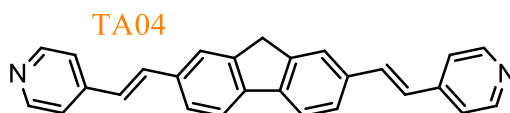
#### 4.10.3. Synthesis of TA03



**((1*E*,1'*E*)-(9*H*-fluorene-2,7-diyl)bis(ethene-2,1-diyl))bis(4,1-phenylene) diacetate**

One gram (1.703mM) of 2,7-diiodo-9*H*-fluorene is dissolved in 50 ml of acetonitrile under Argon and stirred for 30 minutes at room temperature. After, 0.55 g (0.340mM) of acetoxystyrene, 19 mg (0.085mM) of palladium diacetate, 51.66 mg (0.170mM) of tri-*o*-polyphosphine, and 0.393 g (3.9mM) of triethylamine are then added to the mixture and stirred for one night at 95°C. The residue is purified by recrystallization in acetonitrile. 83% yield gray powder is obtained. ATR-IR ( $\nu \text{ cm}^{-1}$ ): 3301 $\text{cm}^{-1}$  ( $\nu$ , OH), 2919-2850 $\text{cm}^{-1}$ ( $\nu$ , CH), 1408-1442 $\text{cm}^{-1}$ ( $\nu$ , C=C Ar), 956 $\text{cm}^{-1}$  ( $\nu$ , -C=CH).  $^1\text{H NMR}$  (400 MHz,  $\text{CDCl}_3$ , 298 K):  $\delta$ (ppm) 2.28(s, 6H), 4.12(s, 2H), 6.95(s, 4H), 7.29(q, 4H), 7.54( dd, 2H), 7.71(d, 2H), 7.82(m, 4H).

#### 4.10.3. Synthesis of TA04



**2,7-bis((*E*)-2-(pyridin-4-yl)vinyl)-9*H*-fluorene**

One gram (1.700mM) of 2,7-diiodo-9*H*-fluorene is dissolved in 50 ml of acetonitrile under Argon and stirred for 30 minutes at room temperature. After, 0.358 g (3.41mM) of 4-vinylpyridine, 57.2 mg (0.085mM) of palladium diacetate, 51.66 mg (0.170mM) of tri-*o*-polyphosphine, and 34.5 mg (3.41mM) of triethylamine are then add to the mixture and stirred for one night at 95 °C. The residue is purified by recrystallization in acetonitrile. 91% yield yellow powder is obtained. ATR-IR ( $\nu \text{ cm}^{-1}$ ) : 3301 $\text{cm}^{-1}$  ( $\nu$ , OH), 2919-2850 $\text{cm}^{-1}$ ( $\nu$ , CH), 1408-1442 $\text{cm}^{-1}$ ( $\nu$ , C=C Ar), 1353 $\text{cm}^{-1}$  ( $\nu$ , CN), 956  $\text{cm}^{-1}$  ( $\nu$ , -C=CH).  $^1\text{H NMR}$  (400 MHz,  $\text{CDCl}_3$ , 298 K):  $\delta$  (ppm) 4.12(s, 2H), 7.25(d, 2H), 7.42(dd, 2H), 7.47( d, 4H), 7.82(d,2H), 7.91(d,2H), 8.54(d ,4H).

---

# **Chapter 5 Organic and inorganic materials with long persistent luminescence and development of persistently luminescent textile fabrics**

## **5.1. Introduction**

In the final chapter of this thesis, we are taking steps toward the development of textiles displaying long persistent “glow in the dark” luminescence, which is the ultimate goal of this work. The overall strategy was to create luminescent textile fabrics by incorporating photoluminescent materials through various methods. To achieve fabrics that emit light for an extended period of time, it is necessary to use materials with strong and long-lasting luminescence emission. According to previous research, strontium aluminate-based inorganic phosphors are currently the most effective persistently luminescent materials for this purpose [88,97,253]. However, there is also growing interest in using organic luminescent materials, which have been shown to exhibit promising persistent luminescent behavior [133,134,137,194].

In the first part of this chapter, a selection of organic compounds is synthesized, which have been reported in the literature to display long persistent luminescence (LPL) in the crystalline state. Their luminescent properties are investigated with a specific time-resolved luminescence spectroscopic set-up. In the second part, commercial doped strontium aluminate phosphors were investigated and compared with the organic luminescent materials. The persistent luminescence of the commercial inorganic materials was found to be much more intense and

lasted for a long duration. The third part of the chapter describes the incorporation of the inorganic persistently luminescent phosphors into textiles and the characterization of their luminescence.

## **5.2. Set-up for spectrotemporal characterization of luminescence**

Before discussing the studies of LPL materials, we describe a specific set-up that measures the emission spectrum of a material as a function of time with a sub-millisecond resolution while at the same time being able to measure luminescence on the second to minute timescales. Conventional time-resolved luminescence equipment is usually limited to very short time scales, either nanosecond timescale for fluorescence or microsecond timescale for phosphorescence measurements. The new set-up will be used throughout this chapter to characterize the long-lived luminescence of the various materials. Other instruments, standard measurements, and analysis procedures have been described earlier in Chapter 2.

The set-up is based on fiber-coupled spectrometers described earlier in this thesis (*section 2.5.3*) and installed on an optical breadboard (*Figure 5.1*). The excitation light is typically a 365 nm wavelength LED (Thorlabs M365L2) equipped with an aspheric condenser lens (ACL25416U-A, Ø1", f=16 mm, NA = 0.79). The excitation light illuminates the sample under a 45° angle. In the front, a bare-optical fiber (600 µm internal diameter) coupled with a high-pass filter (Ocean Optics OF2-GG395) transmits wavelengths > 395 nm to reduce the emission of the excitation LED itself. The optical fiber is positioned above the sample holder to be the closest to the sample. The other side of the fiber is connected to a calibrated CMOS spectrophotometer from Avantes (ULS2048CL-EVO). The samples were deposited on a thin metal plate. The excitation source is connected to a LED driver (Thorlabs LEDD1B) controlled by a function generator for generating periodic pulsed excitation (defined by its period and pulse width).

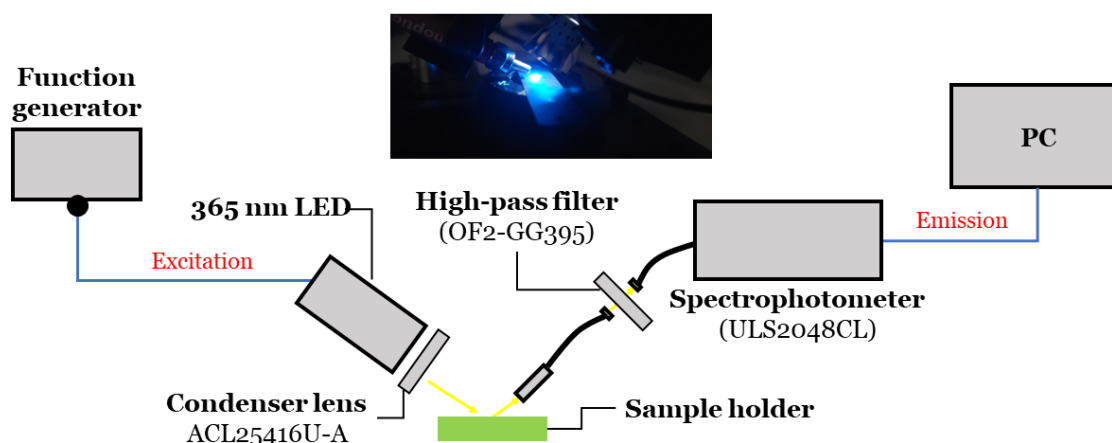


**Figure 5.1.** Set-up for the spectrotemporal measurement of long persistent luminescence of solid materials. The image depicts a sample being measured in dark conditions

The advantage of the fiber-coupled assembly is that it can be adjusted for each type of sample. In this case, the same set up was used to investigate the phosphorescent compounds in their powder form and the textile fabrics. Whereas most of the time, the 365 nm LED was used, use was made of a home-built 260 nm LED excitation source when required. This source was built around a TSLC N3535U LED (260 nm, TSLC, Taiwan) mounted on an ILR-XN01-S260-LEDIL-SC201 board (Intelligent LED Solutions, UK) with a thermal dissipator and connected to the Thorlabs LEDD1B driver that acts as the LED current source.

Different measurement parameters were adjusted depending on the type of analyte. The basic parameters are as described here, except when indicated. The function generator was set to flash the excitation source every 100 seconds, with a pulse width of 5 seconds (“p100s, w5s” for “period 100 s, width 5 s”) for several cycles. The spectrometer is synchronized to start recording simultaneously with the LED, and the recording is averaged over several excitation cycles.

### ***Part One: Organic room-temperature luminescent materials***

As mentioned in the introduction, various organic materials in the solid state can exhibit long-lived luminescence, which can last for a few minutes to a few hours at room temperature [136,137]. Two types of mechanisms are known in the literature. The first type of mechanism is the “intramolecular mechanism”, where the excitation energy remains in the initially excited molecule. The best-known example is room-temperature phosphorescence, in which the long-lived emission comes from the triplet state of the compound, which is directly populated from the initially excited singlet state. Alternatively, in certain cases, the triplet state may repopulate the fluorescent singlet state, leading to delayed fluorescence [104, 107].

The second type of mechanism is the “intermolecular mechanism”, where photoexcitation of the chromophore in its singlet state leads to the creation of an electron-hole due to intermolecular charge transfer processes. The electrons and holes separate and diffuse in the material (hop from chromophore to chromophore) to end up in trap sites, where they are stored. These trapped charge carriers then slowly recombine either by direct exciplex or excimer emission or via a population of an emissive singlet or triplet state [119,122,135].

The chosen materials for the present investigation are those studied in work by Alam *et al.* [135], which involves the growth of crystals (aggregates) and their doping with electron donor molecules. Previously described materials were chosen since the field of organic materials with long-persistent luminescence is new, and it is important to reproduce previous work to have a starting benchmark for comparison with future materials.

## **5.3. Synthesis of organic room temperature molecules**

### **5.3.1. Chemicals**

All used chemicals were of high purity and used as received. Triphenylphosphine (TPP, 99.5%), 1,3-dibromopropane (C3Br2, 99%), *N,N,N',N'*-tetramethylbenzidine (TMB, 95%), hexafluorophosphoric acid solution (HPF<sub>6</sub>, ~55 wt. % in H<sub>2</sub>O). Ethanol (EtOH, 95%, 4% water),

acetonitrile (ACN, 96%), dichloromethane (DCM, 99%), ethyl acetate (EA, 99.7%), diethyl ether (DE, 99%, anhydrous) were supplied by Sigma-Aldrich/Merck and VWR International.

### 5.3.2. Synthesis routes

The electron acceptor molecule (*TPPC3Br2*) was prepared using a simple one-step synthesis similar to that used in the reference [135]. The two steps synthesis route of the donor-acceptor binary system (*TPPC3Br2-TMB*) is identical to what has been reported in references [119,122,135]. The ions metathesis with  $PF_6^-$  anion is made following the reported synthesis pathway described in reference [124] with minor changes.

#### 5.3.2.A. Preparation of acceptor (guest) molecule

**TPPC3Br2.** One molar equivalent of triphenylphosphine (3.00 g, 12 mM) and 1 molar equivalent of 1,3-dibromopropane (2.31 g, 12 mM) were mixed neatly in a bottle with a screw cap. The reaction mixture was left for 6-8 hours with stirring at 95°C, and the product was recovered as a white precipitate. The obtained product was washed three times with small portions of diethyl ether to eliminate unreacted compounds. The product was subsequently purified twice by recrystallization from absolute ethanol to have transparent crystals of different sizes.

#### 5.3.2.B. Growth of OLPL crystals

**TPPC3Br2-TMB.** In order to dope the *TPPC3Br2* crystals (host molecule) with an electro-donor, the molar ratio of *TMB/TPPC3Br2* was (10:1) was used. 500 mg (10 mmol) of *TPP-C3Br2* was dissolved in 5 mL of *DCM*, followed by the addition of 2.40 g (100 mmol) of *N,N,N',N'*-tetramethylbenzidine, and finally, 5 mL of ethyl acetate was layered on top. The mixture was left undisturbed for a few days until small crystals formed. No additional purification was performed.

#### 5.3.2.C. Metathesis: exchange of the bromide ion for hexafluorophosphate

**TPPC3Br1PF6.** The bromide counterion in the host molecule is exchanged with a hexafluorophosphate counterion through a metathesis reaction. To do this, 1 molar equivalent

## Organic and inorganic materials with long persistent luminescence and development of persistently luminescent textile fabrics

of  $TPPC3Br_2$  (1.00 g, 30 mmol) and 1 molar equivalent of hexafluorophosphoric acid solution (0.44 g, 30 mmol) were mixed with 20 mL of acetonitrile. The reaction mixture was stirred overnight at  $95^\circ\text{C}$ , resulting in the formation of a white precipitate. The product was washed three times with small amounts of diethyl ether to remove unreacted compounds. It was then purified twice through recrystallization from absolute ethanol to obtain crystals for spectroscopic measurements.

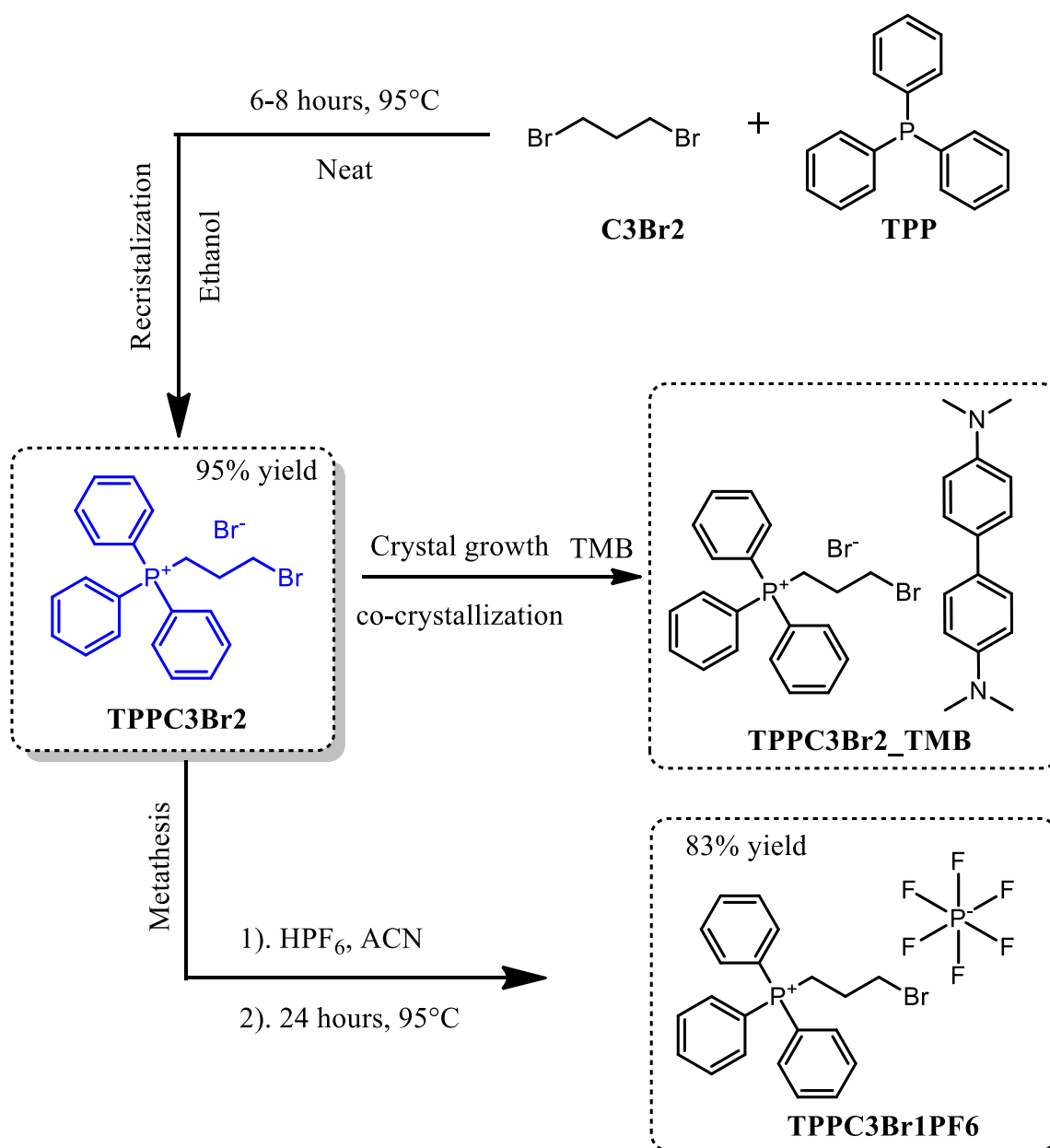


Figure 5.2 Synthesis route of the prepared organic persistent luminescent materials



### 5.3.3. Spectroscopic measurements

The spectroscopic measurement setup is the one shown in *section 5.2* with the use of a 260 nm excitation LED and changes in the period and width of the excitation. The setup was set to a period of 2 seconds and a width of 1 second. The data were analyzed as follows :

First, data were collected, corrected, and averaged over several excitation cycles (*Figure 5.3*).

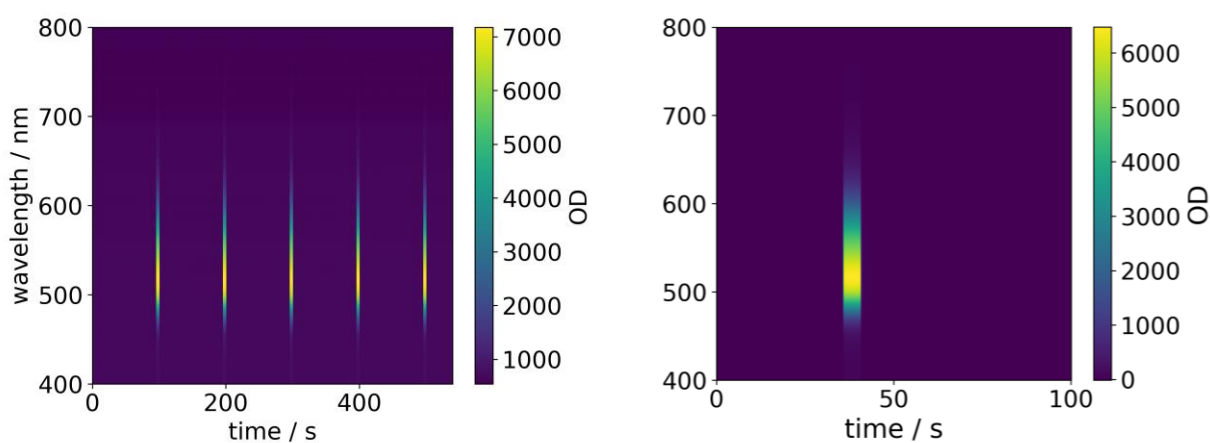


**Figure 5.3.** Excitation and emission intensities as a function of time and wavelength (left). Averaged over cycles (right). Example of TA1

When the excitation source is operating, the emission spectra are the (prompt) fluorescence of the material. After switching off the excitation source, the recorded spectra are the persistent luminescence of the compounds.

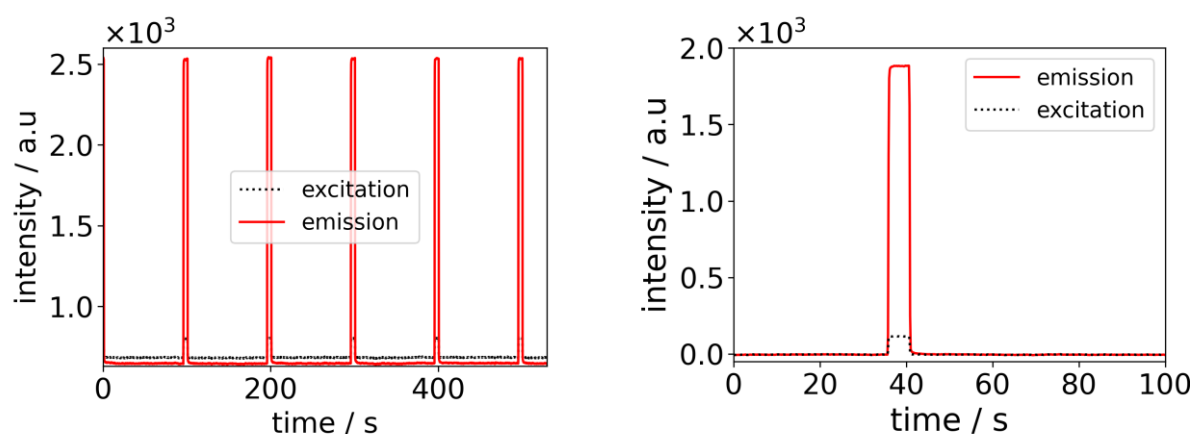


**Figure 5.4.** Excitation and emission intensities over cycles (On-Off cycles) as a function of time (left). Averaged (right). Example of TA1

Second, the decay times of luminescence, which are obtained from *Figure 5.4\_right*, were fitted using a single exponential fit represented in a logarithmic scale, as shown in *Figure 5.7*. The persistent luminescence spectra were also recorded (*Figure 5.6*), displaying a typical heterogenous luminescence behavior.

#### **5.4. LPL of the host molecule alone**

As previously mentioned in the literature review of this thesis, the emission of long persistent luminescent materials (LPL) is caused by the intramolecular charge transfer (CT) between two or more molecules (or ions). The luminescence occurs during the process of charge recombination (CR), and the slower this process occurs, the longer the luminescence lasts.

At the beginning of this chapter, we emphasized the importance of reproducing literature results due to the novelty of this field. In this work, we aimed to prepare LPL materials using a modified version of the strategy described in references [124,135], including the use of a stronger electro-donor molecule. The first step was to create a host molecule that could accept electrons and separate the charge between the acceptor molecules. This was achieved using a quaternary phosphonium ion with a bromide counterion that acts as an inter-electro-donor. Next, we made two modifications to the acceptor molecule. The first was to exchange the bromide counterion for a larger anion through a metathesis reaction, as described in *section 5.6*. The second modification was to use a separate electro-donor molecule, doped in the host molecule, to form a host/guest binary system, resulting in exciplex emission as described in *section 5.5*.

Quaternary phosphonium ions are known for their ability to withdraw electrons, facilitating charge transfer and separation. The molecule *TPPC3Br2* is a quaternary phosphonium salt with bromide as a counterion that was obtained through simple recrystallization in ethanol and characterized without further purification.

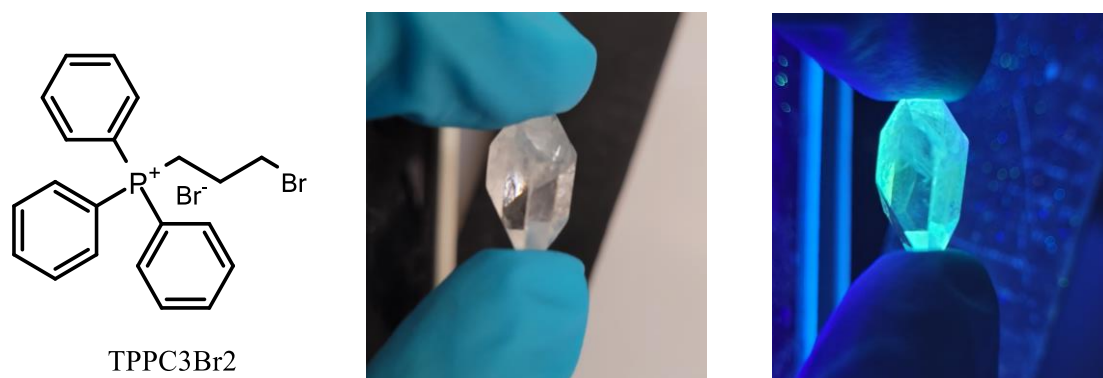


**Figure 5.5.** TPPC3Br<sub>2</sub> molecule and crystal (1.5 cm) at daylight and under 254 nm excitation lamp. The TPPC3Br<sub>2</sub> crystal, when excited under 260 nm, shows an emission maximum at 488 nm (Figure 5.6\_left). As shown in Figure 5.7, the luminescence of TPPC3Br<sub>2</sub> decays on the sub-second time scale after switching off the excitation.

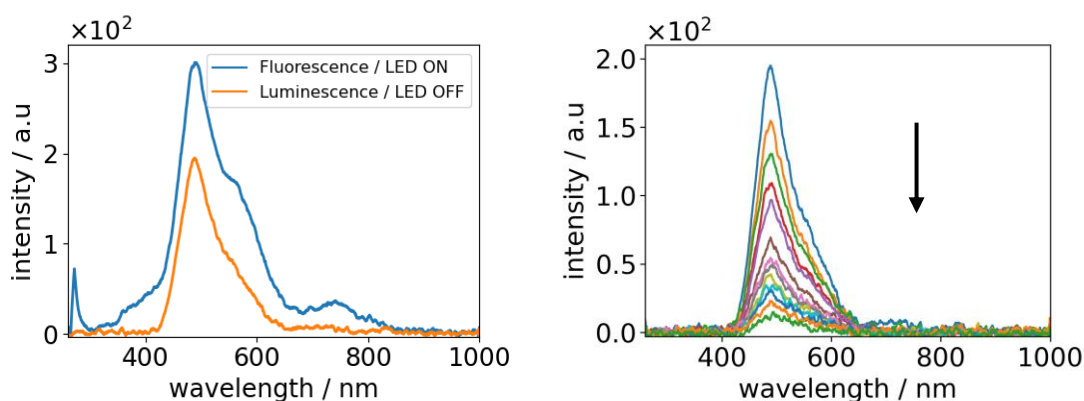


**Figure 5.6.** Emission spectra of crystalline TPPC3Br<sub>2</sub> upon excitation using 260 nm LED (left, the fluorescence / LED ON is the last spectrum recorded when the LED is ON, just after, the Luminescence / LED OFF is the exact first spectrum recorded). The persistent luminescence after switching off the excitation source (right).

In this study, the luminescence lifetime and the rate of luminescence decay (as depicted in the decay profile shown in Figure 5.7) were examined as part of the analysis. Although these two parameters are related, they represent distinct concepts. The luminescence lifetime refers to the amount of time it takes for the intensity of the emitted light to decrease to a certain level (specifically,  $1/e$ , where  $e$  is the base of the natural logarithm) from its initial value [254]. The luminescence lifetime was calculated from the luminescence decay profiles to compare the optical properties of the materials after introducing molecular modifications.

According to *Figure 5.7*, the resolved PL (photoluminescence) decay profile was analyzed using a monoexponentially fit function. This allowed for the determination of the lifetime of the luminescence of the host molecule (*TPPC3Br2*), which was found to be 0.129 seconds based on the analysis of the decay profile.

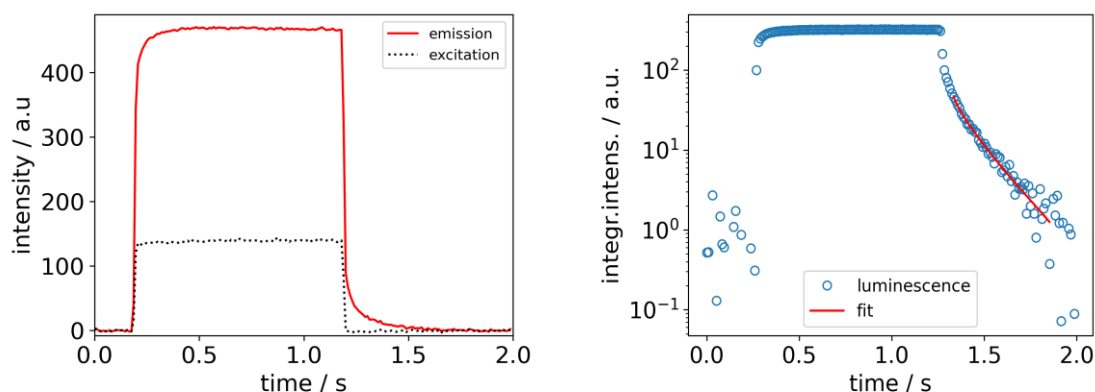


**Figure 5.7.** Averaged decay luminescence of TPPC3Br2 (left). PL decay profile on a semi-logarithmic scale with a mono exponential fit (right)

### 5.5. Host-guest binary molecule | doping

One way to change the optical properties of a host molecule is to dope it with a guest molecule through a process called co-crystallization. In this method, the host and guest molecules are mixed together and allowed to crystallize together, resulting in the incorporation of the guest molecule into the crystal structure of the host. This type of chemical modification is often used to introduce new functionalities or modify the properties of the host molecule [255,256].

In this study, *N,N,N',N'-Tetramethylbenzidine (TMB)*, which is a strong electro-donor, was used as a guest molecule to dope the host molecule (*TPPC3Br2*) using the molar ratio of (10:1), respectively (*Figure 5.2*). Crystals were obtained by recrystallization from ethanol and characterized without further purification (*Figure 5.8*).



**Figure 5.8.** Shows a crystal of TPPC3Br<sub>2</sub>\_TMB, with the central image showing the crystal while under excitation and the image on the right showing the crystal right after the excitation source (wavelength 260 nm) has been turned off

*Figure 5.8* illustrates that TPPC3Br<sub>2</sub>-TMB crystals emit green light when excited by a 260 nm LED light source, with some impurities also emitting blue light. The blue emission is classified as fluorescence because it disappears when the excitation source is immediately turned off.

*Figure 5.9<sub>right</sub>* shows that the emission maximum of TPPC3Br<sub>2</sub>-TMB crystals is at 530 nm. The sharp peak at 406 nm is due to the presence of small crystals of blue fluorescence (*Figure 5.9<sub>left</sub>*), which are considered impurities as no purification was performed after doping.

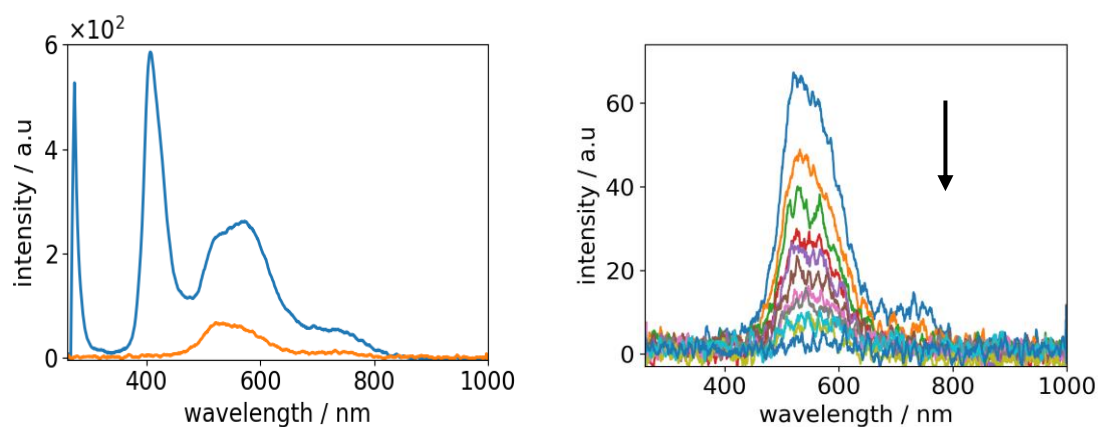


**Figure 5.9.** Emission spectra of TPPC3Br<sub>2</sub>\_TMB when excited using 260 nm LED. The sharp peak at 406 nm corresponds to the presence of a small amount of fluorescent impurities (left panel, the fluorescence / LED ON is the last spectrum recorded when the LED is ON, just after, the Luminescence / LED OFF is the exact first spectrum recorded). Evolution of the persistent luminescence spectrum after switching off the excitation source (right panel).

The lifetime of the luminescence of TPPC3Br<sub>2</sub>-TMB was determined to be 0.073 seconds using a mono-exponential fit of the decay profile shown in *Figure 5.10*. Compared to the host

molecule (seen in *section 5.4*), the donor-acceptor binary system exhibits a shorter emission time but shifts towards longer wavelengths (488 nm to 530 nm). This shorter emission time may be due to the used molar ratio, as an increase in the ratio of the donor molecule can lead to a longer emission time, according to the literature [124,135]. This is because the charge recombination rate is influenced by the number of charge transfer states available, with more charge transfer states resulting in a slower recombination rate. However, it is important to note that other factors, such as the nature of the donor and acceptor molecules, the presence of impurities, and the temperature of the sample, can also impact the emission time and the rate of charge recombination.

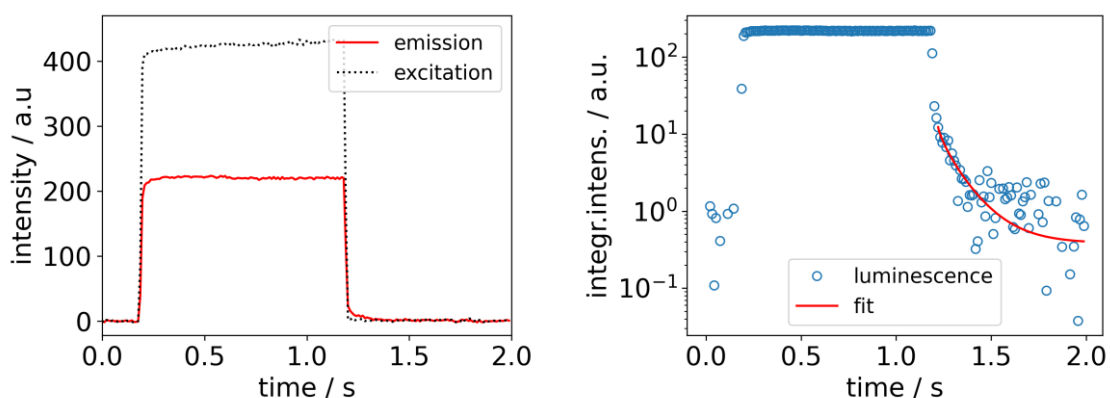


**Figure 5.10.** Averaged decay luminescence of TPPC3Br2\_TMB (left). PL decay profile on a semi-logarithmic scale with a mono exponential fit (right)

### 5.6. Ion exchange | metathesis

In *section 5.4*, it was observed that the compound (host molecule alone) exhibits long-lasting luminescence, which is thought to be caused by the transfer of charge from the bromide anion to the phosphonium cation and the resulting charge separation in the crystal. In this study, we sought to investigate the effect of the counterion by replacing the small bromide anion ( $\text{Br}^-$ ) with the larger hexafluorophosphate anion ( $\text{PF}_6^-$ ). This was done by performing a metathesis reaction to exchange the bromide anion for the  $\text{PF}_6^-$  anion and recrystallizing the resulting compound from ethanol (*Figure 5.11*).

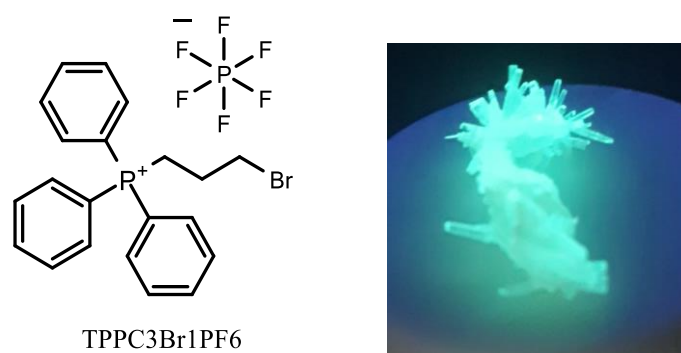


**Figure 5.11.** Crystal of TPPC3Br1\_PF6 under excitation source (254 nm)

When exposed to 260 nm light, the crystals exhibit an emission maximum at 490 nm. *Figure 5.12* shows the fluorescence spectrum when the crystals are excited (blue curve) and the emission spectrum (luminescence) when the excitation source is turned off (orange curve)

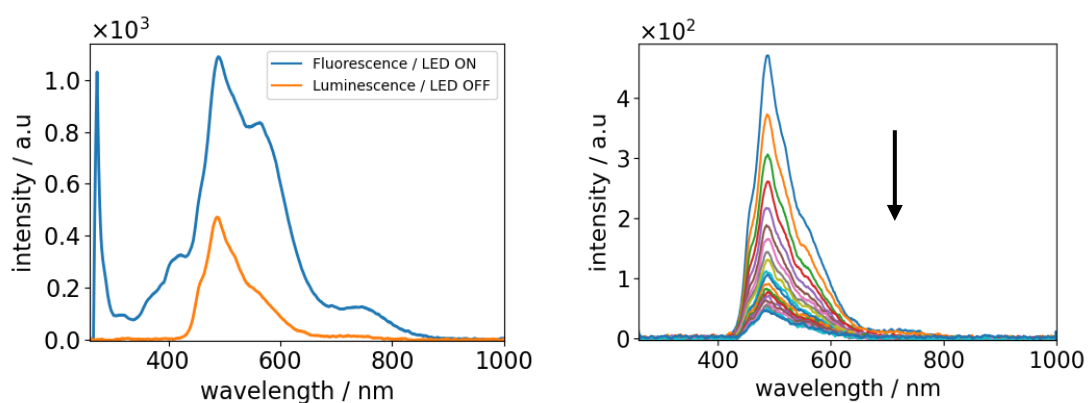


**Figure 5.12.** Shows the emission spectra of TPPC3Br1\_PF6 when excited by a 260 nm LED (left panel, the fluorescence / LED ON is the last spectrum recorded when the LED is ON, just after, the Luminescence / LED OFF is the exact first spectrum recorded) and the persistent luminescence after the excitation source has been turned off (right panel).

The lifetime of this luminescence (TPPC3Br1\_PF6) was calculated from the decay profile presented in *Figure 5.13* and found to be 0.142 seconds.

The lifetime of the luminescence is slightly longer when the hexafluorophosphate counterion is used instead of the bromide counterion. Additionally, the luminescence intensity is more than double when the hexafluorophosphate counterion is used ( $5.10^2$  counts) compared to the bromide counterion when it is used ( $2.10^2$  counts). As a result, using larger counterions enhances the emission intensity while also leading to a slight increase in the lifetime of the emission.

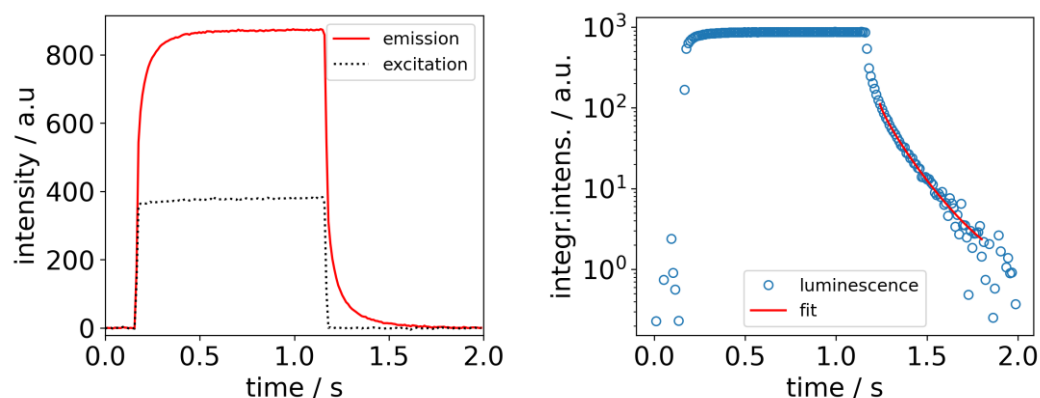


**Figure 5.13.** Averaged decay luminescence of TPPC3Br1\_PF6 (left). PL decay profile on a semi-logarithmic scale with a mono exponential fit (right)

## 5.7. Summary

In this first part, organic room-temperature luminescent materials were synthesized and investigated (*Table 5-1*). The host molecule *TPPC3Br2* showed clear green persistent luminescence at 488 nm, which is attributed to charge-recombination fluorescence from trapped photogenerated charge carriers. Exchanging the bromide counterion with hexafluorophosphate increased the emission intensity (at 490 nm) with a slight increase in luminescence duration. The use of donor dopant (TMB) causes a redshift of the emission spectrum (488 nm to 530 nm) with a decrease of the emission intensity.

**Table 5-1.** Summary of the three materials and comparison of their photophysical parameters

<i>Material</i>	<i>System</i>	<i>Chemical reaction</i>	$\lambda_{max\ EM}$ (nm)	$\tau$ (seconds)
TPPC3Br2	Host molecule	Nucleophilic reaction	488	0.129
TPPC3Br2_TMB	Host-guest (donor-acceptor)	Co-crystallization	530	0.073
TPPC3Br1PF6	Host molecule with exchanged anion	Metathesis	490	0.142



### ***Part Two: Persistent phosphorescence / inorganic phosphors***

In the second part of this work, we studied commercially available doped strontium aluminate powders that emit light in the dark (also known as "phosphors"). These phosphors were obtained from TRITART (Germany) and are intended for use in acrylic and resin applications for design and decoration purposes. They have a non-glowing white state and can be excited using UV and blacklight to produce various colors. The supplier did not provide the exact composition of these phosphors, but they are known to be strontium aluminate-based. We examined two phosphors, TA1 and TA2, and compared their optical performance to that of our experimental organic luminescent materials from the first part of this chapter. The aim was to compare the performance of these commercially available inorganic phosphors with our synthesized organic materials.





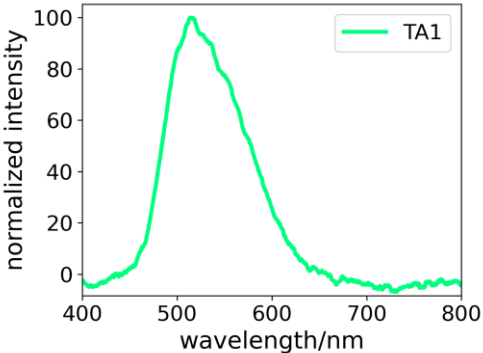
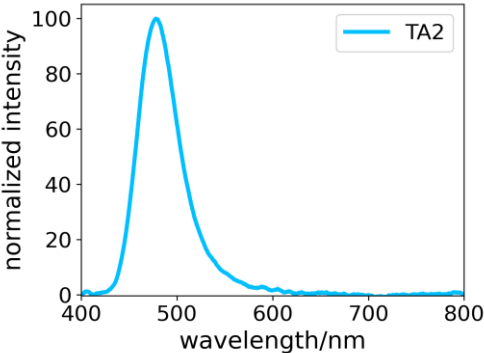
#### **5.8. Characterization of phosphors in their powder form**

The phosphors TA1 and TA2 are presented in their powder form, with a non-glowing white appearance. They are microscale (10-30 $\mu$ m) powders that emit blue and green light, respectively, in dark conditions after being excited.

The emission spectra of the compounds were recorded using the measurement setup shown in *section 5.2*. **Table 5-2** shows the appearance of the powders under daylight and immediately after the excitation light source is turned off. The phosphors show a strong emission at 515 nm and 478 nm wavelengths for TA1 and TA2, respectively.

## Organic and inorganic materials with long persistent luminescence and development of persistently luminescent textile fabrics

**Table 5-2.** Photographs of the compounds TA1 and TA2 under daylight (first row) and immediately after a full-off of the excitation (second row). Emission spectra (third row) and maximum emission (Forth row)

Sample	TA1	TA2
<b>Under daylight</b>		
<b>In dark conditions*</b>		
<b>Emission spectra</b>		
<b>Emission maximum</b>	515 nm	478 nm

\* After excitation at 365 nm for a few seconds

Subsequently, the time-dependent luminescence behavior of the compounds TA1 and TA2 was studied. To this end, the samples were excited (under 365 nm) with pulses having a width of 5 seconds that were repeated every 100 seconds. This periodic excitation was repeated continuously. A time series of emission spectra with an integration time of 10 milliseconds were recorded over 5 excitation cycles (*following the same steps as in section 5.3.3*).

According to literature, the luminescence decay of these phosphor materials can be divided into three stages, each with different intensities and time constants [87,153]. The duration of

each stage varies among different compounds, but in general, the total duration of photoluminescence emission can last for several hours. The first stage of the afterglow decay is relatively short (up to 5 minutes) but very intense. The second stage is 5-8 times longer than the first stage but with less intensity. The third and final stage can last for hours with a low intensity that can be seen as a faint emission and glow. This final stage is what gives rise to persistent luminescence [153,257].

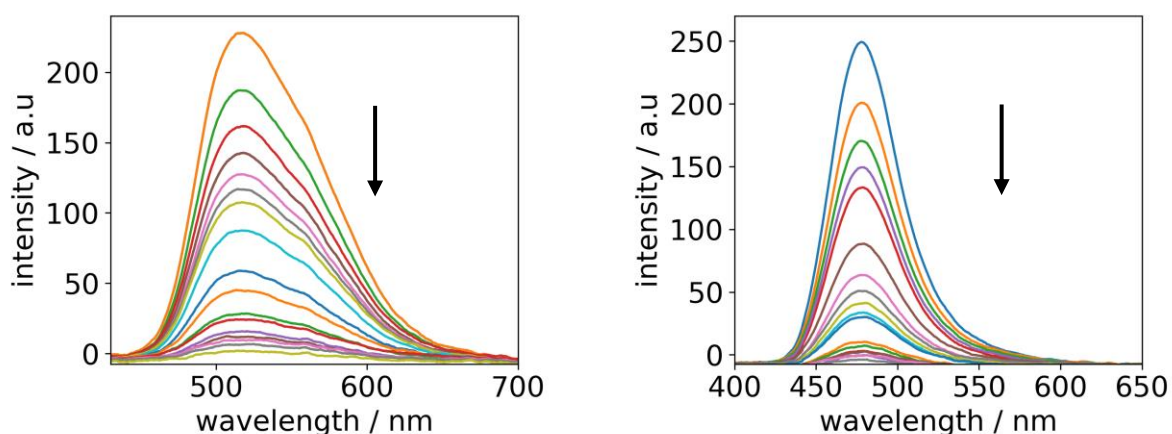


**Figure 5.14.** Persistent luminescence spectra of sample TA1 (left) and TA2 (right) after the full off of the excitation source.

The lifetime, or time constant, of the phosphorescence process is defined as the time it takes for the intensity to decrease to  $1/e$  of the initial emission  $I_0$  [254]. From the time-resolved PL decay curves (*Figure 5.15*), the average lifetimes of TA1 and TA2 at 365 nm measured at room temperature (298 K) were 1.07 and 1.54 seconds, respectively.

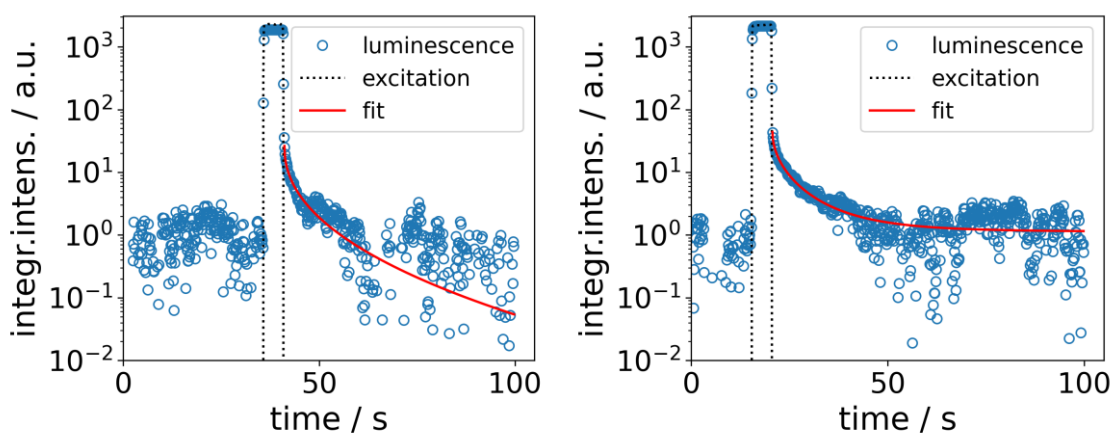


**Figure 5.15.** Decay luminescence profiles on a semi-logarithmic scale of TA1 (left) and TA2 (right)

These values seem too low for persistent luminescence, which is typically observed for several hours. Two reasons can explain these values. First, the experimental protocol used in the first part of this work, where organic long persistent luminescent materials (OLPL) were studied, was also used to characterize the inorganic phosphors. The spectra were recorded in intervals of 100 seconds, which only allowed the first stage of luminescence decline to be investigated (out of the three stages). To fully characterize the luminescence decay of these materials, new experiments with longer time intervals must be conducted (several hours intervals). Second, it is necessary to use a mathematical multi-exponential fit function to properly describe the decay profile, as it differs in each stage. In this case, the lifetime is the sum of the lifetimes at each stage. It is also important to reproduce the same experimental conditions used in the first part of this work to investigate the OLPL to make meaningful comparisons between the results.

### ***Part Three: Development of luminescent textiles***

The previous studies have shown that developing textile fabrics that can emit light after being exposed to an excitation source requires using powerful and intense materials with a long emission duration. Strontium aluminate-based phosphors have been found to be the most suitable compounds for this purpose [258,259]. However, organic luminescent materials have also shown promising results [133,134].

In this final section of this chapter, we attempted to create self-luminous textile fabrics by adding inorganic phosphors (TA1 and TA2, *section 5.8*) to a raw polymer base and applying the mixture directly to textile fabrics using the spray coating method.

### **5.9. Sample preparation**

As mentioned earlier, selecting an appropriate functionalization technique for a particular application can be challenging, particularly when working with insoluble inorganic compounds. In this part of the work, we adopted a simple and direct approach to incorporate the luminescent compound into the textile fabric (*Figure 5.16*) using raw polymer via the spray coating method (*section 2.3.3*). We chose this method over others because our previous

experiments using other functionalization methods, such as sol-gel, pad-dry-cure, and knife coating, were unsuccessful with these insoluble inorganic particles.

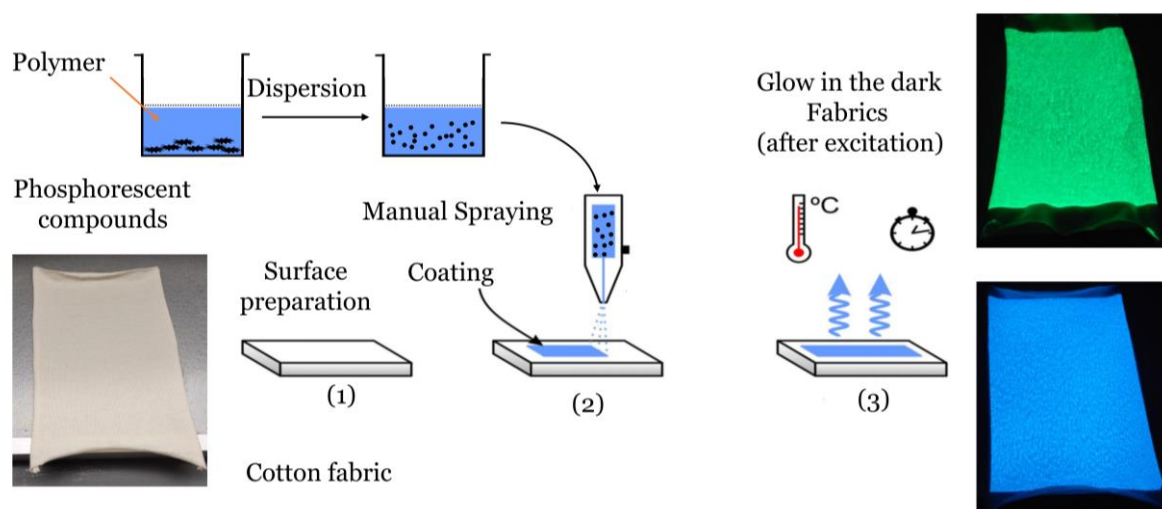


**Figure 5.16.** The adopted strategy to prepare photoluminescent fabrics using the spray coating technique.

To create self-luminous textile fabrics, 10% by weight (*wt %*) of a phosphorescent compound (TA1 or TA2) was added to 10 ml of liquid polyurethane (used as received, with a viscosity of 1.08). The mixture was stirred manually and then dispersed using an ultrasonic device set at 10W and 20kHz for 10 minutes. The resulting mixture was placed in a spray gun and applied to one side of the fabric using multiple passes from a distance of 20 cm (filtered air was used at a pressure of 4 bar and a controlled medium debit). The fabric was left to air dry for 30 minutes and then dried at 105°C for 1 hour. This process is designed to coat the fabric with a layer of the phosphorescent mixture, which should allow the fabric to emit light after being exposed to an excitation source. It is important to ensure that the mixture is properly dispersed and applied to the fabric to obtain good results.

### 5.10. Morphological aspect of the textile fabrics

A scanning electron microscopy (SEM) analysis was conducted to examine the surface of the fabrics. The results revealed that the polymer was wrapped around the fibers and that there were welds present between the fibers. Additionally, the SEM analysis showed a compact mass of particles on the fabric's surface, which appeared as agglomerates with a heterogeneous

distribution. These particles were identified as the powders that were added to the blend formulation, which contained luminescent compounds.

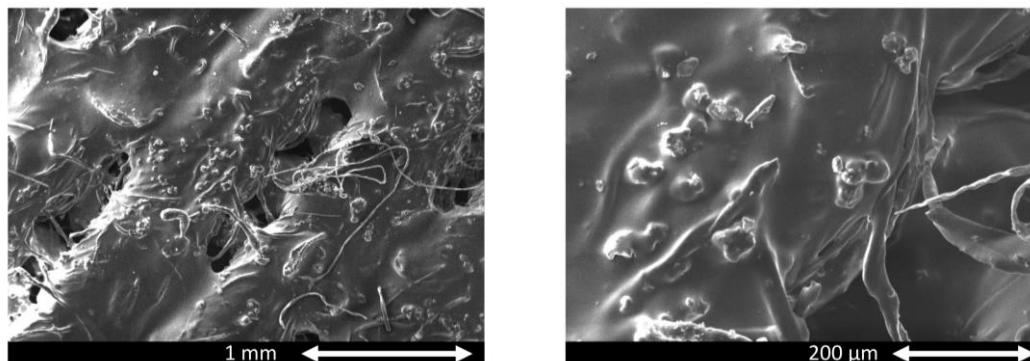


**Figure 5.17.** SEM photographs of a sample obtained by the spray coating method (example of TA01). The luminosity of the images was adjusted using the processing software ImageJ.

### 5.11. Visual aspect of the samples as a function of the time

The prepared textile fabrics were excited under a 365 nm lamp for 1 minute. The photographs were taken after excitation was turned off (20-30 seconds between each take). *Figure 5.18* gathers photographs of the prepared textiles at various times.

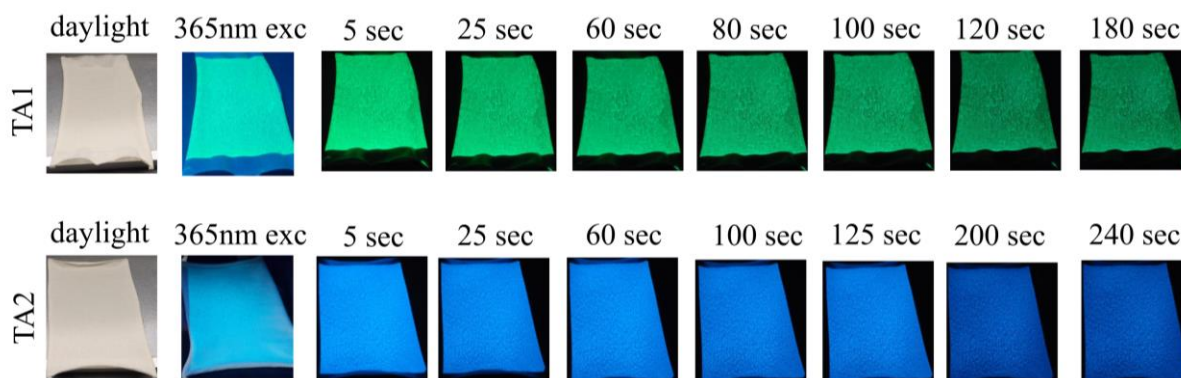


**Figure 5.18.** Photographs (taken by a mobile phone) of a 10 wt% of phosphorescent compounds dispersed in 10 ml of polyurethane (R-PU) and applied via the spray coating. Images under daylight, under UV 365 nm excitation, and after various times after turning off the excitation

The textile fabrics were observed in dark conditions for over 6 hours. The fabrics represent an intense emission for the first 5-8 minutes, depending on the sample, then the intensity starts to decrease slowly. After 30 minutes, the intensity continues to decrease to reach the final emission stage, which is the persistent luminescence that lasts for hours of emission as a faint glow in the dark.

Since this emission is low, it can be detected through the naked eye, using spectrometers (as in the setup in *section 5.2*), or using a special camera that is very sensitive to light emission (most of these cameras have a CMOS detector as the one used in the ULS2048CL Evo spectrometer from Avantes).

### **5.12. Conclusion and future perspectives**

In this chapter, we studied the phosphorescence of various materials. We found that inorganic phosphors had, in the main, an intense emission with extended luminescence duration, and these compounds showed good luminescence duration, with intense emission at first that gradually decreased to lower intensities, resulting in a faint glow in the dark.

We also explored using organic persistent luminescent materials based on exciplex formation. However, these materials had relatively low luminescence duration compared to inorganic phosphors, and further improvements are needed. One way to potentially extend the duration of their luminescence is to prepare these compounds under nitrogen conditions to limit oxygen quenching (using a glove box).

Also, according to the literature review of this thesis, an effective method to prepare pure organic long persistent luminescent thin films is when a molecule with a polymeric nature is used as the host material and doped later using a strong electro-donor molecule. This will provide a favorable environment for the triplet exciton state to be protected from external conditions and also slow the charge recombination, resulting in extending the emission duration. In future work, we intend to use the electrospinning technique to elaborate a polymeric blend of donor-acceptor electrospun mixed directly inside the syringe to have thin

films. This will provide a favorable environment for charge transfer between the molecules and protect the triplet state excitons from external conditions.

As for the main goal of this research work, we successfully elaborated luminous textile fabrics using a simple direct method involving incorporating materials into a raw polymer base with suitable viscosity, which could be applied to textiles using the spray coating method. The applying method showed good results in incorporating these luminescent particles into a thin polymeric layer adhered to the textile matrix. The resulting fabrics showed persistent luminescence in the dark after being excited for several minutes. Visually, the textile fabrics present a similar behavior to the compounds where the luminescence decay is not gradual, and the intensities of each stage of luminescence differ from one to another. Sophisticated functionalization methods can also be employed as long as the experimental conditions are respected. Currently, we are investigating the same compounds to be applied in the preparation of films using a blend of polymers via the electrospinning method. The aim is to elaborate a very thin electrospun that exhibit the luminescence property.



---

## General conclusion

The goal of this thesis was to create a luminous textile using materials with this property. In the process of preparing and applying the materials to the textile fabric to produce the final product, we sought to answer several questions: what material is most effective? what is the best method for adhering the elaborated material to the textile fabric? what are the sustainable and optimal conditions for this process?

First, we studied the functionalization method to stabilize an efficient process for applying the prepared material to the textile. We improved and optimized the process to obtain the most satisfactory results using organic model dyes as the required functionality. Based on the results we obtained, we proposed a new eco-friendly dyeing process for textiles that can be used as an alternative to existing methods.

We further improved and tested the effectiveness of the process for incorporating luminescent molecules. To do this, we synthesized several fluorescent molecules and characterized them using a new experimental measurement setup developed during this thesis. This method showed reliable results in measuring photoluminescence quantum yields of luminescent molecules in solution, using LEDs as an excitation source. We then elaborated fluorescent textiles using the previous dyeing process, which showed good results.

In the final part of this work, we sought to prepare phosphorescent materials that could be applied to textile fabrics and transfer their luminous property to create a luminescent textile. To do this, we first established a spectrottemporal measurement setup to measure the photophysical parameters of the luminescent analyte. We then attempted to prepare organic molecules that exhibit luminescence at room temperature for later application using the previously developed process. However, these materials had a short emission time, which was insufficient for our main goal of developing a luminescent textile with long persistent emission. As a result, we turned to inorganic phosphorescent materials and were able to create luminescent textiles with long persistent emissions using a direct-facile method. This work demonstrates the potential for developing sustainable and effective methods for creating luminescent textiles using various materials

---

## References

1. Bancroft WD, Ackerman JW (1931) The solid solution theory of dyeing. *Proc Natl Acad Sci USA* 17: 480–482.
2. Shindy H (2016) Basics in colors, dyes and pigments chemistry: A review. *Chem Int* 2: 2016.
3. Gürses A, Açıkyıldız M (2016) Dyes and pigments: Their structure and properties, *Dyes Pigm.*, 13–29.
4. Witt ON (1876) On the knowledge of the structure and the formation of coloring carbon compounds. *Berichte der deutschen chemischen Gesellschaft* 9: 522–527.
5. Pigot C, Noirbent G, Brunel D, et al. (2020) Recent advances on push–pull organic dyes as visible light photoinitiators of polymerization. *Eur Polym J* 133: 109797.
6. Pigot C, Péralta S, Bui T-T, et al. (2022) Push-pull dyes based on Michler’s aldehyde: Design and characterization of the optical and electrochemical properties. *Dyes Pigm* 202: 110278.
7. Dewar MJS, Llano CD (2002) ACS Publications, Ground states of conjugated molecules. Improved treatment of hydrocarbons, 2002. Available from: <https://pubs.acs.org/doi/pdf/10.1021/ja01032a001>.
8. Coulson CA, Longuet-Higgins HC, Bell RP (1947) The electronic structure of conjugated systems I. General theory. *Proc Math Phys Eng Sci* 191: 39–60.
9. Chen R, Lockwood DJ (2002) Developments in luminescence and display materials over the last 100 years as reflected in electrochemical society Publications. *J Electrochem Soc* 149: S69.
10. Jüstel T, Nikol H, Ronda C (1998) New developments in the field of luminescent materials for lighting and displays. *Angew Chem Int Ed* 37: 3084–3103.
11. Stokes A, George G (1852) On the change of refrangibility of light. *Philos trans R Soc Lond, A* 142: 463–562.
12. Wiedemann E (1889) On the mechanics of luminosity. *Lond Edinb Dublin philos mag j sci* 28: 149–163.
13. Kitai A (2008) Luminescent materials and applications, John Wiley & Sons.
14. Hamilton PA, Murrells TP (1986) Mechanism for the chemiluminescence in oxygen-phosphorus systems. *J Phys Chem* 90:1.
15. Maxwell K, Johnson GN (2000) Chlorophyll fluorescence—a practical guide. *Journal of Experimental Botany* 51: 659–668.

16. Lakowicz JR (1999) Introduction to fluorescence, *Principles of Fluorescence Spectroscopy*, Boston, MA, Springer US, 1–23.
17. Randall JT, Wilkins MHF, Oliphant MLE (1945) The phosphorescence of various solids. *Proc Math Phys Eng Sci* 184: 347–364.
18. Lastusaari M, Laamanen T, Malkamäki M, et al. (2012) The Bologna Stone: history's first persistent luminescent material. *Eur J Mineral* 24: 885–890.
19. Zhang Z, Guo X, Huang K, et al. (2022) Lead-free bright yellow emissive Rb<sub>2</sub>AgCl<sub>3</sub> scintillators with nanosecond radioluminescence. *Journal of Luminescence* 241: 118500.
20. Walton AJ (1977) Triboluminescence. *Adv Phys* 26: 887–948.
21. Brooks WP (1965) Shock-induced luminescence in quartz. *J Appl Phys* 36: 2788–2790.
22. Chapman GN, Walton AJ (1983) Triboluminescence of glasses and quartz. *J Appl Phys* 54: 5961–5965.
23. Bergeron NP, Hollerman WA, Goedeke SM, et al. (2008) Triboluminescent properties of zinc sulfide phosphors due to hypervelocity impact. *International Journal of Impact Engineering* 35: 1587–1592.
24. Henisch HK (1964) Electroluminescence. *Rep Prog Phys* 27: 369.
25. Kafafi ZH (Ed.) (2017) Organic electroluminescence, Boca Raton, CRC Press.
26. Zhang D-W, Li M, Chen C-F (2020) Recent advances in circularly polarized electroluminescence based on organic light-emitting diodes. *Chem Soc Rev* 49: 1331–1343.
27. Wilson T, Hastings JW (1998) Bioluminescence. *Annu Rev Cell Dev Biol* 14: 197–230.
28. White EH, Steinmetz MG, Miano JD, et al. (1980) Chemi- and bioluminescence of firefly luciferin. *J Am Chem Soc* 102: 3199–3208.
29. Haddock SHD, Moline MA, Case JF (2010) Bioluminescence in the Sea. *Ann Rev Mar Sci* 2: 443–493.
30. Hastings JW, Potrikusv CJ, Gupta SC, et al. (1985) Biochemistry and physiology of bioluminescent bacteria, *Advances in Microbial Physiology*, 235–291.
31. Lu X, Zhan Y, He W (2022) Recent development of small-molecule fluorescent probes based on phenothiazine and its derivatives. *Journal of Photochemistry and Photobiology B: Biology* 234: 112528.
32. Thoof AM, Cassaidy K, VanVeller B (2017) A small push–pull fluorophore for turn-on Fluorescence. *J Org Chem* 82: 8842–8847.
33. Genin E, Hugues V, Clermont G, et al. (2012) Fluorescence and two-photon absorption of push–pull aryl(bi)thiophenes: structure–property relationships. *Photochem Photobiol Sci* 11: 1756–1766.

- 
34. Rémond M, Zheng Z, Jeanneau E, et al. (2019) 4,5,5-Trimethyl-2,5-dihydrofuran-Based electron-withdrawing groups for nir-emitting push-pull dipolar fluorophores. *J Org Chem* 84: 9965–9974.
  35. Ipuy M, Liao Y-Y, Jeanneau E, et al. (2016) Solid state red biphotonic excited emission from small dipolar fluorophores. *J Mater Chem C* 4: 766–779.
  36. Filho MS, Fiorucci S, Martin AR, et al. (2017) Design, synthesis and photophysical studies of styryl-based push-pull fluorophores with remarkable solvatofluorochromism. *New J Chem* 41: 13760–13772.
  37. Redon S, Eucat G, Ipuy M, et al. (2018) Tuning the solid-state emission of small push-pull dipolar dyes to the far-red through variation of the electron-acceptor group. *Dyes and Pigments* 156: 116–132.
  38. Wong K-L, Bünzli J-CG, Tanner PA (2020) Quantum yield and brightness. *Journal of Luminescence* 224: 117256.
  39. Rubin MB, Braslavsky SE (2010) Quantum yield: the term and the symbol. A historical search. *Photochem Photobiol Sci* 9: 670–674.
  40. Gold V (Ed.) (2019) The IUPAC compendium of chemical terminology: The Gold Book, research triangle park, nc, international union of pure and applied chemistry (IUPAC).
  41. Crosby GA, Demas JN (1971) Measurement of photoluminescence quantum yields. A Review. *J Phys Chem* 75: 991–1024.
  42. Tomasini EP, San Román E, Braslavsky SE (2009) Validation of fluorescence quantum yields for light-scattering powdered samples by laser-induced optoacoustic spectroscopy. *Langmuir* 25: 5861–5868.
  43. Würth C, González MG, Niessner R, et al. (2012) Determination of the absolute fluorescence quantum yield of rhodamine 6G with optical and photoacoustic methods – Providing the basis for fluorescence quantum yield standards. *Talanta* 90: 30–37.
  44. Brannon JH, Magde D (1978) Absolute quantum yield determination by thermal blooming. Fluorescein. *J Phys Chem* 82: 705–709.
  45. Magde D, Wong R, Seybold PG (2002) fluorescence quantum yields and their relation to lifetimes of rhodamine 6G and fluorescein in nine solvents: improved absolute standards for quantum yields. *Photochem Photobiol* 75: 327–334.
  46. Fischer M, Georges J (1996) Fluorescence quantum yield of rhodamine 6G in ethanol as a function of concentration using thermal lens spectrometry. *Chem Phys Lett* 260: 115–118.
  47. Baesso ML, Bento AC, Andrade AA, et al. (1998) Absolute thermal lens method to determine fluorescence quantum efficiency and concentration quenching of solids. *Phys Rev B* 57: 10545–10549.
  48. Bindhu CV, Harilal SS, Varier GK, et al. (1996) Measurement of the absolute fluorescence quantum yield of rhodamine B solution using a dual-beam thermal lens technique. *J Phys D: Appl Phys* 29: 1074.
-

49. Laverdant J, Marcillac WD de, Barthou C, et al. (2011) Experimental determination of the fluorescence quantum yield of semiconductor nanocrystals. *Materials* 4: 1182–1193.
50. Chartier A, Georges J, Mermet JM (1990) Limitation of the thermal-lens method in fluorescence quantum-yield measurements. *Chemical Physics Letters* 171: 347–352.
51. Galanin MD, Kutyonkov AA, Smorchkov VN, et al. (1982) Measurement of photoluminescence quantum yield of dye solutions by the Vavilov and integrating-sphere methods. *Opt Spectrosc* 53: 405–409.
52. Suzuki K, Kobayashi A, Kaneko S, et al. (2009) Reevaluation of absolute luminescence quantum yields of standard solutions using a spectrometer with an integrating sphere and a back-thinned CCD detector. *Phys Chem Chem Phys* 11: 9850–9860.
53. Porrès L, Holland A, Pålsson L-O, et al. (2006) Absolute measurements of photoluminescence quantum yields of solutions using an integrating sphere. *J Fluoresc* 16: 267–272.
54. Rurack K, Spieles M (2011) Fluorescence quantum yields of a series of red and near-infrared dyes emitting at 600–1000 nm. *Anal Chem* 83: 1232–1242.
55. Würth C, Lochmann C, Spieles M, et al. (2010) Evaluation of a commercial integrating sphere setup for the determination of absolute photoluminescence quantum yields of dilute dye solutions. *Appl Spectrosc, AS* 64: 733–741.
56. Würth C, Pauli J, Lochmann C, et al. (2012) Integrating sphere setup for the traceable measurement of absolute photoluminescence quantum yields in the near infrared. *Anal Chem* 84: 1345–1352.
57. Resch-Genger U, Hoffmann K, Nietfeld W, et al. (2005) How to improve quality assurance in fluorometry: fluorescence-inherent sources of error and suited fluorescence standards. *J Fluoresc* 15: 337–362.
58. Velapoldi RA, Tønnesen HH (2004) Corrected emission spectra and quantum yields for a series of fluorescent compounds in the visible spectral region. *Journal of Fluorescence* 14: 465–472.
59. Grabolle M, Spieles M, Lesnyak V, et al. (2009) Determination of the fluorescence quantum yield of quantum dots: suitable procedures and achievable uncertainties. *Anal Chem* 81: 6285–6294.
60. Würth C, Grabolle M, Pauli J, et al. (2013) Relative and absolute determination of fluorescence quantum yields of transparent samples. *Nat Protoc* 8: 1535–1550.
61. Leyre S, Coutino-Gonzalez E, Joos JJ, et al. (2014) Absolute determination of photoluminescence quantum efficiency using an integrating sphere setup. *Rev Sci Instrum* 85: 123115.
62. Green AP, Buckley AR (2012) Application of gauge R&R to the rigorous measurement of quantum yield in fluorescent organic solid state systems. *Rev Sci Instrum* 83: 073108.

- 
63. Eaton DF (1988) Reference materials for fluorescence measurement. *Pure Appl Chem* 60: 1107–1114.
  64. Williams ATR, Winfield SA, Miller JN (1983) Relative fluorescence quantum yields using a computer-controlled luminescence spectrometer. *Analyst* 108: 1067–1071.
  65. Chen RF (1967) Fluorescence quantum yields of tryptophan and tyrosine. *Analytical Letters* 1: 35–42.
  66. Kubin RF, Fletcher AN (1982) Fluorescence quantum yields of some rhodamine dyes. *Journal of Luminescence* 27: 455–462.
  67. Brouwer AM (2011) Standards for photoluminescence quantum yield measurements in solution. *Pure Appl Chem* 83: 2213–2228.
  68. Gills, T.E. (1994) Standard reference material 936a: Quinine Sulfate Dihydrate.
  69. Griffith DJ, Bone EL, Thomalla SJ, et al. (2018) Calibration of an in-water multi-excitation fluorometer for the measurement of phytoplankton chlorophyll-a fluorescence quantum yield. *Opt Express* 26: 18863.
  70. Barlier-Salsi A (2014) Stray light correction on array spectroradiometers for optical radiation risk assessment in the workplace. *J Radiol Prot* 34: 915–930.
  71. Nawara K, Waluk J (2017) Improved method of fluorescence quantum yield determination. *Anal Chem* 89: 8650–8655.
  72. Ostapko J, Nawara K, Kijak M, et al. (2016) Parent, Unsubstituted hemiporphycene: synthesis and properties. *Chem Eur J* 22: 17311–17320.
  73. Nawara K, Waluk J (2020) Fluorescence quantum yield determination using simultaneous double-beam absorption measurement. *Measurement* 165: 108159.
  74. Aaboub T, Boukhriss A, Gmouh S, et al. (2022) Determination of photoluminescence quantum yields in dilute solution using non-monochromatic excitation light. *Photochem Photobiol Sci*.
  75. Xu J, Tanabe S (2019) Persistent luminescence instead of phosphorescence: History, mechanism, and perspective. *Journal of Luminescence* 205: 581–620.
  76. Khosravi AA, Kundu M, Jatwa L, et al. (1995) Green luminescence from copper doped zinc sulphide quantum particles. *Appl Phys Lett* 67: 2702–2704.
  77. Shakil MA, Das S, Rahman MA, et al. (2018) A review on zinc sulphide thin film fabrication for various applications based on doping elements. *Mater sci appl* 9: 751–778.
  78. Lahariya V, Dhoble SJ (2022) Development and advancement of undoped and doped zinc sulfide for phosphor application. *Displays* 74: 102186.
  79. Prener JS, Williams FE (1956) Activator systems in zinc sulfide phosphors. *J Electrochem Soc* 103: 342.
-

80. Murugadoss G (2013) Synthesis and photoluminescence properties of zinc sulfide nanoparticles doped with copper using effective surfactants. *Particuology* 11: 566–573.
81. Vijayan S, Umadevi G, Mariappan R, et al. (2020) High luminescence efficiency of Copper doped Zinc Sulfide (Cu: ZnS) nanoparticles towards LED applications. *Materials Today: Proceedings*.
82. Abd El-Gawad AHM, Khalil AAI, Gadallah A-S (2020) Influence of preparation conditions on the properties of silver doped copper-zinc sulfide thin films prepared via sol-gel spin coating technique. *Optik* 223: 165561.
83. Matsuzawa T, Aoki Y, Takeuchi N, et al. (1996) A new long phosphorescent phosphor with high brightness, SrAl<sub>2</sub>O<sub>4</sub>: Eu<sup>2+</sup>, Dy<sup>3+</sup>. *J Electrochem Soc* 143: 2670.
84. Qiu J, Li Y, Jia Y (2021) Persistent phosphors, *Persistent Phosphors*, Woodhead Publishing, 127–215.
85. Dorenbos P (2005) Mechanism of persistent luminescence in Eu<sup>2+</sup> and Dy<sup>3+</sup> codoped aluminate and silicate compounds. *J Electrochem Soc* 152: H107.
86. Li Y, Gecevicius M, Qiu J (2016) Long persistent phosphors—from fundamentals to applications. *Chem Soc Rev* 45: 2090–2136.
87. Van den Eeckhout K, Smet PF, Poelman D (2010) Persistent luminescence in Eu<sup>2+</sup>-doped compounds: A review. *Materials* 3: 2536–2566.
88. Dutczak D, Jüstel T, Ronda C, et al. (2015) Eu<sup>2+</sup> luminescence in strontium aluminates. *Phys Chem Chem Phys* 17: 15236–15249.
89. Rojas-Hernandez RE, Rubio-Marcos F, Rodriguez MÁ, et al. (2018) Long lasting phosphors: SrAl<sub>2</sub>O<sub>4</sub>: Eu, Dy as the most studied material. *Renew Sust Energ Rev* 81: 2759–2770.
90. Abbruscato V (1971) optical and electrical properties of SrAl<sub>2</sub>O<sub>4</sub>: Eu<sup>2+</sup>. *J Electrochem Soc* 118: 930.
91. Vitola V, Millers D, Bite I, et al. (2019) Recent progress in understanding the persistent luminescence in SrAl<sub>2</sub>O<sub>4</sub>: Eu, Dy. *J Mater Sci Technol* 35: 1661–1677.
92. Clabau F, Rocquefelte X, Jobic S, et al. (2005) Mechanism of phosphorescence appropriate for the long-lasting phosphors Eu<sup>2+</sup>-doped SrAl<sub>2</sub>O<sub>4</sub> with codopants Dy<sup>3+</sup> and B<sup>3+</sup>. *Chem Mater* 17: 3904–3912.
93. Clabau F, Rocquefelte X, Le Mercier T, et al. (2006) Formulation of phosphorescence mechanisms in inorganic solids based on a new model of defect conglomeration. *Chem Mater* 18: 3212–3220.
94. Turro NJ (1969) The triplet state. *J Chem Educ* 46: 2.
95. Andrews DL, Lipson RH (2021) After light is absorbed: photophysics in an excited electronic state. *Molecular Photophysics and Spectroscopy (Second Edition)*.

- 
96. Baryshnikov G, Minaev B, Ågren H (2017) Theory and calculation of the phosphorescence phenomenon. *Chem Rev* 117: 6500–6537.
  97. Murthy KVR, Virk HS (2014) Luminescence phenomena: an Introduction. *Defect Diffus Forum* 347: 1–34.
  98. Valeur B, Berberan-Santos MN (2012) Molecular fluorescence: principles and applications, Wiley-VCH Verlag.
  99. Nazarov VB, Gerko VI, Alfimov MV (1996) Phosphorescence lifetime of naphthalene and phenanthrene in aggregated aromatic molecule- $\beta$ -cyclodextrin-precipitant complexes. *Russ Chem Bull* 45: 2109–2112.
  100. Lower SK, El-Sayed MA (1966) The triplet state and molecular electronic processes in organic molecules. *Chem Rev* 66: 199–241.
  101. Tian S, Ma H, Wang X, et al. (2019) Utilizing d-p $\pi$  bonds for ultralong organic phosphorescence. *Angew Chem Int Ed* 58: 6645–6649.
  102. Kuno S, Akeno H, Ohtani H, et al. (2015) Visible room-temperature phosphorescence of pure organic crystals via a radical-ion-pair mechanism. *Phys Chem Chem Phys* 17: 15989–15995.
  103. Perumal S, Minaev B, Ågren H (2013) Triplet state phosphorescence in tris(8-hydroxyquinoline) aluminum light emitting diode materials. *J Phys Chem C* 117: 3446–3455.
  104. Mao Z, Yang Z, Mu Y, et al. (2015) Linearly tunable emission colors obtained from a fluorescent-phosphorescent dual-emission compound by mechanical stimuli. *Angew Chem Int Ed* 54: 6270–6273.
  105. Wang J, Gu X, Ma H, et al. (2018) A facile strategy for realizing room temperature phosphorescence and single molecule white light emission. *Nat Commun* 9: 2963.
  106. Zhao W, He Z, Tang BZ (2020) Room-temperature phosphorescence from organic aggregates. *Nat Rev Mater* 5: 869–885.
  107. Schulman SG (2017) Fluorescence and phosphorescence spectroscopy: physicochemical principles and practice, Elsevier.
  108. Lewis GN, Lipkin D, Magel TT (1941) Reversible photochemical processes in rigid media. a study of the phosphorescent state. *J Am Chem Soc* 63: 3005–3018.
  109. Yuan WZ, Shen XY, Zhao H, et al. (2010) Crystallization-induced phosphorescence of pure organic luminogens at room temperature. *J Phys Chem C* 114: 6090–6099.
  110. Wang B, Lei B, Tang Y, et al. (2018) Facile fabrication of robust superhydrophobic cotton fabrics modified by polysiloxane nanowires for oil/water separation. *J Coat Technol Res* 15: 611–621.
  111. Pilloff HS, Albrecht AC (1966) Direct measurement of a biphotonic photo-ionization in liquid solution. *Nature* 212: 499–500.
-



112. Ohkita H, Sakai W, Tsuchida A, et al. (1997) Charge recombination luminescence via the photoionization of a dopant chromophore in polymer solids. *Macromolecules* 30: 5376–5383.
  113. Xu S, Chen R, Zheng C, et al. (2016) Excited state modulation for organic afterglow: materials and applications. *Adv Mater* 28: 9920–9940.
  114. Hoshino M, Uekusa H, Tomita A, et al. (2012) Determination of the structural features of a long-lived electron-transfer state of 9-Mesityl-10-methylacridinium ion. *J Am Chem Soc* 134: 4569–4572.
  115. Fukuzumi S, Kotani H, Ohkubo K, et al. (2004) Electron-transfer state of 9-Mesityl-10-methylacridinium ion with a much longer lifetime and higher energy than that of the natural photosynthetic reaction center. *J Am Chem Soc* 126: 1600–1601.
  116. Benniston AC, Harriman A, Li P, et al. (2005) Charge shift and triplet state formation in the 9-Mesityl-10-methylacridinium cation. *J Am Chem Soc* 127: 16054–16064.
  117. Ohkubo K, Kotani H, Fukuzumi S (2005) Misleading effects of impurities derived from the extremely long-lived electron-transfer state of 9-mesityl-10-methylacridinium ion. *Chem Commun* 4520–4522.
  118. Deotare PB, Chang W, Hontz E, et al. (2015) Nanoscale transport of charge-transfer states in organic donor–acceptor blends. *Nature Mater* 14: 1130–1134.
  119. Kabe R, Adachi C (2017) Organic long persistent luminescence. *Nature* 550: 384–387.
  120. Vandewal K, Albrecht S, Hoke ET, et al. (2014) Efficient charge generation by relaxed charge-transfer states at organic interfaces. *Nature Mater* 13: 63–68.
  121. Lin Z, Kabe R, Nishimura N, et al. (2018) Organic long-persistent luminescence from a flexible and transparent doped polymer. *Adv Mater* 30: 1803713.
  122. Nishimura N, Lin Z, Jinnai K, et al. (2020) Many exciplex systems exhibit organic long-persistent luminescence. *Advanced Functional Materials* 30: 2000795.
  123. Xk L, Z C, Cj Z, et al. (2015) Prediction and design of efficient exciplex emitters for high-efficiency, thermally activated delayed-fluorescence organic light-emitting diodes. *Adv Mater* 27.
  124. Alam P, Cheung TS, Leung NLC, et al. (2022) Organic long-persistent luminescence from a single-component aggregate. *J Am Chem Soc* 144: 3050–3062.
  125. Jinnai K, Kabe R, Adachi C (2018) Wide-range tuning and enhancement of organic long-persistent luminescence using emitter dopants. *Adv Mater* 30: 1800365.
  126. Kuila S, George SJ (2020) Phosphorescence energy transfer: ambient afterglow fluorescence from water-processable and purely organic dyes via delayed sensitization. *Angewandte Chemie International Edition* 59: 9393–9397.
  127. Louis M, Thomas H, Gmelch M, et al. (2019) Blue-light-absorbing thin films showing ultralong room-temperature phosphorescence. *Adv Mater* 31: 1807887.
-

- 
128. Li W, Li Z, Si C, et al. (2020) Organic Long-persistent luminescence from a thermally activated delayed fluorescence compound. *Adv Mater* 32: 2003911.
  129. DeRosa CA, Daly ML, Kerr C, et al. (2019) Methoxy-substituted difluoroboron benzoylacetate complexes with color-tunable phosphorescence. *ChemPhotoChem* 3: 31–36.
  130. Gao R, Fang X, Yan D (2018) Direct white-light emitting room-temperature-phosphorescence thin films with tunable two-color polarized emission through orientational hydrogen-bonding layer-by-layer assembly. *J Mater Chem C* 6: 4444–4449.
  131. Kwon MS, Lee D, Seo S, et al. (2014) Tailoring intermolecular interactions for efficient room-temperature phosphorescence from purely organic materials in amorphous polymer matrices. *Angew Chem Int Ed Engl* 53: 11177–11181.
  132. Reineke S, Seidler N, Yost SR, et al. (2013) Highly efficient, dual state emission from an organic semiconductor. *Appl Phys Lett* 103: 093302.
  133. Wang X, Dong M, Li Z, et al. (2022) Recent advances of room temperature phosphorescence and long persistent luminescence by doping system of purely organic molecules. *Dyes and Pigments* 204: 110400.
  134. Yan X, Peng H, Xiang Y, et al. (2022) Recent advances on host–guest material systems toward organic room temperature phosphorescence. *Small* 18: 2104073.
  135. Alam P, Leung NLC, Liu J, et al. (2020) Two are better than one: a design principle for ultralong-persistent luminescence of pure organics. *Adv Mater* 32: 2001026.
  136. Kenry, Chen C, Liu B (2019) Enhancing the performance of pure organic room-temperature phosphorescent luminophores. *Nat Commun* 10: 2111.
  137. Lei Y, Yang J, Dai W, et al. (2019) Efficient and organic host–guest room-temperature phosphorescence: tunable triplet–singlet crossing and theoretical calculations for molecular packing. *Chem Sci* 12: 6518–6525.
  138. Zhang X, Du L, Zhao W, et al. (2019) Ultralong UV/mechano-excited room temperature phosphorescence from purely organic cluster excitons. *Nat Commun* 10: 5161.
  139. Wieszczycka K, Staszak K, Woźniak-Budych MJ, et al. (2021) Surface functionalization – The way for advanced applications of smart materials. *Coordination Chemistry Reviews* 436: 213846.
  140. Michael FM, Khalid M, Walvekar R, et al. (2018) 2 - Surface modification techniques of biodegradable and biocompatible polymers, In: Shimpi NG (Ed.), *Biodegradable and Biocompatible Polymer Composites*, Woodhead Publishing, 33–54.
  141. John MJ, Anandjiwala RD (2009) Surface modification and preparation techniques for textile materials, In: Wei Q (Ed.), *Surface Modification of Textiles*, Woodhead Publishing, 1–25.
  142. Nadi A, Boukhriss A, Bentis A, et al. (2018) Evolution in the surface modification of textiles: a review. *Text Prog* 50: 67–108.
-

143. Boukhriss A, Messoudi ME, Roblin J-P, et al. (2020) Luminescent hybrid coatings prepared by a sol–gel process for a textile-based pH sensor. *Mater Adv* 1: 918–925.
  144. Tao C, Zou X, Du K, et al. (2018) Fabrication of robust, self-cleaning, broadband TiO<sub>2</sub>SiO<sub>2</sub> double-layer antireflective coatings with closed-pore structure through a surface sol-gel process. *J Alloys Compd* 747: 43–49.
  145. Kianfar P, Abate MT, Trovato V, et al. (2020) Surface functionalization of cotton fabrics by photo-grafting for pH sensing applications. *Front Mater* 7.
  146. Liu H, Yin Y, Zhou J, et al. (2022) Fabrication of durable fluorescent and hydrophobic cotton fabrics by multiple surface modifications. *Industrial Crops and Products* 175: 114238.
  147. Hameed A, Aljuhani E, Bawazeer TM, et al. (2021) Preparation of multifunctional long-persistent photoluminescence cellulose fibres. *Luminescence* 36: 1781–1792.
  148. Chung C, Lee M, Choe EK (2004) Characterization of cotton fabric scouring by FT-IR ATR spectroscopy. *Carbohydrate Polymers* 58: 417–420.
  149. Moussa A (2021) Textile color formulation using linear programming based on Kubelka-Munk and Duncan theories - Moussa - 2021 - Color Research & Application - Wiley Online Library, 2021. Available from: <https://onlinelibrary.wiley.com/doi/abs/10.1002/col.22626>.
  150. Schindler WD, Hauser PJ (2004) Chemical finishing of textiles, Elsevier.
  151. Cherrington R, Goodship V, Middleton B (2016) Design and manufacture of plastic components for multifunctionality: structural composites, injection molding, and 3d printing, William Andrew is an imprint of Elsevier.
  152. Chmielarz P, Król P (2017) Poly(urethane-methacrylate) copolymers prepared by the atom transfer radical polymerization methods as a new material for hydrophobic coatings, *Polyurethane Polymers*, Amsterdam, Elsevier, 247–260.
  153. Khattab TA, Rehan M, Hamdy Y, et al. (2018) Facile development of photoluminescent textile fabric via spray coating of Eu(II)-doped Strontium Aluminate. *Ind Eng Chem Res* 57: 11483–11492.
  154. Samanta A, Bordes R (2020) Conductive textiles prepared by spray coating of water-based graphene dispersions. *RSC Adv* 10: 2396–2403.
  155. Ly BCK, Dyer EB, Feig JL, et al. (2020) Research techniques made simple: cutaneous colorimetry: a reliable technique for objective skin color measurement. *J Invest Dermatol* 140: 3-12.e1.
  156. Maitra S, Chatterjee D, Bandyopadhyay AR (2019) Skin color variation: A study on Eastern and North East India. *Asian j med pharm sci* 10: 13–16.
  157. McLaren K, Taylor PF (1981) The derivation of hue-difference terms from CIELAB coordinates. *Color Res Appl* 6: 75–77.
  158. Marcuse D (2012) Principles of optical fiber measurements, Elsevier.
-

- 
159. Okoshi T (2012) *Optical Fibers*, Elsevier.
  160. Stöber W, Fink A, Bohn E (1968) Controlled growth of monodisperse silica spheres in the micron size range. *Journal of Colloid and Interface Science* 26: 62–69.
  161. Rao KS, El-Hami K, Kodaki T, et al. (2005) A novel method for synthesis of silica nanoparticles. *Journal of Colloid and Interface Science* 289: 125–131.
  162. LeBaron PC, Pinnavaia TJ (2001) Clay nanolayer reinforcement of a silicone elastomer. *Chem Mater* 13: 3760–3765.
  163. Wang ZJ, Kumagai T, Kokawa H, et al. (2008) Preparation of hafnium oxide thin films by sol–gel method. *J Electroceram* 21: 499–502.
  164. Checucci S, Bottein T, Gurioli M, et al. (2019) Multifunctional metasurfaces based on direct nanoimprint of titania sol–gel coatings. *Adv Opt Mater* 7: 1801406.
  165. Brenier R, Mugnier J, Mirica E (1999) XPS study of amorphous zirconium oxide films prepared by sol–gel. *Applied Surface Science* 143: 85–91.
  166. Gabriel AO, Riedel R (1997) Preparation of non-oxidic silicon ceramics by an anhydrous sol–gel process. *Angew Chem* 36: 384–386.
  167. Milea CA, Bogatu C, Duta A (2011) The influence of parameters in silica sol-gel process. *Bull Transilvania Univ* 4: 59.
  168. Corriu RJP, Leclercq D (1996) Recent developments of molecular chemistry for sol–gel processes. *Angew Chem* 35: 1420–1436.
  169. Periyasamy AP, Venkataraman M, Kremenakova D, et al. (2020) Progress in sol-gel technology for the coatings of fabrics. *Materials* 13: 1838.
  170. Dehghanhadikolaei A, Ansary J, Ghoreishi R (2018) Sol-gel process applications: A mini-review. *Proc Nat Res Soc* 2: 02008–02029.
  171. Mackenzie JD, Bescher EP (2000) Physical properties of sol-gel coatings. *J. Sol-Gel Sci. Tech* 19: 23–29.
  172. Chen S, Carraro G, Barreca D, et al. (2015) Growth and electro-optical properties of Ga-doped ZnO films prepared by aerosol assisted chemical vapour deposition. *Thin Solid Films* 584: 316–319.
  173. Franco E, Dussán R, Amú M, et al. (2018) Statistical optimization of the sol–gel electrospinning process conditions for preparation of polyamide 6/66 nanofiber bundles. *Nanoscale Research Letters* 13: 230.
  174. Bentis A, Boukhriss A, Gmouh S (2020) Flame-retardant and water-repellent coating on cotton fabric by titania–boron sol–gel method. *J Sol-Gel Sci Technol* 1–12.
  175. Bentis A, Boukhriss A, Grancaric AM, et al. (2019) Flammability and combustion behavior of cotton fabrics treated by the sol gel method using ionic liquids combined with different anions. *Cellulose* 26: 2139–2153.
-

176. Sakai RT, da Cruz FMDL, de Melo HG, et al. (2012) Electrochemical study of TEOS, TEOS/MPTS, MPTS/MMA and TEOS/MPTS/MMA films on tin coated steel in 3.5% NaCl solution. *Progress in Organic Coatings* 74: 288–301.
177. Tai ZS, Othman MHD, Mustafa A, et al. (2021) Development of hydrophobic polymethylhydrosiloxane/tetraethylorthosilicate (PMHS/TEOS) hybrid coating on ceramic membrane for desalination via membrane distillation. *Journal of Membrane Science* 637: 119609.
178. De G, Kundu D, Karmakar B, et al. (1993) FTIR studies of gel to glass conversion in TEOS-fumed silica-derived gels. *Journal of Non-Crystalline Solids* 155: 253–258.
179. Favre-Besse F-C, Poirel O, Bersot T, et al. (2014) Design, synthesis and biological evaluation of small-azo-dyes as potent Vesicular Glutamate Transporters inhibitors. *Eur J Med Chem EUR* 78: 236–247.
180. Fettouche S, Boukhriss A, Tahiri M, et al. (2019) Naked eye and selective detection of copper (ii) in mixed aqueous media using a cellulose-based support. *Chem Res Chin Univ* 35: 598–603.
181. Puchtler H, Sweat F, Gropp S (1967) An investigation into the relation between structure and fluorescence of azo dyes. *J R Microsc Soc* 87: 309–328.
182. Pastore A, Badocco D, Bogialli S, et al. (2021) Behavior of sulfonephthalein and azo dyes as effective pH sensors in hybrid materials. *Microchemical Journal* 160: 105605.
183. Benkhaya S, M'rabet S, El Harfi A (2020) Classifications, properties, recent synthesis and applications of azo dyes. *Heliyon* 6: e03271.
184. Ziarani GM, Moradi R, Lashgari N, et al. (2018) Azo Dyes, *Metal-Free Synthetic Organic Dyes*, Elsevier, 47–93.
185. De Meyer T, Hemelsoet K, Van der Schueren L, et al. (2012) Investigating the halochromic properties of azo dyes in an aqueous environment by using a combined experimental and theoretical approach. *Chem Eur J* 18: 8120–8129.
186. Shu D, Fang K, Liu X, et al. (2019) Cleaner pad-steam dyeing technology for cotton fabrics with excellent utilization of reactive dye. *Journal of Cleaner Production* 241: 118370.
187. Sicardi S, Manna L, Banchemo M (2000) Diffusion of disperse dyes in PET films during impregnation with a supercritical fluid. *The Journal of Supercritical Fluids* 17: 187–194.
188. Sakka S, Kozuka H (2005) Handbook of sol-gel science and technology. Sol-gel processing, Springer Science & Business Media.
189. Wysecki G, Stiles WS (1982) Color science: Concepts and methods, quantitative data and formulae. *New York, London, Sidney*.
190. Weatherall IL, Coombs BD (1992) Skin color measurements in terms of CIELAB color space values. *J Invest Dermatol* 99: 468–473.

- 
191. Ulery AL, Drees LR, America SSS of (2008) Methods of soil analysis: Mineralogical methods.
  192. Becerir B (2005) A novel approach for estimating the relation between K/S value and dye uptake in reactive dyeing of cotton fabrics. *Fibers Polym* 6: 224–228.
  193. Faustini M, Nicole L, Ruiz-Hitzky E, et al. (2018) History of organic–inorganic hybrid materials: prehistory, art, science, and advanced applications. *Adv Funct Mater* 28: 1704158.
  194. García-Martínez J-M, Collar EP (2021) Organic–inorganic hybrid materials. *Polymers* 13: 86.
  195. Berkowitz J, Ellison GB, Gutman D (2002) ACS Publications, Three methods to measure RH bond energies, 2002. Available from: <https://pubs.acs.org/doi/pdf/10.1021/j100062a009>.
  196. Wang Q-M, Yan B (2006) Designing a family of luminescent hybrid materials by 3-(triethoxysilyl)-propyl isocyanate grafted 2-hydroxynicotinic acid bridge molecules. *Journal of Organometallic Chemistry* 691: 3567–3573.
  197. Schiffer D, Tegl G, Vielnascher R, et al. (2015) Fast Blue RR—siloxane derivatized materials indicate wound infection due to a deep blue color development. *Materials* 8: 6633–6639.
  198. Lai C-W, Wang Y-H, Lai C-H, et al. (2008) Iridium-complex-functionalized Fe<sub>3</sub>O<sub>4</sub>/SiO<sub>2</sub> core/shell nanoparticles: a facile three-in-one system in magnetic resonance imaging, luminescence imaging, and photodynamic therapy. *Small* 4: 218–224.
  199. Yazdanshenas ME, Shateri-Khalilabad M (2012) The effect of alkali pre-treatment on formation and adsorption of silver nanoparticles on cotton surface. *Fibers Polym* 13: 1170–1178.
  200. Brouwer AM (2011) Standards for photoluminescence quantum yield measurements in solution. *Pure and Applied Chemistry* 83: 2213–2228.
  201. Crosby GA, Demas JN (1971) Measurement of photoluminescence quantum yields. A Review. *J Phys Chem* 75: 991–1024.
  202. Valeur B, Berberan-Santos MN (2012) Molecular fluorescence: principles and applications, Wiley-VCH Verlag.
  203. Lakowicz JR (2013) Principles of fluorescence spectroscopy, Springer Science & Business Media.
  204. Würth C, Grabolle M, Pauli J, et al. (2013) Relative and absolute determination of fluorescence quantum yields of transparent samples. *Nat Protoc* 8: 1535–1550.
  205. Resch-Genger U, Rurack K (2013) Determination of the photoluminescence quantum yield of dilute dye solutions. *Pure Appl Chem* 85: 2005–2013.
-

206. Klán P, Wirz J (2009) Photochemistry of organic compounds: from concepts to practice, John Wiley & Sons.
207. Hofstraat JW, Latuhihin MJ (1994) Correction of fluorescence spectra. *Appl Spectrosc* 48: 436–447.
208. Braslavsky SE (2007) Glossary of terms used in photochemistry. *Pure and Applied Chemistry* 79: 293–465.
209. Nawara K, Waluk J (2017) Improved method of fluorescence quantum yield determination. *Anal Chem* 89: 8650–8655.
210. Hart SJ, Jiji RD (2002) Light emitting diode excitation emission matrix fluorescence spectroscopy. *Analyst* 127: 1693–1699.
211. Herman P, Maliwal BP, Lin H-J, et al. (2001) Frequency-domain fluorescence microscopy with the LED as a light source. *J Microsc* 203: 176–181.
212. Lamb J, Forfang K, Hohmann-Marriott M (2015) A practical solution for 77 K fluorescence measurements based on LED excitation and CCD array detector. *PLoS ONE* 10: e0132258.
213. Moe AE, Marx S, Banani N, et al. (2005) Improvements in LED-based fluorescence analysis systems. *Sens Actuator B-Chem* 111–112: 230–241.
214. Nawara K, Waluk J (2019) Goodbye to quinine in sulfuric acid solutions as a fluorescence quantum yield standard. *Anal Chem* 91: 5389–5394.
215. Pantke ER, Labhart H (1972) On the temperature dependence of non-radiative deactivation processes. *Chem Phys Lett* 16: 255–259.
216. Suzuki K, Kobayashi A, Kaneko S, et al. (2009) Reevaluation of absolute luminescence quantum yields of standard solutions using a spectrometer with an integrating sphere and a back-thinned CCD detector. *Phys Chem Chem Phys* 11: 9850–9860.
217. Taniguchi M, Lindsey JS (2018) Database of absorption and fluorescence spectra of >300 common compounds for use in PhotochemCAD. *Photochem Photobiol* 94: 290–327.
218. Tran-Thi T-H, Prayer C, Millié Ph, et al. (2002) Substituent and solvent effects on the nature of the transitions of pyrenol and pyranine. Identification of an intermediate in the excited-state proton-transfer reaction. *J Phys Chem A* 106: 2244–2255.
219. Magde D, Brannon JH, Cremers TL, et al. (1979) Absolute luminescence yield of cresyl violet. A standard for the red. *Journal of Physical Chemistry* 83: 696–699.
220. Pant D, Tripathi UC, Joshi GC, et al. (1990) Photophysics of doubly-charged quinine: steady state and time-dependent fluorescence. *J of Photochem and Photobio A: Chem* 51: 313–325.
221. Olmsted J (1979) Calorimetric determinations of absolute fluorescence quantum yields. *J Phys Chem* 83: 2581–2584.

- 
222. Martin MM (1975) Hydrogen bond effects on radiationless electronic transitions in xanthene dyes. *Chem Phys Lett* 35: 105–111.
223. Zhang X-F, Zhang J, Liu L (2014) Fluorescence properties of twenty fluorescein derivatives: lifetime, quantum yield, absorption and emission spectra. *J Fluoresc* 24: 819–826.
224. Würth C, González MG, Niessner R, et al. (2012) Determination of the absolute fluorescence quantum yield of rhodamine 6G with optical and photoacoustic methods – Providing the basis for fluorescence quantum yield standards. *Talanta* 90: 30–37.
225. Fischer M, Georges J (1996) Fluorescence quantum yield of rhodamine 6G in ethanol as a function of concentration using thermal lens spectrometry. *Chem Phys Lett* 260: 115–118.
226. Rurack K, Spieles M (2011) Fluorescence Quantum yields of a series of red and near-infrared dyes emitting at 600–1000 nm. *Anal Chem* 83: 1232–1242.
227. Lewis JE, Maroncelli M (1998) On the (uninteresting) dependence of the absorption and emission transition moments of coumarin 153 on solvent. *Chem Phys Lett* 282: 197–203.
228. Prazeres TJV, Beija M, Fernandes FV, et al. (2012) Determination of the critical micelle concentration of surfactants and amphiphilic block copolymers using coumarin 153. *Inorganica Chimica Acta* 381: 181–187.
229. Cser A, Nagy K, Biczók L (2002) Fluorescence lifetime of Nile red as a probe for the hydrogen bonding strength with its microenvironment. *Chem Phys Lett* 360: 473–478.
230. Avnir Y, Barenholz Y (2005) pH determination by pyranine: medium-related artifacts and their correction. *Analytical Biochemistry* 347: 34–41.
231. Ulrich S, Osypova A, Panzarasa G, et al. (2019) Pyranine-modified amphiphilic polymer conetworks as fluorescent ratiometric pH sensors. *Macromol Rapid Commun* 40: 1900360.
232. Finkler B, Spies C, Vester M, et al. (2014) Highly photostable “super”-photoacids for ultrasensitive fluorescence spectroscopy. *Photochem Photobiol Sci* 13: 548.
233. de Borba EB, Amaral CLC, Politi MJ, et al. (2000) Photophysical and photochemical properties of pyranine/methyl viologen complexes in solution and in supramolecular aggregates: a switchable complex. *Langmuir* 16: 5900–5907.
234. Gardecki JA, Maroncelli M (1998) Set of secondary emission standards for calibration of the spectral responsivity in emission spectroscopy. *Applied Spectroscopy* 52: 1179–1189.
235. Isak SJ, Eyring EM (2002) Fluorescence quantum yield of cresyl violet in methanol and water as a function of concentration. *ACS Publications*.
236. Hatami S, Würth C, Kaiser M, et al. (2015) Absolute photoluminescence quantum yields of IR26 and IR-emissive Cd<sub>1-x</sub>Hg<sub>x</sub>Te and PbS quantum dots – method- and material-inherent challenges. *Nanoscale* 7: 133–143.
-



237. Würth C, Pauli J, Lochmann C, et al. (2012) Integrating sphere setup for the traceable measurement of absolute photoluminescence quantum yields in the near infrared. *Analytical Chemistry* 84: 1345–1352.
238. Braun CL, Smirnov SN (1993) Why is Water Blue? *J Chem Ed* 70: 612–614.
239. Zong Y, Brown SW, Johnson BC, et al. (2006) Simple spectral stray light correction method for array spectroradiometers. *Appl Opt* 45: 1111.
240. Nawara K, Rana A, Panda PK, et al. (2018) Versatile approach for reliable determination of both high and low values of luminescence quantum yields. *Anal Chem* 90: 10139–10143.
241. Kulinich AV, Ishchenko AA, Bondarev SL, et al. (2021) Effect of donor and acceptor end-groups on electronic structure and spectral-fluorescent properties of merocyanines in frozen ethanol. *Journal of Photochemistry and Photobiology A: Chemistry* 405: 112932.
242. Mahesh K, Karpagam S, Pandian K (2019) How to design donor–acceptor based heterocyclic conjugated polymers for applications from organic electronics to sensors. *Top Curr Chem (Z)* 377: 12.
243. Yamaguchi Y, Matsubara Y, Ochi T, et al. (2008) How the  $\pi$  Conjugation Length Affects the Fluorescence Emission Efficiency. *J Am Chem Soc* 130: 13867–13869.
244. Nijegorodov N, Zvolinsky V, Luhanga PVC (2008) Photonics and photochemical stability of aromatic molecules, family related in  $\pi$ -structure but different in planarity, rigidity and molecule symmetry. *Journal of Photochemistry and Photobiology A: Chemistry* 196: 219–226.
245. Sugihara Y, Inai N, Taki M, et al. (2021) Donor–acceptor–acceptor-type near-infrared fluorophores that contain dithienophosphole oxide and boryl groups: effect of the boryl group on the nonradiative decay. *Chem Sci* 12: 6333–6341.
246. Werts MHV, Gmouh S, Mongin O, et al. (2004) Strong modulation of two-photon excited fluorescence of quadripolar dyes by (de)protonation. *J Am Chem Soc* 126: 16294–16295.
247. Lakowicz JR (1983) Effects of solvents on fluorescence emission spectra, *Principles of Fluorescence Spectroscopy*, Boston, MA, Springer US, 187–215.
248. Haidekker MA, Brady TP, Lichlyter D, et al. (2005) Effects of solvent polarity and solvent viscosity on the fluorescent properties of molecular rotors and related probes. *Bioorganic Chemistry* 33: 415–425.
249. Ahmed R, Manna AK (2022) Understanding high fluorescence quantum yield and simultaneous large stokes shift in phenyl bridged donor– $\pi$ –acceptor dyads with varied bridge lengths in polar solvents. *J Phys Chem A* 126: 4221–4229.
250. Qin X, Yang X, Du L, et al. (2021) Polarity-based fluorescence probes: properties and applications. *RSC Med Chem* 12: 1826–1838.
251. Velapoldi RA, Mielenz KD (1980) A fluorescence standard reference material. *National Bureau of Standards (US) Special Publication* 2060–64.
-

- 
252. Kreller DI, Kamat PV (1991) Photochemistry of sensitizing dyes: spectroscopic and redox properties of cresyl violet. *J Phys Chem* 95: 4406–4410.
  253. Tiwari R, Dubey V, Singh V, et al. (2021) Luminescence: Theory and applications of rare earth activated phosphors, De Gruyter.
  254. Allison SW, Gillies GT (1997) Remote thermometry with thermographic phosphors: Instrumentation and applications. *Rev Sci Instrum* 68: 2615–2650.
  255. Krupp F, Frey W, Richert C (2020) Absolute configuration of small molecules by co-crystallization. *Angew Chem* 132: 16009–16013.
  256. Aakerøy CB, Sinha AS (2018) Co-crystals: introduction and scope, *Cryst. Growth Des.* CRY., 1–32.
  257. Khattab TA, Abd El-Aziz M, Abdelrahman MS, et al. (2020) Development of long-persistent photoluminescent epoxy resin immobilized with europium (II)-doped strontium aluminate. *Luminescence* 35: 478–485.
  258. Van der Heggen D, Joos JJ, Feng A, et al. (2022) Persistent luminescence in strontium aluminate: a roadmap to a brighter future. *Adv Funct Mater* 32: 2208809.
  259. Huang Z, Chen B, Ren B, et al. (2022) Smart mechanoluminescent phosphors: a review of strontium-aluminate-based materials, properties, and their advanced application technologies. *Adv Sci (Weinh)* :2204925.



**Titre :** Développement et caractérisation de matériaux moléculaires luminescents et leur application dans des textiles techniques

**Mots clés :** Luminescence, fibres optiques, spectroscopie, fonctionnalisation, sol-gel

**Résumé :** L'objectif de ce projet de recherche était de développer des matériaux qui présentent une émission lumineuse dans le but ultime d'utiliser ces matériaux sur des textiles pour des applications techniques. Afin de réaliser cet objectif, une série d'expériences ont été menées pour mieux comprendre ces matériaux et maîtriser la technique de transfert de la propriété lumineuse au substrat choisi (textiles). Le travail accompli dans cette thèse peut être divisé en deux sections, qui sont complémentaires l'une de l'autre. La première partie se concentre sur les aspects techniques et instrumentaux, dans lesquels diverses méthodes de caractérisation et techniques de mesure basées sur des instruments couplés à des fibres optiques ont été développées, examinées et validées.

La seconde partie traite principalement de la préparation et de la synthèse de molécules et de matériaux, ainsi que de leur intégration dans des textiles. Pour ce faire, plusieurs techniques ont été utilisées, telles que la méthode sol-gel, l'enduction et la pulvérisation à polymère brut. Ces méthodes ont été utilisées pour fonctionnaliser les matériaux développés pour les intégrer au sein de la matrice textile. Le processus, allant des molécules aux tissus finaux, a été étudié et optimisé du point de vue optique en utilisant les ensembles de couplage de fibres développés dans la première partie. En fin de ligne, des textiles luminescents ont été élaborés, qui pourraient être utilisés dans la conception d'une tente de camping auto-lumineuse.

**Title:** Development and characterization of luminescent molecular materials and their application in technical textiles

**Keywords:** Luminescence, optical fiber devices, spectroscopy, textile processing, sol-gel

**Abstract:** The objective of this research project was to develop materials that exhibit luminous emission, with the ultimate goal of using these materials on textiles for technical applications. In order to accomplish this aim, a series of experiments were conducted to gain a deeper understanding of these materials and to master the technique for transferring the luminous property to the chosen substrate (textile fabrics). The work undertaken in this thesis can be divided into two main sections, which are complementary to each other. The first part focuses on the technical and instrumental aspects, in which various characterization methods and measurement techniques based on optical fiber coupling instruments were developed, reviewed, and validated.

The second part primarily deals with the preparation and synthesis of molecules and compounds, as well as their integration into textile fabrics. There are several techniques that can be used for this purpose, and in the context of this work, the sol-gel chemistry, polymer knife coating, and raw-polymer spray-coating methods were employed as functionalization pathways. The entire process from molecules to the final fabric was optically investigated, studied, and further optimized using the fiber coupled assemblies established in the technical part. Ultimately, luminescent textile fabrics were produced that have the potential to be used in the design of a self-luminous camping tent.